Trinity College Dublin
Coláiste na Tríonóide, Baile Átha Cliath
The University of Dublin

Effect of groundwater-surface interactions on coastal areas hosting aquaculture activities

A Thesis Presented to the Academic Faculty in Fulfilment of the Requirements for the Degree of Doctor of Philosophy

2022

Maxime Savatier

School of Natural Sciences
Discipline of Geography
Biogeochemistry Research Group

The University of Dublin
Trinity College Dublin

iCRAG
IRISH CENTRE FOR RESEARCH IN APPLIED GEOSCIENCES

I declare that this thesis has not been submitted as an exercise for a degree at this or any other university and it is entirely my own work.

I agree to deposit this thesis in the University's open access institutional repository or allow the library to do so on my behalf, subject to Irish Copyright Legislation and Trinity College Library conditions of use and acknowledgement.

Maxime Savatier

"The oceanographic and hydrogeological communities should recognize the local and global importance of SGD and work together to achieve a better understanding of processes that control SGD and its constituents."

Willard S. Moore, 2010.

-

"The modeler, as an artist, must determine which aspects of the natural process are important, and must be sure that these aspects are simulated correctly in the model"

Hugo B. Fischer, 1979.

Summary

Submarine groundwater discharge (SGD) is crucial for the nutrient budgets of coastal areas and global oceans. However, its role in the function of coastal ecosystems is still poorly characterised. This study aimed to (1) investigate the effect of nutrient fluxes from submarine groundwater discharge on Irish coastal ecosystems hosting aquaculture activities and (2) determine how this effect vary during the year, to (3) assess the value of SGD for coastal areas hosting aquaculture activities.

Two sites of contrasting hydrogeology and depth were selected to represent the two extreme ranges of the effect of SGD on coastal ecosystems: Kinvarra Bay, a shallow bay connected to a productive aquifer of karstic limestone, and Killary Harbour, a fjord fed by rivers and surrounded by an unproductive aquifer, mainly of impermeable sandstone. Radium isotopes, radon, nutrient, salinity, dissolved oxygen, temperature data and other water chemistry parameters were collected in these two bays between August 2017 and April 2019. These were combined with modelling to investigate the effect of changes of SGD composition, quantity and variability of flushing on coastal system's nutrient balance, primary production and aquaculture. In Kinvarra Bay, nitrogen inputs from fresh SGD amplified the primary production, directly benefiting the mussel aquaculture activity. Saline SGD can also provide added solute to the system, including limiting nutrient such as phosphorus or radiotracers such as radium, in particular when drought occurs following spring tides. In Killary Harbour, SGD was negligible in this bay by comparison to river flow, except potentially in the most inner part of the bay, where an intertidal area is present. However, solutes fluxes from deep sediment were significant, and likely provides limiting nutrients such as phosphorus for local phytoplankton growth, in addition to the inputs from rivers. This fluxes could be amplified by the resuspension of fine sediments due to cyclic currents in deep waters. In both bays, the transfer of solutes from sediment to surface waters, either through sediment resuspension or SGD, is a key factor driving phosphorus availability. Phosphorus availability affects both phytoplankton biomass and composition, thus the food source and/or ecosystem services providers (maintain water quality, oxygen levels) for aquaculture production. Consequently, solutes inputs from sediments via SGD (in sites with high SGD inputs) or via suspended sediments (in sites with fine sediments) are likely to affect the interannual variability of aquaculture production by controlling in part the limiting nutrients for primary production and the bay nutrient balances.

This work includes an introduction section, followed by six chapters, each of them going one step further to understand the effect of SGD on coastal areas nutrient balance.

After an introduction of the research aims in section 1, Chapter 2 provides a review of the current knowledge on the processes driving SGD composition and quantity, the methods to estimate it, and its effect on coastal nutrient balance and aquaculture.

In Chapter 3, radon and salinity measurements and a comparison to modelling and earlier work are used to assess the range of fresh SGD fluxes during the year in Kinvarra Bay. This review is also used to improve the existing tracer-based methods to quantify the total SGD coming to coastal areas. This work shows that correcting for the effect of spatial variations of flushing in coastal sites can improve the reliability of mass balances of non-conservative elements used to assess SGD. This correction is particularly useful for sites where SGD occurs in a specific location and is not equally distributed across the system, such as in karst systems. Similarly, the method chosen to calculate inventory of a tracer can significantly modify the final discharge estimate, particularly when solute inputs occur in shallow areas. For example, as they are not accounting for the true distribution of depths, averages and median can overestimate the effect of a source present in shallow areas on the inventory of a solute.

In Chapter 4, increase of radium isotopes in coastal waters are related to periods of increasing seawater recirculated through coastal aquifers and are used to assess the magnitude of recirculated seawater fluxes in a karst system (Kinvarra Bay). This section suggests that saline groundwater can supply additional phosphorus to coastal areas following periods of saline intrusions in coastal aquifers. These fluxes are likely to lead to periods of increased primary production by reducing ecosystem phosphorus limitation, thus affecting Chl-a, dissolved oxygen … in the bay.

Chapter 5 assesses the effects of stratification and of the spatial and temporal variability of flushing on the time of contact between land-derived solute fluxes and non-mobile organisms such as mussels. To do so, six radium salinity and nutrients transects of surface and deep waters were carried out in a variably stratified fjord (Killary Harbour) under a range of river discharge and stratification conditions. In this bay, increased stratification during periods of high discharge limit further the transfer phosphorus from deep to surface waters. Consequently, this amplify the increase of surface N:P ratio following increased water inputs from river, compared to what can be expected from changes of nutrient loads from rivers. A review of past studies suggests

that this effect could influence phytoplankton species and the frequency of harmful algae blooms (HABs) in coastal systems. This combined information can support and validate the description of flushing and estuarine mixing in models, or be applied to test the effect of potential catchment management strategies on the value of SGD for aquaculture.

In Chapter 6, a lower trophic model and the analysis of the EPA transitional water database for Kinvarra Bay showed that primary production is amplified by nutrient inputs from SGD, particularly when phosphorus availability in the bay is high. Nutrient inputs from SGD lead to an increase of modelled phytoplankton biomass by 67%, suggesting that the economic value of SGD flow to Kinvarra bay mussel and oyster aquaculture is between 86 400 and 121 200 Euro. Historical data and modelling suggest that residence time, salinity, nutrient levels, and chlorophyll-a fluctuate seasonally in the bay as a result of the combined effect of neap/spring tidal variability and changing SGD rates. Residence time and the effect of SGD on the chemistry of the system are lowest during spring tides and low groundwater discharge periods but are highest during neap tides and high groundwater discharge periods. Considering this, water inputs from land to the bay are likely to have the highest impact on the bay biogeochemistry during neap tides.

The effect of climate change and anthropogenic driven changes for Kinvarra Bay and systems receiving large SGD fluxes in general are also discussed in Chapter 6. The lower trophic model is applied to test the effect of two direct effects of climate change: the increased sea water temperatures on phytoplankton growth, and changes of rainfall frequency creating changes of SGD seasonal patterns. As the future trends of SGD discharge are not known, we analyse model results for a fourteen years timeserie including several extreme events (drought, flood) and compare them with observed data to estimate the effect that climate related change of SGD discharge could have on the bay nutrient balance, phytoplankton biomass and mussel production. Other effect that could be indirectly modified by climate change are also tested using the lower trophic model: phosphorus availability, changes of marine currents in Galway Bay (modifying the return flow to Kinvarra Bay), and changes of nutrient ratios of phytoplankton. Among other findings, the model results suggest that modifications of the timing of SGD flow relative to periods of phytoplankton growth (for example, as a result of change of rainfall patterns) can lead to significant changes of phytoplankton biomass, thus could modify the quantity of aquaculture production that aquatic systems can support.

Finally, the nutrient mass balance of Kinvarra bay and Killary Harbour are compared using the LOICZ approach in chapter 7 and the results are related to the observations in previous chapters. This thesis ends with two short sections giving recommendations for water management around bays receiving large SGD fluxes (section 9) and summing up the key knowledge gaps identified in this work (section 10).

Acknowledgement

Firstly, I would like to thank Prof. Carlos Rocha for giving me the opportunity to conduct this research, and for providing his support during the development of this work. His guidance and patience during the review of the numerous drafts of papers and chapters boosted the quality and multiplied the qualities of this work.

Maria Teresa and Jennifer Murphy, my PhD colleagues and team workers within the biogeochemistry research group also were of great support during this project for the design of sampling strategies and their views on natural processes in estuaries from both the aquatic biology and geoscience viewpoint. Their support during challenging times was also an immense help.

I would like to thank also the School of Natural Sciences of Trinity College Dublin and the Irish Centre for Research in Applied Geoscience for providing the funding and organisation structure to carry out this research, along with the many opportunities to discuss, exchange with different researchers. Thank you also to the Marine Institute, and the Environment Protection Agency and the Office of Public Works for allowing me to use some of their datasets to the analysis presented here.

Thank you to Dr Jan Scholten from Kiel University for his advice on radium measurement with a Radium Delayed Coincidence Counter and his contribution and help during the first fieldwork. Thank you to Mark Kavanagh from the Trinity Centre for the Environment for his advices and positive support on reagent preparation, quality checks and methods when using continuous flow analysers for nutrient analysis. Thank you also to Prof. Laurence Gill, Patrick Jerome Morrissey, Philip Schuler, for sharing their experience on karst system characteristics in western Ireland. Thank you also to my family and my fiancée, Vitória Dos Santos Acerbi.

Last but not least, I am grateful to the support of the fishermen, landowners and people of western Ireland who contributed to this work through their advice and guidance when accessing the bays, finding boats, getting access to wells. Thank you particularly to Vincent Kayne, Simon Kennedy, and Rayner Krause.

Table of contents

List of Figures

Chapter 2:

Chapter 3:

Chapter 4:

Chapter 5:

Chapter 6:

Chapter 7:

List of Appendices

Chapter 6:

General appendix - datasets:

List of Tables

Chapter 2:

Chapter 3:

Chapter 4:

Chapter 5:

Chapter 6:

List of Abbreviations and notations

BH	Borehole in Kinvarra catchment, close to the main karst conduit feeding Kinvarra springs.
Chl-a	Chlorophyll-a
DIP	Dissolved Inorganic Phosphorus
DIN	Dissolved Inorganic Nitrogen
DIN:Si	Dissolved Inorganic Nitrogen to dissolved reactive silicon ratio
DO	Dissolved Oxygen
DOC	Dissolved Organic Carbon
DON	Dissolved Organic Nitrogen
DRSi	Dissolved Reactive Silica
dpm	Decay per minute
EPA	Environment Protection Agency
EM	Marine end member (sample taken the most seaward in a transect)
FW	Freshwater
HABs	Harmful Algae Blooms
ICES	International Council for the Exploration of the Sea
KE	Kinvarra East.
KW	Kinvarra West.
LOICZ	Land-ocean interactions in the coastal zone
N	Nitrogen
NO_3^{2-}	Nitrate
NO_2^-	Nitrite
NH_4^+	Ammonium
NTU	Nephelometric Turbidity Units
N:P	Nitrogen to phosphorus ratio
NFM	Natural Flood management
OM	Organic Matter
P	Phosphorus
p-r	Primary production-respiration
POC	Particulate Organic Carbon
PO_4^{2-}	Phosphate
RCP	Representative Concentration Pathway
Ra	Radium
Rn	Radon
SGD	Submarine Groundwater Discharge
Si:	Silicon
SP	Spring (sample notation for Kinvarra springs)
SPM	Suspended Particulate Matter
SRP	Soluble Reactive Phosphorus

SW	Seawater
SWTP	Sewage treatment plant
Temp	Water temperature
TDS	Total Dissolved Solids
TP	Total Phosphorus in water

1 Introduction

The contribution of coastal ecosystems to human welfare and the economy was estimated to reach $12.5 Trillion (US dollars) globally at the end of the 20th century, compared roughly to the annual GDP of $18 trillion/year (Costanza et al., 1998). This value is decreasing (Costanza et al., 2014) as additional nutrient inputs to rivers and groundwater from human activities (e.g. agriculture, insufficiently treated wastewater, increased land erosion by changes of land use) impact themselves on the coastal ecosystem health. The observed changes include inter-alia, more frequent development of toxic algae blooms (Silke et al. 2005), low oxygen (hypoxic) zones (Altieri and Gedan, 2015; Rabalais et al., 2002), blooms of nuisance or harmful micro or macroalgae (Green et al., 2014; Li et al., 2017; Liu et al., 2013; Pihl et al., 1999) and the overdevelopment of specific species such as jellyfish (Bosch-Belmar et al., 2017; Condon et al., 2012; Dong et al., 2010; Palmieri et al., 2014). These events impact coastal ecosystem services directly and have detrimental knock-on effects on the fishing and aquaculture industries, coastal communities, tourism, and in some cases for marine and coastal infrastructure (Barbier et al., 2011). They require an understanding of the biogeochemistry of coastal areas to be appropriately managed, and for their effect on ecosystems and human activities to be reduced (Barbier et al., 2011).

Seminal studies conducted over the past two decades have demonstrated the significance of subsurface water sources and pore water exchange for coastal ecosystem biogeochemical budgets and dynamics (Basterretxea et al., 2010; Burnett et al., 2006; Carpenter et al., 1998; Church, 1996; Knee and Paytan, 2011; Lecher et al., 2016; Rocha et al., 2015; Rodellas et al., 2015; Sadat-Noori et al., 2016; W. Finkl and L. Krupa, 2003). The earlier paradigm, that rivers represent the dominant pathway for solute fluxes from land to coastal areas, may need to be reassessed; water fluxes coming to coastal zones from the seafloor and coastal sediments may represent globally solute fluxes up to 3 to 4 times the inputs from rivers (Kwon et al., 2014).

While nutrient inputs to coastal areas from channelled freshwater flows such as rivers are relatively well-gauged, the role of sub-surface sources (e.g. submarine groundwater discharge or SGD) is more difficult to quantify in coastal areas. Early global estimates of

fresh groundwater discharge were between 6 to 10% of the surface waters discharging into the ocean (Zektser and Loaiciga, 1993). As a result, ocean nutrient balances frequently ignore groundwater/seawater interactions in comparison with river fluxes (e.g. Hansell and Follows 2008; Gruber 2008).

However, land derived groundwater is not the only water flow going through the seafloor. The majority of the flow crossing the seafloor is seawater, recirculated through the seafloor and mixed with land derived groundwater. This additional flow occurs at short time and space scale, by recirculation driven by tides and waves through coastal sediments (Li et al., 1999), or at a larger scale through the repositioning of the salt/freshwater interface within groundwater by seasonal changes and tides (Edmunds, 2003; Michael et al., 2005; Isaac R Santos et al., 2009). For this reason, Burnett et al. (2003) define submarine groundwater discharge (SGD) as any flow of water across the seafloor, regardless of fluid composition or driving force. The reactions occurring when meteoric and seawater mix and travel through porous media significantly modify the composition of the discharging water compared to the seawater and freshwater composition (Moore, 2010, 1999). As a result, the rates of transfer, mixing and the original water chemical signatures are not uniform at the system scale (Slomp and Van Cappellen, 2004; Spiteri et al., 2008). This variability makes any estimation of SGD-driven nutrient fluxes challenging. In most cases, nutrient fluxes from SGD cannot be derived directly from discharge figures and the concentration of nutrient in aquifers, but also requires considering the mixing and reaction patterns affecting nutrients during their transfer within coastal and submarine aquifers.

In Ireland, around 35 sites with potentially SGD related temperature anomalies were identified using sea surface temperature (SST) derived from Landsat ETM+TIR (Wilson and Rocha, 2012). However, only Kinvarra Bay has been studied extensively to determine the potential impacts of SGD on ecosystem function (Cave and Henry, 2011; Einsiedl, 2012; Einsiedl et al., 2009; McCaul et al., 2016; McCormack et al., 2014; Rocha et al., 2015; Schubert et al., 2015; Smith and Cave, 2012).

A multi-tracer approach (combining pH, Electric conductivity (EC) and radon) differentiated fresh SGD from surface runoff (Schubert et al., 2015). One of the first nutrient balances in Ireland for an SGD-dominated coastal system was built with a

combination of tracers during summer 2010, 2011 and 2013 (Rocha et al., 2015). The SGD flow rates estimated from tracers confirmed the freshwater flow predictions from hydrogeological modelling and water balances (Gill et al., 2013; McCormack et al., 2014). Furthermore, dissolved inorganic nitrogen inputs from SGD were shown to be the primary driver of eutrophication during summer.

As SGD can supply an important part of the nutrients supporting primary production in coastal areas, it may strongly modify coastal ecosystems, which support aquaculture activities. Enhanced primary production due to the nutrient provided by SGD can promote filter feeders growth in both natural environments (e.g. Piló et al., 2018) and aquaculture sites (e.g. Hwang et al., 2010; Wang et al., 2014).

Conversely, freshwater fluxes and changes of physicochemical parameters (pH, aragonite saturation index, turbidity) at SGD sites can also lead to metabolic stress for organisms present in these systems, particularly calcifying organisms such as bivalves or corals (Lecher and Mackey, 2018). Indeed, these organisms depends on specific pH and aragonite saturation index to be able to form and maintain their protective shells. Deciding under which conditions and where in Ireland SGD has a negative or positive impact will require to answer to the following challenges.

First, while SGD is a crucial source of solutes for the ocean (Moore, 2010), and many nutrient transformations take place in coastal aquifers (e.g. Slomp and Van Cappellen, 2004), the annual variability of nutrient loads from SGD fluxes have been characterised only for few coastlines in the world. SGD fluxes have higher Nitrogen: Phosphorus ratios than river waters (Slomp and Van Cappellen, 2004). As a result, they can drive ecosystems further towards phosphorus limitation, or modify phytoplankton or macroalgae communities (Lecher and Mackey, 2018). However, only one coastal spring site in Ireland is routinely sampled by the Environmental Protection Agency, Kinvarra springs, while 1392 river locations and 221 inland springs and boreholes are monitored for water chemistry under the water framework directive (EPA, 2004). There is no national sampling program specific to SGD yet.

Secondly, the combined effect of discharge, tide, marine current and winds leads to variable flushing patterns in most coastal systems, which change the contact time between SGD waters and aquaculture or other marine organisms, thus the effect of SGD

on them. Lower freshwater discharge to an estuary tend to increase flushing times exponentially (Alber and Sheldon, 1999). Moreover, the discharged waters can remain longer preferentially in the inner part of bays under low tidal forcing, thus particularly during neap tide (e.g. Gregory et al., 2020). Longer retention times are favourable for larger phytoplankton biomass when nutrient, temperature light levels are not limiting growth (e.g. Cloern et al., 1983). Non-mobile marine organisms (bivalves, corals, macroalgae) found in or next to retention areas can also be more exposed to the changes of water chemistry driven by SGD fluxes than organisms far from these zones. In addition to this, stratification can contain some of the solute inputs from SGD next to their discharge point, either in surface or deep waters. This can for example, modify the nutrient ratio available for phytoplankton growth in deep and surface waters. Existing hydrodynamic models for Irish transitional waters provide depth-averaged currents for Irish estuaries (Marine Institute, 2020a). Still, they do not provide information on the rate and frequency of stratification nor identify specific retention zones in Irish coastal systems. Assessments of the variability of residence time between transitional waters of Ireland exists (O'Boyle et al., 2015). However, they assume well-mixed systems and do not estimate the spatial and temporal variability of flushing. The spatial and temporal variability of flushing due to the effect of neap/tide cycle or discharge is known for only a few sites in Ireland. Where assessed, discharge (e.g. Donohue, 2012) or tide (e.g. Gregory et al., 2020) have a significant effect on the flushing characteristics of Irish coastal systems, as expected from estuarine dynamics (e.g. Sanford et al., 1992). Irish transitional waters are frequently not well mixed (Donohue, 2012; Gregory et al., 2020), as expected from previous work (Monsen et al., 2002) and have variable flushing depending on tides, SGD inputs (Gregory et al., 2020) or river inputs (e.g. Donohue, 2012). Assessing the spatial variability of flushing in more systems should help to understand further the effect of SGD discharge on coastal ecosystems.

Finally, to date, few studies assessed the effect of SGD on marine biota (see review by Lecher and Mackey, 2018). SGD can amplify the primary production of ecosystems by the nutrient inputs it provides, but fresh SGD also creates salinity fluctuations that may negatively impact some marine organisms (Lecher and Mackey, 2018). For example, reduced salinity can reduce growth of mussels (e.g. Davenport, 1979; Gruffydd et al.,

1984). So far, studies which assess the effect of SGD on entire ecosystems, beyond phytoplankton or macrophytes, are the least common worldwide (Lecher et al., 2015). It was suggested that more studies combining the measurement of radon and radium isotopes as tracers of SGD discharge, with chlorophyll-a, as an indicator of phytoplankton biomass, were required to assess the effect of SGD-borne nutrients on marine ecosystems (Lecher and Mackey, 2018). Few studies assessed the effect of SGD on sites hosting aquaculture activities or filter feeders to date, but showed that SGD could support the majority of the production of shellfish farming in some sites (e.g. Hwang et al., 2010; Wang et al., 2014). SGD sites with salinity above 34 could also have more abundant benthic filter feeders (mussels) on rocky shores (Piló et al., 2018). No similar studies in Ireland were found during review.

In this context, estimating the impact of nutrient fluxes from SGD for a range of sites hosting aquaculture activities will help develop better management strategies to (1) maintain coastal ecosystem services required to sustain human interests and (2) protect the local aquaculture-derived revenue from negative effects due to the anthropogenic perturbations of coastal ecosystems where SGD is present.

Objectives.

This work aims to assess the effect of nutrient loads from submarine groundwater discharge on coastal areas hosting aquaculture activities. It focusses on enclosed bays as they have a restricted exchange with the open ocean and are the most likely to be affected by SGD fluxes. Moreover, they provide sheltered environments favourable for aquaculture organisms. To highlight the range of possible effect of SGD in these systems, this work compares two bays hosting aquaculture activities and with distinct catchment hydrogeology: Kinvarra Bay, receiving most of its freshwater inputs as fresh SGD, and Killary Harbour, a bay surrounded with unproductive aquifer, receiving most of its freshwater inputs as river discharge.

The SGD variability across the year is characterized in the two systems using salinity, ^{222}Rn, ^{223}Ra and ^{224}Ra. The salinity, ^{223}Ra and ^{224}Ra isotopes transects also can quantify flushing patterns in these sites (water ages), and, where appropriate, differentiate the

effect of saline SGD from diffuse solute fluxes from sediment. Nutrient transects and mass balances based on SGD estimates from tracers are also supporting the characterisation of internal nutrient sources and sinks in the two sites. These information are then used to build a lower trophic model to assess the effect of the annual variability of SGD fluxes on nutrient levels and primary production supporting aquaculture in Kinvarra Bay.

Our applied strategy involved:

1) A desk-based study to a) define the catchment hydrology and hydrogeology of the sites of study to assess the potential magnitude of freshwater input and their pathway across the catchment, b) collect past estimate of fresh SGD/river discharge and nutrient concentrations in the bays, surrounding aquifers or rivers they receive, to give a first assessment of the relative role of SGD as a nutrient source on a typical year and c) determine when possible the flushing time of water in the bays.

2) Sampling of natural geochemical tracers of SGD through the coastal aquifer (salinity, radium, radon) in groundwater, intertidal springs and surface water, to (a) determine the contribution of SGD to the overall nutrient balance feeding phytoplankton growth, and (b) the water residence time of the bays (with radium isotopes).

3) In parallel, sampling for nutrients analysis of bay, groundwater, river, and springs water to assess the different sources/sinks of nutrients and their transformation along the groundwater-coastal water-aquaculture pathway.

4) Building nutrient mass balances using the LOICZ approach (Gordon et al., 1996) based on sampling surveys and to characterise the variability of nutrient sinks and sources in the systems studied.

5) Applying a lower-trophic ecosystem model (Cranford et al., 2007) to an SGD dominated site, Kinvarra Bay. This model aimed to assess the effect of nutrient loads from SGD and variable flushing rates on phytoplankton growth and from this, on the nitrogen assimilation of filter feeders (mussels). This model was setup and validated, using the nutrient, discharge and residence time data derived from steps 1 to 4 and using a ten-year nutrient, water chemistry and Chl-

a dataset on Kinvarra Bay, Kinvarra springs and the limestone aquifer feeding it from the environment protection agency. Mussel production data from Kinvarra Bay, and results from previous studies was then used to put in perspective the findings.

6) Comparing the water, salt, nutrient mass balance for Kinvarra Bay and Killary Harbour to illustrate the difference between bays receiving dominant river inputs and bay receiving dominant SGD inputs, in light of the findings from point 1 to 5.

This strategy identified the following differences between the water and nutrient balance of a bay receiving large SGD inputs (here Kinvarra Bay) compared to a bay receiving large river discharge (Killary Harbour):

-Kinvarra Bay during spring tide survey was always a sink of DIN (larger during periods of high discharge), and either a source (during low fresh discharge) or a sink of DIP (during high fresh SGD discharge). Killary Harbour on the other hand is either a source or sink of DIN/DIP depending on the magnitude of deep sources and surface sink of these nutrient, which can vary as a function of discharge, tidal current (for deep nutrient fluxes amplified by sediment resuspension) and seasons (for surface nutrient losses).

- In Kinvarra Bay, the large N inputs from SGD led to maximum DIN inputs when the peak SGD inputs occurred during neap tides, when residence times in the bay were maximum. The bay thus had larger average dissolved N concentrations compared to Killary Harbour, and potentially greater transfer of DIN to organic N.

-An increase of ^{223}Ra and ^{224}Ra activities in Kinvarra Bay was observed during spring tides with low groundwater level (<6m in a reference borehole connected to the conduit feeding Kinvarra springs). This increase was attributed to saline SGD fluxes. These fluxes may provide added nutrients for the local primary production (such as phosphorus, a limiting nutrient) during periods of spring tides occurring during low groundwater level periods. Nutrient mass balances in Kinvarra Bay during these periods had a net gain of SRP and a net loss outside of these periods.

-Conversely, this work demonstrates that the nutrient level in Killary Harbour is strongly driven by changes of river discharge, vertical mixing and fluxes from bottom sediments.

Fluxes from bottom sediment were identified though an increase of Ra, and in some case turbidity in deep waters in the fjord and are most likely due to sediment resuspension during periods of peak tidal current, followed by deposition during periods of lower tidal currents. Vertical mixing is also strongly driven by the tidal variability creating cyclic solute exchanges. The increase of vertical mixing following an increase of discharge from land can amplify the changes of DIN/SRP ratios in the bay.

-The lower trophic model in this work and observations of Chl-a in the bay indicated that nitrogen inputs from SGD significantly amplify the local primary production in Kinvarra Bay by ≈67% and may directly benefit the local mussel production by between 864 K euros and 121 K euros.

- Nutrient balance in bay with and without major fresh SGD inputs during high and low discharge periods are compared in chapter 7.

Moreover, the following method improvements were developed and may be applied to characterise other sites. For example, this work:

-Reviewed the assumptions of tracer-based estimates of SGD fluxes (Chapter 3). This showed that SGD discharge estimations using non-conservative tracers can underestimate SGD during periods of high discharge, particularly where SGD fluxes occur in shallow areas of a bay. This section suggests to correct for the spatial variability of water ages either (a) by using Ra isotopes, as tested here, or by (b) by coupling tracers measurements with hydrodynamic models or advective-dispersive model (not tested here but likely to be more robust).

-Carried out a systematic analysis of Ra end members in a bay connected to a karst, Kinvarra Bay (Chapter 4), to characterise the effect of saline SGD on karst systems during spring tides, and explain an increase of ^{223}Ra ^{224}Ra activity observed in the bay during droughts. This analysis highlighted that saline intrusion could occur both within superficial sediments and the karst aquifer when groundwater level is low during periods of seasonally high sea level (here spring tides), leading to additional solutes fluxes to coastal areas during these periods. Therefore, the increase of Ra in the water column during such periods can originate from a mix of several end members. This can widen the range of

discharge explaining a given Ra increase and provide added phosphorus or other limiting nutrients to coastal bays following periods of greater saline intrusion.

-Studied the spatiotemporal variability of Ra isotopes, nutrients and salinity in a variably stratified fjord (Killary Harbour, Chapter 5). The section reviewed the condition when the Ra age method can be applied in estuaries. It also confirmed previous findings that the Ra ratio difference between surface and deep waters increase with stratification.

-Adapted the lower trophic model of Cranford et al. (2007) for an SGD dominated site and analysed previous EPA datasets in Kinvarra Bay using the LOICZ approach to characterise the variability of shallow sites receiving large fresh SGD fluxes (Chapter 6). The LOICZ showed a net gain of SRP in the bay during spring tides surveys when groundwater level was below 6m and a net loss of SRP when groundwater level was above 6m at a reference well recording the long-term variability of groundwater head close to the main conduit feeding Kinvarra springs. The Cranford et al. (2007) model adapted in this work allowed to test the effect of different environmental changes on the bay nutrient level and Chl-a concentration. Furthermore, these model outputs, along with past mussel production data in the bay, allowed to give a first assessment of the potential effect of SGD on the bay mussel production, and illustrated how environmental changes may affect it in the future.

2 Literature review: the role of Submarine Groundwater Discharge (SGD) in coastal nutrient cycling.

2.1 Submarine groundwater discharge: Definition

Water interactions between land and sea are not limited to inputs from surface waters, but also occur through water exchanges between coastal aquifers and the ocean. Water fluxes between coastal aquifers and the ocean have two origins: (1) groundwater initially coming from inland recharge and (2) recirculation of seawater within coastal and marine aquifers. Groundwater flows continuously towards the sea through porous rocks and sediments because of the inland recharge creating a hydraulic gradient in coastal aquifers. On the other hand, seawater continuously recirculates through coastal and marine aquifers by the effect of tide, wave setup and sea level changes modifying the groundwater gradient, and water convection due to differences of temperature and density (Rocha, 2000, 1998; Taniguchi et al., 2002). This recirculated flux interacts and mixes with water coming from shallow and deep aquifers, before flowing back to the sea. Flows of seawater and freshwater to the sea are grouped under the term of Submarine Groundwater Discharge (SGD), defined as any flow of water across the seafloor, regardless of the fluid composition or driving force (Burnett et al., 2003). To distinguish it with porewater exchanges due to shear flow, Moore (2010) added a "scale of meter to kilometres" to the definition. This was justified as the conventional techniques used to assess SGD "do not quantify shear flow because seepage meters block waves and currents, concentrations of SGD tracers released by shear flow are expected to be low, and current SGD models do not consider this process" (Moore, 2010).

2.2 Methods to estimate SGD

Seven types of methods have been applied most often to detect or assess the magnitude of SGD flows in coastal areas (see reviews by Burnett et al., 2006; Moore, 2010): thermal images; seepage meters; electromagnetic techniques; water budgets; hydrograph separation techniques; groundwater flow modelling; and tracer techniques.

A short review of these methods and their conditions of application follows, and afterwards a review of their use in SGD related studies in Ireland.

Firstly, seepage meters (Lee, 1977) can measure directly the discharge occurring from permeable sediments. They are composed of a benthic chamber inserted in sediments, connected to sampling bags. The change of volume of the sampling bag due to SGD is recorded either manually or automatically, if coupled with an automatic measurement device (e.g. Paulsen et al., 2001; Sholkovitz et al., 2003; Taniguchi and Fukuo, 1993). Seepage meters quantify both the fresh and saline SGD on specific locations but work best in unconsolidated sediments. When combined with measurements of hydraulic gradient in piezometers, they can be used to assess the large scale hydraulic conductivity of aquifers (Barwell and Lee, 1981; Taniguchi, 1995). As they modify the natural water currents around them, they cannot however, appropriately quantify water fluxes occurring at scales smaller than the size of the seepage meter, such as shear flow.

Secondly, SGD waters normally have different temperature than ocean waters. Temperature anomalies in coastal areas can be thus used to detect potential areas of SGD discharge, for example using satellite images of seawater temperature (e.g. Roxburgh, 1985; Wilson and Rocha, 2012).

Thirdly, electromagnetic techniques measure changes of sediment resistivity, which vary with porosity and fluid conductivity in porous sediments, to detect changes of porewater composition associated with SGD fluxes (e.g. Hoefel and Evans, 2001; Paepen et al., 2020; Stieglitz et al., 2008). Here too, however, electromagnetic techniques are most used along soft sediment coastlines, as they require a good contact between the measurement electrodes and the surrounding medium, and heterogeneous porosities may also lead to changes of resistivities independent of SGD fluxes.

Fourthly, water balances in a catchment may be an appropriate tool to assess fresh SGD fluxes, once the different water sources and sinks in the catchment are characterised (e.g. Allen, 1976; Muir, 1968; Oberdorfer, 1996; Pluhowski and Kantrowitz, 1964; Sekulic and Vertacnik, 1996; Schuler et al., 2018). However, the uncertainty of the variables required to build water mass balances may be larger than the SGD flow that is to be determined (Burnett et al., 2006), in particular where SGD is a minor component of the water balance. Water balances are thus appropriate as a first approach for assessing expected changes

in simple groundwater basins (Oberdorfer, 1996) or in sites where fresh SGD fluxes are the main pathway for freshwaters to the seas (Schuler et al., 2018).

Fifthly, hydrograph separation techniques analyse river flow patterns to determine groundwater fluxes to rivers and to assess fresh SGD fluxes. They have been used historically to assess fresh SGD to large areas, assuming similar fresh groundwater flows per area inland and at sea (e.g. Boldovski, 1996; Tanaka and Ono, 1998; Williams and PinderIII, 1990; Zektser and Dzhamalov, 1981; Zektzer et al., 1973). This technique does not include groundwater discharge downstream of river gauging stations (Buddemeier, 1996), ignoring thus the spatial variability of permeabilities and recharge usually present when getting from lowland floodplains to coastal areas. The uncertainty of hydrograph separation techniques for SGD estimation may be comparable to the magnitude of discharge being estimated (Burnett et al., 2006).

Sixthly, groundwater flows to coastal areas have also been assessed using a range of hydrogeologic models. The simplest version of these approaches use the Darcy's law (Darcy, 1856) to assess potential fresh SGD fluxes from the hydraulic gradient measured from piezometers or mini-piezometers close to the shore (e.g. Barwell and Lee, 1981; Freeze and Cherry, 1979; Taniguchi, 1995). Seepage in coastal settings can also be modelled with semi empiric equations accounting in different ways for the shape of the zone of SGD discharge (e.g. Bokuniewicz, 1992; Fukuo and Kaihotsu, 1988; McBride and Pfannkuch, 1975). These methods supply simple first-order estimates for SGD flow, but generally require an assessment of hydraulic conductivity or other aquifer properties often spatially variable. To account for the spatial variability of groundwater properties, numerical models (e.g. finite element models such as MODFLOW, McDonald and Harbaugh (1984)) are also frequently used to investigate catchment hydrology and assess freshwater flow. However, it is often difficult to have sufficient representative aquifer values such as hydraulic conductivity and porosity (Burnett et al., 2006), particularly in coastal areas.

In karst aquifers, Kresic and Panday, (2021) distinguish four types of models: (1) time series models, (2) numerical models using the equivalent porous medium approach (EPM), (3) hydraulic models of pipe or reservoir network and (4) coupled continuum conduit flow models (CCFF). Time series model use statistical and probabilistic methods

to model the changes observed during a time period on one or several selected locations. They usually require long timeseries of data and to distinguish between multiple input drivers (current recharge, operation of wells) but cannot predict the effect of changes on the catchment (new pumping well, dams). EPM models approximate the karst as an equivalent porous media. Examples include MODLFOW, FEFLOW. They can be valuable as a first approach at large scale but cannot simulate flow in conduits and exchange of water between the conduits and the surrounding rock matrix. As a result, they are generally not appropriate to mimic the dynamic of flow and solute propagation in karsts. Hydraulic model of pipe or reservoir models consider mainly the preferential flow pathways to simulate karsts network, and either do not consider the exchange with the rock matrix or consider it with a lumped parameter. As a result, these cannot model the future effect of common groundwater management or future engineering interventions in karsts. Examples include the Stormwater Water Management Model (SWMM), developed by the US EPA. The CCFF models couple the Darcian equivalent continuous flow model with a network of conduit to consider both the matrix of the aquifer, conduit flow and their interactions. Example of these models include modflow USG, modflow CFP (Kresic and Panday, 2021).

In coastal environments, one of the challenges met by numerical models is the effect of density on the SGD flow (Smith and Zawadzki, 2003). Model such as MODFLOW (McDonald and Harbaugh, 1984) often use single density of fluid flow and thus can only assess fresh SGD and cannot account for the effect of density on the location of the SGD flow (Smith and Zawadzki, 2003). To account for both saline and fresh SGD, dual density models, such as FEFLOW (Diersch, 1992) or SEAWAT (Guo and Bennett, 1998; Langevin, 2003), have been developed and applied to model SGD flows (e.g. Langevin, 2003; Smith and Zawadzki, 2003). They allowed to assess fresh SGD, investigate the effect of variable physical drivers on the discharge of SGD of marine origins or to assess the locations on the ocean floor where most continental-derived SGD was likely to seep out (e.g. Robinson et al., 2006; Robinson, 1998; Smith, 2004; Wilson, 2005;Thompson et al., 2007). It was also noted that models assuming steady state (thus ignoring tidal fluctuations) did not reproduce the magnitude of total SGD suggested by other method, highlighting the need for transient models (e.g. Smith and Zawadzki, 2003).

Finally, tracer techniques use the measurement of elements which concentration change as a result of SGD flows relative to seawater (e.g. for total SGD: radon, radium, stable isotopes, methane or silicon) to detect SGD locations and quantify SGD fluxes (Burnett et al., 2006). The quantification of SGD fluxes with the tracer methods requires to evaluate the other sources of the tracer and choose an "end member" concentration representative of SGD discharge.

In this thesis, three tracers of SGD were measured: ^{222}Rn ^{224}Ra and ^{223}Ra. They are naturally produced in sediments as a result of the uranium-lead decay chain for ^{223}Ra and ^{222}Rn, and the thorium-lead decay chain for ^{224}Ra (IAEA, 2014). They tend to be enriched in groundwater and porewater relative to seawater, which make them good indicators of SGD (e.g. Burnett et al., 2008, 2001; Burnett and Dulaiova, 2003; Moore and Arnold, 1996; Rama and Moore, 1996).

Radon, in gaseous form at ambient temperature, can be extracted from water samples by degassing and measured by alpha spectrometry (RAD7, AlphaGard). To measure single water samples, the detector (in this study a RAD7) is connected to the water sample with a closed loop of air-tight tubes continuously circulating a flow of air through the sample to extract the radon gas. The detector's pump circulates air through a porous stone submerged in the sample and in line with the closed loop of tubes (e.g. RADH2O module Durridge, 2015). This creates agitation in the sample which extract the radon gas. The air leaving the sample is then dried by flowing through a cylinder full of desiccant (e.g. anhydrous calcium sulfate) placed between the sample and the detector. This air reaches the measurement chamber of the detector, before flowing back to the sample and extracting additional radon. For continuous measurements of radon, for example in coastal waters containing low radon activities, the detector is coupled with a module extracting the gas from a pumped water flow, by a spray nozzle such as in the RADAQUA module (Burnett et al., 2001a; Dulaiova et al., 2005) or using a gas exchange membrane, such as the Liquicell module (Schmidt et al., 2008). To increase detection limits further, three or more radon detectors can be coupled together in parallel sets of tubing (e.g. Dulaiova et al., 2005).

^{224}Ra and ^{223}Ra are generally measured in SGD related studies using a Radium Delayed Coincidence Counter (RaDeCC). To make the low radium activities in seawater detectable,

samples are preconcentrated by pumping at low flow rate (less than 1 L min^{-1}) large known volumes of sampled water through acrylic fibres coated with Mn oxides, which have the properties to adsorb on their surface radium isotopes (Moore, 1976; Moore et al., 1985). Alternatively, where only the $^{224}Ra/^{223}Ra$ ratio is of interest, the fibres can be let for several tidal cycles attached to moored buoys on selected location in the bays under study to absorb radium (e.g. such as in Rocha et al., 2015). Then, the sample is rinsed with Ra-free waters to remove salts and dried until reaching a water- fibre weight ratio of 0.4-1.1 (as recommended by Sun and Torgersen, 1998). Finally, the fibres containing the Ra from the sample are connected to a closed loop to the RaDeCC detector, filled with helium and the ^{223}Ra and ^{224}Ra are measured as described in Moore (2008), following the calibration procedure of Moore and Cai (2013).

In Ireland, remote sensing using satellite thermal images (sea surface temperatures) allowed to identify 35 potential SGD locations along the Irish coastline (Wilson and Rocha, 2012). 52.1% of Irish coastline is composed of rocky shores (cliffs, rock, stones), while 31.7% are sandy sediment and 10.1% muddy sediments (Neilson and Costello, 1999). As the majority of Irish coastlines is composed of rocky shores, more studies to date have been carried out in these environments, where seepage meters and electromagnetic techniques involving the measurement of conductivity in unconsolidated sediment are rarely useable. Tracer-based estimates of total SGD rates have been build using ^{222}Rn, ^{224}Ra, ^{223}Ra and salinity (e.g. Rocha et al., 2015; Schubert et al., 2015) in a selected site, Kinvarra Bay. Conduit models have also been applied to quantify fresh SGD for the same sites (Cave and Henry, 2011; Morrissey et al., 2020), but have not yet been compared with radon or radium-based SGD estimates. The small number of locations investigated for SGD in Ireland does not allow to estimate the overall effect of SGD flows on Irish coastlines but as shown in the next part, recent global studies suggest that it is likely to represent an important nutrient flux compared to river flow.

2.3 Role of SGD in the water cycle and nutrient cycling in the ocean

A large scale study in the upper Atlantic Ocean using radium isotopes estimated that SGD represents a water discharge of 2–4 $\times 10^{13}$ m^3 yr^{-1}, thus between 80 to 160% of the amount of freshwater entering the upper Atlantic Ocean from rivers (Moore et al., 2008). Other studies suggest that the global SGD discharge is (12±3) $\times 10^{13}$ m^3 yr^{-1}, which is 3-4 times higher than river discharge to the Atlantic and Indo-Pacific oceans (Kwon et al. 2014). These findings imply that SGD is a major pathway for transport and reactivity of solutes between land and sea, and that in light of this information, the global cycles of the major elements need reassessment.

The majority of SGD fluxes occurring globally is saline SGD, with fresh SGD representing around 0.2-1.4% (Luijendijk et al., 2019; Zhou et al., 2019) to 6% (Zektser and Loaiciga, 1993; Zektzer et al., 1973) of the total river fluxes. Despite the small volumes of fresh SGD globally compared to saline SGD, solute inputs from fresh SGD can represent by themselves potentially 50 percent of the total salt loadings by rivers (Zektser and Loaiciga, 1993). Nutrient fluxes from SGD (fresh + saline) to the global ocean were estimated from radium isotopes to represent discharges of dissolved inorganic nitrogen, dissolved inorganic phosphorus and dissolved silica of approximately 1.4 ; 1.6; and 0.7 times the river discharge to the global oceans (Cho et al., 2018). SGD was also shown to represent comparable fluxes to river flow for nitrogen, phosphorus and silica in the Mediterranean sea (Rodellas et al., 2015b). While saline SGD fluxes are likely to be important globally, large fresh SGD fluxes are probably more specific to certain locations of the world: a recent global study estimated that the flow of fresh SGD represents more than 25 percent of river flow for 26% of the world's estuaries, 17% of the salt marshes and 14% of the coral reefs (Luijendijk et al., 2020). Thus, focusing on sites with strong SGD inputs may be an appropriate first step to better assess the effect of SGD on the ocean.

To sum up, understanding the ecological effect of SGD for coastal areas is important: (1) in most of the open ocean and coastal areas because of solutes provided by saline SGD and (2) close to sections of the world's coastlines where large fresh SGD fluxes are present due to favourable hydrogeological conditions.

The next section will review the various aspects necessary to understand the effect of SGD fluxes on nutrient balance in coastal areas and aquaculture. This will first introduce the drivers of the magnitude and composition of SGD fluxes coming to coastal areas, then review the current knowledge of the spatial and temporal variability of SGD, and the variable residence time of solutes coming from SGD in coastal areas. The last part of section 2.4 will discuss the effect of SGD nutrient fluxes on the nutrient balance and primary production of coastal ecosystems, before introducing the key research questions that will be answered in chapters 3 to 6 of this work.

2.4 Requirements to understand the ecological effects of SGD into coastal systems

2.4.1 Magnitude and composition of SGD fluxes

2.4.1.1 The subterranean estuary

Two zones of distinct salinity are generally present in coastal aquifers. In the upper section of coastal aquifers, fresh groundwater flows towards the coast as a result of inland recharge. In the lower section of the aquifer, saline waters infiltrate from the sea and tend to remain under the fresh groundwater as a result of their larger density (Figure 1). At the limit between these two zones, a saline/fresh interface is present, where mixing occurs (Cooper, 1965). The brackish waters created by this mixing tend to flow towards the coast as brackish SGD, as a result of the changes of the hydraulic gradient during the year and of density difference between the fresh and saline waters. The saline waters leaving the aquifer through saline groundwater flow are replaced by new saline waters coming from the coast. This promotes the recirculation of seawater under the saline-fresh interface through a convection cell (Figure 1) (Cooper, 1965). Consequently, a saline circulation cell is present under the freshwater plume, with a direction reversed at depth compared to groundwater flow, similarly to what may happen in an estuary (Figure 1). Because of this similarity with estuaries, Moore (1999) introduced the term of 'subterranean estuary' to describe the mixing zone between freshwater and seawater in coastal aquifers.

In a surface estuary, mixing between fresh and saline waters is promoted by tides and the flow difference between surface and deep waters (e.g. Geyer and MacCready, 2014;

Geyer and Ralston, 2011). Conversely, in a subterranean estuary, mixing is amplified by the changes of tides, and recharge/loss of groundwater creating movements of the saline fresh interface. During these movements of the interface, the pore space network forces water to follow a non-linear trajectory within the aquifer, promoting dispersion. This added dispersion in the aquifer promotes the mixing between saline and freshwater more considerably than what could be expected from molecular diffusion or from the spatial difference of flow rate alone (Cooper, 1965). This added mixing amplifies the thickness of the saline/fresh transition layer in the aquifer. As a result, homogeneous aquifers are likely to have a more abrupt change of salinity at the interface between the fresh and saline plume in the subterranean estuary than heterogeneous aquifers such as layered aquifer of alternating sand and clay, aquifers of fractured bedrock or karst (Cooper, 1965).

The position of the saline-fresh interface may vary as a function of changes of hydraulic gradient, which affect the magnitude of SGD fluxes. For example, during groundwater recharge, the position of the saline-fresh interface can move towards the sea, which can drive large fluxes of recirculated saline waters to the sea (Kohout, 1965). Other potential causes for modifications of the hydraulic gradient in coastal aquifers and porewater include tide, waves, or marine currents, for example. Changes of the sea level (e.g. due to tide) create fluctuations of groundwater level in coastal aquifers (e.g. Ferris, 1952). Local increase of permeability and porosity due to bioturbation, gas bubble upwelling or compaction can also promote fluid circulation, affecting the SGD fluxes (Santos et al., 2012) and or the hydraulic head in sediment.

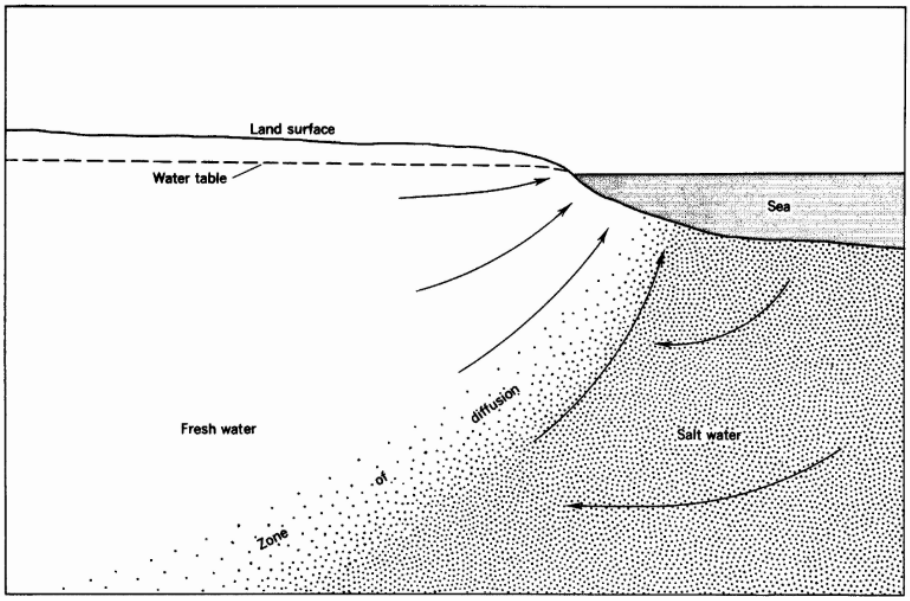

Figure 1: Circulation of saline water from the sea to the zone of diffusion and back to the sea (Cooper, 1965). The position of the saline-fresh interface tends to move seawards and landwards as a function of groundwater recharge and sea-level change, which can drive additional fluxes of recirculated seawater to the coast during recharge events or during periods of temporarily decreasing sea level (Reproduced from Kohout, 1965, work in the public domain).

2.4.1.2 The role of the subterranean estuary in nutrient cycling

The concentrations of dissolved constituents in porewater/groundwater can change greatly in the mixing zone of the subterranean estuary (Beck et al., 2007; Slomp and Van Cappellen, 2004; Spiteri et al., 2008). For example, the mixing between seawater and freshwater can lead to a decrease of about 50% of NO_3 and PO_4 along the pathway from fresh groundwater to sea (Beck et al., 2007). This section reviews first the key parameters affecting N and P in fresh groundwater, before describing the effect on N and P cycles of the mixing with seawater occurring in the subterranean estuary.

2.4.1.2.1 N and P dynamics in freshwater aquifers

The flux of N and P from coastal aquifers and sediments to coastal areas are generally controlled by: (1) water flow rates and water pathways within the aquifer (2) the form and rate of inputs of the N and P from anthropogenic and natural sources and (3) redox conditions in the aquifer (Slomp and Van Cappellen, 2004).

Increasing supply rates of N and P to coastal aquifers may occur as a result of (a) nearshore urban development and additions of N and P through agricultural activities (Valiela et al., 1990) (b) saltwater intrusions due to groundwater mining and sea level rise

(Krest et al., 2000; Moore, 1999). Salinity intrusions in previously freshwater saturated aquifers lead to the replacement of Ca^{2+} by Na^{+} and Mg^{2+} ions on sorption sites, which can lead to aquifers going from undersaturation to saturation relative to calcite. Precipitation dissolution reactions may occur (Slomp and Van Cappellen, 2004).

In fresh groundwater, N is generally under the form of NO_3, since NH_4 is diluted and nitrified in the oxic zone during infiltration (Jordan et al., 1997; Wilhelm et al., 1994). In some cases, there can be a complete turnover of nitrogen during the pathway through aquifers, leading to observable changes of N and O stables isotopes in NO_3 compared to the original sources (Lamontagne et al., 2018). The decomposition of NO_3 may occur under anoxic condition through denitrification, Mn or Fe oxide reduction, sulfate reduction or metagenesis (Hansen et al., 2001; Jakobsen and Postma, 1999; Korom, 1992; Lovley and Chapelle, 1995). Dissimilatory nitrate reduction to ammonium (DNRA) may also lead to NO_3 losses, but through production of NH_4, keeping N in a biologically available form unlike denitrification which produce gaseous N. Under suboxic to anoxic conditions, the oxidation of NH_4 coupled with NO_2 reduction through Anaerobic Ammonium Oxidation may also occur, provided there is a source of NO_2 (Smith et al., 2015). While initially, infiltrated waters are oxic, oxygen is consumed along the groundwater flow path by the degradation of dissolved organic carbon (DOC). Once few oxygen is available, other electron donors are used for the decomposition of DOC: NO_3, MnO_2, FeOOH then SO_4^{2-} in this order (Korom, 1992). Thus, aquifers with large DOC levels or long water residence time can become anoxic, which leads to the reduction of nitrogen. In many cases, the DOC inputs from surface sources tend to be diluted and consumed in the vadose zones, directly after infiltration, and manure and sewage have usually no effect on the organic matter content of aquifers (Richards and Webster, 1999; Wilhelm et al., 1994). However, during periods when groundwater is close to the surface, or if groundwater recharge occurs without going through a thick vadose zone (e.g.: in Karst when groundwater level are high) the loss of DOC may be limited and lead to larger inputs to the aquifer during recharge events (e.g. Deirmendjian et al., 2018; Mudarra et al., 2014). Increasing DOC may lead to faster consumption of oxygen and more favourable conditions for the consumption of DIN in the aquifer. However, when the ratio DOC to

NO_3 is low Anammox may be favoured and amplify the degradation of dissolved N as NH_4 and NO_2 to N_2 (Smith et al., 2015), with NO_3 as a by-product.

In karst environments, Nitrogen can be subject to distinct reactions in fractures or conduits, where oxygen availability is high, compared to porespace, where longer residence times can favour depleted oxygen (Visser et al., 2021). This can lead to large spatial variability of NO_3, independently from land uses (e.g. Visser et al., 2021). For example, micropores in iron bearing carbonate formations can provide locally suboxic to anoxic conditions (Visser et al., 2021) favourable for NO_3 reduction processes such as denitrification. In this context, N reductions reactions may occur in porespace with restricted oxygen availability and may be coupled at times with N oxidations processes in conduits or fracture richer in oxygen. This may amplify the NO_3 spatial and temporal variability in sections of the karst network not connected to major phreatic conduits, and create locally increase of NH_4 or NO_2, particularly during low recharge periods, when "older" water circulates in the karst network and when porespace is more likely to contribute significantly to the composition of water, for example through the degradation of organic N (dissolved or particulate). This could be also the case for slow moving saline water within deep sections of coastal aquifers.

Dissolved phosphorus, on the other hand, is generally lost in freshwater aquifers under oxic condition directly after infiltration through sorption to Fe oxides or co-precipitation with dissolved Al, Ca or Fe (Robertson, 1995; Welskel and Howes, 1992; Zanini et al., 1998), except when the removal capacity of the soil is overwhelmed due to high P loading, for example from fertilisers (Robertson, 1995; Slomp and Van Cappellen, 2004; Van der Molen et al., 1998). Karst network can have a high retention capacity for phosphorus, which can be adsorbed to sediment and colloids (Jarvie et al., 2014). However, it may be subsequently released and/or progressively transferred downstream during storms events (Jarvie et al., 2014). In Irish karst springs, Dissolved reactive phosphorus (DRP) is the dominant phosphorus component present in water (Kilroy and Coxon, 2005), which seems to be also valid in Kinvarra springs, as the maximum turbidity level we observed in Kinvarra spring was 0.2 NTU in April. We cannot exclude however an influence of particulate P during periods of heave rainfall as particulate P and dissolved unreactive P

can also increase to a greater degree than DRP during such periods in Ireland(Kilroy and Coxon, 2005).

2.4.1.2.2 Effect of mixing with saline waters in the subterranean estuary

Nitrogen and phosphorus are frequently released, stored or transformed within the subterranean estuary.

Reactions involving nitrogen and phosphorus are favoured mainly when recirculated seawater mix with groundwater and a least one of the two water masses is anoxic, below 1 mg L^{-1} of dissolved oxygen (DO) (Slomp and Van Cappellen, 2004) (see Figure 2). These reactions may involve: the storage and release of phosphorus by sorption/desorption or precipitation with calcium or iron (e.g. Ca-P and Fe-P in Figure 2), losses of NO_3 and NO_2 by denitrification, the transformation of NH_4 in NO_3 and then NO_2 by nitrification (Figure 2). As a result of these reactions, N:P ratio of the SGD waters are more likely to be lower if one of the two water masses is anoxic (Case 2, 3 and 4 in Figure 2), than when both fresh and saline SGD are oxic (Case 1 in Figure 2). Indeed, NO_3 can be lost by denitrification, whereas P is stored in the transition zone and may be later released (see Slomp and Van Cappellen, 2004).

When the subterranean estuary position moves inland (saline intrusion), NH_4 and PO_4 may be released in the aquifer (Slomp and Van Cappellen, 2004). In oxic aquifers (Case 1 and 2), PO_4 sorbed to Fe oxides may be displaced by anion in seawaters and the release of N and P from organic matter decomposition may increase. In anoxic groundwater, (Case 3 and 4) NH_4^+ present on sorption sites may be released by replacement by Na^+ and the decomposition of organic matter may be enhanced. Thus, the N:P ratio of SGD may decrease following salination and decrease in anoxic aquifers down to below Redfield values (Slomp and Van Cappellen, 2004), as a result of the P release from the previous position of the subterranean estuary.

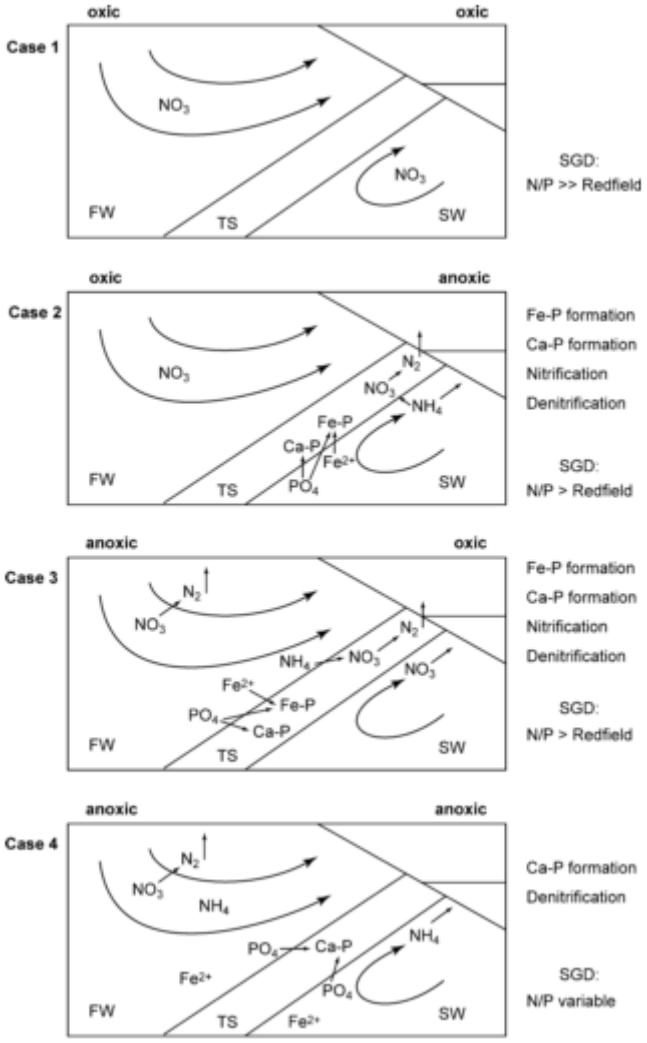

Figure 2: The redox dependence of biochemical processes leading to transformation, removal or release of NH_4, NO_3 and PO_4, when groundwater (FW) meets seawater (SW) in the mixing, transition zone (TS). Case 1: oxic groundwater meets oxic seawater, Case 2: oxic groundwater meets anoxic seawater, Case 3: anoxic groundwater meets oxic seawater, Case 4: anoxic groundwater meets anoxic seawater. (Reproduced from: from Slomp and Van Cappellen, 2004 with permisssion from Journal of Hydrology).

The mixing between waters of different chemical composition can also favour dissolution/precipitations reactions in the aquifer. For example, in limestone, the mixing of waters with different saturation levels of CO_2 can lead to localised dissolution, an essential mechanism for cave formation (Bogli, 1964) and pore space formation. This phenomenon can also be present when seawater and freshwater mix with freshwater (Plummer, 1975; Slomp and Van Cappellen, 2004) and can promote for example the later replacement of calcite by dolomite (Badiozamani, 1973; Luczaj, 2006). According to Slomp and Van Cappellen (2004) two main mechanisms may lead to dissolution precipitation of

carbonates during salination: ion exchanges and sulphates inputs from seawater. First, the replacement on sorption sites of Ca^{2+} by Na^{+} and Mg^{2+}, can lead to increase of Ca^{2+} concentrations during salinations. Secondly, the inputs of sulphates from seawater (seawater [SO_4] = 29.3 mM, groundwater [SO_4] generally < 0.5mM Appelo and Postma, 1993) may promote the reduction of Fe oxides and favour sulphate reduction instead of methanogenesis in anoxic waters, leading to an increase of alkalinity and Ca^{2+} concentration (Slomp and Van Cappellen, 2004). Both alkalinity increase and Ca^{2+} input can enhance carbonate precipitation at the salinity front (Appelo and Postma, 1993).

Another critical variable for nutrient reactions is the oxygen and organic carbon availability in the aquifer, as the supply of organic carbon is a primary energy source for nutrient reactions in aquifers (Korom, 1992). Surface infiltration and recirculated seawater may deliver oxygen and particulate organic carbon (POC) to porewaters (see Figure 3). This input of POC can lead to a local reduction of dissolved oxygen levels. For example, within a well-oxygenated beach aquifer, the local respiration was sufficiently high to lower the porewater O_2 concentration near the sediment surface during active seepage, thus favouring the occurrence of suboxic biogeochemical processes near the sediment surface (Figure 3) (Ibánhez and Rocha, 2016). The coexistence of carbon, oxygen and nutrient supplies can create a biogeochemical hotspot in permeable material such as sands and drive the mineralisation of organic material and production of additional Dissolved N and P (Boudreau et al. 2001; Rocha, 2008; Santos et al. 2014; Billerbeck et al. 2006; Charbonnier et al. 2013; Erler et al. 2014; Santos et al. 2009).

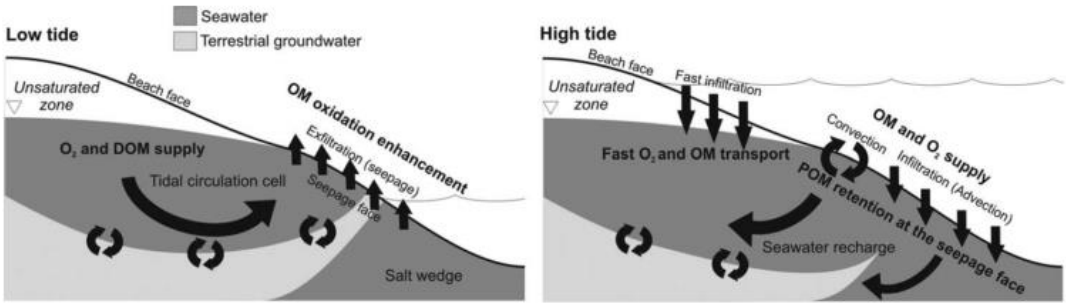

Figure 3: The main transport processes in a beach aquifer and their influence on O_2 and OM supply and reactivity in the seepage face (Reproduced from: Ibánhez and Rocha, 2016, with permission from Limnology and Oceanography).

In karst aquifers, the input of anthropogenic labile organic matter can increase bacterial activities oxidising manganese, which is likely to influence nutrient and trace element's biogeochemical cycles (Carmichael et al., 2015). Indeed, sorption sites of oxidised manganese and other oxides can sorb/desorb both Ra, PO_4 and NH_4. A release of phosphorus can occur by the dissolution of iron-bound phosphorus from sediments (Loveless and Oldham, 2010), and in limestone under the effect of a saline intrusion (Price et al., 2010). Cave surface can accumulate Fe and Mn oxides (e.g. Frierdich et al., 2011) and thus may act as preferential sorption sites for nutrients.

Finally, the nitrate reactions in the subterranean estuary also vary with the level of nutrient contamination of an aquifer (see Figure 4). When nutrient levels in groundwater are high, the subterranean estuary can function as a nutrient sink (Loveless and Oldham, 2010), while at low nutrient levels it can act as a source (Santos et al., 2009d). For example, remineralisation of organic N can provide added dissolved oxidised N in subterranean estuaries (e.g. Isaac R. Santos et al., 2009; Charbonnier et al., 2013). Since nutrient levels in groundwater can be variable, especially in karst or other aquifers well connected to surface waters, the subterranean estuary may act as an alternating sink/source of nutrients. (Erler et al., 2014).

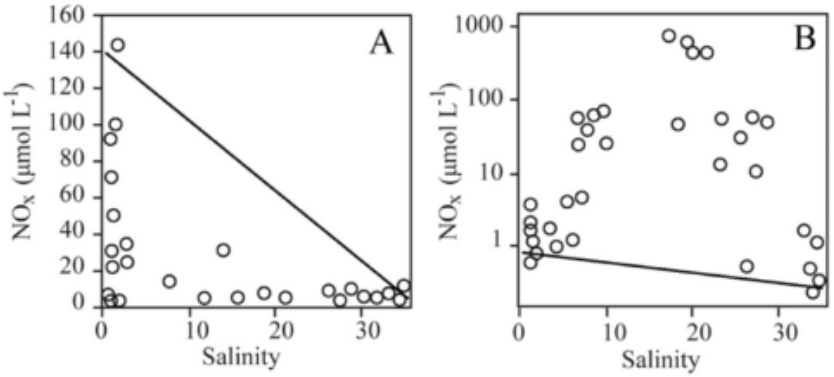

Figure 4: Examples of nitrate versus salinity scatter plots in (A) a nutrient-contaminated (Loveless and Oldham, 2010) and (B) an uncontaminated subterranean estuary (Santos et al., 2009). The solid lines represent the theoretical conservative mixing line. In the contaminated aquifer (A), nitrate was attenuated in the subterranean estuary. In the uncontaminated aquifer (B), nitrate was produced within the subterranean estuary due to seawater inputs at high tide combined with mineralisation within the subterranean estuary. Notice the log scale on the coordinate axis in B. (Reproduced from: Robinson et al., 2017 with permission from Advances in Water Resources).

Therefore, the mixing between groundwater and recirculated seawater in the subterranean estuary can cause multiple reactions, leading to the temporary storage, production, or release of nutrients to the water column. These reactions in the

subterranean estuary can modify the nutrient concentrations in SGD discharge compared to what would be expected from simple mixing between inland groundwater and sea water. Consequently, simultaneous sampling of both SGD discharge points and coastal groundwaters may allow to better characterise changes occurring in specific subterranean estuaries. Data from both boreholes and coastal springs located along the same preferential karst conduit are thus included in this study, and the results are discussed in chapter 4 and 6.

2.4.2 Spatial and temporal variability of SGD fluxes

2.4.2.1 SGD occurs at multiple scales with distinct compositions

In most natural environments, zones of lower permeability may separate different layers of aquifers. As a result, zones of mixing between saline and fresh groundwater are present in different locations along the coastal and continental slope **(**Figure 5) (Bratton, 2010). Consequently, the attribution of volumes and composition to the total SGD depends largely on the scale considered, as the mixing between freshwater and seawater within aquifers occurs at a wide range of scales and through aquifers with distinct porosity networks and geochemical characteristics. Depending on the scale considered, the SGD fluxes can have distinct age, history and thus, chemistry.

For this reason, Bratton (2010) suggests the use of a three scale classification for SGD processes: nearshore, embayment and shelf scale. The two first scales are of interest in this work.

At the nearshore scale (Figure 5a), tides and waves drive the infiltration of seawater through beach sands at high tide, followed by the seepage of pore water out of the coastline at low tide. This process, called tidal pumping, creates a zone of recirculation of seawater in homogeneous aquifers (such as beach aquifers), referred to as the upper saline plume (Li et al., 2000; Robinson et al., 2007). This plume most frequently forms on coastlines with a small slope and large tidal fluctuations, where the intertidal area covers a large part of the coastal floor (Robinson et al., 2007b), and is composed of permeable sediments. When the groundwater level is low, more seawater can infiltrate in the permeable sections of the coastline (ex.: sand or rock with a high density of fractures), allowing larger saline SGD fluxes. On the top and under this plume, direct seepage of

continental groundwater can occur, if the head difference between sea level and inland groundwater level is high enough (Figure 5a). Finally, as shown previously in section 2.4.1.1, the freshwater flow can drive additional recirculation of sea water under the freshwater plume, creating a lower saline plume (lower left in Figure 5a). This lower saline plume is present in both homogenous aquifers such as sandy beach slopes (Robinson et al., 2007b) and heterogeneous aquifer such as karst (Cooper, 1965), as soon as a hydraulic connection is present between the sea and the deep aquifer.

At the embayment scale, fresh groundwater inputs can also occur, along with slow recirculation of sea water by density difference, when a confined aquifer comes in contact with the overlaying seawater (see Figure 5b). When this occurs, a zone of mixing will develop between the fresh and saline waters and favour recirculated SGD (or Saline SGD).

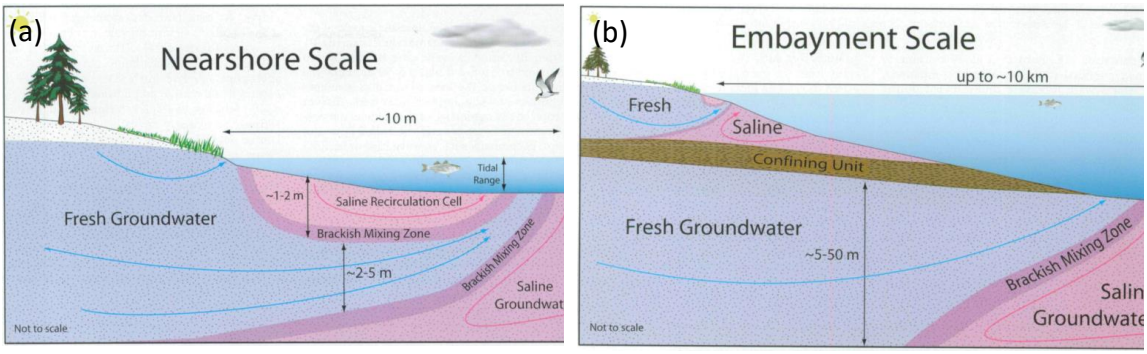

Figure 5: The nearshore and embayment scales of SGD in homogenous aquifer. (Reproduced from: Bratton, 2010, work in the public domain). The nearshore scale figure (on the left) describes the surface fresh SGD, the upper saline plume (saline recirculation cell) and the lower saline plume (lower brackish mixing zone). The embayment scale (right) includes the previous element, with mixing between groundwater and recirculated seawater within confined aquifers.

Aquifers with heterogeneous pore space promote a larger dispersion and a greater mixing zone between fresh and saline water than homogeneous aquifers such as sands (Cooper, 1965). As a result, Cooper, (1965) postulated that the rates of dispersion will be larger in karst or fractured bedrock than in one of laminated sand. While the intensity of the mixing is likely to be larger where it does occur in karst aquifer, it is also likely to occur dominantly in restricted zones of the aquifer where fractures or conduit allow significant water movements. It is thus not certain whether this localised increased dispersion could systematically lead to an increase of the thickness of the saline/fresh interface at the aquifer scale. In any case, the mixing interface can amplify the saline recirculation in the

aquifer as a result of the movement of the freshwater in the upper part of the aquifer and the density difference between the brackish and fresh waters (Figure 5).

Saline recirculation is possible in the aquifer if pore spaces are present to allow the saline intrusion in the aquifer below sea level (natural permeability is sufficient or preferential flow paths are present). Fleury et al. (2007) define three types of coastal karst aquifers depending on the extent of the connection between the karst network and the sea. Type 1 are poorly developed karst network, similar to fractured aquifers, where most of the flow occurs through diffuse fracture networks. Spring flow in these types of aquifer are relatively weak and vary little during the year, with rarely saline intrusion present. Type 2 are well developed karst aquifers, often on several levels, with conduit often too large compared to the current flow, which favour large saline intrusion in the network. Spring flow in these systems have typically large mean rates with strong seasonal variability. The fraction of salinity in these systems is generally low during high flow but rise with decreasing flow rates. Type 3 are systems with well-developed karstification developed under sea level, but free of saline intrusion due to closed network under sea level, as a result of clogging, impermeable layers of specific geological features. Flow rates in these systems are variable but remain fresh or slightly salty during the year.

In karst aquifers and fractured bedrock, the depth of the deepest cave or developed fracture network often is a function of the lowest historical sea level in this area. Historical sea levels are not homogeneous worldwide but are a function of the cyclic growth and decay of ice sheets. The presence of more massive ice sheets on continental landmass during the last ice age led to historical sea levels 130 m lower in areas far from ice sheets` areas of influence (Fairbanks, 1989; Lambeck and Chappell, 2001), and up to 250 m higher in areas previously covered with ice sheet (Lambeck and Chappell, 2001). Deep karst networks of type 2 and type 3 karst are thus likely to be widely present in locations of the world where ice sheet cover was low during the latest glacial maximum, but less so close to areas that were previously covered with massive ice sheets (>500m depth) and were further under sea level than present days (e.g. see maps of Peltier, 1994). Indeed there is extensive evidence of incursion of seawater within karst aquifers worldwide (Bonacci, 1987; Arfib et al., 2007; Fleury, Bakalowicz and de Marsily, 2007; Menning, Wynn and Garey, 2015). In Ireland, the majority of karst forms developed during the Holocene

(Drew, 1991; Tratman, 1969), but also during previous periods (Drew and Jones, 2000) when sea level was at least 30m lower than present-day (Shennan et al., 2018).

As demonstrated previously in section 2.4.1.2, the effect of reactions in the subterranean estuary on SGD composition is likely to increase with the time water remains in the aquifer. The upper and lower saline plume identified in relatively homogeneous aquifers (Figure 5) have distinct residence times, and thus chemical history. Modelled transit times for the upper saline plume are short (e.g. nine days, Robinson et al. 2007), while simulated water ages in permeable coastal aquifer sands range from 1000 days to thousands of years (Post et al., 2013; C. Robinson et al., 2007a). Due to this longer pathway, the lower saline plume waters are more likely to be influenced by the aquifer biogeochemistry. Groundwater typically becomes more reducing along its flow path as biogeochemical reactions consume dissolved oxygen, in particular, the oxidation of organic matter (Bear et al., 1999). Thus, long transit times often results in low levels of dissolved oxygen in groundwater (Slomp and Van Cappellen, 2004), favouring potentially anoxic reactions (See section 2.4.1.2.2). In karst, estimation of transit times in the aquifer is problematic as these are site-specific. Karst typically present three type of porosity: intergranular, fractures and conduit (Worthington, 1999). Fracture porosity can be lumped with either the matrix or conduit network depending on aperture widths (White, 1988; Worthington et al., 1995). The three porosity types generally keep waters during distinct timescale. For example, transit times for an alpine karst system varied between 2-13 days for conduits and open fractures; 3-5 month in well drained fissures and fractures; to a few years in poorly drained fissures and rock matrix (Lauber and Goldscheider, 2014). Non karst units such as superficial soil may also contribute to the water fluxes in karst, with distinct compositions and timescale of renewal (Hartmann et al., 2021).

As a result of these different groundwater transit times and different biogeochemical histories, multiplying tracer-based estimates of SGD over large regions by end-member concentrations found in fresh groundwater seems likely to give only a first-order estimate of solute fluxes crossing the land-ocean boundary, and is often misguided. As shown in section 2.4.1, sampling directly SGD waters is a better estimate of the actual SGD composition than groundwater samples, but this approach may be limited if other SGD

locations in the system not detected have different compositions as a result of their transit times, the pathway taken in the subterranean estuary, and the fraction of saline SGD in them. The current work will discuss where possible the role of the spatial variability of the composition of SGD fluxes and other fluxes from sediments for the interpretation of the changes observed in both SGD and river dominated systems (e.g. Chapter 3, 4 and 5).

2.4.2.2 SGD rates vary across time scales going from hours to years.

Multiple drivers can modify the magnitude of SGD (see review by Robinson et al. 2017; Santos et al. 2012), frequently leading to changes of flow rates of one order of magnitude over timescales going from hours to years (e.g Charette et al., 2013; Taniguchi et al., 2005).

A series of studies measured the temporal variability of SGD in specific sites (e.g. Charette et al., 2013; Hatta and Zhang, 2013; Hsu et al., 2020; Kohout, 1965; Mallast et al., 2013; Sadat-Noori et al., 2015; Taniguchi et al., 2005). The following observations were made by these works: (1) Periods of groundwater recharge are more favourable for large SGD rates (e.g. Hsu et al., 2020; Kohout, 1965; Mallast et al., 2013; Sadat-Noori et al., 2015; Taniguchi et al., 2005). (2) Maximum SGD rates tend to occur at low tides. For example, Taniguchi et al. (2005) observed after low tide SGD rates two to eight time larger than at high tide (Figure 6). The same study showed peak flows (Figure 6a) when the groundwater level was high or rising (Figure 6b). As originally observed by Kohout (1965), periods of recharge can push the saline-fresh interface towards the sea, creating large fluxes of saline and fresh groundwater (Kohout, 1965).

As a result of this variability the relative flow of SGD compared to river discharge also vary in time. For instance, SGD discharge in a river-dominated Florida estuary represented between 2 to 140% (the average is 43%) of the river discharge, depending on the time of the year (Charette et al., 2013).

Similarly, the fraction of saline and fresh waters present in the total SGD fluxes can vary in time. For example, a study based on ^{222}Rn and radium (Sadat-Noori et al., 2015) showed that in “wet” conditions, deep fresh groundwater discharging into an estuary contributed 65% of the total SGD discharge, while during drier conditions, most of the SGD flow was saline groundwater (80%).

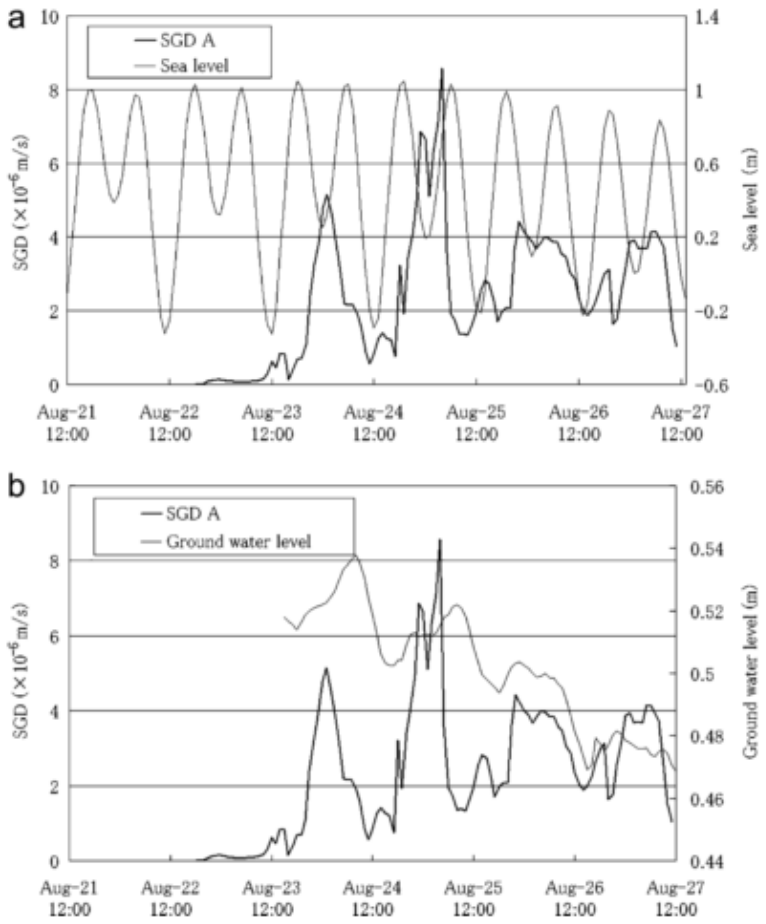

Figure 6: Effect of tide and groundwater level on SGD rates (a) SGD rates measured with seepage meter in Suruga Bay and sea level. (b) SGD measured with seepage meter in Suruga Bay and groundwater level in the nearby aquifer. (reproduced from: Taniguchi et al., 2005, with permission from Ground Water).

Thus, as a result of the multiple drivers of SGD, the same site can either show very low or high SGD rates depending on the time of the year, location and year considered. It is, therefore, crucial to adapt the timing of sampling to the processes which dominate the variability of SGD flow in the site that is studied. In some sites, the SGD variability may be also driven by other drivers than tidal and groundwater level variability (See full list of drivers in Table 1). In such a context, annual averages of SGD based on single surveys (e.g. only summer) or randomly selected surveys during the year are unlikely to be representative of the annual conditions. In theory, incorporating all potential drivers during fields investigations should require continuous measurement of tracers or other indicators of SGD on different locations simultaneously, because different SGD sites may behave in distinct manner.

Table 1: Timescale of sampling to capture the effect of the drivers of variability for SGD flux rates (based on reviews from Robinson et al. 2017; Santos et al. 2012).

Drivers of SGD variability	Usual time scales of effect on SGD rates.	Conditions of most significant variability.	Suggested sampling strategy to account for its effect in integrated annual SGD rates estimates.
Main drivers			
Wave setup	Usual waves: few seconds to the tenth of seconds. Storms: Up to 100 days after.	Storm event/tsunami, especially on exposed coastlines.	SGD measurement after/before a storm event.
Tides	Daily	Changes for High/low tide, and spring/neap tide.	Full tidal cycle samplings, including spring/neap tide.
Groundwater level	Weekly to yearly Karst: Hourly to daily	Seasonal High/low flow condition and after a rainfall event. Especially for good aquifers and groundwater with low residence time.	Seasonal sampling at the High/Low groundwater level condition and continuous sampling through the response signal of a rainfall event.
Density driven recirculation	Days to thousands of years.	Significant change of other drivers, (acting as combination or amplifier of other drivers). E.g period of recharge.	Difficult to estimate without modelling. Continuous measurement of Rn222 or Ra during a period of groundwater recharge, close to a change of bedrock/sediment type?
Others (example)			
Current	Variable	Strong variability of current	Measurements at low/high periods.
Organism	Organism specific	High density of benthic organisms	Sampling at periods of high/low activity of organisms. Summer/winter?
Compaction	Exceptional event	Submarine landslides, earthquakes	Sampling after one of the events cited.

This variability of SGD rates makes the closure of annual budgets of nutrients in coastal areas challenging without continuous measurements. Submersible probes to measure salinity are common but cannot differentiate fresh SGD from surface waters inputs and cannot detect saline SGD fluxes. Total SGD fluxes may be assessed continuously by the measure of tracers specific of SGD such as radon or radium. The method for continuous measurements of radon using a pump, a module for radon extraction and a RAD7 or an

AlphaGard allows continuous measurements (Burnett and Dulaiova, 2003). However, the setting requires continuous pumping at high flow rate (>1L min^{-1}) which is power consuming (Dulai et al., 2016) and the sensitivity of the equipment to humidity require to change drying cylinders relatively frequently. Alternative techniques have been developed to suppress the need for pumping, such as the Water Probe (Durridge inc.), but they do not allow the temporal resolution required to assess the tidal variation of the SGD signature (Dulai et al., 2016). As an attempt to make long term measurements possible, techniques to measure radon using submersible gamma ray spectrometers have been also applied (e.g. Dulai et al., 2016; Povinec et al., 2006; Tsabaris et al., 2012), but were generally limited to measurement periods going from days to week. A recent study succeeded in maintaining continuous measurement on a single location during yearly timescale (Dulai et al., 2016). For radium isotopes, the main measurement technique using a Radium Delayed Coincidence Counter (RaDeCC) is lab-based and sampling require to filtrate large volumes of waters through Mn Fibres on site which limit the length of studies. Radium-228 and Radium-224 (Eleftheriou et al., 2017) can be also made with submersible gamma ray detectors to record the variability of SGD flow. A last option to detect SGD is the measurement of the enrichment of methane close to certain submarine springs using submersible detectors (Dulaiova et al., 2010).

The resource and time requirements to measure continuously SGD discharge tend to limit the studies measuring continuously SGD discharge to seawater to studies length from one to several days at best (e.g. Burnett and Dulaiova, 2003; Hsu et al., 2020; Sadat-Noori et al., 2015; Taniguchi et al., 2005). To date rare studies succeeded in continuous measurement of SGD tracers over several month to years scale (e.g. the SGD sniffer in Dulai et al., 2016), and were limited to single locations.

As continuous measurements of tracers of SGD are generally possible on single locations and short timescales, assessing SGD discharge across the year in between periods or points of measurements require strategies to assess the SGD variability outside of known measure points. Detailing how the survey timing compare to the range of changes of SGD drivers in an average year can be an option to do so (e.g. groundwater level, tide, and other listed in Table 1). This is the approach that was generally used in studies over days timescales, generally with a focus on sea level variability and recharge

(e.g. Burnett and Dulaiova, 2003; Hsu et al., 2020; Sadat-Noori et al., 2015; Taniguchi et al., 2005). Some studies have used the rainfall patterns in the days preceding a survey to assess the potential for SGD discharge due to recharge (e.g. Gregory et al., 2020). Using rainfall to assess recharge indirectly however do not consider the effect of the water storage present in the aquifer before recharge on the SGD flows. In that sense, changes of groundwater level on one or several representative locations (area for preferential groundwater flow feeding the spring under study) may be a more appropriate way to account for the effect of the long-term storage in the aquifer on SGD flow. Another strategy is to use models to assess the potential SGD discharge variability across the year. However these estimates generally can only assess freshwater SGD, and can be generally validated only using inland groundwater levels (e.g. McCormack et al., 2014; Morrissey et al., 2020). Estimates of submarine spring flow are rarely included in the validation or calibration steps of such models because of the difficulty to have such estimates.

Current Irish SGD estimates using geochemical tools (Rocha et al., 2015; Schubert et al., 2015; McCaul et al., 2016) allowed to differentiate the components and spatial variation of SGD for specific seasons or time of the year. The potential temporal variability of SGD beyond specific seasons have been assessed using modelling approaches (Cave and Henry, 2011; McCormack et al., 2014; Morrissey et al., 2020). These three studies showed a significant temporal and interannual variability of the fresh SGD discharge. For example, the daily averaged flow modelled for Kinvarra springs goes from close to zero flow in July 2016 to 30 $m^3 s^{-1}$ in January 2016 (Morrissey et al., 2020), and the mean flow modelled for Kinvarra West for July goes from 4 to 10 $m^3 s^{-1}$ between 2010 and 2013, depending on the year considered (McCormack et al., 2014). However, so far, the outputs of these models have not been compared with tracers-based estimates of total SGD, and the variability of saline vs fresh SGD during the year remains unknown. Tracer-based estimates of total SGD and models are compared for different periods of the year in a selected SGD site in chapter 3 in this work, and the variability of saline vs fresh SGD ratios are investigated in chapter 4.

2.4.3 The variable residence time of nutrient inputs from SGD in a coastal bay

Water inputs into coastal areas, such as SGD or river discharge, are generally creating a gradient of concentrations and non-uniforms reactions across a system. Such sites may not be fully mixed and water inputs may frequently take several days to leave them. For example, early studies for “classical” estuaries showed that nutrient could be stored and react preferentially in their inner parts (e.g. Figure 2 in Edmond et al., 1981). More recent studies showed that peaks of phytoplankton in coastal areas could be related to areas of older waters (Tomasky-Holmes et al., 2013). Thus, the effect of any input of waters on a coastal bay nutrient balance is not only a function of the flow rates of inputs to coastal areas and their compositions, but also depends on how long and where the discharged waters remain preferentially. The next section defines the main indicators used to study the flushing of coastal systems, reviews their methods of estimation and the causes for their variability.

2.4.3.1 Definitions of residence times, water ages and flushing times

According to Monsen et al. (2002), “no single transport time scale is valid for all time periods, locations, and constituents, and no one time scale describes all transport processes”. These authors advise rigorous definitions of the terms used and to make sure the transport timescale concept used are appropriate for the questions to be answered.

Definitions of residence time, flushing time and water ages may be variable between publications from different years or authors. In this work, we will use the definitions of Monsen et al. (2002), who distinguish three transport timescales commonly used to describe the retention of waters or solutes transported in water in a water body: Flushing time, residence time and water ages.

According to Monsen et al. (2002), following Geyer et al., (2000) flushing time is “a bulk or integrative parameter that describes the general exchanges-characteristics of a water body, without identifying the underlying physical processes, the relative importance of those processes, or their spatial distribution”. The flushing time is the most widely used parameter to compare the transport timescale for different periods or systems, due to its simplicity. For a given well-mixed water body, the flushing time (T) can be calculated as:

$$T = \frac{V}{Q} \quad (1.1)$$

Where V is the volume in the water body, and Q is the volumetric flow rate through the water body (Geyer et al., 2000, p 191;Monsen et al., 2002).

The definition of flushing time in Monsen et al. (2002), following Geyer et al., (2000) is distinct from the earlier definition of flushing time used in Officer, (1976) and cited in Luketina, (1998) as "the time needed for the river flow to replace all of the river water in the estuary". As a result of these distinct definitions, the tidal prism methods defined by Luketina, (1998) as methods to calculate "residence time" are cited in Monsen et al. (2002) as methods to calculate "flushing time". We use in this work, the more recent definitions of Monsen et al. (2002) as this definition explicitly allow to account for the effect of other physical drivers than river discharge on flushing (e.g. SGD), and this work also include discussions on the effect of spatial variability.

Where tides are driving most of the variability of the exchange with the outside of the water body, the tidal prism method defines flushing time as (Dyer, 1973):

$$T = \frac{(V_l+P)T}{(1-b)P} \quad (1.2)$$

Where P is the volume between the high and low tide mark, T is the tidal period, V is the volume of the bay at low tide, b is a return flow factor (defined as in Sanford et al., 1992), the fraction of water that left during ebb tide that comes back during the next flood tide. Multiple versions of the tidal prism method have been tested by Luketina, (1998) and will be tested for an estuary receiving large volumes of fresh SGD in Chapter 3.

In systems where significant water inputs from land are present (river flow or net flows from submarine groundwater discharge, equation 1.2) tend to underestimate flushing time and the effect of these inputs on flushing can be accounted for using the following equation (Sanford et al. 1992; Luketina, 1998):

$$T = \frac{V_l+P}{(1-b)\frac{P}{T}+(1+b)\frac{Q}{2}} \quad (1.3)$$

Where Q is the water input to the estuary, and other terms are defined as in equation 1.2.

However, most water bodies are not fully and instantaneously mixed and accounting for spatial variability requires to introduce two other timescales (as defined in the work of Monsen et al., 2002).

Water ages is: 'the time [a water parcel] has spent since entering the estuary through one of the boundaries' (Zimmerman, 1988). Unlike flushing time, it is unique of each water parcel in the water body. Consider for example an input of radioactive elements in the inner boundary of a coastal bay. As the time goes, water parcels originating from the initial inputs are flushed towards the bay mouth and the element decay progressively with time. If no other inputs of the element are present in the system, the quantity present in a given water parcel would be then a function of the time that the water parcel took to go from the source to the measured location, water ages. If the source of radioactive element is continuous, then each location will have water parcels with a distribution of ages, which averaged value can be determined with sampling (for example the Ra age method in section 2.4.3.2).

Residence time is ''the time it takes for any water parcel of the sample to leave the lagoon through its outlet to the sea'' (Dronkers and Zimmerman, 1982; Monsen et al., 2002). It is measured from an arbitrary location of a system (Monsen et al., 2002), generally, but not always, a source of an element of interest, for example an aquaculture activity site providing nutrient to a system. When the reference location is a dominant source of the element of interest, for example a river located on one boundary of the system, then residence time following this definition is equivalent to the transit time of this element in the system, as defined by Sierra et al. (2017) as the: "random variable that describes the ages of the particles at the time they leave the boundaries of a system". In numerical models, residence time are defined practically as the time taken by a particle or element to leave a control region without returning on the next tide (e.g. Monsen et al., 2002).

In systems where relative water ages increase with distance from a source, the residence time can be equivalent to the average water age in the outlet of the system. The term residence time is also frequently used to describe a bulk estimate of the renewal time of a system or of a section of system vertically well-mixed at high tide, when this estimate is including both the influence of tides and water inputs such as river discharge

(e.g. Gordon et al., 1996; Luketina, 1998; Sanford et al., 1992). Indeed, the residence time of a system can be equivalent to the flushing time as defined by Monsen et al. (2002) when it describes the time it takes for a water parcel coming from a single or dominant source (ex: a river or spring) to leave a system vertically well mixed at high tide through its outlet.

2.4.3.2 Methods to assess flushing times, residence times and water ages

Five types of methods are used either alone or combined to assess the retention of waters in coastal systems: Compartment models, numerical modelling, drifters, flow rates measurements, and tracer methods.

Compartment models generally assess the flushing times of coastal systems by approximating them in one or a series of well mixed boxes, and using information on estuaries dimensions, water inflow and salinity (for an intercomparison of these models see Sheldon, J. E. and Alber, 2002). Can be included in this type of models: flushing times estimates, tidal prism models (B. H. Ketchum, 1951; Luketina, 1998; Sanford et al., 1992; Wood, 1979) and box models, which are closely related (Officer, 1980). A review of the different ways to implement the tidal prism methods in a single box system is given in Sanford et al. (1992); and a review of the different versions of such single box tidal prism models is given in Luketina (1998). Both of these works are used in this study.

Hydraulic and numerical modelling (e.g. Oliveira and Baptista, 1997) generally divide coastal systems in a large number of cells to assess the spatial variability of residence time and water ages of specific areas. They generally require high resolution data from flow rate measurements observations, drifters observations, or observation of the spatial variability of a scalar of interest to be calibrated or validated.

Drifters consist in using drifting device to record movements of water parcels in time. When large numbers of drifters are used (e.g. 400 drifters and 6000 driftcards in Pawlowicz et al., 2019), residence time may be determined by combining drifters observations with a box model or numerical model. Alternatively, flow rates in coastal systems can be measured to support modelling effort, but a large density of measurements is generally required to limit uncertainty.

Tracers methods use the measurement of a solute fed in a system to assess residence time of a system. The most common method involves the measurement of salinity combined with a model, but cannot distinguish between the timescales of different freshwater sources. More recently, a method using the measurement of naturally occurring radium isotopes in the ocean, elements which are continuously released by coastal springs and sediment have been developed (Moore, 2000; Moore et al., 2006). In this method, water ages within a system can be determined by measuring the ratio between radium isotopes of distinct decay rates. Knowing the decay rates of the different radium isotopes, and assuming that all significant Ra sources in the system have close Ra ratio, water ages can be then calculated (Moore, 2000; Moore et al., 2006). Two methods exists to do so, the "mummy model" (Moore, 2000) is applicable in systems where a single source of radium is present; and the "continuous model" (Moore et al., 2006) is applicable to systems where the radium inputs occurs continuously from the bay floor, with a constant Ra ratio. The "mummy model" does not require a system at steady state relative to mixing (Moore, 2000), while the continuous model does require a system at steady state (Moore et al., 2006). The "mummy model" allows to assess the time since the solutes in a water parcel left contact with a Ra source of known Ra ratio. For example, for the ^{224}Ra and ^{223}Ra activity ratios the age of the solute (or water age) is given by:

$$A = \frac{ln\left(I(\frac{^{224}Ra}{^{223}Ra})\right) - ln\left(F(\frac{^{224}Ra}{^{223}Ra})\right)}{\lambda_{224} - \lambda_{223}} \quad (1.4)$$

Where A is the mean water age (in days) in the bay relative to a reference point (or mixing end member), $\mathrm{F}(\frac{^{224}Ra}{^{223}Ra})$ is the observed ^{224}Ra/^{223}Ra activity ratio (AR) at the sampling location, $\mathrm{I}(\frac{^{224}Ra}{^{223}Ra})$ is the ^{224}Ra/^{223}Ra activity quotient at the radium source (e.g. a coastal spring or intertidal area releasing Ra), and λ_{223} and λ_{224} are the decay constants of ^{223}Ra (0.0608 day^{-1}) and ^{224}Ra (0.19 day^{-1}) respectively. This approach assumes that the radium activity ratios of the freshwater end member are constant during the survey period, and that there is no inputs of new radium to the system large enough to modify Ra ratios along the transect (Moore, 2000).

The continuous water model (Moore et al., 2006) defines water ages from the ^{228}Ra and ^{224}Ra as follows:

$$A = \frac{F(^{224}Ra/^{228}Ra) - I(^{224}Ra/^{228}Ra)}{\lambda_{224} \times I(^{224}Ra/^{228}Ra) - \lambda_{228} \times F(^{224}Ra/^{223}Ra)} \approx \frac{F(^{224}Ra/^{228}Ra) + I(^{224}Ra/^{228}Ra)}{\lambda_{224} \times I(^{224}Ra/^{228}Ra)} \quad (1.5)$$

Where $F(\frac{^{224}Ra}{^{228}Ra})$ is the observed $^{224}Ra/^{228}Ra$ activity ratio (AR) at the sampling location, $I(\frac{^{224}Ra}{^{228}Ra})$ is the $^{224}Ra/^{228}Ra$ activity quotient at the radium source (e.g. a coastal spring or intertidal area releasing Ra), and λ_{22} and λ_{224} are the decay constants of ^{224}Ra ($2.8\ 10^{-4}$ day^{-1}) and ^{224}Ra ($0.19\ day^{-1}$) respectively.

Similarly, for ^{224}Ra and ^{223}Ra we can demonstrate (as shown in appendix 1.1), with same notations than equation 1.4:

$$A = \frac{F(^{224}Ra/^{223}Ra) - I(^{224}Ra/^{223}Ra)}{\lambda_{224} \times I(^{224}Ra/^{223}Ra) - \lambda_{223} \times F(^{224}Ra/^{223}Ra)} \quad (1.6)$$

As SGD leads generally to large sources of radium to coastal areas, tracers-based method using radium seems particularly suited for the assessment of the variability of the ageing of SGD fluxes within coastal systems. However, this method requires a single source of radium in the system with a known Ra ratio (the “endmember”). This approximation thus requires either negligible Ra inputs along the bay after the main source, for example as a result of stratification limiting the Ra inputs to surface samples (for the “mummy” model), or similar Ra ratios between the Ra fluxes from deep sediment and SGD fluxes along the coastlines (for the “continuous” model). If other sources are present, then the water ages will tend to be underestimated if Ra ratios in these sources are larger than the Ratios in the water column. On the other hand, both compartment models and numerical models are frequently reliant on known inputs of water from land, and their estimation of residence time might be potentially modified if large fresh SGD inputs are present in addition to river discharges. Drifters are not influenced by these limitations but require very large number of measurement points, and to be coupled with modelling to assess residence time. Ra isotopes are thus used in this work to assess the variability of water ages in SGD (see Chapter 3) or river influenced systems (see Chapter 5). Finally, the water age and residence time provide limited information on time-dependant variability in systems where multiple solute sources/sinks contribute on similar scale to the solute budget. For these systems, advective-dispersive models or other type of numerical model including the different sources/sinks and the transport mechanisms would more appropriately represent the solute dynamic. An example of such model for

one dimensional cross-shelf transport of SGD is provided in Lamontagne and Webster, (2019).

Nevertheless, developing a detailed advection dispersion model for a dynamic system such as an estuary require a detailed characterisation of the elemental balance of the element in the system and can be time and cost demanding. In this context, the residence time or water age concept is a valuable approximation to characterise the time-dependant variability of solute flushing in systems where one solute endmember, such as a river or a spring, dominate the solute budget. It could be also valuable to identify and highlight specific retention zones when a model specific to every solute of interest cannot be developed. The next subsection describes the variability of residence time in coastal systems and its effect on the spatially variable flushing of SGD in coastal areas.

2.4.3.3 Causes for variable residence times, water ages and flushing times and their effects on the storage of SGD waters in coastal systems.

Periods of stronger tides tend to increase the rate of flushing of coastal systems (Luketina, 1998), while periods of increasing water inputs in estuaries tend to decrease residence time of elements in estuaries (Alber and Sheldon, 1999). For example, a log-normal relationship between flushing time and discharge (Alber and Sheldon, 1999) was previously identified (Figure 7). As a result of this relationship, the effect of a changing discharge on flushing time may be either very high if the initial range of discharge is low, or lower if the initial range of discharge is high.

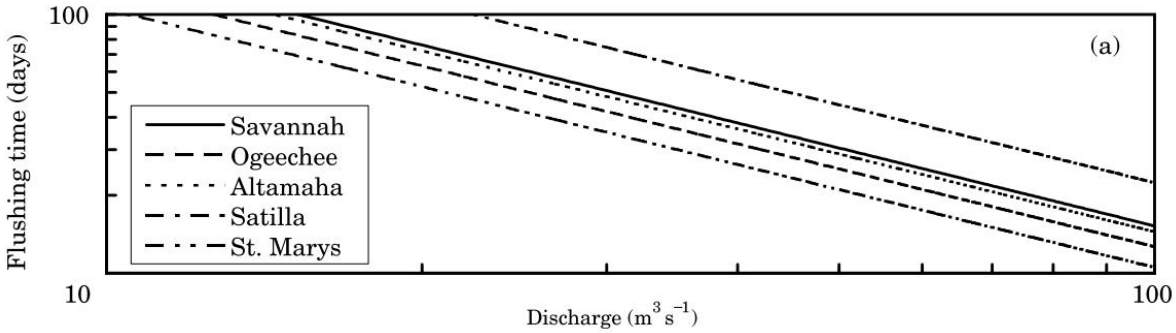

Figure 7: Effect of discharge on flushing time in five Georgia estuaries (modified figure with a log-normal scale from Alber and Sheldon, 1999 with permission from Estuarine, Coastal and Shelf Science)

Moreover, the combined effect of tides and marine currents outside of a bay may drive some of the discharged water from SGD or rivers back to the bay or coastal area. This flow

occurs if the plume of discharged water is not entirely dispersed outside of the bay (e.g. Figure 8) and can be returned partially during the next rising tide. Studies attempting to account for this fact introduce a return flow factor term, defined as the percentage of water leaving on the ebb that is returning during the next flood tide (Sanford et al., 1992). For Kinvarra Bay, Rocha et al. (2015) determined with Ra isotopes during low discharge a return flow factor of 0.86+-0.4, suggesting that the bay retain the majority of the discharged water to the system for several tidal cycles. The retention of discharged water in the inner bay was recently confirmed (Gregory et al., 2020), which validate this observation. The effect of the tide was also highlighted, with larger retention of freshwater during neap tide periods than during spring tide periods. Interestingly, recent sea temperature observation in Kinvarra Bay also identified a plume of similar shape (Figure 9b) that what found in the original Sanford (1992) paper (Figure 9a). This similarity suggests that the Sanford method to assess return flow may work well in Ireland for enclosed bays like Kinvarra Bay, discharging in a broader coastal area.

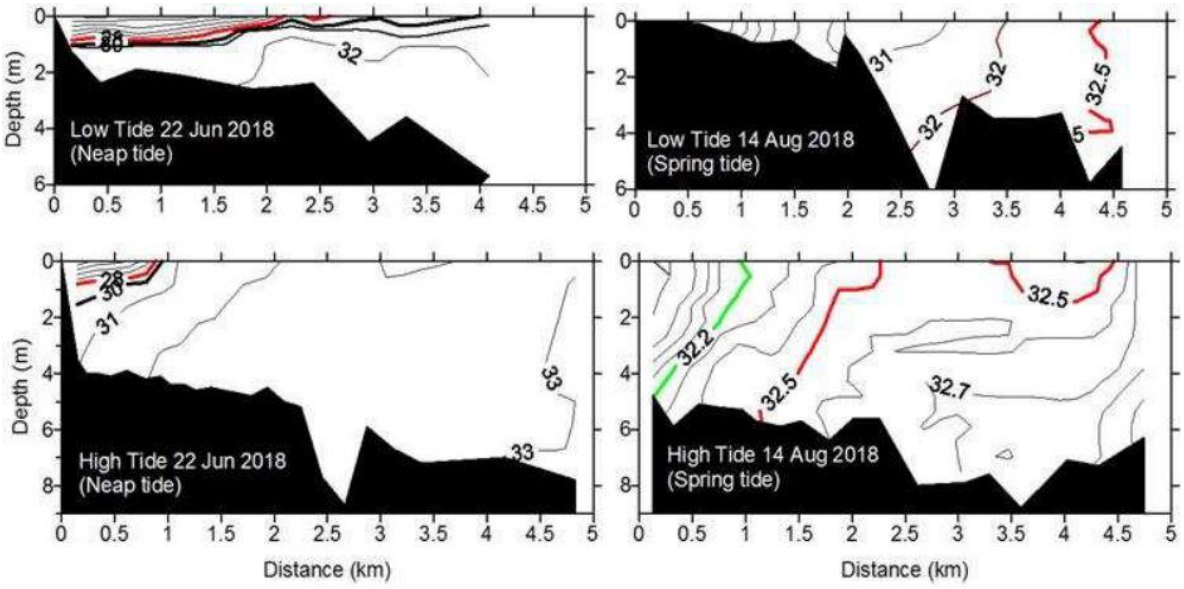

Figure 8: Effect of tidal stages on the storage of fresh SGD waters in Kinvarra Bay (Reproduced from: Gregory et al., 2020 with permission from Estuarine, Coastal and Shelf Science). Salinity data for neap and spring tides show tidal excursion of approximately 1.5km and 3km respectively, as shown by the movement of the S=28 contour (neap tide) and S= 32.5 contour spring tide), marked in red. Neap sampling was completed with very light to no wind while spring sampling had stiff northerly (opposing) breeze (>15 knots).

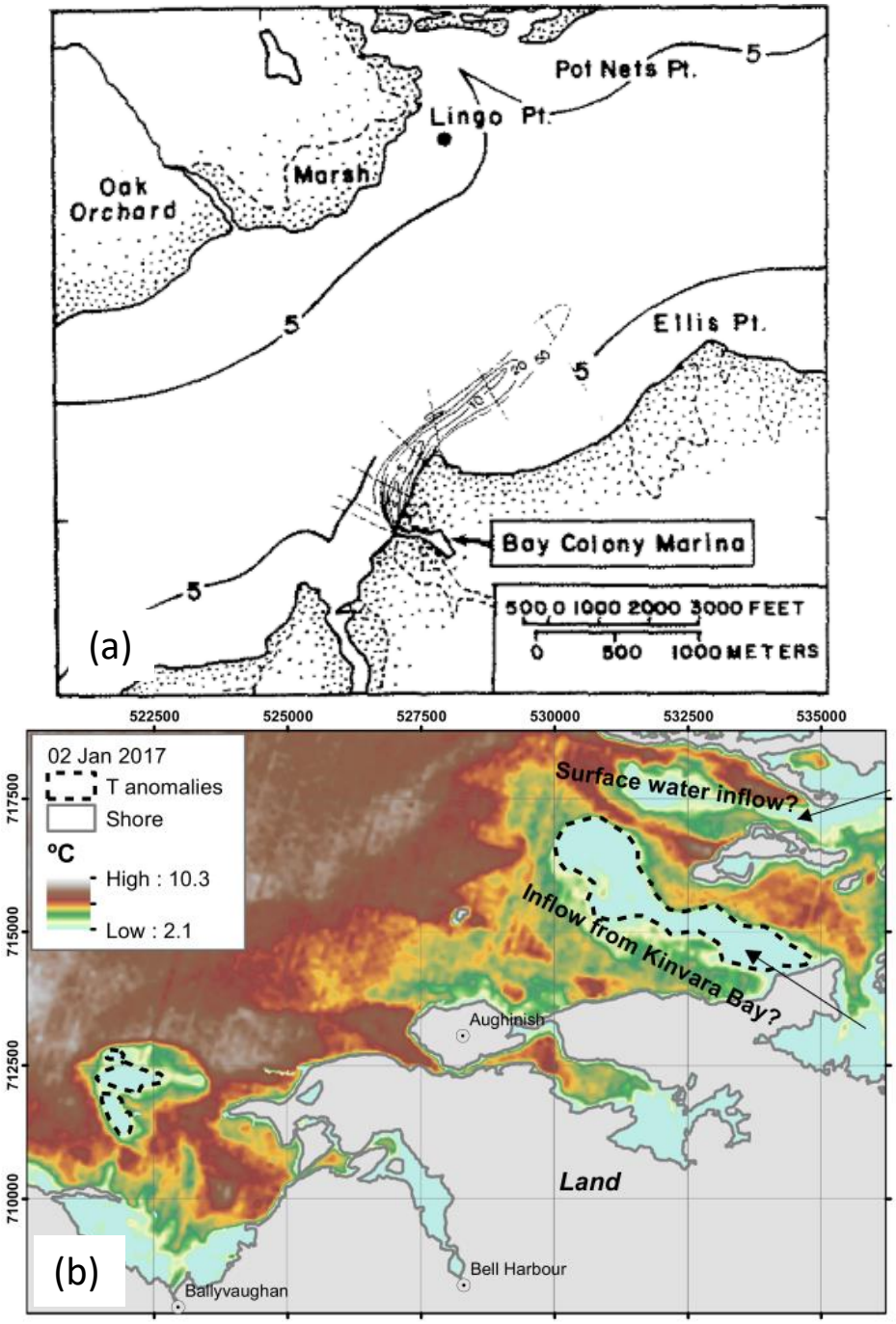

Figure 9: Illustration of two plumes of water remaining outside of a coastal bay where inputs of solutes occur. (a) in the paper that introduced the concept of return flow factor (Figure reproduced from Sanford et al., 1992) and (b) in Kinvarra Bay (Figure reproduced from Lecher and Mackey, 2018, with open access Creative Commons CC BY license). (a) represents the measured surface dilution of dye from bay colony Marina on 15th June 1990, while (b) represents sea surface temperature anomaly taken the 2nd of January 2017 in Kinvarra Bay outlet (centre-right of the map).

Our review of the effect of residence time for the storage of SGD in coastal systems suggest that the joint effect of tide and river flow can lead to large changes of the fraction of coastal water affected by SGD for a given SGD flow. In Kinvarra, the residence times and the spatial variability of water ages were measured with $^{224}Ra/^{223}Ra$ in summer low

discharge surveys (Rocha et al., 2015). However, the spatial variability of ages and its response to varying conditions of discharge and time of the year is currently unknown and will be investigated in this study in chapter 3.

2.4.3.4 Limits of the residence time and water ages concepts

While useful as a simple way to compare the spatial and temporal variability of aquatic systems, the concepts of residence time and water age also have limitations. When diffusion is important, the apparent ages derived from radio-tracers typically underestimate the "true" water ages, with a difference increasing with the time difference between the half-life of the tracer and the timescale of the exchange in the system of interest (Deleersnijder et al., 2001; Delhez et al., 2003). To limit this drawback, radiotracers with half-life in the order of the age of the system might be selected. Moore, (2000) already noticed in its original development a better performance of certain tracer couple of tracers, through a lower spread of water ages results from specific pairs of tracers: "the $^{224}Ra/^{223}Ra$ methods is better for ages in the range 1-7 days and the $^{224}Ra/ex^{228}Ra$ method is better for age in the range 7-40 days".

Moreover, mixing processes in aquatic environments can lead to different ages for different constituents (Deleersnijder et al., 2001). Radio-age computed from the ratio of the activities of two radioactive tracers is always intermediate between the ages of these two tracers (Delhez et al., 2003). This could, if different isotopes of an atom have distinct sources and sinks, lead to distinct ages when using different isotopes pair. To avoid these limitations of radiotracers, it has been suggested in hydrogeology to use the tracer measurements directly to calibrate models (Suckow, 2014). Such a model would provide additional meaningful information if sufficient information on the different sources is available.

Despite their limitations, apparent water ages derived from radiotracers allow to quantify the variability of flushing without deployment of an advective-dispersive model, which is more time and resource demanding, and require more computational power and information on the system. Probably for this reason, apparent water ages derived from radiotracers are still commonly applied to quantify water ages variability in aquatic systems (e.g. Tamborski et al., 2017; Tomasky-Holmes et al., 2013; Rocha et al., 2015). The

present thesis uses the concepts of apparent water ages and residence time as a way to highlight the spatial and temporal variability of flushing. This approach aims to give a preliminary interpretation of the effect of variable flushing on the reactive elements of interest, before an advective-dispersive model or a more detailed model can be eventually applied for the systems studied. Such approach using advective-dispersive models for Radium tracers has been recently described in Lamontagne and Webster, (2019) and adaptation of the method in the estuaries studied here could be applied when sufficient resources and information are available to do so.

2.4.4 Effect of SGD on aquaculture and coastal ecosystems.

A review of the effect of submarine groundwater discharge on marine biota was recently published (Lecher and Mackey, 2018). SGD affects marine biota by (1) modifying water physicochemical properties (reducing temperature, adding nutrients, changing pH), (2) modifying rates of vertical mixing (either creating salinity stratification or reducing stratification) and (3) adding microorganisms from land to the sea (virus, bacteria). (Figure 11). When SGD changes vertical mixing or supplies fluxes of microorganisms to coastal areas, it also modifies water physicochemical properties or provides additional solutes to coastal areas at the same time. This section will thus focus on the variable effect of SGD on solute fluxes and physicochemical changes in coastal areas.

SGD provides marine ecosystems with more sustained and stable nutrient inputs than surface inputs, which vary quickly as a response to net rainfall events. These nutrients sustain across the year the primary ecosystem production of phytoplankton, algae and plants. As a result, elevated chlorophyll-a and high radon activities, an indicator of SGD fluxes, often occurs together (Honda et al., 2018; Su et al., 2014; Valiela et al., 1992). This sustained primary production has cascading effects on other organisms and higher trophic levels, which may have positive, or negative impacts on the marine ecosystems depending on the prevailing conditions (Lecher and Mackey, 2018).

Fresh SGD and saline SGD have a distinct effect on marine ecosystems. Fresh SGD decreases coastal areas salinity which may negatively impact organisms adapted to marine environments and can reduce the marine primary production around the coastal

springs. However, it also provides new nutrients to the overall system, which amplify primary production on locations where the water inputs are sufficiently dilute. Saline SGD supplies recycled or new nutrient to coastal systems without decreasing bay water salinities. As a result of these differences, primary production is more likely to be amplified at the locations where mainly saline SGD is present than at locations where mainly fresh SGD is present. For example, locations close to saline SGD inputs favours more diatoms species such as *Pseudo nitzchia* than locations close to freshwater inputs (Lecher and Mackey, 2018; Liefer et al., 2009) (Figure 11 b).

Moreover, both saline and fresh SGD are frequently enriched in Si compared to seawater. Si enrichments can also amplify primary production when this nutrient is limiting (Lecher and Mackey, 2018), and favour specifically the growth of diatoms over other species (Figure 11a). This amplified growth of diatoms can convert more dissolved inorganic nutrients in organic nutrients, which benefits other species such as cyanobacteria, criptophytes and dinoflagellates (Figure 11a).

SGD transports a variable quantity of nutrients (nitrogen, phosphorus…) to coastal areas depending on the scale considered (see section 2.4.2), and frequently transforms them along the flow path (see section 2.4.1.2). As phosphorus has a greater affinity with particles than nitrogen, the N:P ratios in groundwater are generally higher than the Redfield ratio (N:P=16). Changes of the nitrogen: phosphorus ratios or quantity of nutrient loads to coastal areas can modify primary production and promote eutrophication (e.g. see Figure 10). Groundwater discharge might thus drive primary productivity in coastal areas to P limitation (Welskel and Howes, 1992), which was already observed in Ireland for Kinvarra Bay during summer (Rocha et al., 2015).

As shown previously in part 2.4.1.2.2, the reactions occurring within the subterranean estuary are also affecting the N:P ratio, potentially decreasing or increasing the ratio at different times of the year, depending on oxygen levels, inputs of labile organic matter, salinity changes, and the structure of the subterranean estuary (Slomp and Van Cappellen, 2004). This larger N:P ratio can modify the ratio in marine plants and algae, increasing macrophyte biomass but reducing their diversity (Lecher and Mackey, 2018). It can also favour the development of phytoplankton species adapted to P limitation.

Partly for these combined reasons, SGD nutrient loading influences the occurrence of harmful algal blooms (HAB) (Cheng et al., 2020; Laroche et al., 1997; Lecher et al., 2015; Liefer et al., 2009), formed by the proliferation of phytoplankton species producing marine toxins (Gerssen et al., 2010) or leading to oxygen depletion in the water column (Silke et al., 2005). For example, a study showed that blooms occur on average 10-20 days after the occurrence of a peak of nutrient inputs from SGD (Cheng et al., 2020). In such a context, understanding the drivers and the timing of changes of N:P ratios and nutrient loads from SGD in a coastal system may be highly beneficial for aquaculture, coastal ecosystem and communities (Lecher and Mackey, 2018).

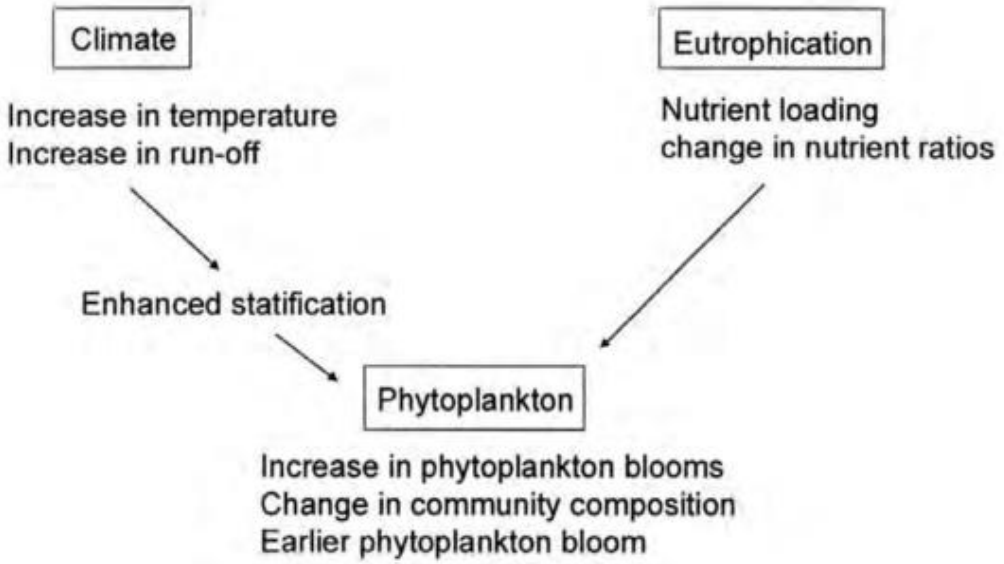

Figure 10: Simplified representation of the links between the physical and chemical environment and plankton productivity, with possible consequences on climate change and an increase in eutrophication on phytoplankton (reproduced from Edwards, 2000, with author's permission, based on Beusekom and Diel Christiansen (1994) and Dickson (1992)).

In Ireland, so far, few studies assessed the effect of SGD inputs on periods of increasing primary production and harmful algae blooms. However, harmful algae blooms have notable impacts on aquaculture and fisheries since 1976 (Parker et al., 1982). Early phytoplankton long term datasets noted a decrease of diatoms relative to flagellates between 1958 and 1974 (Reid, 1977), an apparent change also present in other parts of the word, under different periods (Hallegraeff, 1993). This shift towards larger dinoflagellates communities is concomitant with an apparent global increase of harmful algae blooms frequency (Hallegraeff, 1993). Potential causes for this apparent increase include: increasing nutrient loads to coastal areas due to the growth of population,

favourable climate conditions, transport of invasive phytoplankton species in ship ballast, and a growing perception of HAB due to the increasing scientific awareness and increasing use of coastal areas for aquaculture (Hallegraeff, 1993).

Beyond a concentration threshold of phytoplankton or macroalgae in the water column, blooms can lead to mortality of coastal and aquaculture organisms. The large presence of phytoplankton and macroalgae can favour (1) oxygen super-saturation during daylight hours followed by (2) oxygen depletion during the late hours of darkness (Marine Institute et al., 2005), and (3) irritation and clogging of gill membranes by the algal biomass (Parker et al., 1982). The toxins produced by some species under stress conditions (e.g. nutrient limiting conditions at the end of blooms for Pseudo-nitzschia (Bates et al., 1998; Trainer et al., 2012)) are also causing concerns. To date, seven important human illnesses associated with microalgae toxins are known (Hallegraeff, 1993; Lagos, 1998; Ló Pez-Rivera et al., 2009; Yasumoto et al., 1995; Yasumoto and Murata, 1993), among which four are occurring during algae blooms in Irish waters (Marine Institute et al. 2005, p. 5). The direct and indirect effect on human society was estimated to be between $33 and $82 million for the U.S. alone (Anderson et al., 2000). In addition to this, increasing development of macroalgae blooms (e.g. Ulva blooms, Wan et al. 2017), with the associated H_2S production by decomposition (Great Britain. Environment Agency., 2009; Reiffenstein et al., 1992), was related with odour nuisance (Melia, 2014; The Irish Times, 2010) with the associated impact for tourism and coastal activities. At least one case of death was suspected linked to H_2S accumulation from seaweed (BBC news, 2009; Pouchar, 2015). In this context, investigation the role of SGD for supplying nutrient for blooms in coastal areas will favour a better management of the impacts of HAB on coastal communities, ecosystem and aquaculture. The potential effect of SGD nutrient fluxes on phytoplankton growth and N assimilation of mussels is investigated using a lower trophic model in chapter 5.

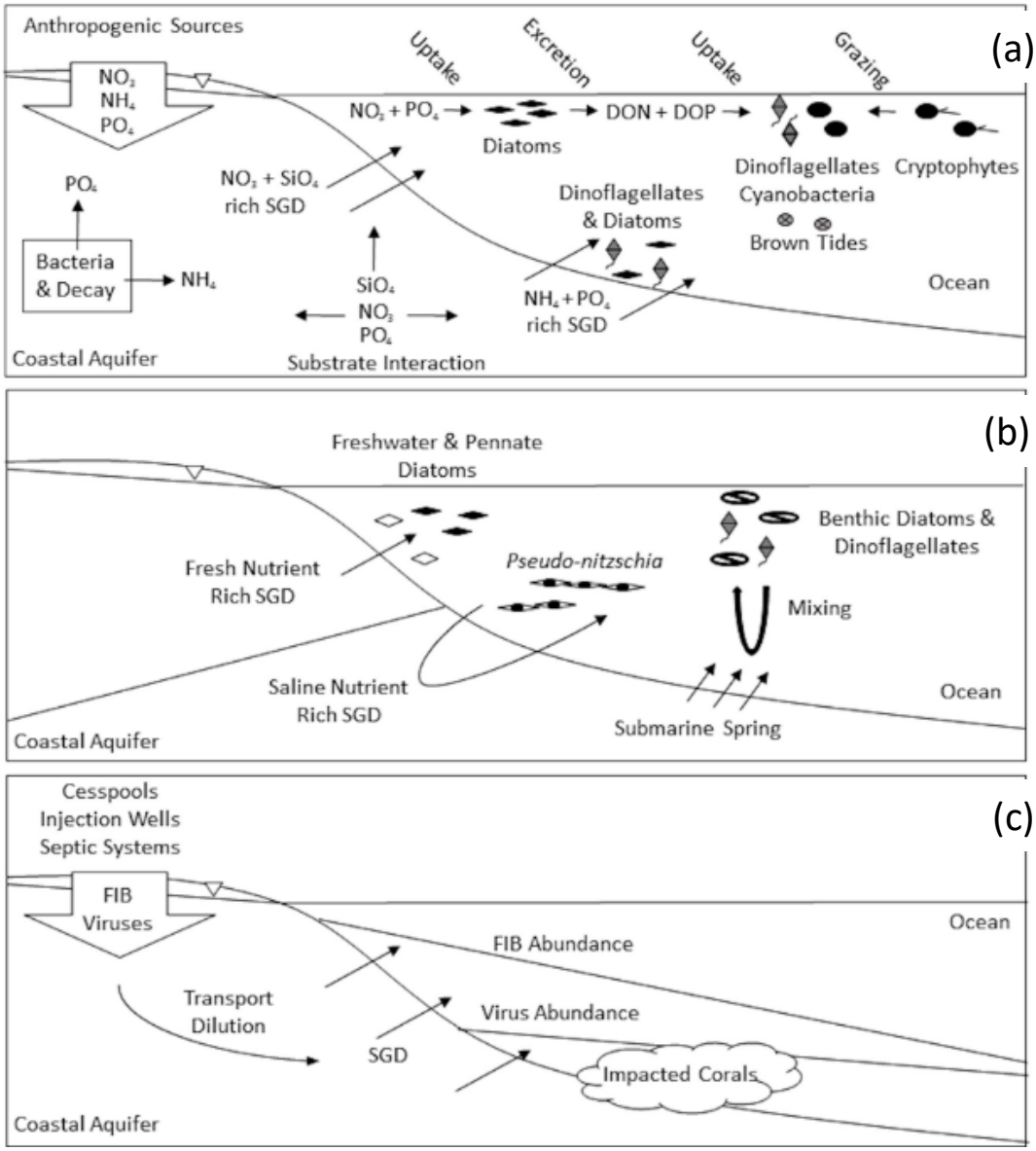

Figure 11: Summary of the effect of SGD on marine biota (reproduced from Lecher and Mackey, 2018, under open access Creative Commons CC BY license). In (A), inputs of nitrate and dissolved silica from SGD induces the growth of diatoms that consume nitrate and phosphate in the water column. The diatoms transform the inorganic nutrients into organic nitrogen and phosphorous, which are used by dinoflagellates and cyanobacteria or brown tides. Cryptophytes graze the dinoflagellates and cyanobacteria. The discharge of groundwater high in ammonium and phosphate aids the development of dinoflagellates in addition to diatoms. In (B), the discharge of fresh groundwater increases the abundance of freshwater-preferring and pennate diatoms. Saline SGD from seawater that has circulated through the coastal aquifer spurs the growth of Pseudo-nitzschia. Vertical mixing from high discharge submarine springs suspends benthic diatoms and dinoflagellates. In (C), faecal indicator bacteria (FIB) and enteric viruses enter the groundwater system from anthropogenic waste sources. The FIB are diluted as salinity increases until FIB and viruses are output to the coastal ocean via SGD. Concentrations of FIB abundance decrease faster than viruses, due to their faster degradation time in seawater. Viruses and FIB negatively affect corals, in addition to causing beach closures.

2.5 Questions arising from the literature review.

The earlier sections reviewed the drivers of SGD, its methods of measurements and its effect on coastal areas nutrient balances. This review gives a theoretical framework to study (1) the timing and spatial variability of the total water fluxes to coastal areas coming from rocks and sediment (2) the nutrient flux into coastal areas driven by Submarine Groundwater Discharge and (3) its effect on the water column chemistry and phytoplankton abundance and communities.

SGD is composed of a mix of seawater, recirculated through rocks and soils, and groundwater, with a variable relative proportion depending on tides, groundwater level, wave setup, geology. As a result of this variable, mixed composition, the effect of nutrients fluxes from SGD on coastal areas is complex to estimate: only a small proportion of the total SGD flux is directly measurable in coastal springs and models to assess saline SGD require assumptions difficult to verify. The freshwater component of the SGD fluxes to coastal areas have been the most studied. However, the variability of SGD during the year is generally poorly characterised and rarely account for the combined effect of the natural drivers (effect of storms, effects of density difference in the subterranean estuary) and the nutrient reactions involved in Irish subterranean estuaries. In addition to this, the effect of saline SGD in Irish water is still to be described, as current estimate focused on the freshwater component, or only sampled coastal springs, without considering the potential processes occurring during the mixing of freshwater and seawater in the aquifer (the subterranean estuary). The effect of recirculated seawater on the composition of the discharged waters is poorly characterised so far for karst. Most of the study of saline intrusion so far was related to its effect on the pumping of coastal resources for water supply (e.g. in Geological Survey, 1965), and less so for characterising its effect on the balance of elements in coastal areas.

Furthermore, the impact of SGD on the frequency of eutrophication by the additional nutrient inputs it provides to coastal areas is difficult to quantify for additional reasons: Nutrients level within the water itself are non-conservative, both along time and along its pathways (Ibánhez and Rocha, 2016; Slomp and Van Cappellen, 2004). The mixing zone between recirculated seawater and groundwater is changing the nutrients levels within SGD when saline and freshwaters mix, particularly if the two water masses are under

different redox conditions. The so-called subterranean estuary can act either as a source or as a sink of nutrient depending, for example, on nutrient levels, organic carbon, and oxygen availability. Finally, the SGD fluxes are not instantly flushed to the open ocean once leaving the aquifer but can remain variable times in specific locations in coastal systems, as a function of tides and changes of marine currents outside of the system. A given load of solute from SGD is more likely to significantly affect a site if it occurs during neap tides periods than if it occurs during spring tides periods. This effect of tide on flushing characteristic was confirmed recently for Kinvarra Bay (e.g. Figure 2 in Gregory et al., 2020), but the potential practical implication for the coastal management of sites with solute inputs from SGD is still to determine.

In this context, developing further the understanding of the parameters driving (1) the changes of SGD compositions, (2) their quantity and (3) where when and how long the SGD waters remain the longer in coastal systems will benefit the management of coastal systems. The next chapters will investigate how to do so, as follows.

The changes in SGD composition and abundance during the year are investigated in Chapters 3 and 4 using the example of a study site with major SGD inputs, Kinvarra Bay. Chapter 3 compare a series of methods applicable to assess total SGD. A potential issue is highlighted in the tracer methods based on non-conservative solutes. Improvements of the methods are developed to correct SGD figures for the spatial variability of flushing in an estuary affected by SGD. Chapter 4 assesses in Kinvarra Bay the saline SGD (or recirculated SGD), and investigate its potential effect on the nutrient composition of the total SGD fluxes to the bay.

Chapter 5 use radium isotopes, nutrient and salinity measurements in Killary Harbour to illustrate how variable stratification and flushing rates modifies the nutrient availability of a given solute for primary production when solute fluxes occur from deep sediments.

The sixth chapter of this work combined the observations on the variability of SGD fluxes and the information on flushing rates in the system with nutrient mass balances and models to study the effect of SGD on aquaculture for Kinvarra Bay. This last chapter derive a series of conclusions applicable for the development of policies to ensure the preservation and optimisation of the SGD value for coastal ecosystems and aquaculture activities.

Chapters 3 to 6 are organised as journal articles, to allow each of them to be read as a standalone work and facilitate their future publication. Chapters 3 and 5 have been already submitted respectively to the Journal of Hydrology and Marine Chemistry and published. The current version of Chapter 5 and Chapter 3 are modified following feedbacks from Marine Chemistry's and Journal of Hydrology's reviewers respectively and were updated following suggestions from the reviewers of this thesis.

Appendix 1.1: Adaptation of the continuous model to $^{224}Ra/^{223}Ra$:

Following a similar approach than previously done for $^{222}Ra/^{228}Ra$ (Moore et al., 2006) the continuous model for $^{224}Ra/^{223}Ra$ to get water ages can be expressed as :

The equation for the ^{224}Ra balance can be expressed similarly as in Moore, Blanton and Joye, (2006):

$$F^{224}Ra = I^{224}Ra\left(\lambda_{224} + \frac{1}{t}\right) = {}^{224}Ra\ Decayed + continuous\ {}^{224}Ra\ \ input \quad (11)$$

Where F ^{224}Ra is the total flux of ^{224}Ra to the system, I ^{224}Ra is the inventory of ^{224}Ra in the system, λ_{224} is the decay constant for ^{224}Ra, and t is the apparent age of water in the system. We can write a similar equation for ^{223}Ra:

$$F^{223}Ra = I^{223}Ra(\lambda_{223} + \frac{1}{t}) \quad (12)$$

Now divide equation (11) by equation (12):

$$F(^{224}Ra/^{223}Ra) = I^{224}Ra(\lambda_{224} + \frac{1}{t})/(I^{223}Ra(\lambda_{223} + \frac{1}{t})) \quad (13)$$

Eq. 13 can be rearranged:

$$T = \frac{F(^{224}Ra/^{223}Ra)+I(^{224}Ra/^{223}Ra)}{\lambda_{224}*I(^{224}Ra/^{223}Ra)-F(^{224}Ra/^{223}Ra)*I^{223}Ra*\lambda_{223}} \quad (14)$$

Which give the general equation for the continuous model:

$$T = \frac{F(^{224}Ra/^{223}Ra)-I(^{224}Ra/^{223}Ra)}{\lambda_{224}*I(^{224}Ra/^{223}Ra)-F(^{224}Ra/^{223}Ra)*\lambda_{223}} \quad (15)$$

3 PAPER A: Rethinking tracer-based (Ra, Rn, salinity) approaches to estimate point-source submarine groundwater discharge (SGD) into coastal systems.

Keywords: Submarine groundwater discharge, Karst, Radon, Radium, Modelling, Salinity, Ireland

Highlights:

- Marine tracer-based approaches to estimate SGD are evaluated for a small bay
- The tracer-derived SGD magnitude is dependent on budget model assumptions.
- Inventorying tracers by different methods raises large differences in SGD estimates.
- Bay-ocean exchange rates and spatial variability of water ages affect SGD assessment.
- A method is suggested to correct for this effect using radium relative water ages.

3.1 Abstract

Submarine groundwater discharge (SGD) is a potentially more important source of solutes to the global oceans than river flow. As a result, the accuracy of predictions of the magnitude and seasonal variability of SGD to the sea is critical for the management of coastal marine ecosystems. For a model site (Kinvarra Bay, Ireland) dominated by point source SGD inputs, different ways to consider water residence time within the system and water exchange across its boundaries could lead to massive differences between estimates provided by different marine tracer-based methods. For example, results from tidal-prism and freshwater fraction models, the most widely used approaches to quantify freshwater fluxes into marine areas of restricted exchange, vary by one order of magnitude depending on the chosen method to consider the water exchange across the outer system boundaries and whether Snapshot or Eulerian data are used. As demonstrated, SGD estimates based on single location time series (Eulerian) outside of a retention area can lead to consistently lower estimates than when using transect data (Snapshot data).

Moreover, the outcome of radon (^{222}Rn) based SGD estimates depends on the way the effect of water age variability on radon decay and degassing is accounted for. A solution to this conceptual problem is provided by developing a correction to ^{222}Rn budgetary approaches to estimate SGD, based on the spatial variation of water ages estimated from radium isotopes (^{223}Ra, ^{224}Ra) in solution. New data is used to compare the different sets of approaches while examining the validity of their underlying assumptions to verify internal consistency. The substantial range of published data on Kinvarra Bay to assess the quality of results produced with the new method.

3.2 Introduction

Increasing evidence shows that Submarine Groundwater Discharge (SGD), defined as the flow of water from the seabed to the coastal ocean regardless of fluid composition or driving force (Burnett et al., 2003), is a larger source of dissolved chemicals to the ocean than river water (Kwon et al., 2014; Moore et al., 2008; Rodellas et al., 2015a). Hence accurate SGD rates are necessary to validate marine biogeochemical budgets of ecosystem sensitive elements such as carbon, nitrogen and phosphorus.

Taniguchi et al. 2019 reviews the array of methods to quantify SGD in use to date. Seepage meters (Lee, 1977) measure total SGD fluxes over small areas (typically ~0.25-1 m^2 e.g., Leote et al., 2008). Salt or catchment-based water budgets help estimate fresh groundwater flows over larger coastline lengths. Radioactive tracers of SGD, such as radium (Kwon et al., 2014; Moore et al., 2008; Rodellas et al., 2015a) or radon (Burnett and Dulaiova, 2003) have been increasingly employed to estimate total SGD (fresh groundwater plus recirculated seawater) at regional scales (Burnett et al., 2008, 2001; Dulaiova et al., 2010; Rocha et al., 2016; Sadat-Noori et al., 2015). Finally, hydrogeological models can be used to predict fresh and occasionally saline SGD rates, but require calibration, making direct or tracer-based quantification of SGD essential for validation. Yet, quantifying SGD remains challenging because of its spatial and temporal variability.

Tracer budgets, while time consuming, integrate a measure of temporal variability producing snapshots of discharge for entire coastal systems. But to measure annual or multiannual SGD, its temporal variability (intra- and inter-annual) has to be evaluated. However, flow rates derived from tracer budget methods are sensitive to the sampling strategy, how whole-system tracer inventories are obtained, and to the mathematical simplifications that allow closure of mass balances. Combined, these sensitivities lead to large disparities in SGD magnitude estimates, even when the same tracer data are used. For example, water exchange between coastal systems and the open ocean can be quantified in multiple ways, with different results (e.g. Dyer and Taylor, 1973; Gordon et al., 1996; Ketchum, 1951; Luketina, 1998; Sanford et al., 1992a). Hydrodynamics driven by winds, tides and watershed inputs makes mixing within coastal systems spatially variable, so rather than a homogeneous volume, they comprise a distribution of water masses with distinct biogeochemical histories. The water age, defined as the time since a water parcel

was separated from a solute source (here Kinvarra springs) and its distribution is therefore essential to develop accurate non-conservative elemental budgets in areas of restricted exchange (Monsen et al., 2002). Groundwater generally contain much larger ^{222}Rn activity than seawater, and sediment release ^{223}Ra and ^{224}Ra when in brackish to saline waters. Consequently, these elements are valuable tracers of SGD in seawater. However, they are subject to radioactive decay, and for Radon, degassing and consequently, their use in SGD budgets requires to constrain the transport processes in the studied system and this is most often lacking.

We show how these factors affect SGD estimates and develop potential ways to overcome bias using Kinvarra bay, a groundwater dependant coastal system, as a testbed. Groundwater-surface water interactions in Kinvarra have been intensively studied since the 90's (Drew and Daly, 1993; Drew, 2003, 2008; Cave and Henry, 2011; Smith and Cave, 2012; Einsiedl, 2012; Petrunic, Einsiedl and Duffy, 2012; McCormack et al., 2014; Rocha et al., 2015; Schubert et al., 2015; McCormack et al., 2016; Gregory et al., 2020; Morrissey et al., 2020). Seepage meters are impractical there because of its karstic shoreline, which hosts multiple points of focused discharge. Thus SGD studies to date estimated groundwater inputs using tidal prism and freshwater fraction models or whole system salt budgets (e.g., inter-alia, Cave and Henry, 2011; McCormack et al., 2014), occasionally combined with radiotracer methods (Rocha et al., 2015). However, very few studies (Rocha et al., 2015; Schubert et al., 2015) combined radiotracer budgets with independent approaches to evaluate internal consistency of SGD quantification, and the majority of tracer data available for the system was collected during low flow periods (spring, summer). Catchment-based approaches, including karst flow models (McCormack et al., 2014, Morrissey et al., 2020) have been developed beside tracer-based studies on the seaward side, but they require discharge measurements at the modelled location for calibration and validation.

While estimates of SGD into Kinvarra have been available since 1993 (Drew and Daly, 1993), they differ sometimes considerably, with assessments varying from ~10^4 m^3 d^{-1} during summer (Rocha et al., 2015) to 10^6-10^7 m^3 d^{-1} for annual projections (Cave and Henry, 2011). Most studies were carried out independently and provide figures that cover only short periods of time, and SGD is subject to tidal, seasonal and interannual variability.

Nevertheless, hydrogeological models, which aim to integrate discharge estimates over timescales beyond short-term (snapshot) assessments, require reliable quantification of SGD flow rates at matching timescales to ensure calibration and confidently offer predictive capability. Understanding the cause of discrepancy of SGD fluxes between different studies will ensure derivation of reliable annual water, carbon or nutrient balances for the system.

Here, we revisit past estimates of SGD for Kinvarra Bay, conduct new radiotracer (Rn, Ra) surveys, close mass balances under a range of different assumptions, and compare the results with those provided by hydrogeological models (McCormack et al., 2016). Our study aims to explain the difference between SGD estimates across different hydrological seasons and years. To this end, we first review the methods used to determine SGD into coastal areas from karst aquifers. We test the assumptions underpinning these methods using data collected in successive surveys of salinity, ^{222}Rn, ^{224}Ra and ^{223}Ra, and ancillary environmental monitoring data available for different groundwater level conditions. We then compare the results of disparate SGD flow estimates resulting from different tidal prism and hydrogeological models, radon and water mass balances, using the groundwater head in the nearby karst aquifer as an indicator of the hydraulic gradient driving the flow.

3.3 Site description

Kinvarra Bay in the west coast of Ireland is fed by a major karst network (Figure 12). The bay hosts significant mussel (*Mytilus Edulis*) and oyster (*Crassostrea Gigas*) aquaculture (Tully and Clarke, 2012; Marine Institute, 2019). Tourism is the main tertiary industry in the region and the largest employer (Gallagher et al., 2010), bringing a seasonal (higher during summer) peak influx of pollution that was transferred into the bay as sewage up to May 2017, when a wastewater treatment plant entered service.

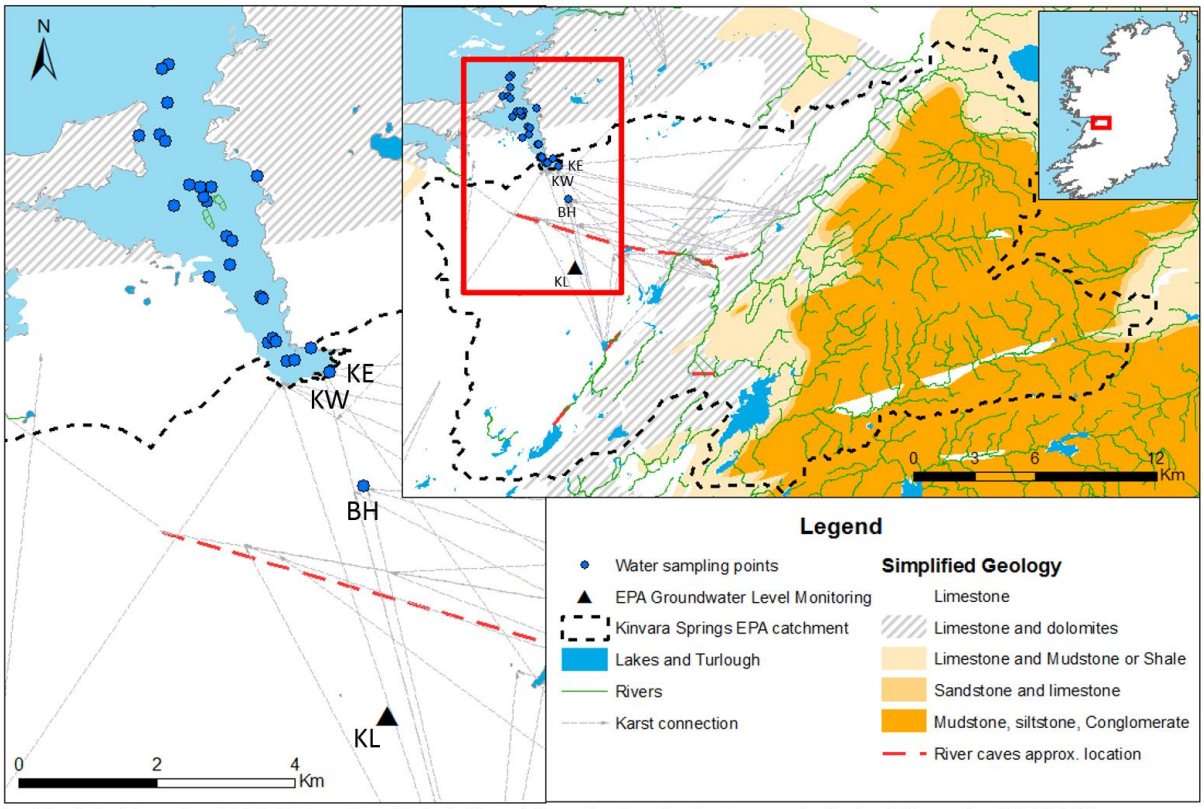

Figure 12: Location of water sampling sites in Kinvarra Bay and of the catchment feeding the two main springs of the bay, Kinvarra West/Arch (KW) and Kinvarra East/Castle (KE). "BH" mark the location of the borehole used in this study as representative of groundwater composition flowing to Kinvarra. Killiny Borehole (KL) is the location were the EPA monitor groundwater level continuously. The geology shown (Geological Survey, 2019) is grouped by main lithologies relevant for water circulation within the catchment. Grey lines connect points identified by previous tracing studies (Geological Survey, 2019) as linked by a karst network. The approximate location of a major cave network (e.g.: underground river) identified by cave exploration and surface features is shown in red and taken from Drew (Drew, 2003).

Groundwater inputs (5-30 $m^3 s^{-1}$ as per Drew, 2008) originate mainly from two springs located in the upper part of the bay. These drain a catchment of approximately 500 km^2, in which the lower basin is well-developed limestone karst that is partly fed by river water

draining an upper sandstone basin (Clare and Mcnamara, 2009; Morrissey et al., 2020) (Figure 12). Previous studies used different names to describe the two dominant springs in Kinvarra Bay: they are referred to as the Castle spring and the Arch spring (e.g. Cave and Henry, 2011; Smith and Cave, 2012) or as Kinvarra East and Kinvarra West (McCormack et al., 2014; Morrissey et al., 2020). According to Cave and Henry, (2011), the Arch spring is not perennial and is thought to drain shallower karst conduits. In contrast, the Castle spring, located next to Dunguaire castle is perennial and thus thought to drain a deeper karst network. According to McCormack et al., (2014): "Kinvarra West (KW) (..) serves as the outlet of a major, primarily allogenically fed, karst conduit network and Kinvarra East (KE) (…) discharges water from more diffuse/autogenic sources".

Following Cave and Henry, (2011) the Castle spring is perennial, fed by a deep karst network, and is located next to Dunguaire Castle. Thus the Castle spring as defined by Cave and Henry, (2011) is likely to be the spring marked as Kinvarra East on the map of McCormack et al., (2014). Furthermore, Cave and Henry, (2011) states that the Arch spring drains shallower sources. This also correspond to the description of McCormack et al., (2014) of Kinvarra West as fed mainly from "allogenic sources" (ex: river water from the upper catchment). According to McCormack et al., (2014), Kinvarra East drain 20%, from the catchment size, and is thus expected to represent a minor fraction of the total fresh water flow. Further modelling work by Morrissey et al., (2020) also consider that the majority of the flow from the catchment flows to Kinvarra West. Conversely, Smith and Cave, (2012), showed that under normal winter condition the freshwater source to the bay is 70% Castle 'type' source water and 30% Arch 'type' source. The cause for this apparent contradiction with the statement of Smith and Cave, (2012) may need to be investigated. For the purpose of this work, we will consider that Kinvarra East is equivalent to Kinvarra Castle and Kinvarra West is equivalent to Kinvarra Arch as defined by Cave and Henry, (2011).

Nevertheless, despite the distinct flow paths these two springs are connected (Drew, 2003; see also Karst connections in Figure 12). During summer, outflowing water is undistinguishable by radon or stable isotope signature (Schubert et al., 2015). The Irish Environmental Protection Agency monitors groundwater head at the Killiny borehole (KL, Figure 12) and groundwater quality at Loughcurra South borehole (BH, Figure 12).

3.4 Material and methods

3.4.1 Systematic review of past SGD estimates

Studies providing estimates of SGD flow rate in Kinvarra Bay using a range of different methods (Drew, 2008; Cave and Henry, 2011; McCormack et al., 2014; Rocha et al., 2015; Schubert et al., 2015) were reviewed. Groundwater flow into Kinvarra was then determined from the results of four bespoke sampling surveys that evaluated the reproducibility of SGD rates estimated with different approaches. In order to compare these with prior SGD estimates, all individual rates were referenced to the regional groundwater level at Killiny Borehole (EPA, 2020). This choice was supported by (1) tracer experiments (Drew 2003) and cave exploration (Boycott et al., 2003) show the Killiny borehole is less than 1km away from a network of conduits connected to Kinvarra springs (Figure 12) (2) no known pumping station is present in the direct proximity the well and (3) SGD estimated using salinity (Cave and Henry, 2011; Rocha et al., 2015), radon (Rocha et al., 2015) and hydrogeological modelling of the karst network (McCormack et al., 2014) were correlated with groundwater level at Killiny (e.g.: Figure 13 and Figure 15).

To compare our results with the output of the model of McCormack et al (2014) we sought an empirical relationship between their results (Figure 13b) and the groundwater level at the time of their study (Figure 13a). Typical relationships between flow and discharge require information on the karst network geometry, conduit roughness, size etc… which needs to be determined or calibrated. As the aim here was not to accurately model flow at a given time, but to model the general annual long term annual trend using the less assumptions possible for validation purposes, we used two alternative scenarios which required minimum assumptions and/or parameterization on the karst geometry. The first approximated the karst as an equivalent continuous medium and assumed a linear dependence on groundwater head derived from Darcy's law (Q=1.6H, Figure 13 b). The second approximated the karst as a medium with fractal properties following the method developed by Maramathas and Boudouvis, (2010). ($\mathrm{Q} = 1.1\sqrt{2\mathrm{g}(\mathrm{H} - \mathrm{T} - 1)}$ in Figure 13b), to derive flow rates from the net groundwater level (H-T).

Discharge depends linearly on hydraulic head only if the groundwater flow is laminar (Bear, 1979) and the karst is constrained within a relatively homogenous layer of limestone of constant cross-sectional area. In practice, as a first approximation karst can be approximated at large scale and for sufficiently long timescale outside of storm periods as equivalent continuous medium: For example, Debieche et al., (2002) observed in a phreatic karst aquifer a linear relationship between discharge and flow rates for 80% of a five year time series, periods with low flow rates outside of storms periods. The fractal approximation was shown to give good results to model the flow rate change with head in karst aquifers by Maramathas and Boudouvis (2010). The equation describes the karst system as a reservoir filled with porous material with fractal properties and does not require prior assumptions on the Reynolds number. The introduction of a correction factor to account for head losses by friction within the aquifer (-1) improved the fit. The two relationships produced a relatively narrow range of annual variability for the daily averaged flow (Figure 13b), so we use the first as a benchmark for comparison with other estimates of daily averaged groundwater flow. To obtain the total flow through Kinvarra springs (West and East) we note that 2 $m^3.s^{-1}$ (the flow value attributed by McCormack, 2014 for Kinvarra East) needs to be added to Kinvarra West flow values.

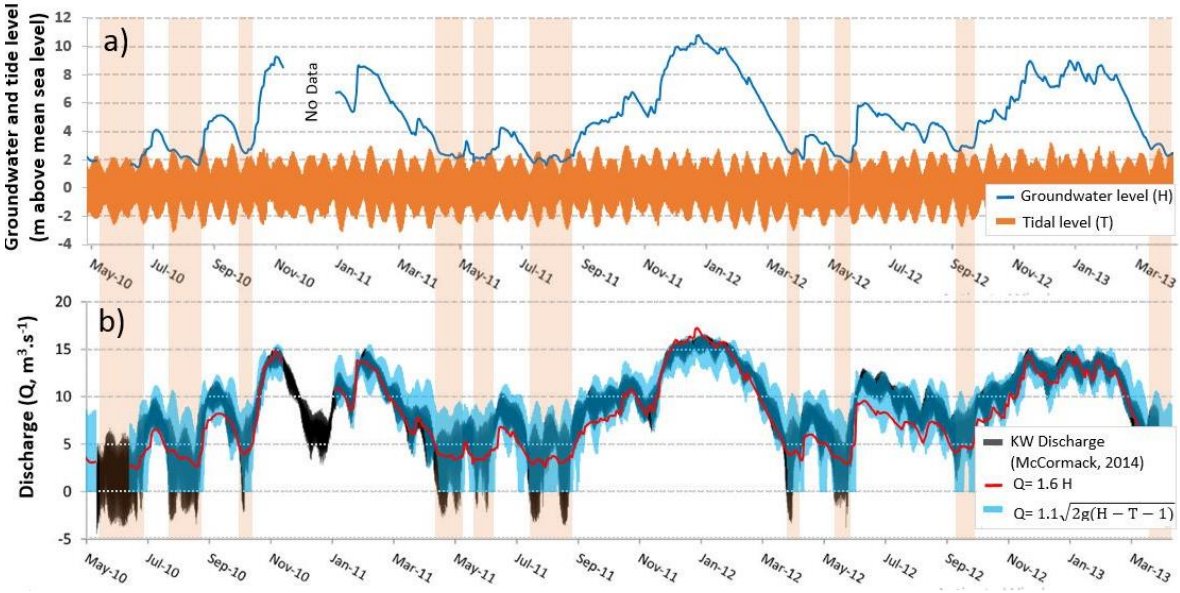

Figure 13: Compared seasonal variability of groundwater level (EPA) and modelled groundwater flow in McCormack, (2014). a: Groundwater level, measured at Killiny Borehole (EPA, 2020), and tidal level measured at Galway bay (Marine Institute, 2020). b: Modelled flow rate of Kinvarra west, and its relationship with groundwater level and tidal level. KW Discharge is taken from Fig 5 in McCormack 2014, (reproduced with permission of Elsevier). Q=1.6 H and Q=1.1√(2g(H-T-1)), are two distinct approximations of the annual variability of flow modelled by McCormack (2014), using groundwater level measured in Killiny Borehole (H in Fig 2a) and tidal level measured in Galway bay (T). g is the acceleration of gravity ($9.81 m^2.s^{-1}$). The first relationship assumes a Darcian flow in the karst system (approximate the karst as an equivalent continuous medium) to derive a linear relationship with groundwater level above mean tide level (H). The second relationship approximate the karst as a medium with fractal properties using the method developed by Maramathas and Boudouvis, (2010) to approximate the daily flow variability from (H-T), as an attempt to represent the effect of tide on the potential short-term variability. The addition of a term to account for head losses within the karst conduit between the main network of conduit and the spring (-1), improved the fit for the second relationship. Vertical light red areas highlight periods when the relationship between groundwater level and flow is the most affected by sea level fluctuations (groundwater level close or lower to high spring tide level and/or negative/low modelled flow in McCormack 2014). For KW Discharge and Q=1.1√(2g(H-T-1)), the thickness of the line is due to the daily variation of flow.

3.4.2 Fieldwork strategy

Variability of flow at Kinvarra springs is driven by groundwater level dynamics (Figure 13). Thus four surveys were planned to a) cover the local range of groundwater level oscillation (2m, 12-14 July 2018; 4m, 20-23 October 2018; 7.2m 25-28 January 2019; 9.4m, 06-08 April 2019), and b) collect tracer data within the bay during spring tides to ensure maximal tidal mixing. Each survey sampled water along the longitudinal axis of the bay by boat during spring tides and high tide (except October 2018 when samples were taken

from land) for the determination of salinity, ^{222}Rn, ^{224}Ra and ^{223}Ra and included the acquisition of 24-h time series of salinity and radon activity at selected locations, every 3 hours at least. Our objective was to characterize both spatial and temporal variability of bay water composition for each sampling period while limiting any possible bias due to non-homogenous flushing of the system by tidal mixing. During each survey, samples for ^{222}Rn were also taken in triplicate at the spring at low tide in locations directly after the discharge point and in a selected borehole connected to the main karst network feeding the bay. Spring radon activities at the spring were generally around 8 Bq L^{-1} except on the April 2019 survey, when significantly lower values were observed at 5.5±1.5 Bq L^{-1}. A new series of samples was taken on a different deep location of the spring and activities around 8±1 Bq L^{-1} were found again. As a precaution, activities measured during the same survey were used as an endmember in the radon mass balances as in Rocha et al., (2015).

Water samples from the bay were collected with a NISKIN bottle from 0.5 – 1 m depth and stored in sealed 250ml glass bottles for radon analysis. Rn in water was determined with a RAD7 monitor (Durridge, 2015) using the WAT250 protocol, with corrections for the time elapsed between sampling and measurement. Salinity was measured with an Aquaread® Aquaprobe, calibrated according to standard manufacturer protocol (Aquaread, 2013). Results were independently verified with a Carl Stuart Limited Cond197 i WTW electrical conductivity probe. Water column activities of ^{224}Ra and ^{223}Ra were determined after pre-concentration of natural radium levels (Moore, 1976) achieved by pumping a large water volume (60-100 L) at a low flow rate (1 L min^{-1}) through MnO_2 coated fibre cartridges (Moore and Arnold, 1996). After rinsing with Ra-free water and drying to a water/Mn fibre ratio of ~ 0.4-1.1 by weight (Sun and Torgersen, 1998) ^{224}Ra and ^{223}Ra activities were measured by Radium DEcay Coincidence Counter (RaDECC) (Moore and Arnold, 1996). At least three separate measurements were taken from each sample: immediately after collection, 7-10 days after the first measurement to improve the ^{223}Ra estimate, and after 25 days, to correct for ^{228}Th supported ^{224}Ra levels (Moore, 2007). The ^{227}Ac supported activity for ^{223}Ra, determined after 80 days for selected samples, fell within the uncertainty of ^{223}Ra quantitation. Depth was measured at each sampling location using a handheld sonar (Hawkeye Digital). When water was sampled from land, the representative depth was estimated from the mean depth of the local

bathymetric cross section derived from the 30m INFOMAR DTM (INFOMAR and GSI, 2019), considering the tidal height at the moment of collection.

3.4.3 Determination of water ages

Monsen et al. (2002) highlight the fact that in reality bays and estuaries are not flushed homogeneously and are rarely fully mixed horizontally. As a result, a water sample taken at any time within such a system includes freshwater with different travel times to the sampling location. This has important consequences for the closure of biogeochemical budgets of non-conservative elements such as radon or short-lived radium isotopes. Following Zimmerman (1988), Monsen (2002) use water age, defined as 'the time [a water parcel] has spent since entering the estuary through one of the boundaries', to describe this travel time. We determined water ages in Kinvarra using the solute $^{224}Ra/^{223}Ra$ activity ratios corrected for supported activity following Moore (2000):

$$A = \frac{ln\left(\left(\frac{^{224}Ra}{^{223}Ra}\right)_i\right) - ln\left(\left(\frac{^{224}Ra}{^{223}Ra}\right)_{obs}\right)}{\lambda_{224} - \lambda_{223}} \quad (2.1)$$

Where A is the mean water age (in days) at any location in the bay relative to a reference point (or mixing end member), $\left(\frac{^{224}Ra}{^{223}Ra}\right)_{obs}$ is the observed $^{224}Ra/^{223}Ra$ activity ratio (AR) at the sampling location, $\left(\frac{^{224}Ra}{^{223}Ra}\right)_i$ is the $^{224}Ra/^{223}Ra$ activity quotient at the radium source (here Kinvarra Springs), and λ223 and λ224 are the decay constants of ^{223}Ra (0.0608 day^{-1}) and ^{224}Ra (0.19 day^{-1}) respectively. This approach assumes that the radium activity ratios of the freshwater end member are constant during the survey period, and no significant inputs of new radium to the system occur within the water age profile (Moore, 2000). This approach was previously applied in Kinvarra Bay by Rocha et al., (2015) and showed to lead to reliable results for the system.

3.4.4 Calculating tracer inventories from transect data

Estimating SGD or fresh water inputs into a basin of restricted exchange usually involves calculating the inventory of a tracer element within the system (Luketina, 1998; Taniguchi

et al., 2019). The method chosen to determine the inventory is crucial because it strongly affects the result of mass balances based on measurements of the tracer. For example, the average of tracer concentrations at different sampling locations is the simplest path to estimate the tracer inventory in a bay or estuary, but this approach is only valid if water depth within the system follows a normal distribution. In natural systems the depth distribution of the submerged area does not usually comply with normality (e.g. Figure 14). As a result, point concentrations or depth distributions of elements in shallow, narrow areas will strongly affect averages, while only representing a small fraction of the whole volume. The concentration mean may thus lead to a non-representative inventory. Methods involving 2D or 3D integration with depth are always preferable.

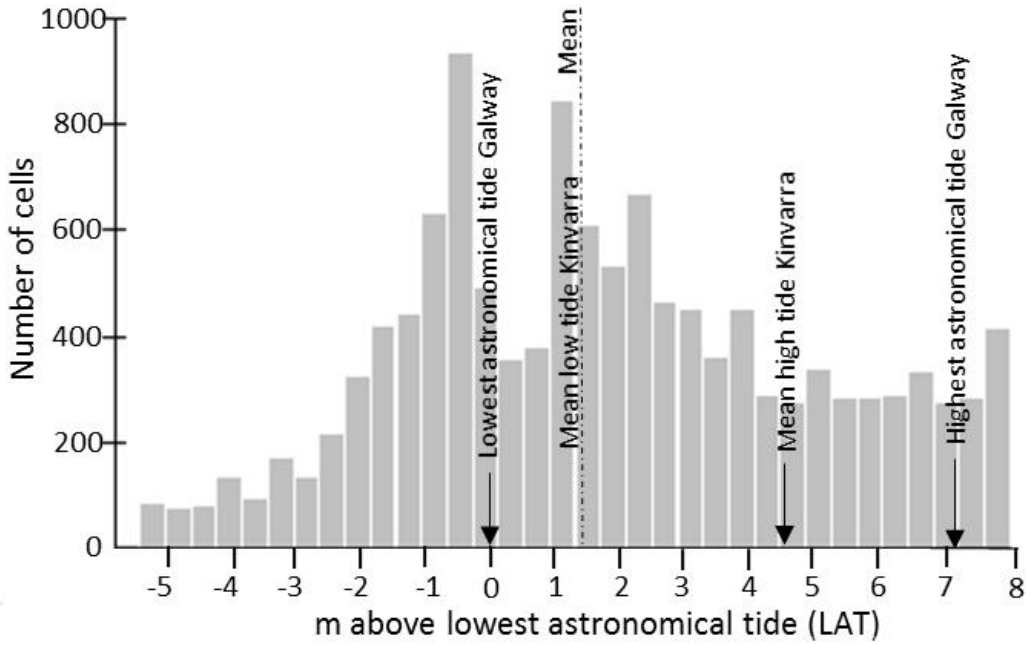

Figure 14: Frequency distribution of depth (determined using a Digital Terrain Model with 30 m resolution) for Kinvarra Bay, showing an asymmetric, non-normal distribution of depth throughout the system. Depths are expressed with reference to mean tide level. The right-hand bound of the horizontal axis corresponds to the approximate maximal spring tide level. Vertical texts show the depths corresponding to the mean tidal height in Kinvarra as reported by Rocha et al. (2015), and the maximum and minimum tide level in the nearby Galway bay (Marine Institute, 2020).

We used salinity, the most common indicator of fresh and saltwater mixing, to assess the effect of the most common approaches to calculate solute inventories when closing coastal mass budgets. Six ways to calculate the salt inventory were compared using data from our four surveys: (1) the average all the sampling point data, (2) the median of all sampling point data, (3) one-dimensional integration over distance, (4) two-dimensional integration over distance and depth, (5) three-dimensional integration using interpolated

salinity and bathymetric maps of the system and finally, (6) quasi three-dimensional integration by sample grouping into four areas of known volume (box modelling).

Methods 1 and 2 involved salinity measurements obtained for four successive transects. For method 3, salinity was plotted as a function of distance from Kinvarra spring, and the curve functions then integrated over the transect length to yield a depth-averaged inventory. For method 4, the local 'inventory' was determined by multiplying each salinity value by depth, inventories plotted as a function of distance, then integrated over the transect length and normalized by the bay's longitudinal cross-sectional area to determine the salt content of the system. For method 5, the salinity distributions were first interpolated using ArcGIS to create a raster of 30m*30m cells, the salinity for each cell then multiplied by the average cell depth (at mean tide), derived from a 30 m resolution bathymetry raster. The results were added, then divided by the bay volume to complete a 3D integration of salinity over the volume of the bay. Finally, in method 6, the bay was divided into four different areas (boxes) and averages of salinity calculated for each. Each mean was then multiplied by box volume. Resultant box inventories were added, and the total divided by the volume of the bay. The results of each distinct tracer inventory estimate were compared with reference to the change in salinity observed during a 24hour period.

3.4.5 Salinity-based estimates of freshwater inputs to the system.

Salt inventories in coastal systems yield multiple ways to estimate watershed freshwater contributions to the sea. Because of their relative simplicity, the most commonly used are the tidal prism mixing models developed from the seminal paper of Ketchum (1951). We tested four different tidal prism models to investigate how the way salinity data is used might affect the resulting estimate of freshwater input. The model used in Kinvarra Bay by Cave et al. 2010, derived from the segmented tidal mixing models of Dyer & Taylor (1973), was compared with three (Models A, B, C) tidal prism mixing models reviewed in Luketina (1998). All of these are only applicable to vertically well mixed systems at the scale of a tidal cycle (stratification can be present at low tide locally but most of the surface waters are mixed with deep waters during the rising tide).

Whether or not they are may be tested according to Schultz and Simmons (1957): if R = Qr T/P < 0.1, where Qr is the flow coming to the system (the maximum expected for Kinvarra is 30 m s^{-1} following Drew 2008), T is the tidal period and P the tidal prism (from $1.5*10^7 m^3$ for an average tidal cycle to $2.5*10^7$ m^3 for highest spring tide), then the system can be taken as vertically well mixed at the scale of one tidal cycle. For Kinvarra R = 0.08 for the mean tidal amplitude and R=0.05 for the highest spring tide under high discharge conditions, so we accept that the water column is well-mixed during a given tidal cycle even for high flow, and tidal prism approximations are reasonable to use.

3.4.5.1 Tidal prism Model A as per Luketina 1998.

The classic tidal prism model assumes that the volume of seawater, Vp, entering an estuary during flood tide is entirely of ocean salinity So, and that it is completely mixed with a corresponding volume of freshwater Vr flowing into the system measured over a tidal cycle. It further assumes that this quantity of mixed water is completely removed from the estuary upon ebb (Officer, 1976). As a result, the dilution of a steady source of freshwater by seawater in a coastal basin depends only on the tidal period and the tidal prism (Luketina, 1998). Effects of varying discharge on internal mixing of the system are thus ignored. By rearranging Equation 3 in Luketina (1998), and using Qr= Vr*T where Vr is the volume of freshwater flowing to the system over one tidal period (m^3.tidal $period^{-1}$), Qr the fresh water flow rate (in m^3 d^{-1}) and T the tidal period (in days), the flow rate of freshwater into an embayment described by this model is given by:

$$Qr = \frac{P\left(1-\frac{S}{So}\right)}{T} \quad (2.2)$$

With P the tidal prism volume (m^3), S the salinity of the estuary at high tide (kg m^{-3}), assuming a well-mixed estuary (here either taken from our 24-hour salinity time-series, or derived from the various inventory calculations explained in 3.4.4), So the salinity of the ocean (kg m^{-3}, taken here at 35 or equal to the marine end member).

3.4.5.2 Tidal prism Model B as per Luketina 1998.

Model B considers ebb and flood separately to derive a flow rate. It assumes that flow between the ocean and the estuary occurs in either direction for equal duration (Luketina, 1998). This will not be true if discharge has a significant effect on water exchange between

the embayment and the ocean. Because the residence time of water in the system is ~seven days during summer (Rocha et al., 2015), and our surveys showed that it was at least 3 days during other times of the year, we accept this as a reasonable first order approximation at the scale of 24 hours, to illustrate the difference with other estimates. By rearranging Equation 11 in Luketina (1998) we find:

$$Qr = \frac{2P(1-\frac{S}{So})}{T\left(1+\frac{S}{So}\right)} \quad (2.3)$$

3.4.5.3 Tidal prism model C as per Luketina 1998.

Model C extends B by considering changes to the duration of ebb and flood flows and variation in the level of flushing through the estuary mouth. It accepts changing discharge affects flushing. To do so, the model includes a return flow factor b to represent the fraction of water that had previously left the bay during ebb returning during flood tide. By rearranging Equation 26 in Luketina (1998) with $QrT/(\pi P) << 1$ we have:

$$Qr = \frac{2P(1-\frac{S}{So})}{T\left(1+\frac{S}{So}*\frac{1+b}{1-b}\right)} \quad (2.4)$$

The return flow factor can be estimated using equation 4 in Sanford (1992):

$$\mathrm{b} = 1 - \frac{\mathrm{V}_{mt}\mathrm{T}}{\mathrm{T}_f\mathrm{P}} \quad (2.5)$$

Where V_{mt} is the volume of water within the bay at mean sea level, T is the tidal period, T_f the freshwater flushing period and P the mean tidal prism. T_f can be calculated according to the fraction of freshwater method (Dyer and Taylor, 1973) as recommended by Alber and Sheldon, (1999) and used previously by Rocha et al. (2015). We highlight the effect on discharge estimates arising from inclusion or exclusion of the return flow factor on discharge estimates at Kinvarra using b= 0 and b= 0.86 as the mean determined for summer (low discharge conditions) by Rocha et al., (2015).

3.4.5.4 Tidal prism model as in Cave and Henry (2011).

Cave and Henry (2011) used two different equations derived from the tidal prism concept (Dyer and Taylor, 1973; B. Ketchum, 1951) to determine freshwater discharge to Kinvarra Bay. This adaptation was made originally to assess the variability of freshwater

inputs from time series of salinity data collected in the bay. It implicitly assumes that high and low water concentrations are represented by the range found within 24 hours at a single site and that the entire bay constitutes one well mixed volume. If no ebb water returns during flood tide, this model yields one order of magnitude higher freshwater inputs than all the other approaches considered here. Allowing for some return flow yields freshwater input rates in closer agreement with our other estimates. We therefore employ equation 2 from Cave and Henry, (2011) to estimate fresh water flows to Kinvarra here:

$$Q = \frac{S_{hw} - S_{lw}}{Max\ salinity\ of\ flood\ tide} * (H_{hw} - H_{lw}) * A_b \quad (2.6)$$

Where Q is the net volume of fresh water flowing into the system ($m^3\ d^{-1}$), S_{hw} and S_{lw} the salinity at high and low tide respectively (kg m^{-3}, derived from 24h data), H_{hw} and H_{lw} the tidal height (m, derived here from Galway bay data), and A_b the mean horizontal surface area of the bay (m^2).

3.4.6 Radon mass balance

We estimate SGD from radon measurements in Kinvarra in two different ways. The first uses the raw (uncorrected for water ages) radon in water activities to close a Rn mass balance for the system considering all the potential sources and sinks. These include degassing to the atmosphere, radioactive decay, water exchange with outer water bodies, diffusive sediment-water fluxes and total SGD into the system (Burnett and Dulaiova, 2003). However, water ages in Kinvarra Bay are spatially variable: between 0 at the water source and 8 days at the system boundary with Galway Bay (Rocha et al., 2015). This is not surprising - water ages in estuaries are spatially variable and tend to increase with distance from the main freshwater source (Monsen et al. 2002). As a result, a volume of water located further away from the radon source (here Kinvarra springs) will have lost more Rn to decay and degassing than water found closer to the springs. The system is therefore not well mixed spatially, and consequently, the effect of degassing fluxes on a given part of the bay will depend both on the age of water and on the wind conditions prevalent during a number of days (x) prior to the survey (where x is the age of water in

that portion of the bay). With water ages varying between 0 close to the springs and 8 days further out in the bay, a putative water sample composed of 100 percent SGD collected at the outer rim of the system, even with no loss to the atmosphere during transport by successive tides to its current location will include only a quarter of the radon it originally carried (half-life of radon is 3.82 days). In reality, the additional effect of degassing occurring during that period will result in much lower radon activities at the outlet to Galway Bay. Calculating radon inventories for the system without correcting for water ageing is likely to result in a large underestimate of the Rn inventory, and consequently of the total SGD fluxes into the system. Here we test an amendment of the often employed 'classical' steady state, whole system, radon mass balance approach to solve this conceptual problem. In this new approach, we correct individual radon activities for the degassing and decay occurring from the moment it left contact with the bedrock source before closing radon mass balances for the system.

3.4.6.1 Radon mass balance 1: no spatial variability of water ages.

For the first approach, if all inputs and outputs of radon are balanced over the flushing time of the system (i.e. steady state), we have (all terms in Bq m^{-2} d^{-1}):

$$Rn_{dif} - Rn_{dg} - Rn_{dy} - Rn_{net} + Rn_{adv} = 0 \quad (2.7)$$

Where Rn_{dif} is the diffusive radon flux across the sediment water interface (taken from Rocha et al., 2015); Rn_{dg} is the radon degassing flux, i.e., atmospheric evasion (estimated from wind speed and temperature using the equations of Macintyre et al. (1995) and Turner et al. (1996)); Rn_{dy} is the radon decay within the domain (estimated from radon inventory and the standard decay law); Rn_{net} is the net exchange fluxes across the mouth of the bay, estimated from the slope of the radon vs salinity curve, as described by equation 3 in Officer (1979), and Rn_{adv} the advective radon flux associated with groundwater discharge (unknown here). We use the equation of Officer (1979) conservatively, because Rn_{net} estimates extracted from 24h tidal cycles are overly dependent on each individual tidal cycle, and could lead to high uncertainty over periods scaled to the residence time of water in the system (taken as the oldest age measured

within). With this in mind, and following from equation 2.7, Q_{SGD}, the total SGD flux into the bay ($m^3\ d^{-1}$) is:

$$Q_{SGD} = \frac{(Rn_{dg}+Rn_{dy}-Rn_{dif})*A_b}{Crn_{spring}-\left(Crn_{mouth}-S_{mouth}*\frac{dCrn}{dS}\right)} \quad (2.8)$$

Where Crn_{spring} is the activity of the main radon source to the bay (here Kinvarra spring, Bq m^{-3}), CRn_{mouth} and Sal_{mouth} the radon activity (Bq m^{-3}) and salinity (kg m^{-3}) at the mouth of the bay and dCrn/dS the slope of the radon vs salinity curves at the mouth of the bay (Bq kg^{-3}).

3.4.6.2 Radon mass balance 2: accounting for ageing of water.

We improve on the previous mass balance by correcting radon activity data for the effect of degassing and decay as water ages toward the sea. To correct Rn in water activities for radioactive decay as water ages within the system we use the standard decay law:

$$^{222}Rn\ corrected\ for\ decay = {}^{222}Rn\ measured * e^{A\,\lambda_{Rn}} \quad (2.9)$$

Where A is the time elapsed since the sampled parcel of water left contact with the radon source (d), estimated from the Ra relative water ages (Equation 2.1) and λ_{Rn} the decay constant of ^{222}Radon (d^{-1}). Similarly, for degassing, we use the equation:

$$^{222}Rn\ Corrected\ for\ degassing = {}^{222}Rn\ corrected\ for\ decay * (1-K)^{-A} \quad (2.10)$$

Where K is the gas transfer velocity of radon (m d^{-1}) calculated using the equations of Macintyre et al. (1995) and Turner et al. (1996) for the period corresponding to the age of the water parcel preceding the measurement.

3.5 Results

3.5.1 Review of methods to estimate SGD in a karst environment

Most of the methods tested here yield flow rates that covary with groundwater level on land (Figure 15). However, exceptions exist (e.g. j, m in Figure 15), and all methods yield different SGD flow rate magnitudes. This is the case even when different methods

employ the same salinity (full triangles, Figure 15, h, i, j, f) or radon dataset (full squares, Figure 15, m, n).

We classify water balances and SGD estimates based on hydrogeological models as catchment-based approaches (Table 2). The resulting SGD rates are inter-comparable for this system because surface runoff is a minor component of the water balance in Kinvarra. The only exception is when groundwater level is at its highest, at which time surface drainage may represent a larger fraction of the freshwater input into the bay (Coxon and Drew, 2000). During summer, Rocha et al. (2015) found the ratio between total freshwater fluxes and SGD varied between 1.3±0.4 and 0.65±0.19. The catchment-based approaches reviewed here yield a relatively similar range of groundwater flows (Figure 15, b, k). This consistency suggests that the range of SGD rates derived from these methods is reproduceable if the catchment limits are accurate and spatial resolution of net rainfall estimates are sufficient to represent the actual rainfall distribution in the models.

Tidal prism models (Figure 15, c to j) assume that the bay is well mixed vertically at the scale of a tidal cycle (assumption 6, Table 2). In addition, radon (Figure 15, m, n) and radium mass balances require accurate identification of their main source into the system, both in location and magnitude (assumption 12, Table 2). Assumptions 6 is common to all tidal prism methods applied here and assumption 12 is common to all radon mass balances methods analysed here. Consequently, differences between different methods based on salinity or between different methods based on radon are not likely to be due to these two assumptions., so these are not analysed further here. Other pre-requisites to estimate SGD flow rates are three-fold: (1) inventories of the tracer of choice are calculated in a manner that is physically representative of the system (assumption 5 in Table 2), (2) exchange of water across the outer boundary of the system is calculated in a realistic fashion (assumption 7-11, Table 2), and (3) mass balances based on radioactive tracers, which are non-conservative within the time-scale of water retention within the system (e.g. ^{222}Rn, ^{223}Ra, ^{224}Ra) have to account for the effect of ageing water (assumptions 13-15 in Table 2). We show next how choices made within this assumption framework explain the differences shown in Figure 15.

Table 2: Review of methods useable to estimate total SGD and fresh SGD flowing to a system affected by a karst aquifer. The assumptions of each method are listed with numbers

Type of approach	Methods used for flow estimation	Reference for Kinvarra Bay	Assumptions/conditions for it to lead to a realistic estimate of the flow
Direct flow measurement	Direct measurement of localised flow (e.g. karst conduit)	(Drew, 2008)	(1) Method usually gives a minimum value as measuring all main springs and flow is rarely feasible.
Catchment based approach	Water balance using rainfall/ETP	(Cave and Henry, 2011; Schubert et al., 2015)	(2) Catchment size is known (3) Rainfall/ETP data is sampled at scale representative of the spatial variability of the catchment (altitude range, rainfall patterns).
	Hydrogeological model	(McCormack et al., 2014)	(2), (3) (4) Preferential flow pathways/storage (e.g. turlough) of the aquifer and their physical characteristics are known, model parameters can be calibrated using flow and water level data set capturing similar timescales than the model.
Salinity derived estimate (Tidal prism type of method)	Tidal prism A, classical tidal prism method. (Luketina, 1998)	This study (**Eq. 2.2**)	(5) Measurements and method used to derive inventories are representative of real variability in the bay. (6) Bay is well mixed (relatively small). Valid if R=QRT/P< 0.1 (Schulz and Simmons, 1957). (7) Water is completely removed on ebb tide, no return of water on flood tide.
	Tidal prism B. (Luketina, 1998)	This study (**Eq. 2.3**)	(5), (6), (8) Ebb and tide of equal time. (9) Salt crossing the ocean boundary over one tidal cycle is 0. Not valid if the freshwater flow is large enough to change the salinity of the bay (river or freshwater springs).
	Tidal prism C. (Luketina, 1998)	This study (**Eq. 2.4**)	(5), (6), (10) Consider the effect of discharge by allowing to consider some water returned in the next flood tide with the introduction of a return flow factor b.
	Tidal prism (Cave and Henry, 2011)	(Eq 2 in Cave and Henry, 2011), (Guerra et al., submitted) This study (**Eq. 2.6**)	(5), (6), (11) Allows inclusion of some water returned during the following flood tide by using the maximum salinity during the flood tide as reference.
Radon derived estimate	Radon mass balance ignoring spatial variability of decay and degassing due to change of ages within the system.	(Rocha et al., 2015) This study (**Eq.2.8**)	(5) (12) Source end member is known dominant source of solute is known for the bay. (13) The effect of the spatial variability of ages on radon decay and degassing can be ignored.
	Radon mass balance corrected for spatial variability of decay and degassing due to change of ages within the system.	This study (**Eq. 2.8-2.10**)	(5), (12) (14) Valid if radium derived water ages used to correct for age derived spatial variability of decay and degassing are representative of the actual water ages in the system.
Radium derived estimates	Simple mass balance, ignoring spatial variability of ages and depth.	Not applied here (assumption 16 not verified)	(5), (12) (15) The effect of the spatial variability of ages on radium decay can be ignored. (16) Fluxes from suspended sediment and bottom sediment affect inventories in a homogenous way.
	Considering spatial variability of depth and water ages.	To be developed.	(5), (12), (14)

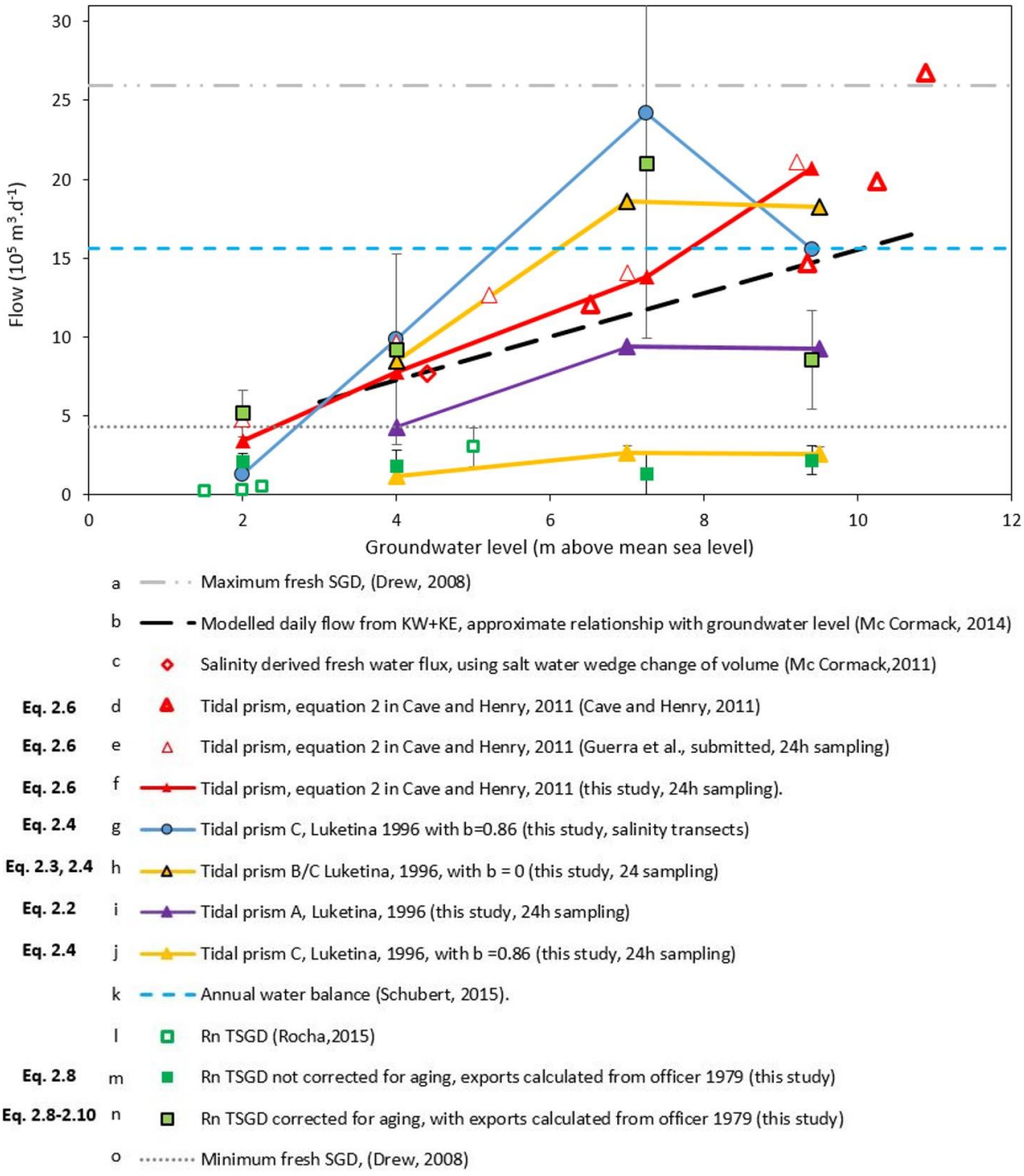

Figure 15: Compared estimates of SGD flow rates as a function of groundwater level in the karst aquifer connected to Kinvarra Bay. Each estimate is related to the groundwater level at Killiny Borehole (EPA, 2020) in the period of the surveys. Studies where the date of measurement was unknown are shown with a line covering the range of likely groundwater level during the sampling or study periods. Equation number for each method are shown on the left part of the legend. For estimates based on salinity the type of data on which the study is based (transect of salinity or measurement of changes on a given part of the bay) is shown in parenthesis.

3.5.2 How tracer inventories are calculated affects SGD estimates

Tracer-based methods to determine freshwater or SGD flow into a coastal system depend on mass inventories (Assumption 5, in Table 2). However, in most systems with a significant source of solute such as a river or a spring the spatial variability of this solute is often much larger than the measurement uncertainty. The way point measurements throughout these systems are used to estimate the total inventory of a given solute at any given time is a key aspect of biogeochemical budgets.

Table 3 illustrates the results of the comparison between six methods of estimating whole system inventories within Kinvarra Bay using the same salinity dataset. Methods are ordered by increasing complexity. The last column lists the average inventory resulting from each approach and associated standard deviation, with salinity observed at high tide for reference.

	Salinity inventories from transects (kg m^{-3})								High tide salinity average of 24h samples
	Average	Median	1D integral	2D integral	3D integral	3D integral using boxes	Average of all previous	Standard deviation of all previous	
Summer 2018 (07)	29.9	29.1	27.2 ±0.2	29	28.6	29.8	28.9	3.8%	35.7
Autumn 2018 (10)	24.1	27.9	24.1 ±0.2	23.8	26.3	28.9	25.8	8.5%	28.6
Winter 2019 (01)	15.3	17.6	17.6 ±0.1	22.9	20.1	20.5	19.0	14.2%	28.5
Spring 2019 (04)	24.5	27.1	25.7 ±0.2	35	29.3	31.0	28.8	13.4%	30.2

Table 3: Effect of the method used to integrate high tide salinity transects on the inventories used to calculate SGD estimates from transect data. Uncertainty shown is one standard deviation. Combined averages and uncertainties are calculated for the six methods used to assess inventory from transects to highlight the effect of method choice on the final inventory (method choice induces here a standard deviation of between 4 and 14% even for a well-known parameter like salinity where uncertainty is <0.5%). High tide salinity observed during 24h sampling is shown in the last column for comparison.

A series of insights arise from the results. Firstly, with the exception of summer, when freshwater inflow is lower, the salinity inventory derived from the mean or median of available data are consistently lower than those resulting from spatial integration of the same data. For example, the average and median of cross-system salinity for the winter 2019 survey are respectively 26 and 15 percent lower than the inventory calculated by 3D

integration (Table 3). An average by definition assumes normal distribution of depths in the system, so the true depth distribution is ignored. When data are not normally distributed the median is used instead of the mean to describe the central tendency of the dataset. The difference between the median salinity and the inventory resulting from 3D integration is less than for that between the latter and the mean (Table 3), but the median still overestimates the effect of springwater inputs during high discharge surveys by comparison to more sophisticated approaches. As shown in Figure 14 shallow areas predominate in Kinvarra, like in many coastal bays, contributing to an asymmetric distribution of depths in the system. An elemental inventory using measures of central tendency is likely to be disproportionally affected by any solute source located in the shallow portions of the basin, compared to methods that either fully or partially consider the actual spatial distribution of depths (e.g. 2D integration or 3D integration). We observe this for surveys conducted for all other than low discharge periods.

Secondly, even when the uncertainty associated with a given inventory estimate is as low as 0.5 % (e.g. inventories of salinity derived from 1D integration, Table 3), the choice of one method over another by itself leads to much larger uncertainties (cf. STDEV in last column, Table 3). This likely results from the way the geometry of the bay is considered in the different calculations of inventories. While averaging ignores the effect of variance in distance and depth between sampling points on the resulting tracer inventory, the 1D integration considers the effect of distance but ignores depth distribution, the 2D integration considers the effect of depth and unequal distribution of sampling points along the length of the sampling path, and the 3D integration considers the actual changes of distance and depth within the system.

Finally, regardless of the method used, the high tide salt inventories derived from transect data are consistently lower than the values drawn from 24h measurement time series (Table 3). As a result, using transect data (a Snapshot approach) to support SGD quantification is likely to yield consistently larger SGD rates than when a Eulerian approach is employed, i.e., using the same budgeting method on data resulting from 24h time-lapse sampling at point locations. The observations in Figure 15 confirm this: for tidal prism model C, assuming a return flow factor of b =0.86, the SGD magnitude drawn from a measure of the salinity inventory taken from transect data (Figure 15 g) is three to four

times higher than that produced by processing a 24h time series, all else being equal (Figure 15 h).

3.5.3 Basin mixing is spatially and temporally heterogeneous

The salinity and water age profile at high tide (Figure 16) show that the volume of fresh SGD stored within the bay is highly heterogeneous in space. This is accentuated by the low salinity, mostly low water age plume in the inner bay. In July 2018, when groundwater level was the lowest, the plume of water with salinity <10 was constrained to the immediate vicinity of Kinvarra springs, but in January 2019, when groundwater level was high, it covered most of the inner half of the bay (Figure 16). Our first three surveys, carried out when groundwater level ranged between 2m and 7m, showed this low salinity plume extended further out into the bay with increasing groundwater level. However, when groundwater level was highest (9.7 m), this correlation stopped. At this point the water ages within the bay were much higher than observed during the other surveys and were more heterogeneous in the outer bay. This suggests that the circulation patterns driving water exchange between Kinvarra and Galway Bay are also temporally and spatially variable.

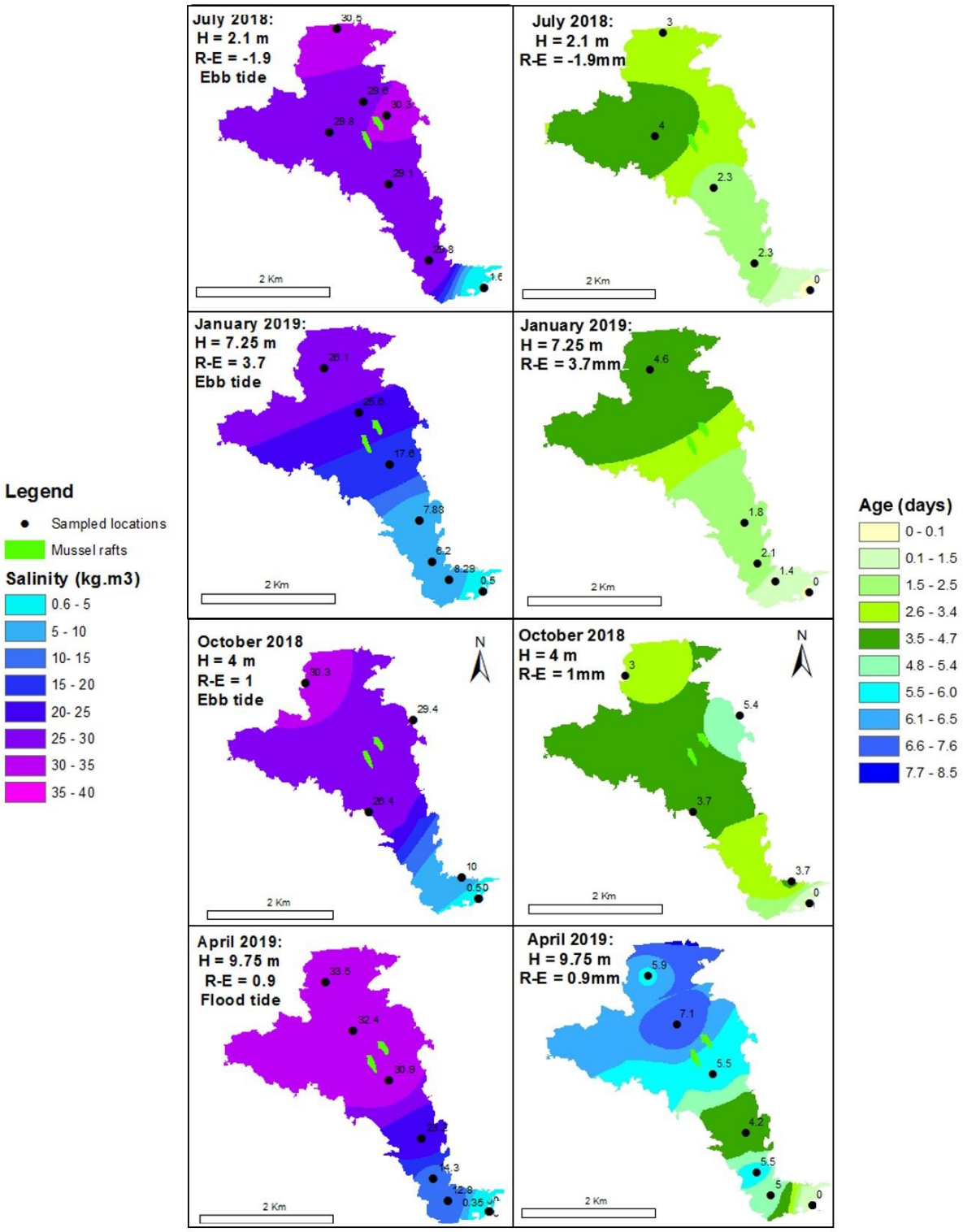

Figure 16: Interpolated maps of water ages (estimated from $^{224}Ra/^{223}Ra$) and salinity in Kinvarra Bay. For each interpolation the date, the groundwater level (H), the averages and net rainfall (R-E in mm) during the ten days leading to each survey are shown on the upper left corner. The tidal stage at which sampling was carried out is also specified.

This will also affect SGD quantification by radon, radium or salt mass balances, if the internal circulation pattern is assumed equal for all attempts, irrespective of season or freshwater discharge. How we accept the water moves across outer system boundaries (Assumptions 7-11, Table 2) is particularly important for tidal prism models (eqs. 2.2-2.6). This is not considered in the methods reviewed here (tidal prism A and B, Figure 15 I and h), or described either by an empiric modification of the tidal prism model (Figure 15 d, Cave and Henry, 2011) nor by the introduction of a return flow factor b (model C, in Figure 15 g, h, j).

It is however possible to reconcile all different estimates of discharge within one order of magnitude difference by considering the mathematical descriptor of the water exchange through the outer system boundary. We show this using our 24h timeseries (Figure 15 f, h, I, j). Models that seem to perform best toward internal consistency (i.e., results match at least one other method using another tracer) consider the return flow into the bay in some manner (Figure 15, f, h, j). When the groundwater level rises above 4m, applying model C with no return flow factor (Model C with b = 0, Figure 15 h) leads to SGD estimates that are consistent with catchment water balances (Figure 15k), modelling (Figure 15 b) and discharge based on the tidal prism derivation of Cave and Henry (Cave 2011, Figure 15 d, e, f). On the other hand, using the same dataset with a return flow factor of b= 0.86 leads to lower SGD estimates. These are consistent with radon mass balances uncorrected for ageing water (model C with b = 0.86, Figure 15 j) and close to previous estimates derived from radon and salinity under low groundwater level (low flow) conditions (Figure 15 l). When longitudinal transects are used to determine inventories (Snapshot approach) and include data collected from the inner part of the bay in the calculations, the effects of the inclusion or not of return flow are different. In this case, b=0.86 in model C leads to high flow estimates (Model C with b = 0.86, transects Figure 15 g) now consistent with the annual catchment water balance (Figure 15 k), modelling based on rainfall or groundwater level (Figure 15 b) and estimates based on Cave derivation of the tidal prism approach (Figure 15 d, e, f). Methods to estimate the SGD flow rate based on 24-hour time-series (Eulerian approaches) can thus underestimate the effect of retention areas on return flow, and thus lead to lower full system return flow factors than those suggested by Snapshot approaches. The effect of retention areas on water age distribution throughout the system is visible in

Figure 16, with most of the bay showing ages older than 3 days. If this lack of uniformity in water age is ignored by using 24h data from a single site similar SGD flow results as those arising from the use of transects for inventories (Figure 15 g) might be obtained, but with different insights regarding the return flow factor (b=0 for model C using 24h data, in Figure 15 h). SGD flow values derived from Eulerian surveys thus only account for freshwater in sections of the bay close to the sampling point that are fully mixed, and do not necessarily include SGD retained elsewhere for longer periods. Transect (Snapshot data) are in that sense less sensitive to this problem (Figure 15 g).

3.5.4 Water age profile and budgets of non-conservative solutes

SGD flow estimates obtained from radon mass balances are strongly affected by the way the heterogeneity of water ages is accounted for (eq. 2.8 vs eq. 2.8-2.10, Figure 15 m and n). Closing radon mass balances without correcting for the ageing of water within the system yields lower SGD discharge (Figure 15 m) with lower sensitivity to groundwater level (Figure 15, estimate m). Accounting for the spatial distribution of water age leads to more realistic results during higher groundwater level periods, up by a factor of 4 to 8 on the alternative (Rn SGD corrected for age variability, Figure 15 n). These approximate the fresh SGD estimates obtained by catchment-based methods (annual water balance, Model KW, Figure 15 k and b). This closure of the gap breaks down however when groundwater head raises above 8 m, radon-driven SGD estimates corrected for ageing water (Figure 15 m) fall to about half of SGD calculated by catchment-based approaches (Figure 15 k and b), the tidal prism model C with b=0 (Figure 15 h) and the Cave and Henry tidal prism approach (Figure 15 d-f).

3.6 Discussion

Our observations illustrate the importance of inspecting the assumptions that support mass balance models used to estimate SGD in coastal systems. They also underscore the value of intercomparisons between hydrogeological and oceanographic SGD assessments, as highlighted by Burnett et al. (2001). A cross disciplinary approach allows better

understanding of the temporal variability of flushing and the dynamism of elemental inventories in coastal systems due to changes in freshwater discharge. In turn, this allows the validity of priors to the application of catchment and tracer-based approaches to be tested, and consequent development of improvements to account for system characteristics. Our intercomparison identifies a series of critical points that require attention when estimates of SGD discharge are sought from tracer mass balances in a surface water basin. These are summarized in Figure 17 and discussed in detail below.

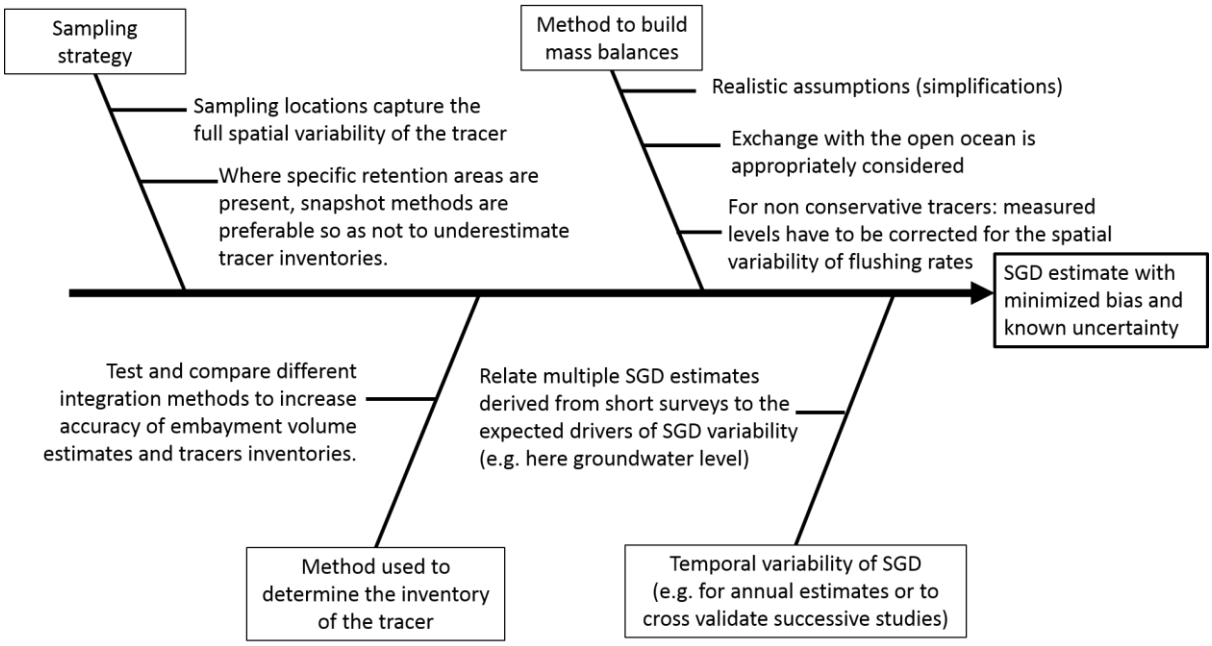

Figure 17: Research decisions leading to reproduceable tracer-based SGD estimates with known, minimized uncertainty and bias.

3.6.1 Sampling strategy

SGD estimates based on snapshot sampling (transects) of a tracer may be consistently higher than when Eulerian time series of the same tracer are used in Kinvarra Bay. A choice between Snapshot or Eulerian datasets could also yield different values of the return flow factor during spring tide (section 3.5.2). Water from Kinvarra springs is preferentially retained in upper Kinvarra Bay for several tidal cycles at least part of the year (Rocha et al., 2015). During these periods, it is less likely to be sampled by 24-h tidal cycle measurements in a single location in the outer part of the bay, and when this happens SGD is likely underestimated. The effect is observed here during spring tide, so is likely to

be larger during neap tide – this is supported by Gregory et al. (2020), who show that the flushing of the inner bay is minimal during these periods.

Significant spatial variability of water ages is also observed, both along and across the length of the bay, which may be explained by the fact that exchange with Galway bay is not homogenous, and rather occurs through an internal gyre, as previously observed (Rocha et al., 2015). This gyre, when present, would accelerate exchange with Galway bay and result in the significant addition of older, more saline and phytoplankton rich waters to the system. This is also consistent with independent findings (Fig. 3 in Gregory et al., 2020).

Inclusion of a measure of both spatial and temporal variability of the tracer of choice seems thus necessary to limit the potential bias introduced in mass-balance approaches by spatial heterogeneity of residence times. Long term estimates of SGD based on continuous tracer measurements in a coastal system should thus involve the synchronous determination of tracer concentrations over the area covered by the system to account for differences in water residence time (e.g. conceptual model on Figure 18). A more frequent application of remote sensing (McCaul et al., 2016; Wilson and Rocha, 2014), or further development of small, low cost sensors to evaluate the spatiotemporal variability of any tracer in combination with the methods tested here may be advisable to avoid bias of SGD quantification or other mass balance-based approaches. Such a multi-pronged approach would facilitate the determination of system characteristics and limit the mismatch between conceptual assumptions underpinning tracer inventories and the reality on the ground.

3.6.2 Development of SGD tracer inventories

We show that the choice of method employed to calculate the inventory of a tracer could have a significant effect on the results and hence on the final SGD figure. Our comparisons highlight the importance of considering the basin geometry and the spatial variations of water age when calculating inventories from transect data in real world aquatic systems. Since solute inventories are so crucial to coastal oceanography and biogeochemical studies, it also seems important to test the effect of ignoring depth

frequency distribution before using measures of central tendency or other simplified methods to estimate solute amounts in a water basin. Testing and comparing estimates from snapshot survey and from continuous measurement locations may be a way to test the effect of method selection on the final SGD estimates (e.g. conceptual model on Figure 18). This type of approach used in the early stage of projects could help to find a balance between ease of calculation and representativeness. Testing different calculation methods as explained here seems to offer a potential way to test for consistency. Where a sufficient number of data points are available, estimating the uncertainty of a given interpolation by kriging may also be promising (e.g. Murphy et al., 2010).

3.6.3 SGD estimates and spatial variability of water ages

Spatial variability of water ages has a strong effect on SGD estimates based on non-conservative tracer solutes (such as radon or short-lived radium isotopes). Indeed, as a water parcel is transferred from its source in the watershed to the open ocean, time elapses and the effect of internal reactions and mixing within the system on water composition accumulates. Ignoring the biogeochemical history of the water when estimating SGD based on Ra or Rn mass balances can lead to large underestimation of degassing and decay losses. In systems where large water age inhomogeneities are observed (e.g. conceptual model on Figure 18), this will result in a large underestimate of SGD fluxes. We suggest a method based on Ra ages to account for the spatial variability of residence time, applicable in systems where the assumptions of the Ra age model are valid (Moore, 2000). Where they are not, an alternative path, although at greater cost and time requirements, is to develop hydrodynamic models or more simply, employ drifters (e.g. Pawlowicz et al., 2019) to assess the extent of the spatial variability of water ages or residence times in order to produce more accurate mass balances of non-conservative elements.

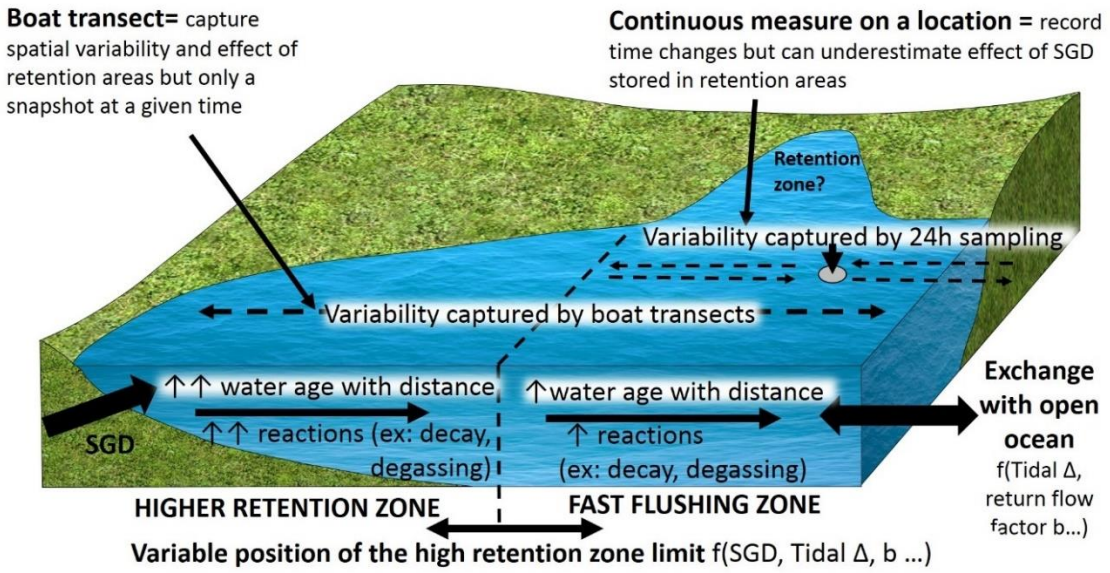

Figure 18: Effect of spatiotemporal changes of water ages and exchange rate on mass balances

3.6.4 Temporal variability of SGD composition and flow rate

SGD rate estimates for Kinvarra Bay correlated with groundwater level measured in Killiny Borehole, our reference well connected to the phreatic karst conduit feeding Kinvarra springs, with few exceptions. This implies that groundwater level measured in a location connected to a preferential flow pathway such as a series of karst conduit is a useful indicator of the potential variability of SGD rate.

Above 8 m of hydraulic head, large differences were found between SGD estimates derived from radon mass balances (Figure 15 m) and all other methods of assessing SGD, i.e., catchment-based (Figure 15 k and b) and tidal prism models (Figure 15 d-f, h). This suggests either (1) that a larger fraction of groundwater flow into the sea may occur via the surface pathway, or (2) groundwater is in greater contact with the atmosphere as groundwater recharge increases and hydraulic head overcomes the 8 m mark, enhancing radon degassing. The second hypothesis is consistent with Coxon and Drew (2000), who found a greater level of groundwater-surface water interactions occurred in the area during periods of higher recharge, with groundwater-fed lakes (turloughs) expanding in volume and area and localized flooding becoming a problem. This view is also supported by our estimates of SGD based on salinity of the bay (Figure 15 c, d, e, f, g, h). These were higher than McCormack's (2014) model predictions when hydraulic head increased above

4 - 6m (Figure 15 b), and the difference between model and tracer-based SGD discharge increased as groundwater level increased. The trend implies that surface pathways become more important for freshwater discharge into the bay as groundwater levels increase in the catchment. Notably, this shift can be detected by salt balance approaches, but not by radon budgeting, since Rn degassing will be stimulated by groundwater-surface water interaction, and water contact with the surface of Rn emanating rock will be reduced by increased volumetric storage and augmented groundwater flow rates driving lower residence times within the aquifer matrix. Maps of overland flooding caused by high recharge of the karstic network have been published recently (Morrissey et al., 2020). Such flooding is likely to be accompanied to a greater contact time of groundwater with the atmosphere, which further support our thesis.

We strongly advocate for caution when conducting radon mass balances during periods of high flow to determine SGD from karst networks into surface water bodies. Higher discharges are driven by higher hydraulic heads and imply a larger volume of the karstic network is taken by the groundwater body. A larger storage and higher discharge yield less surface contact between the flowing groundwater and the Rn-bearing aquifer matrix, since the volume/surface area ratio increases, but also mean that the residence time of water within the aquifer can decreases, which also diminishes the Rn-accumulation potential of the groundwater.

On the other hand, because of the nature of karst, high flow periods also offer greater opportunity for enhanced groundwater-surface water interactions prior to discharge into the sea, which increase degassing of Rn prior to the dilution of groundwater by seawater.

The time of contact between water and the aquifer rock can be much shorter in conduits and fractures than in primary porosity of the aquifer or in sediments above or inside karst systems. Steady state equilibrium radon activity takes a few weeks in porewater to be established. Thus, because of their faster flow conduits are more likely to contain Radon activities below equilibrium than water from the primary porosity or poorly connected fractures. In the karst conduits of Kinvarra catchment, flow rates between 60 and 1000 m/h have been measured (Drew, 2003). Consequently, water that has been in contact with the atmosphere inside a turlough sufficiently close from Kinvarra springs is likely to have Rn

activities lower than equilibrium activities if it went through a well-developed karst conduit to reach Kinvarra springs (half-life of Radon is 3.82 days). For example, the nearest turlough from Kinvarra spring is located in Loughcurra South, 1.8 km inland and was observed to be full during our winter survey. If we assume that a conduit with similar flow rates than observed by Drew, (2003) is present between this turlough and Kinvarra springs it could take between 1.3 days and 2 hours for a water parcel coming from the Loughcurra South turlough to reach Kinvarra springs, thus much lower than the time required to reach equilibrium Radon activities. On the other hand, the ^{226}Ra content of the aquifer matrix may be spatially variable. Radium can coprecipitate and be preferentially adsorbed to specific sections of the aquifer matrix, for example in metal oxides, common in cave surface, or in clay and organic matter rich sediment, which can accumulate in karst conduits. These may also contribute to a faster increase of radon activities in karst conduits and may balance the effect of variable contact time. This may explain why the Radon activities in spring waters taken directly from the discharge point were relatively stable in this study. On the other hand, waters coming from a deeper conduit or from parts of the aquifer further away from the main karst conduits are more likely to contain Rn activities closer from equilibrium.

Finally, the variable density occurring when groundwater mixes with sea water may also lead to more complex patterns than a simple groundwater/head relationship as presented here. This type of variability would require measurements of discharge and salinity at spatial and temporal higher resolution to be characterised. In this work, only changes of salinity of a few units in the spring were observed however, which does not suggest that density effects are very large.

3.7 Conclusion of Chapter 3

We test the most common methods employed to estimate SGD to coastal areas under different discharge conditions in a real-world system, evaluating different mathematical assumptions for the calculation of partial flux terms in mass balance expressions. Our observations show that everything else being equal, the choice of method to assess SGD and the sampling strategy employed to collect relevant tracer data has a large impact on the magnitude of ensuing SGD estimates. These artifacts created by method choice are,

in order of importance, caused by a) how exchange of water between the system and the outer ocean reservoir is described to estimate tidal exchange in mass balances, b) whether the spatial variability of water ages along the net water flow direction is taken into account when mass balances are closed if non-conservative elements are used as tracers of SGD, and finally, c) how representative is the estimated inventory of the tracer solute within the domain of interest, making both the sampling strategy and the method employed to arrive at this figure determine how realistic the outcome is.

Given the high spatial heterogeneity of water ages in real-world systems, including the existence of retention areas that delay flushing of coastal waters toward the ocean, we show that the option for either Snapshot or Eulerian tracer data collection significantly impacts ensuing SGD estimates. Continuous measurements of the concentration of a tracer at a fixed location, if the choice of location is away from an area of higher water retention will underestimate SGD to the system and overestimate its flushing rate. This is particularly relevant for non-conservative tracers and during periods of high discharge, when the system tends to be less well mixed. Spatial awareness of the distribution of the tracer (obtained through a Snapshot sampling approach, i.e., sampling transects for the tracer of choice along the net flow axis) is necessary to characterize de spatial variance of tracer concentrations and, most importantly, the water age profile of the system along its net flow axis. The water age profile can be determined using Ra isotopes. Once this is available, the effect of physical processes that determine the concentration of a tracer along the main water flow path (in the case of Rn degassing and decay) can be corrected for. This approach yields SGD magnitudes that are highly consistent with those obtained by other approaches at any given time, including hydrogeological models and conservative tracer budgets, as well as with those terrestrial drivers of discharge that induce seasonal variability of SGD discharge, represented here by groundwater head on land. These findings are useful to improve the biogeochemical budgets of non-conservative elements in coastal areas of restricted exchange more generally, and SGD quantification in particular.

Acknowledgments

This publication is a result of research supported in part by a research grant from Science Foundation Ireland (SFI) under Grant Number 13/RC/2092 and co-funded under the European Regional Development Fund and industry partners of the Irish Centre for Research in Applied Geosciences (iCRAG). Maxime Savatier was supported through an iCRAG PhD fellowship (TP GW3.2PhD5), co funded by Science Foundation Ireland (SFI) and the European Union. We thank Dr Jan Scholten from Kiel University for his advice on radium analysis, Maria Teresa Guerra, Jennifer Murphy, Gennaro Scarselli and Meabh Hughes for their assistance in field work. We are also grateful towards Mr Rainer Krause, for all the help provided during surveys.

Note: The current version of this paper was accepted for publication to Journal of Hydrology, with minor reviews, after benefiting from reviews and suggestion from two anonymous reviewers. Minor reviews may have been carried out during the last review phase.

4 PAPER B: Seawater recirculation component of SGD from a karst aquifer, determined using radium, and its effects on the biogeochemistry of a small bay.

Keywords: Submarine Groundwater Discharge, Seawater recirculation, Radium, Hydraulic gradient, Nutrient inputs, estuaries.

4.1 Abstract

Recirculation of seawater within sediment and aquifers are essential pathways for solute fluxes between coastal ecosystems. As such, they influence the timing and magnitude of algal blooms and ecosystem changes in coastal areas. Here we give a qualitative assessment of the magnitude of saline submarine groundwater discharge (saline SGD or recirculated SGD) on a coastal karst system previously considered to be dominated by freshwater inputs, using a combined geochemical methodology (^{224}Ra and ^{223}Ra) and one derived from the equations of Schneebeli. Ra isotopes activities were larger in the bay during spring tides when groundwater level was below six meters than when groundwater level was above six meters. The variations of the Ra activities in the successive transects suggested that added Ra inputs from the bay floor were occurring during low groundwater level periods. The activity variations with distance matched the modelled trends expected following Ra input from the bay floor. The review of the potential radium sources in the bay suggest that the Ra increase is due to the intrusion of saline water in porewater previously saturated with freshwater. This may be associated to a flux of recirculated SGD during low groundwater level periods of between 0.2 $\times 10^5$ m^3 d^{-1} to 80 $\times 10^5$ m^3 d^{-1}, according to the end member considered (sediment, karst, or a mix of the two). These values can be compared to the 1 to 20 10^5 m^3 d^{-1} of fresh SGD flow estimated in paper A for these surveys. This range can be refined to 0.3-4.4 $\times 10^5$ m^3 d^{-1} (1% to 440% of fresh SGD rates) if the Ra increase is assumed to be the result of increased saline intrusion through all sediment surface present in the bay (Hypothesis 3). Based on an approximate equation derived from Schneebeli the minimum ratio between saline SGD and fresh SGD is between 5% ±1 and 32% ±2, which is within the range derived from Ra. The highest fraction is predicted for spring tides periods occurring when groundwater level is low (2m). This suggest that the fraction of recirculated SGD should increase during spring tides with decreasing groundwater level, in agreement with the Ra isotope observation. These periods of increasing saline SGD, had increased phosphorus level in the submarine groundwater discharge fluxes, decreased dissolved oxygen, and in some cases increased nitrite level. This simultaneous change may be due to a modification of nutrient reactions occurring in the karst system following the period of greater saline intrusion. The additional fluxes of limiting nutrients such as phosphorus caused by saline

SGD may amplify the intensity of blooms, providing additional nutrient sources to feed phytoplankton growth during drought periods. The evidence provided suggest that periods of spring tide coinciding with low groundwater levels are the most favourable for such a high impact of saline SGD on coastal bay biogeochemistry relative to the fresh SGD discharge.

4.2 Introduction

In a context of global anthropogenic-driven changes of coastal environments, a more detailed understanding of inputs of solute coming to coastal systems is necessary to protect the resources on which human activities depend (aquaculture, fisheries, tourism, among others).

While the traditional approach for such an understanding in coastal areas has placed a great focus on solute inputs from rivers, it is now recognised that the water exchanges between the seafloor and the ocean, grouped under the term of submarine groundwater discharge (SGD) represent for the global ocean a larger source of solute than rivers (Kwon et al., 2014; Moore, 2010; Moore and Shaw, 2008; Rodellas et al., 2015a). These fluxes are generally of two origins: from continental groundwater, fed by the infiltration of net rainfall inland (referred to here as “fresh” SGD), and from the recirculation of seawater and bay water within the aquifer, mainly driven by sea-level fluctuations and density differences (here “saline” SGD). Recirculation of seawater through the bay floor occurs on a wide range of scales (Bratton, 2010), and often represent the majority of SGD-driven solute fluxes during dry periods (e.g. Sadat-Noori et al., 2016). Such fluxes generate additional chemical reactions within sediment porewater and aquifers, such as desorption (Rysgaard et al., 1999; Price et al. 2010), organic matter decomposition (J. Severino P. Ibánhez and Rocha, 2014), or other nutrient transformations (e.g. denitrification, nitrification) (Slomp and Van Cappellen, 2004). Considering the current rate of sea-level rise of 3±1 mm per year between 1993 and 2012 (Dangendorf et al., 2017; Hay et al., 2015), sections of coastal aquifers and sediments previously saturated with freshwater are increasingly flushed by seawater. This trend, combined with an increased frequency

of extreme events (e.g. storm surges), activates additional fluxes of nutrients and other elements previously stored in sediments in coastal areas. In the long term, these added fluxes are likely to modify the cycles of carbon, nutrients and potentially of other elements. Periods of decreased groundwater level coinciding with increasing groundwater use and high sea level periods (e.g. seasonal variation of sea level, summer spring tides and storm surges) are the most likely to be affected first by these additional fluxes, as they represent the most favourable periods for seawater intrusion in coastal aquifers. Wood and Harrington, (2015) previously demonstrated in a groundwater fed laguna, that period of high salinity of the groundwater discharge coincided with periods of seasonally high sea level, suggesting that saline SGD could represent a larger faction of the total discharge during these periods. Estimating the current magnitude of these fluxes for coastal area play thus a key role in managing future ecosystem changes in a context of climate change.

Salinity measurements cannot usually detect saline (or recirculated) SGD in coastal areas (Taniguchi et al., 2019), unless by an increase of salinity associated with evaporation, for example when the recirculation occurs at a small depth in a sandy beach. For this reason, the majority of studies aiming at determining the effect of saline SGD have used measurements of elements naturally present in these fluxes such a radium, radon, silica or methane (See review by Taniguchi et al., 2019). On the other hand, some studies have also aimed at forecasting the seasonal variability of SGD fluxes using numerical models (Li and Barry, 2000; Robinson et al., 2006; Sawyer et al., 2013, Robinson et al., 2007b).

So far, most studies have focused on sandy and muddy coastlines, where the recirculated component is the most evident, and the effect of seawater recirculation on other systems is less well-known. Karst systems are typically considered to be dominated by fresh SGD, and while seawater intrusions on such system are well known (Fleury et al., 2007; Werner et al., 2013), only recently researchers have focused on estimating the volumes of seawater involved, and the potential effect for solute fluxes to coastal ecosystems. For example, Wood and Harrington, (2015) demonstrated that seasonal peaks of sea level enhanced saline intrusion in a karst aquifer, influencing the salinity and chemistry of groundwater discharged to a coastal bay fed by a karst aquifer. Price et al., (2010) showed that recirculation of seawater could drive additional P fluxes to coastal systems, by favouring the

release of phosphorus previously absorbed to limestone by desorption and karst dissolution. We attempt to quantify the seasonal variability of this effect using radium isotopes and equations describing flow rates to cavities from Schneebeli (1986). To do so, we take the example of a coastal bay with large fresh groundwater inputs from a karst aquifer, Kinvarra Bay. This system was selected because its functioning is well known (Drew and Daly, 1993; Drew, 2003, 2008; Einsiedl et al., 2009; Cave and Henry, 2011; Petrunic, Einsiedl and Duffy, 2012; Smith and Cave, 2012; Einsiedl, 2012; Gill et al., 2013; McCormack et al., 2014; Rocha et al., 2015; Schubert et al., 2015; McCaul et al., 2016; Gregory et al., 2020). Moreover, saline intrusions occur in summer in the aquifer (Einsiedl, 2012; Petrunic et al., 2012), with an effect on groundwater chemistry until one to three km inland (Einsiedl, 2012; Petrunic et al., 2012). Previous studies estimating the amount of SGD flowing to the system (Cave and Henry, 2011; McCormack et al., 2014; Rocha et al., 2015; Schubert et al., 2015; Morrissey et al., 2020) did not assess the potential effect of recirculated seawater on the fluxes of solutes to this bay. We thus attempt here (1) to assess the magnitude of saline SGD compared to fresh SGD for this system (2) to develop a method for a rough assessment of the seasonal variability of saline SGD fluxes for a given groundwater level and sea-level variability and (3) to give a first assessment of the effect of these saline fluxes on nutrient and dissolved oxygen concentrations in the total SGD fluxes going to the system. To do so, we use radium isotopes measurements, soluble reactive phosphorus, dissolved inorganic nitrogen and dissolved oxygen measurements made under different groundwater levels. Besides, we attempt to derive a method to assess the minimum saline SGD fraction using equations from Schneebeli (1986).

4.3 Method

4.3.1 Kinvarra Bay

Kinvarra Bay is a small bay located in the west coast of Ireland, which receives important inputs of groundwater from a well-developed lowland karst aquifer. The bay presents significant aquaculture activities, mainly mussels (150 Tonnes in 2018) and oyster production (15 tonnes in 2018) (BIM, 2018a) and is connected to Galway Bay.

A series of springs are present in the bay, with the main one being Kinvarra spring (Kinvarra East/Castle and Kinvarra West/Arch, KE and KW in Figure 19). While the Castle spring is active during all year and is believed to draw from a deep conduit, the Arch spring is irregularly active and draws from a shallower source (Smith and Cave, 2012). Tracers tests (Drew, 2003) and stable isotopes (Schubert et al., 2015) suggest that both these springs are connected to a catchment of approximately 483 km^2. Sea level recorded in the nearby Galway Bay between 2010 and 2020 typically varies during spring tide between +3.67 and -3.77m around Malin head mean sea level (Marine Institute, 2020b). At Killiny borehole, a well more than 4 km inland from the Kinvarra springs with a continuous groundwater level recorder (KI, in Figure 19), groundwater level varies between 1.9 m and 13 m above mean sea level (Environment Protection Agency data). As a result, during spring tides, the tidal level is likely to rise above the local groundwater level during dry periods. Such a scenario probably leads to the recirculation of some of the bay water inside the aquifer sections around the bay shores and deeper in the bay sediment, especially in areas where active major freshwater springs are not present, or are fed by shallow sources, such as here, the Arch spring. Previous studies identified geochemical evidence of intrusion of sea water around Kinvarra Bay on wells sometimes several km inland (Einsiedl, 2012; Petrunic et al., 2012). This evidence suggests that some recirculation of bay water in the aquifer is indeed present during the summer. The approximate locations of these boreholes are shown in Figure 19 with wide circles and seem to correspond to a radius of 2 to 3 km around Kinvarra Bay and the surrounding bays (locations projected from maps of Petrunic et al., 2012). The sediment cover on the bay is only partial, with approximately 60 per cent classified as rocky shore (Figure 19). Consequently, water exchanges between bay water and the aquifer are likely in this area.

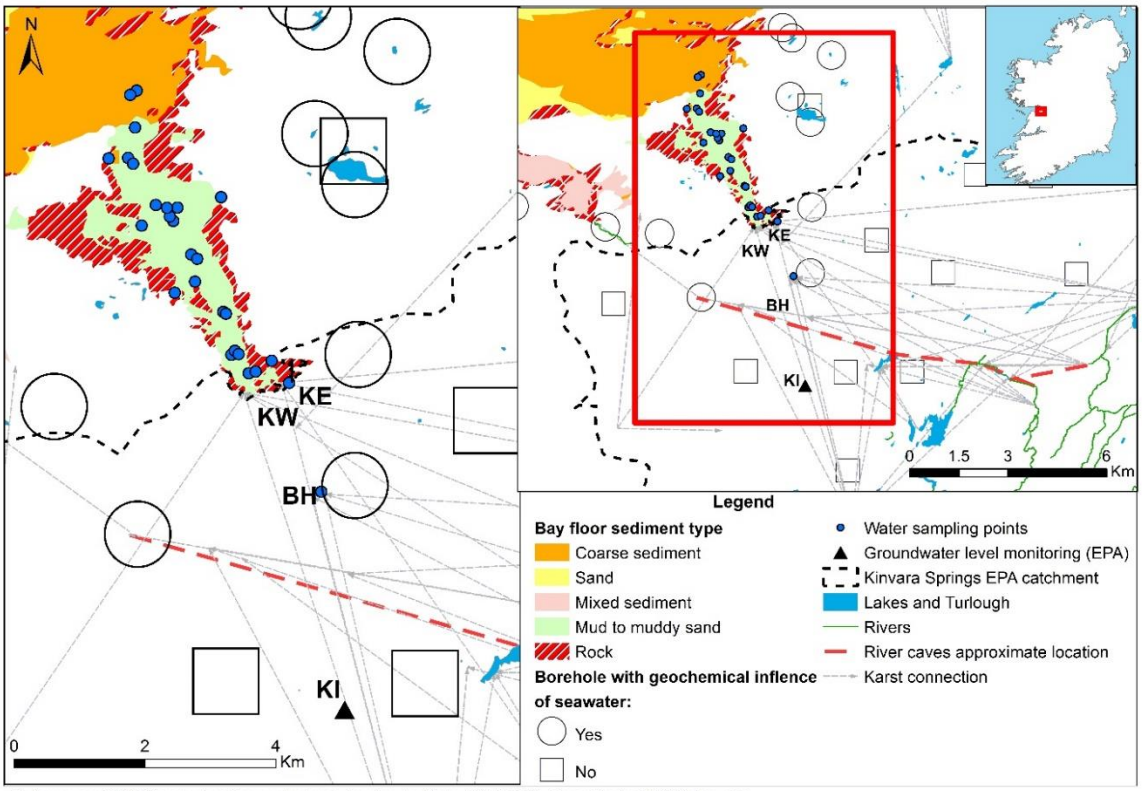

Figure 19: Bay floor types and water sampling locations in Kinvarra Bay, and zones of saline intrusions in the catchment of Kinvarra Bay. Symbols highlight boreholes which have geochemical evidence of seawater influences, and are thus likely to act part of the year as solute sources for saline SGD. (Projected locations taken from Petrunic et al. (2012)). The bay floor typology is from reclassified Marine Institute data. The EPA record groundwater level at Killiny borehole (KI). KE and KW are respectively Kinvarra Arch/East and Kinvarra Castle/west. BH is the borehole location sampled here to study the effect of seawater recirculation on the Karst ^{223}Ra and ^{224}Ra activities.

4.3.2 The potential effect of saline SGD for a given groundwater level

To assess the changes under different groundwater level of the fraction between saline SGD and fresh SGD, publicly available data on groundwater level and sea level variability in the area were first collected and compared. From this data, the minimum relative fraction of saline SGD versus total SGD was assessed using the equation of Schneebeli (1986) as follows.

From Schneebeli (1986), in the case of a semi-infinite groundwater body flowing towards a hemispheric cavity (e.g. a simplified bay, with lateral groundwater fluxes from both sides):

$$Q = \sqrt{2\,\pi}\,K\,H\,\sqrt{S} \qquad (3.1)$$

Where Q is the flow to the cavity per length of cavity ($m^3\ m^{-1}\ d^{-1}$); H is the height difference between the level of water in the cavity and groundwater level (m); K the large-scale hydraulic conductivity ($m\ d^{-1}$); S is storativity (without units), which represents the volume of water released from storage per unit decline in hydraulic head in the aquifer, per unit area of the aquifer. K depends on the intrinsic permeability of the karst, dynamic viscosity and density of the fluid crossing the aquifer.

This equation approximate the karst in the 4-5km around Kinvarra spring where the saline recirculation is known to be most intense (e.g. figure 10 in Petrunic et al., 2012) as an equivalent continuous medium with large scale hydraulic conductivity (K) and storativity (S). As shown previously, a linear relationship with groundwater level (Savatier and Rocha, 2021) can approximate the long term (>1day) variability of Kinvarra spring flow outside of storms periods. This observation is equivalent to concluding that the term $\sqrt{2\,\pi}\,K\sqrt{S}$ in equation 3.1 is approximately constant at large scale. Unlike the section of the catchment further inland, the 3-4 km zone around Kinvarra Bay does not include large turloughs and the known position of the major conduit is outside this zone, this assumption seems thus acceptable for a first-order estimate of the seasonal variability of SGD composition for this system. The effect of salinity changes is considered to have a second-order effect on dynamic viscosity and density of the water crossing the aquifer. The volume of fresh groundwater discharge flowing during a tidal cycle is then:

$$V_{fSGD} = \int_{t=t1}^{t2} Q_{fSGD}^{t}\, dt = \int_{t=t1}^{t2} \sqrt{2\,\pi}\, \mathrm{K} \sqrt{\mathrm{S}}\, (\mathrm{h}_w^t - \mathrm{T}^t)\, dt \qquad (3.2)$$

Where *t1* and *t2* are the start and end time of the tidal cycle; V_{fSGD} is the net volume of groundwater flowing out of the aquifer; Q^t_{fSGD} is the flow to the bay during a short time interval *dt*; h^t_w is the groundwater level in a representative location in the aquifer at time *t* (meters above mean tide level); T^t is the tidal level during a short time interval *dt* in the bay.

While the tidal fluctuations are changing the hydraulic gradient (*h– T*) during a given day, the expression $\int_{t=t1}^{t2} (\mathrm{T}^t)\, dt$ is likely to be close to 0, and negligible compared to $\int_{t=t1}^{t2} (\mathrm{h}^t{}_w)\, dt$, if *t2-t1* is a multiple of *n* tidal periods and if sea level variations are relatively symmetric during a tidal cycle (they can be expressed as a function of sine waves). The tidal variation observed in this system follow such a symmetric, sine wave-like variation (Marine Institute, 2019a). The likelihood of such an approximation can be further verified by comparing the daily averaged flow estimated from groundwater level with the daily averaged flow estimated from groundwater level - tidal level. Chapter 3 showed with a reanalysis of modelling results of McCormack et al. (2014) that although the daily fluctuation could be large due to tidal sea level fluctuations, the changes of daily averaged flow across the year were mainly dependant on groundwater level. The assumption is thus to be verified for this type of system.

While the long-term hydraulic gradient drives fresh SGD, saline SGD tends to be driven by sea-level fluctuations, density difference, as a first approximation to assess a minimum value of SGD recirculation levels, only the effect of tidal fluctuation on saline SGD is considered here. Fresh SGD is thus calculated as the discharge of “new” groundwater, driven to the subterranean estuary by groundwater head difference during a given day. In such conditions, V_{fSGD} the net volume of fresh SGD coming from the groundwater during a full tidal cycle of start and end time t_1 and t_2 is:

$$V_{fSGD} \approx \sqrt{2\,\pi}\, \mathrm{K} \sqrt{\mathrm{S}}\, \int_{t=t1}^{t2} (\mathrm{h}_w^t)\, dt \;\approx \sqrt{2\,\pi}\, \mathrm{K} \sqrt{\mathrm{S}}\, (\mathrm{h}_w)\, (t2 - t1) \qquad (3.3)$$

Where h_w is the daily medium height of groundwater in a representative location of the aquifer during the period *t2-t1*.

If the minimum volume of saline SGD is the volume of bay water that was infiltrated in the aquifer during high tide and is getting out on the next low tide, when the tide is lower than the mean tide level, V_{RSGD} is then given by:

$$V_{\mathrm{RSGD}} = \sqrt{2\,\pi} * \mathrm{k} * \sqrt{\mathrm{S}} * \int \left(\mathrm{h}_t - \mathrm{h}_{moy}\right)\mathrm{dt} = \sqrt{2\,\pi} * \mathrm{k} * \sqrt{\mathrm{S}} * \mathrm{h}_1 \qquad (3.4)$$

Where h_1 is calculated from the integration of the positive height differences between groundwater level and tidal level during 24hours (to get theoretical discharge leaving the groundwater); and h_t is the average tidal height in the area.

From equations 3.3 and 3.4, between two half tides the theoretical ratio between saline recirculated SGD (RSGD) and net fresh SGD is estimated with:

$$\frac{V_{\mathrm{RSGD}}}{V_{\mathrm{fSGD}}} = \frac{\sqrt{2\,\pi} * \mathrm{k} * \sqrt{\mathrm{S}} * \mathrm{h}_1}{\sqrt{2\,\pi} * \mathrm{k} * \sqrt{\mathrm{S}} * \left(\mathrm{h}_w - \mathrm{h}_{moy}\right)(\mathrm{t}_2 - \mathrm{t}_1)} = \frac{\mathrm{h}_1}{\left(\mathrm{h}_w - \mathrm{h}_{moy}\right)(\mathrm{t}_2 - \mathrm{t}_1)} \qquad (3.5)$$

Where h_w is the groundwater level, h_{moy} is the mean level of groundwater close to the coast (assumed equal to mean level of tide = altitude 0), and t_2-t_1 is the tidal period or the length of the period considered.

Equation 3.5 was then applied for the four surveys taken in Kinvarra Bay and the results reliability were evaluated with radium mass balances.

4.3.3 ^{223}Ra, ^{224}Ra, nutrient, and dissolved oxygen measurements

To validate estimates of the variability of V_{RSGD}/V_{fSGD} and assess the effect of changes of saline SGD rates on nutrient fluxes to the system, four surveys of ^{224}Ra, ^{223}Ra, NH_4, NO_2, NO_3, SRP and Dissolved Oxygen were carried out in Kinvarra Bay under different groundwater levels representative of the annual variability (2m, 12th - 14th July 2018; 4m, 20th - 23rd October 2018; 7.2m, 25th - 28th January 2019; 9.4m, 06th - 08th April 2019). Each survey involved sampling of surface water, spring water and of a borehole located close to the main conduit feeding Kinvarra springs, in the area with geochemical evidence of seawater intrusions during the summer (Figure 19).

Radium is a valuable radiotracer to detect recirculation SGD fluxes, as it is naturally produced by the decay of uranium and thorium which are naturally present in low levels in rocks and sediment. This element is usually adsorbed to sediment particles under low

salinity but is desorbed if the ionic strength of the solution increases (Webster et al., 1995). Since seawater recirculation within sediment tends to control desorption and porewater exchange, otherwise unsupported Ra isotopes in the coastal ocean are an indicator of SGD inputs. For this reason, radium mass balances are commonly used to estimate saline SGD fluxes over small or large areas, as they allow the detection of saline circulation through sea floors. The methods used for this sampling campaign to ensure reliable Ra and nutrient results are described in Chapter 3. Ra samples were taken by concentrating large volume of seawater in Ra in acrylic fibres and then measuring using a Radium Delayed Coincidence Counter (RaDeCC).

Each borehole sample was done after a preliminary pumping, until stable parameters (Temperature, EC, pH, DO, TDS) were reached, to ensure samples representative of the aquifer. Samples at intertidal springs were taken during the minimum tide stage, in the upper part of the spring area, to sample discharged waters with minimum bay water content and contact time with the atmosphere. For borehole samples, dissolved oxygen was measured using a calibrated Aquaprobe, by direct pumping through an Aquaprobe flow-through cell, to avoid any contact of the sample with the atmosphere. Samples for dissolved nutrient (NO_3^-, NH_4^+, NO_2^-, PO_4^{3-} as Soluble Reactive Phosphorus - SRP) were filtered directly after sampling through 0.15µm Rhizon membranes into vacutainers for NO_3^-, NH_4^+, NO_2^- (J. S. P. Ibánhez and Rocha, 2014; Jiang et al., 2017), and acid-washed HDPE vials for PO_4^{3-}. These samples were then analysed using standard colourimetric methods (Grasshoff et al., 2009), less than ten days for SRP, and less than 30 days for dissolved inorganic nitrogen (DIN), following recommendations for use with vacutainers (Jiang et al., 2017). Field blanks were taken on each sampling surveys, and each nutrient sample was taken in triplicate tubes filtered separately on the field. SRP was determined at 885 nm using a Hatch DR5000 spectrophotometer using standard colorimetric methods (Grasshoff et al., 2009). NO_3^-, NH_4^+, NO_2^- were analysed with a Lachat Quickchem 8500 flow injection analysis system, following manufacturer-adapted methods for sequential analysis (Lachat instruments, 2002, 2001). Salinity was measured using an Aquaread® Aquaprobe, calibrated according to standard manufacturer procedure (Aquaread, 2013), and values were verified with a Carl Stuart Limited Cond197 i WTW electrical conductivity probe.

In addition to these water samples, the Ra contribution from sediments was determined by taking grab samples in different sections of the bay. Each sediment sample was resuspended in Ra free seawater, and the porewater was then filtered in clean acrylic fibres and analysed as for water samples. Using porewater measurements and bulk density measurement, the radium activities were then converted in equivalent content in porewater (dpm per volume) for later use in Ra balance for the bay, to assess SGD related Ra fluxes through the bay floor.

4.3.4 Radium derived estimates of solutes inputs from the bay floor.

At steady state over the lifetime of the tracer, the radium mass balance for the system for ^{224}Ra and ^{223}Ra is:

$$Ra_{adv} = Ra_{dy} + Ra_{net} - Ra_{dif} \quad (3.6)$$

Where Ra_{adv}, Ra_{dy}, Ra_{net}, Ra_{dif} are the Ra fluxes respectively from SGD, decay, and net exchanges with the outside of the bay (positive values =Ra leaving the system), and Ra fluxes from sediments to the bay.

Since Kinvarra Bay has spatially variable water ages (0-8 days), the actual Ra_{dy} for each of the isotopes (^{224}Ra and ^{223}Ra) will depend on the age of the sample relative to its discharge from a spring or another Ra source (half-life 3.6 and 11.4 days respectively). It is necessary to correct for this fact to satisfy the steady-state assumption. As Chapter 3 demonstrated the importance for spatial variability of age for mass balances of non-conservative elements, the Ra activities in the water were corrected for internal reactions occurring in the bay, considering the spatial variability of water ages in the system. To do so, estimates of water ages variability in Kinvarra Bay (from Chapter 3) were used to correct Ra activities at each location of the bay for the effect of internal reactions in the bay. For Ra short-lived isotopes, decay is the only reaction likely to occur continuously along the pathway of a water parcel within the system. Decay are thus corrected for each sample, considering the time since it left contact with a source (water ages) as follow:

$$\text{Ra corrected for decay} = \text{Ra measured} * e^{A\,\lambda_{Ra}} \quad (3.7)$$

Where A is the time since the sample left contact with a radium source (d), estimated from the relative water ages assessed with $^{224}Ra/^{223}Ra$ ratios (as described in Savatier and Rocha, Submitted); λ_{Ra} the decay constant of ^{224}Ra or ^{223}Ra (d^{-1}); Ra measured and Ra corrected respectively the radium measured in the bay and the radium activities corrected for decay that occurred since the sample left contact with a radium source (Bq m^{-3}): sediment or spring. It is worthy to note that using $^{224}Ra/^{223}Ra$ to assess water ages means that the water ages results are less sensitive to inputs of radium activity than when using an element alone (Moore, 2000), which allows the use of water ages derived from Ra ratios to correct for time-dependent decay as part of a radium mass balance.

To determine Ra_{dif} fluxes from bottom sediment, the spatial variability of radium was modelled following a similar approach as used by Krest et al. (1999). Two alternative models are applied to describe changes of the radium activity with salinity along the bay:

The first model describes a situation in which Ra variance with salinity (after decay corrections) are explained only by binary mixing, i.e., between the freshwater and seawater end members (Krest et al., 1999). In other words, a scenario when there are no further inputs of Ra along the mixing transect, after the area of Kinvarra springs:

$$Cs = C_R(1 - f_o) + f_o C_0 \quad (3.8)$$

Where *Cr* and *Co* are the Ra content in the spring and the marine end-member, and *Cs* is the concentration of Ra at each point of the bay of seawater content f_o. f_o is given by:

$$f_o = \frac{S_S - S_R}{S_O - S_R} \quad (3.9)$$

The second model (from Krest et al., 1999) describes a situation in which Ra changes are explained by mixing between freshwater and seawater, and the addition of Ra from suspended particles and sediments along the mixing gradient. In other words, a scenario in which fresh SGD fluxes from Kinvarra spring explain the radium changes, plus an input of radium from the bay floor, and eventually of particles:

$$C_s = \left(C_R + C_{DES}\left(1 - e^{-\frac{S_S}{S_U}}\right) + F_{DIF} * \frac{t}{d}\right) * (1 - f_o) + f_o C_0 \quad (3.10)$$

Where C_S, S_S, *t*, *d* are respectively the water Ra content (dpm m^{-3}), Salinity (kg m^{-3}), water age (in days) and depth (m) on a given location of the bay; C_R is the Ra content in

the spring (dpm m^{-3}); C_{DES} is the concentration of radium that can be released by suspended sediment present in the water at 100 per cent seawater content (dpm m^{-3}); S_U is the salinity at which desorption is made with a rate *e;* F_{DIF} is the radium flux from the bay floor (dpm m^{-2} d^{-1}, from diffusion and saline SGD), and f_o the fraction of seawater of the location. The range of C_{DES} was estimated from the resuspension of a known quantity of bottom sediment and sediment taken from the spring location in Ra free water. Finally, F_{DIF} was determined by a least-square fitting method of equation 3.10 using the Ra transects.

4.4 Results

4.4.1 Seasonal variability of the ratio between "saline" SGD and "fresh SGD" using the method derived from Schneebeli (1986).

Changes of saline SGD and fresh SGD derived from equations of Schneebeli (1986) are shown in Table 4. The maximum V_{RSGD}/V_{FSGD} occurs during periods of low groundwater level and maximum tidal range (Table 4). Moreover, the predicted relative role of recirculation of bay water through the bay floor compared to fresh SGD inputs (V_{RSGD}/V_{FGD}, Table 4) increases with decreasing groundwater level (h_{gw}, Table 4).

Table 4: Estimated variability of the proportion of saline SGD to fresh SGD for Kinvarra Bay. h_{gw} is the average groundwater level above sea level during the ten days previous to the survey; Maximum high tide is the maximum tidal level during high tide during the period sampled, VRSGD/VFGD, the ratio between the volume of bay water recirculated through the bay floor and the volume of freshwater coming from groundwater to the system. Uncertainties are one standard deviation. The potential range of freshwater inputs derived from tracer-based methods in Paper A are shown for reference in the right column.

Survey	h_{gw} (m)	Maximum high tide (m)	Ratio V_{RSGD}/V_{FGD}	Range of V_{FGD} (10^5 m^3 d^{-1})
201807	2.17 ±0.02	2.29	32% ±2	1-5
201810	3.79 ±0.02	1.62	12% ±2	7-10
201801	7.01 ±0.02	1.22	6% ±1	14-24
201804	9.20 ±0.02	2.19	7% ±2	15-20

4.4.2 ^{224}Ra and ^{223}Ra spatiotemporal variability

Both radium isotopes` activities in the bay and the spring were higher when groundwater level was low (H= 2, 4, Figure 20 a, b) than when groundwater level was high (H= 6, 9.7, Figure 20 a, b).

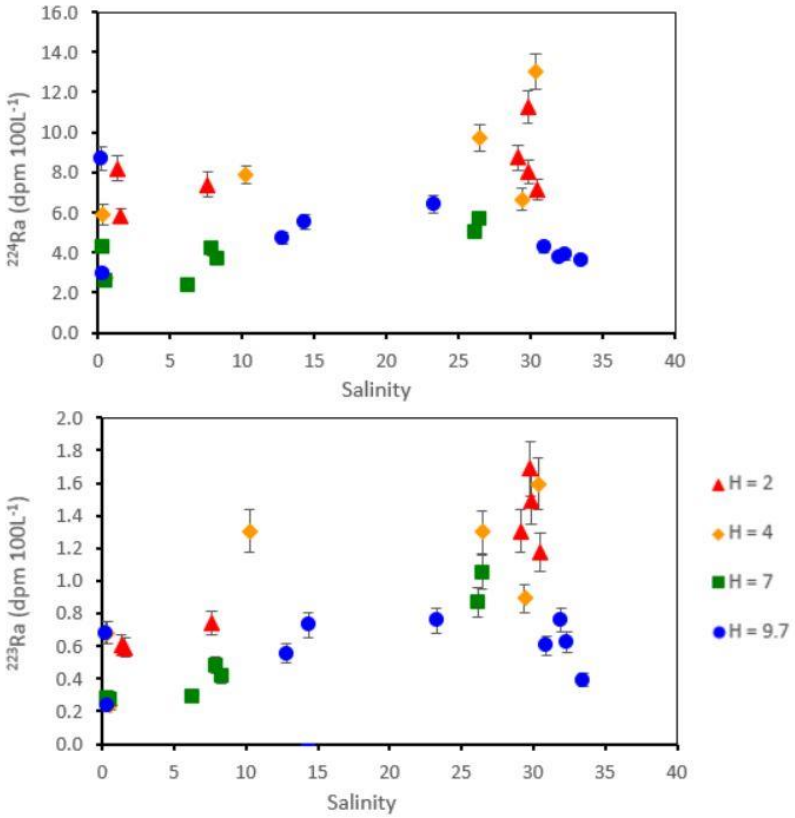

Figure 20: Raw ^{224}Ra and ^{223}Ra for Kinvarra Bay, H is the groundwater level measured at Killiny Borehole during each survey (in m).

Using a similar approach to that of Krest, Moore and Rama (1999), we model these trends to determine which physical process may be more likely to generate the curves after correcting for the water age variability in Figure 21.

For Kinvarra Bay, the release of radium from suspended sediment (CDES in equation 3.10) was negligible: the resuspension of local sediment in a radium free seawater showed that desorbed Ra in sediment was up to 5 dpm 100g^{-1} for ^{224}Ra and 0.6 dpm 100g^{-1} for ^{223}Ra, with most sediment presenting much lower concentrations (Table 5). Suspended sediment levels in the bay are between 5 and 35 mg.L^{-1} (Smith and Cave, 2012). The maximum contribution of suspended sediment to the water column Ra inventory would be thus 0.17 dpm 100L^{-1}and

0.02dpm $100L^{-1}$, which is much smaller (negligible) than the uncertainty associated with the other fluxes.

When groundwater level was high (blue lozenges, Figure 21), the Ra trends (corrected for decay using equation 3.7) were consistent with pure mixing between Galway Bay water and water in direct proximity to Kinvarra springs (blue curve, Figure 21). On the other hand, when groundwater level was low, the higher Ra activities observed (red triangles, Figure 21) corresponded to the predicted trend for simple mixing between seawater and fresh SGD, plus an additional input from the bottom of the bay of 27 dpm m^{-2} d^{-1} for ^{224}Ra and 2.8 dpm m^{-2} d^{-1} for ^{223}Ra (red curve, Figure 21). These calculated fluxes suggest thus $^{224}Ra/^{223}Ra$ ratio of 9.6, similar to the Ra ratio in karst (10) and in subtidal sediment (9+-1), in agreement with Ra fluxes from the bay floor.

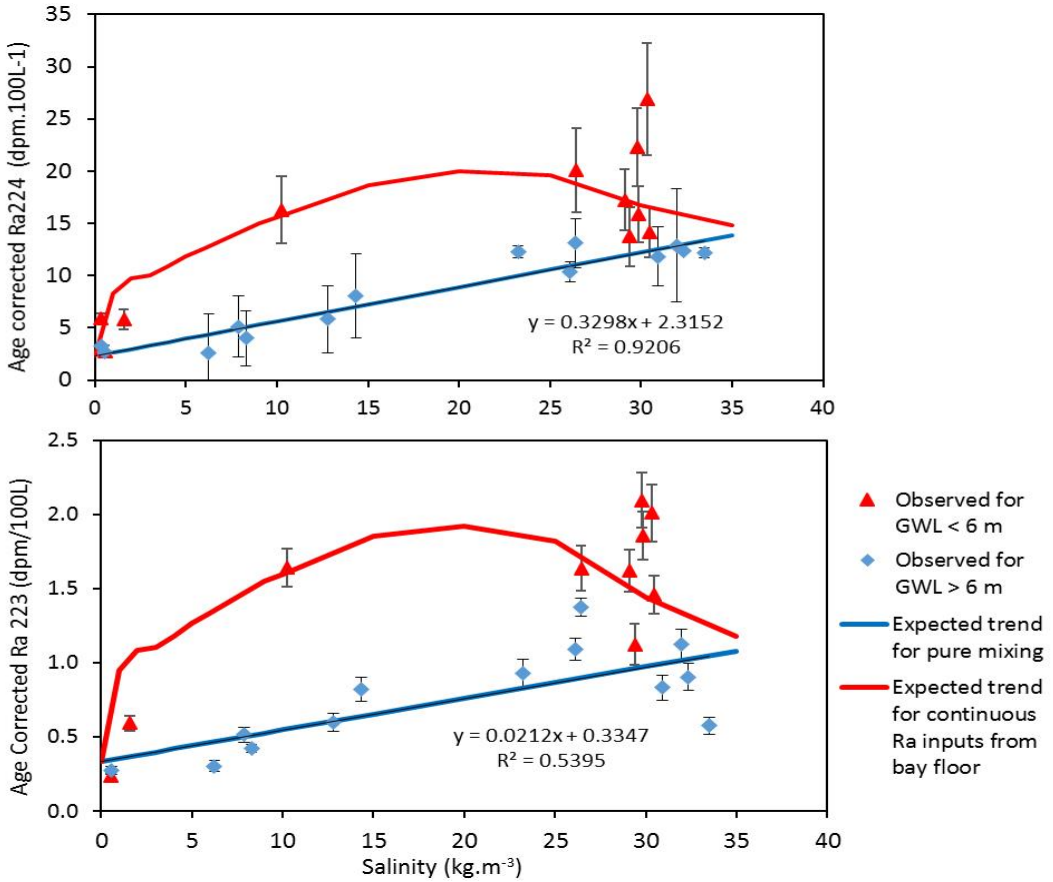

Figure 21: 224Ra and 223Ra transects corrected for spatial variability of ages (equation 3.7) vs salinity and modelled Ra concentration following Krest et al. (1999). Blue lozenges and red triangles are the observed Ra activities in Kinvarra Bay when groundwater level is respectively above or below 6m. Each data series groups two surveys at different times of the year. Blue curves are the expected trends for pure mixing between spring water and seawater, and the red curve is the expected curve for mixing and additional inputs from the bay floor of a radium flux of ^{224}Ra= 270 dpm m^{-2} d^{-1} and ^{223}Ra= 28 dpm m^{-2} d^{-1}.

4.4.3 Effect of groundwater head on nutrient levels in Kinvarra spring and Kinvarra Borehole

During the lowest groundwater level survey (3m), in addition to the Ra increase in the bay, salinity increased in Kinvarra spring and in the borehole representative of the area of seawater intrusion, with a larger increase in the borehole (Figure 19a). Dissolved oxygen also decreased with decreasing groundwater level during our spring tides surveys (Figure 19a). SRP and NO_2 levels were also higher when groundwater levels were below or equal 4m in the borehole (Figure 22b), and the spring (Figure 22c) for one of the surveys.

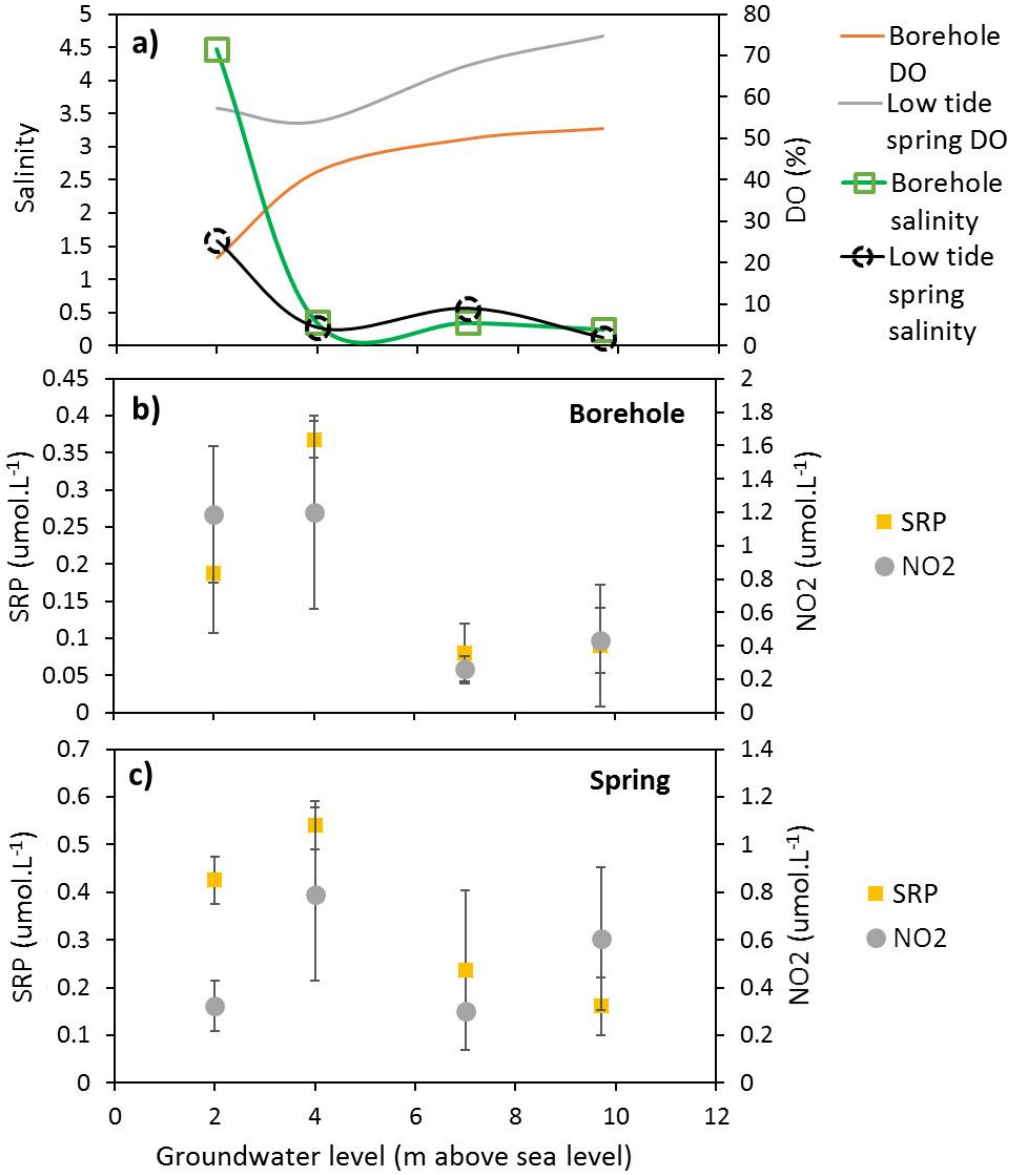

Figure 22: Effect of groundwater level on salinity, SRP and NO_2 levels (a) in the borehole, (b) in Kinvarra spring for spring tide surveys. All samples for the spring were taken at low tide, directly from the discharge point.

4.4.4 Variability of dissolved oxygen in the bay

The minimum dissolved oxygen levels in Kinvarra Bay are generally observed in in the low salinity zone in direct proximity to the spring, and increase with salinity until reaching saturation, or sursaturation when groundwater levels are below 6m (Figure 23b). The variability of dissolved oxygen is larger during periods of low groundwater level than for periods of high groundwater level, with greater saturation or undersaturation observed (Figure 23a).

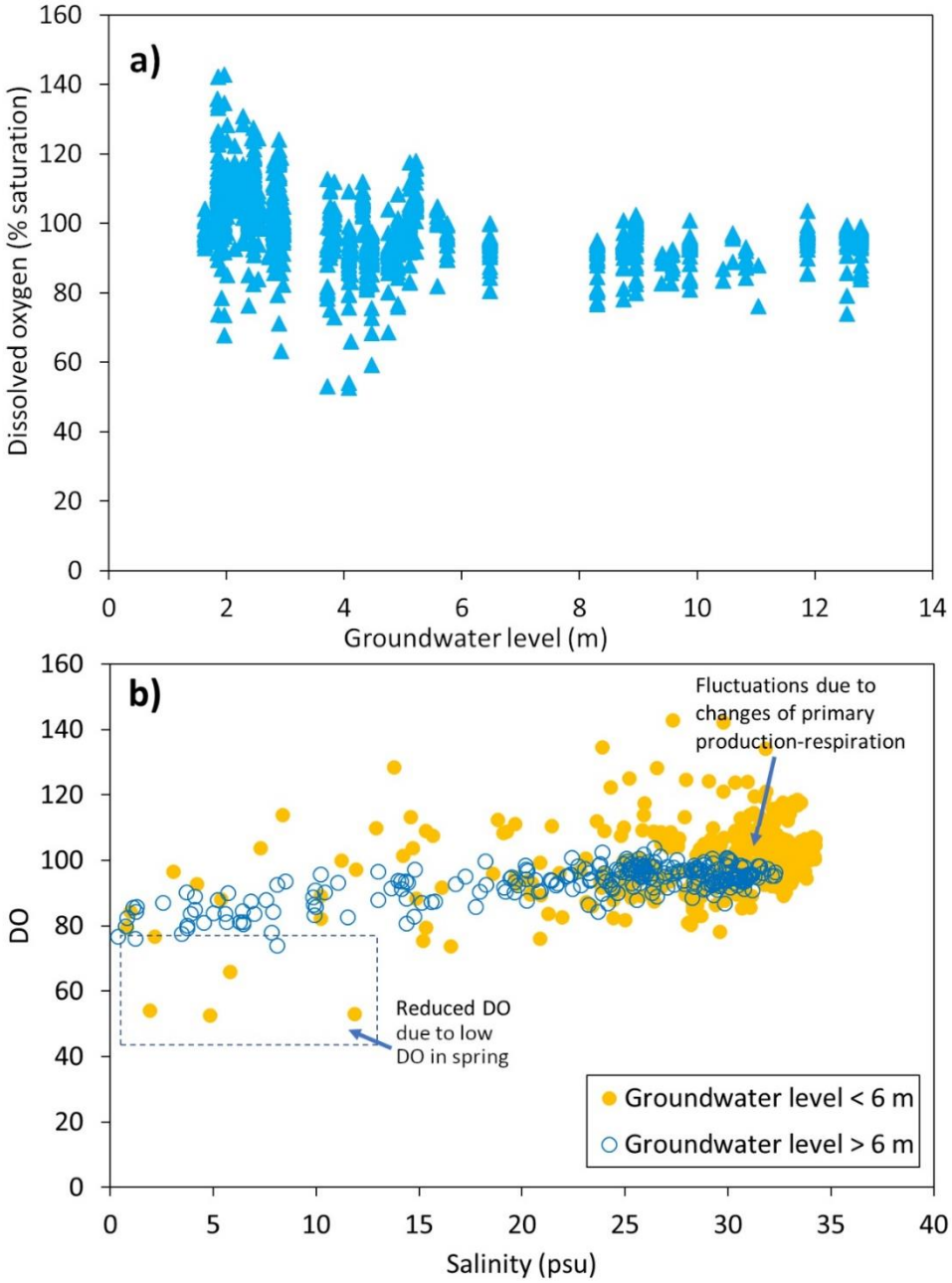

Figure 23: (a) Dissolved oxygen trends in Kinvarra Bay as a function of groundwater level between 2010 and 2018, and (b) dissolved oxygen as a function of salinity in Kinvarra Bay when the groundwater level (GWL) was below or above 6m above mean tide level (EPA, 2018; 2020).

4.5 Discussion

Wood and Harrington, (2015) previously demonstrated that seasonal rise of sea level can increase the salinity in wetlands connected to coastal karst aquifer, sometimes independently of groundwater seasonal recharge. In the current work, surveys were thus carried out only during spring tides to further characterise periods of high recirculated SGD.

During our spring tides surveys, the results from equations derived from Schneebeli (1986) in section 4.4.1 suggest that the magnitude of the saline SGD fraction coming to the bay increases with decreasing groundwater level (Table 4). When during spring tides, groundwater level measured at Killiny (h_{gw}, Table 4) is below the maximum high tide level (e.g. during Survey 201807 in Table 4), a significant proportion of the water present in the bay is likely to be recirculated within the karst superficial aquifer and bay sediment previously saturated with fresh water. Tamborski et al. (2017), also showed that in a system affected by a high hydraulic gradient (coastal bluff), the residence time of water within the subterranean estuary tend to be lower than for a system with a low hydraulic gradient (barrier beach site). When groundwater level are low during spring tides, the release of reactive solute fluxes from sediment and aquifer material to coastal areas is thus likely to be increased by (1) rising salinity due to increasing saline SGD fraction and (2) increasing residence time in the subterranean estuary.

The larger ^{223}Ra and ^{224}Ra activities observed during spring tides surveys with groundwater below 6m confirm that an increase of solute fluxes from sediment is indeed taking place when groundwater level is low during spring tides (Figure 21). A similar increase of radium was previously observed during the summer in other systems and previously attributed to seasonal changes of the storage of organic carbon and rates of bioturbation leading to a net reduction of radium carrier phases (Bollinger and Moore, 1993), or by the joint change of activity of benthic mesofauna during the summer and the lower groundwater level (Rodellas et al., 2017). In Kinvarra Bay, the fact that these fluxes occur only during low groundwater levels suggests that they originate from enhanced recirculation of seawater through the coastal aquifer. To further explore this hypothesis,

we review the main potential Ra sources for the bay in the next section and later attempt to estimate the potential volume involved.

4.5.1 Analysis of all potential ^{224}Ra and ^{223}Ra sources which may contribute to a Ra flux for the bay floor in the bay.

Kinvarra bay is shallow, with 70% of its bay floor less than 2 m below the lowest astronomical tide, and a maximum depth present close to its outlet, at -6m below the lowest astronomical tide (Informar data). The average depth of the bay is 3.4m at mean tide (for a mean tide at +3.77 m above lowest astronomical tide estimated from Galway Bay tide data). 58% of the total bay area is composed of clay to sandy clay, mainly present in the subtidal area. The rest of the bay floor is composed of densely fractured limestone (Informar data), with little or no sediment cover (Figure 19). This limestone covers 70% of the intertidal area.

In tidal systems, saline recirculation over short timescale frequently occurs by infiltration of saline water in the bay floor during flood tide, flowing back to the bay during ebb tide. Recirculation over longer timescales could also occur through the seasonal movement of the fresh/brackish interface within the aquifer. The large coverage of limestone in this area may be favourable for such recirculation to occur, and limestone may contribute significantly to the Ra inputs observed. However, the relative role of sediment for seawater recirculation may not only depend on the area of contact but also of the ability of the surface considered to let water infiltrate within its porewater. Finally, studies in the nearby Bell Harbour identified a deep karst network extending potentially below the bay (Philip Schuler et al., 2018). If such karst network is also present in Kinvarra Bay, it may amplify the contribution of the limestone aquifer to the Ra fluxes in the bay. Other former minor springs along the bay may also allow preferential circulation of seawater through the bay floor, in particular during dry periods.

Considering the previous points, we estimated the likely relative role of each sediment type for Ra fluxes in Table 5, assuming as a first step that it is dependent on both area and infiltration rate using the following equation:

$$F_i = \frac{A_s I_s}{\sum A_i I_i} \quad (3.11)$$

Where *Fi* is the relative role of the bay floor type for the total volume of seawater crossing the bay floor during a given time (% of total fluxes); A_s is the fraction of the bay with this bay floor type; I_s is the infiltration rate of water in this bay floor type (length per time); $\sum A_i I_i$ the sum of the product of area (A_i) and infiltration rate (I_i) (or vertical saturated hydraulic conductivity) for all bay floor types in the bay. As it is not usually feasible to take a representative undisturbed sediment sample to determine the hydraulic conductivity of subtidal sediment, we estimated hydraulic conductivity from soil classification and bulk density, following the soil dataset of Pachepsky and Park (2015) and sediment map for the bay from the Marine Institute (e.g. Figure 19). To assess the range of possible infiltration rates through the limestone bay floor, we took a range of hydraulic conductivity values for Irish Karst limestone from a review of previous estimates in Ireland (Kelly et al., 2015). Using this approach, the contribution of limestone is assessed to represent the majority of discharge volume (88-98 %, Table 5), with potential minor fluxes from other sediment types in the bay.

This observation suggests that direct exchanges with the karst aquifer are likely to play an essential role for Ra fluxes to the bay, but that Ra releases from the superficial layer of fine sediment are also possible and may contribute to the total fluxes. Another potential source of radium is the nearby Galway Bay, in which larger Ra fluxes may also be present during summer.

Three potential radium sources can be thus identified by order of likely importance for the total volume of saline SGD: 1) the karst aquifer, 2) the sediments covering the bay floor and 3) sediments in Galway Bay. We review the potential Ra sources for these different end members in the next subsections.

4.5.1.1 Ra sources in Karstic limestone

The densely fractured limestone may contain fine sediment and oxides favourable for Ra accumulation and release. For example, Fe and Mn oxides can be found in cave and karst systems as sedimentary fills, as a wall, ceiling, and floor coatings/crusts (Hill and Forti, 1997), and can adsorb/release radium (IAEA, 2014). Elevated concentration of Barium – an element which can coprecipitate with radium due to similar properties (IAEA, 2014) – has been identified in Fe and Mn surface formations in karst systems (Frierdich et

al., 2011), suggesting that Ra may also be present in these formations. Moreover, previous studies identified geochemical evidence of seawater intrusion in the karst system in a radius of two km around Kinvarra Bay under low groundwater conditions (Figure 19 and Einsiedl, 2012; Petrunic et al., 2012). Modelling using hydrogeochemical equations also suggests that the recirculation of bay water within the coastal aquifer is a significant part of the total groundwater flow into the bay during low groundwater levels.

From these observations, the karst aquifer itself is likely to play a role as a source of additional radium. To determine what may be the Ra concentration of a section of limestone aquifer affected by seawater intrusion, we used repetitive samplings of radium activities in a borehole close to the main conduits feeding Kinvarra springs, 2 km away from the bay. During summer, higher salinity (up to 7.5 kg m^{-3}) and ^{224}Ra activities higher than usual (up to 8.2 dpm $100L^{-1}$) were observed. ^{223}Ra was less affected with a level of 0.6 dpm $100L^{-1}$ more similar to other surveys. At this level of salinity, most of the radium adsorbed to particles (70-80 per cent) is generally released in solution (Webster, Hancock and Murray, 1995). Kinvarra limestone aquifer, when intruded by pure seawater would be then able to release 10-12 dpm $100L^{-1}$ of aquifer volume for ^{224}Ra and 0.7-0.9 dpm $100L^{-1}$ for ^{223}Ra.

The final Ra activities in the discharged waters may be not only dependent on the salinity level of the recirculated waters, but also depend on the volume of the coastal aquifer where the seawater circulates, and the specific surface and properties of the karst features exposed to the saline intrusion. However, for a karst aquifer, the spatial changes of these values are usually impossible to quantify, and we thus use this estimated value as an end member, which is equivalent to assuming that the porosity in the karst and distribution of oxides and sediment are sufficiently homogeneous at large scale to not depend on groundwater level.

4.5.1.2 Ra sources in bay sediment

The second and third Ra potential sources, the fine sediments in the bay and Galway Bay would be regularly flushed by seawater and are thus less likely to lead to significant fluxes of Ra during summer unless significant bioturbation occurs during summer. Moreover, the typical range of infiltration rates are larger for a karst network than for

sediment, leading to smaller volumes of recirculation in sediment than in the karst network. However, the infiltration rates we used in Table 5 may vary in time, as a result of bioturbation, and may lead to larger Ra values and circulations during summer.

Previous surveys of Benthic organisms within the nearby Galway Bay identified the presence of the polychaete worms *Melinna palmata* with *Magelona spp.*, and the bivalves *Thyasira spp*. in infralittoral sandy mud, and the bivalves *Abra alba* and *Nucula nitidosa* in circalittoral sand (AQUAFACT International Services Ltd, 2012). All these organisms may lead to potential disturbance of sediment, consequently causing additional radium fluxes to the bay as part of their life cycle, if they are present in the system during summer or low groundwater level conditions.

However, previous studies of bioturbation and bioirrigation effect on radium fluxes showed that, while the effect on long-lived radium isotopes (^{226}Ra and ^{228}Ra) was substantial, the effect on short-lived isotopes such as ^{224}Ra was low and mainly diffusion-driven (Hancock et al., 2000). We determined from the measurement of Ra release from these sediments that ^{224}Ra concentration in sediment porewater that has not been in contact recently with seawater could be of up to 3900dpm 100L^{-1} (subtidal sediment, 42% of total bay cover, Table 5). The largest Ra activities that could be released by sediment were observed inside Kinvarra Bay, for subtidal, organic-rich sediment (3900 dpm 100L^{-1}, Table 5). Sediments in Galway Bay, on the other hand, had ten times lower Ra activities (330 dpm 100L^{-1}). Intertidal sediments, coarser sediment in Kinvarra tended to have intermediate values between fine sediment and Galway Bay values (528 – 1528 dpm 100L^{-1}) and represented 15% of the bay floor.

As two sediment types in the intertidal area had distinct Ra porewater activities, we assume for the later calculations that they represent each half of the sediment present in the intertidal area (8% of the total bay floor each). Only a small amount of water circulation in sediment previously not affected by seawater intrusion may thus be enough to explain the increase, and thus we consider this sediment as a potential Ra source.

Table 5: Potential Ra sources and the resulting saline SGD fluxes if they are the primary Ra sources for the bay during low groundwater level period. Hydraulic conductivities for sediments are 25th and 75th quartiles for US sediments classified by texture and bulk density, from Pachepsky and Park (2015). Porewater Ra and surface bound Ra were determined by the resuspension of each sediment type in Ra-free sea water during the current thesis. Bulk density and porosity were also determined in this work.

Sample description	A_i, Area occupied by this bay floor type for each zone (%)			Infiltration rate/Saturated Hydraulic conductivity	F_i, Contribution to total recirculation in each zone of this bay floor type (%)			Porosity (± 0.03)	Bulk density	$C_{i\ desorbed}$ Porewater Ra dpm $100L^{-1}$		Ra^{224}/Ra^{223}	Surface bound Ra dpm $100g^{-1}$		n
	Intertidal	Subtidal	total	mm h^{-1}	intertidal	subtidal	total		kg m^{-3} sample	^{224}Ra	^{223}Ra		^{224}Ra	^{223}Ra	
Limestone waters															
Borehole with saline intrusion in karst network	70	8	42	22-47.5 (Kelly et al., 2015)	83 -91	42-88	77 -90	-	-	11	0.6	10	-	-	1
Intertidal sediment Kinvarra															
Silty sand with oxides and shell debris (1-2%)	15	-	8	8.5-30.2 (Pachepsky and Park, 2015)	11 -7	-	9 -7	0.46	1379 ±30	528 ±127	30 ±7	18 ±2	0.29 ±0.04	0.01 ±0.002	1
Sandy silt with mm rock fragments (1-2%) and oxides	15	-	8	2.2-14.9 (Pachepsky and Park, 2015)	5.6 -2	-	5 -2	0.48	1275 ±30	1528 ±367	97 ±23	16 ±2	0.9 ±0.1	0.037 ±0.009	3
Subtidal sediment Kinvarra															
Organic rich silty clay	-	92	42	0.4-5.7 (Pachepsky and Park, 2015)	-	58 -17	9 -2	0.75	548 ±30	3900 ±936	414 ±99	9 ±1	5 ±1	0.6 ±0.1	1
Galway Bay sediments															
Sandy silt with mm shell debris (2-3%) and 1-2 mm angular rock fragments (5%)	-	-	-	2.4-14.9 (Pachepsky and Park, 2015)	-	-	-	0.45	1474 ±30	252 ±61	17 ±4	15 ±2	0.08 ±0.02	0.005 ±0.001	1
Clayey silt with mm rock fragments and shell debris (1-2%)	-	-	-	1.3-10 (Pachepsky and Park, 2015)	-	-	-	0.46	1387 ±30	330 ±79	44 ±11	7 ±1	0.11 ±0.03	0.015 ±0.004	2

Now that we have reviewed the physical sources of Ra to the bay, we can attempt to quantify the volume of recirculation that needs to be present to explain the observed Ra fluxes from the bay floor observed during summer/low groundwater level periods.

4.5.2 The potential volume of porewater invaded by seawater that must occur when the groundwater level is low to explain the observed Ra increase.

In the intertidal area, the effect of tide tends to create shallow saline recirculation cells, flushed with saline seawater over periods of hours to days (e.g. Fig 1 in Bratton, 2010). Recirculation of seawater also occurs in the subtidal area (e.g. Fig 1 and 2 in Bratton, 2010), where the mixing between seawater and freshwater at the saline/fresh interface continuously drives water from the floor to the sea into the salt/freshwater interface and back to the sea (Cooper, 1965). This flow is a consequence of the mixing between seawater and freshwater by dispersion, diffusion and convection around the saline/fresh interface, driving seawater volume to the sea as a result of the freshwater movement and the density difference between freshwater and seawater (e.g. see Figure 2 in Cooper, 1965). This mechanism is also present at the embayment and shelf scale (e..g. Figure 2 and 3 in Bratton, 2010), which means that Ra fluxes driven by this process may also occur outside of a coastal system.

However, due to the larger water depth present in such deep area, their total effect on Ra inventory is likely to be less significant than the same volume occurring in nearshore areas. From these observations, we can define four potential hypothesis that may explain an added continuous ^{224}Ra and ^{223}Ra fluxes along Kinvarra Bay during low groundwater level, which would not be present during high groundwater level.

1) The volume of the intertidal saline recirculation cell increases when groundwater level decreases, favouring seawater intrusions in previously freshwater-saturated porewater and releasing additional Ra fluxes to the bay from the intertidal circulation cell. In this case, we can consider two sub hypothesis: 1a) The sediments are fully flushed regardless of the groundwater level, limestone aquifer is the only contributor to the Ra increase and 1b) the sediments are not fully flushed by seawater in high groundwater level, and both the limestone and

sediment are contributing to the flux. In both cases, we can expect that only the intertidal area contributes to added Ra fluxes to the bay.

2) The volume of the aquifer where the recirculation of saline groundwater is present (the deep recirculation cell) increase when groundwater level decrease, causing an additional Ra release from the aquifer to the bay. In this case, the limestone is likely to be the primary Ra source, as the increase of volume will dominantly occur in the deep aquifer, and fluxes will preferentially come back to the bay in areas where the karst system is well developed. However, these fluxes may also lead to the resuspension of subtidal sediment, generating added Ra fluxes. The end member for this hypothesis is thus a combination of limestone and subtidal sediment, with a relative fraction function of the percentage of area occupied and infiltration rate of water through the surface.

3) A combination of 1 and 2. The fluxes result from the increase of the volume of both the intertidal recirculation cell and the deep recirculation cell. In such cases, all sediment types in the bay contribute to the fluxes, as a function of their percentage area occupied and infiltration rate of water through them.

4) Ra discharges are not coming from inside the bay but are advected Ra discharges from Galway Bay, either from shallow or deep saline recirculation cells. Given the trend observed in Figure 21, this hypothesis is only possible if the Ra inputs are advected to the system in deep waters, giving a similar pattern to the one of a continuous deep-water source. In such cases, the endmember is likely to have characteristics influenced by sediments in Galway Bay, and Galway Bay Ra activities in sediment might be used to assess the magnitude of the discharge needed to create the observed change. According to Schuler et al., (2020), who identified multiple springs outside of Kinvarra Bay: “Submarine groundwater discharge (SGD) in Galway Bay is likely to occur via sinkholes that are filled by sediments”. These sediment-filled features may provide preferential Ra sources during dry period when the freshwater flow decreases and saline water intrudes deeper in sediment previously saturated with freshwater.

In Table 6, we estimate for these four hypotheses the volume of pore space previously occupied with freshwater that needs to be intruded with seawater to explain the observed Ra increase in the bay. The third column lists the end member values taken for each hypothesis (from Table 5). The volume of pore space intruded by seawater for each hypothesis was calculated as follows:

We considered that recirculated bay water within sediment or the karst aquifer (saline SGD) has a concentration equal to the mean bay water radium activity plus the radium desorbed due to the intrusion of seawater in pore space previously saturated with freshwater. From this, we can estimate the volume of saline SGD as follows:

$$Q_{RSGD} = \frac{A_b * F_{Ra}}{C_b + C_{desorbed}} \quad (3.12)$$

Where Q_{RSGD} is the flow ($m^3\ d^{-1}$) of additional saline SGD (RSGD) necessary to explain the increase of Ra activity within the bay; F_{Ra} is the Ra fluxes from the bay floor (dpm $m^{-2}\ d^{-1}$); C_b is the activity of radium in the bay during winter, when RSGD was minimal (10 dpm m^{-3}); A_b is the area of the bay at mean tide (2×10^6 m^2); $C_{desorbed}$, is the concentration of Ra released per volume of porewater, when seawater invades a volume of porewater previously saturated by freshwater.

For Hypothesis 1a, only one end member contributes significantly to the Ra fluxes in the bay, and the values listed in Table 5 ($C_{i\ desorbed}$) are used for the value of $C_{desorbed}$. However, for hypothesis 1b, 2, 3 and 4, several end members are expected to contribute to the added Ra in the bay. In such cases, $C_{desorbed}$ was calculated using two alternative methods.

The first method assumed that the relative role of a bay floor type for the total recirculation of bay water occurring in a section of the bay (intertidal area, subtidal area or total bay area in Table 5) was mainly dependent on its surface of contact with the bay waters. The second method assumed that the relative role of a bay floor type for recirculation was dependant on both the surface of contact and infiltration rate.

The first method estimates $C_{desorbed}$ from the equation:

$$C_{desorbed} = \sum_{i=1}^{n} C_{i\ desorbed}\, A_i \quad (3.13)$$

Where $C_{i\ desorbed}$ is the quantity of Ra released per volume of porewater intruded with seawater for a given sediment or rock type; A_i the proportion of the bay that is covered by this sediment type or rock type.

The second method estimates $C_{desorbed}$ from the equation:

$$C_{desorbed} = \sum_{i=1}^{n} C_{i\ desorbed}\, F_i \quad (3.14)$$

Where $C_{i\ desorbed}$ is the quantity of Ra released per volume of porewater intruded with seawater for a given sediment or rock type; *Fi* the relative role of the sediment/bay floor type for the total volume of seawater crossing the bay floor (Table 5), calculated from equation 3.11.

The resulting range of potential RSGD flow increases between high and low groundwater level is between 0.2 $\times 10^5$ m^3 d^{-1} and 80 $\times 10^5$ m^3 d^{-1}, depending on the hypothesis on the Ra source and the Ra isotope considered (Table 6). The estimated saline SGD flows are maximal if karsts are the main Ra source for the bay (Hypothesis 1a in Table 6), and the lower range if the subtidal area in the bay is the main Ra source for the bay (Hypothesis 2 in Table 6). As we defined each estimates in term of recirculation processes (deep vs shallow recirculation, in Table 6), this range may be refined with additional Ra measurements in the bay to determine which of these hypotheses is the most likely explanation of the observed increase of Ra fluxes between high and low groundwater level conditions.

Our previous work showed that fresh SGD to Kinvarra Bay during these surveys varies between 1-5 to 15-20 $\times 10^5$ m^3 d^{-1} (Table 4). Saline SGD discharge are thus between one per cent (0.2 $\times 10^5$ m^3 d^{-1}, Table 6) to eighty times the fresh SGD (maximum rate: 8 $\times 10^6$ m^3 d^{-1}, Table 6). The largest saline SGD value (4 $\times 10^6$ -8 $\times 10^6$ m^3 d^{-1}) is found if the karst aquifer is assumed as the primary source of Ra, with no Ra contribution from sediment. Estimates using equations derived from Schneebeli (1986) (RSGD= 5.5-31.6 per cent FSGD during spring tides, depending on groundwater level) are thus in the lower range of these two extreme values. This can be expected as the estimates of minimum saline SGD fraction using Schneebeli (1986) equations did not consider density-driven recirculation, which drives large additional volumes of deep seawater recirculation in a heterogeneous system such as karst (Cooper, 1965). This leads us to think that a shallow recirculation of seawater probably occurs in the intertidal area. Thus, hypothesis 2, which assumed negligible shallow recirculation in Table 6, is unlikely.

Moreover, the borehole had a more marked increase of salinity than the spring (Figure 22), suggesting that deep recirculation is also occurring. Thus, hypothesis 1b is also

unlikely. We can thus reduce the range of likely recirculation affecting the system to 0.3-80 $\times 10^5$ m^3 d^{-1} (hypothesis 1a, 3 and 4).

This range can be further reduced to 0.3-4.4 $\times 10^5$ m^3 d^{-1} (hypothesis 3) if we assume that (1) "saline" SGD through Galway Bay sediment has a negligible influence on the system, (2) the karst is not the only contributor to the increased Ra, but sediment from the bay floor also contributes. A given Ra source can have a detectable effect on Ra activities if : the Ra source is large compared to the volume of the system to lead to a significant change; the timescale of Ra inputs transfers to the measurement points is shorter than the renewal time of the system and the half-life of the isotope considered. Schuler et al., (2020) identified several springs in Galway Bay which may be related to former sinkholes filled with sediments, derived from a period when the sea level in the area was lower. These structures may act as preferential Ra sources during low groundwater level periods. However, the volume of Galway bay is more than one order of magnitude larger than the volume of Kinvarra Bay. As a result, Ra inputs in Galway bay from sediments occurs are likely to be strongly diluted, particularly if they occur as a result of saline recirculation, thus discharging water with similar density to Galway Bay waters, easier to mix than fresh SGD. Moreover, the half-life of ^{224}Ra is 3.6, and 11.4 days for ^{223}Ra, thus decay is likely to be significant during the transfer of such inputs to Kinvarra deep waters. As a result of these combined factors, such sources should not lead to a pattern similar to a continuous Ra source from deep waters as observed here. Moreover, as a result of dilution and decay, and of the lower Ra activities in Kinvarra sediment, the effect of Galway bay sources on Kinvarra Ra activity is likely to be small compared to Ra sources occurring directly within Kinvarra bay.

As a result of this however, using different Ra isotopes to assess "saline" SGD may lead to a different range of figures for this system compared to what was presented here. It can be noted as well that the maximum high tide levels during the periods sampled here are 1m lower than the maximum possible level in Galway Bay long-term recordings (3.6 m). A larger saline SGD proportion may be thus present during periods with larger tide fluctuations than considered here. In the next section, we discussed how the composition of the total SGD fluxes is modified as a result of this larger fraction of saline SGD in the karst during spring tides low groundwater level periods.

Table 6: Potential saline SGD discharge derived from Ra isotopes, using five different hypotheses of recirculation mechanism.

Hypothesis for the observed Ra increase during low groundwater level periods	End member contributing to the Ra fluxes	Volumes of porewater invaded by seawater explaining the observed Ra increase (10^5 m^3 d^{-1})			
		Estimated from equation 3.13 (relative role of bay floor types dependant on area)		Estimated from equation 3.14 (relative role of bay floor types dependant on area and Infiltration rate)	
		Using ^{224}Ra	Using ^{223}Ra	Using ^{224}Ra	Using ^{223}Ra
Hypothesis 1a: Increase of shallow or deep recirculation, driven by tidal pumping of bay water in karst network only (diffuse and conduit).	Limestone diffuse karst in the intertidal area and conduit karst aquifer throughout the bay	45	80	45	80
Hypothesis 1b: Increase of shallow recirculation driven by tidal pumping of bay water in both karst network and sediment.	Limestone diffuse karst aquifer and sediment in the intertidal area	1.7	2.9	3.5 –6.9	6 -12
Hypothesis 2: Increase of deep recirculation coming back to the bay with Ra throughout the bay floor, increasing salinity levels in both limestone and sediment.	Sediment and limestone karst aquifer in the subtidal area.	0.1	0.1	0.2 – 0.8	0.2 – 0.8
Hypothesis 3: Increase of both deep and shallow recirculation	All sediment and limestone in the bay	0.3	0.3	1.1 – 3.5	1.2 – 4.4
Hypothesis 4: The Ra increase only comes from advection of water from outside of the bay.	Galway Bay sediment	1.6 - 2.1	1.2-3.1	1.6 - 2.1	1.2 - 3.1
Range of R SGD from all hypothesis (10^5 m^3 d^{-1})		0.1- 80		0.2 - 80	

4.5.3 Effect of low groundwater level periods on nutrient reactions and fluxes in the surface/groundwater interface

Coastal aquifers such as karst, basalt or laminated sand usually have a thick brackish interface layer between saline and fresh groundwater, as a result of the heterogeneity of permeability and porosity of these aquifers driving larger dispersion than in homogeneous aquifers (Cooper, 1965). Here, we observe a slight salinity increase instead of a sharp salinity increase with decreasing groundwater level in the borehole (Figure 22), which confirms that a relatively thick brackish transition layer indeed exists in the deep sections of this aquifer at the interface between pure seawater and pure freshwater (potentially similar to figure 5 in Cooper, 1965). The presence of such interface tends to amplify the recirculation of seawater in the deep aquifer (Geological Survey, 1965), thus increasing saline SGD compared to what would be expected considering the groundwater head. Besides, it suggests that deep recirculation of seawater is indeed occurring. Thus, this confirms that hypothesis 1b is unlikely: the movement of the deep saline/fresh interface in the aquifer is contributing in part to the observed change of composition of the SGD fluxes. This movement could be related to the seasonal fluctuation of groundwater level and potentially sea level (see conceptual model in Figure 24).

The peak of salinity coincided with a decrease of dissolved oxygen and change of SRP values in the borehole when groundwater level is below 3m. This may occur if the borehole was tapping in part in the brackish transition layer (e.g. as a result of the movement of the brackish/fresh interface in the deep aquifer towards the borehole as shown in Figure 24). A decrease of dissolved oxygen was also visible at groundwater level 4m or lower in the spring (Figure 22), thus the effect does not seem to be limited to the direct proximity of the borehole.

Such change of dissolved oxygen and SRP suggests either increased rates of biological reactions consuming oxygen or longer pathways of the discharged water. These may be due to:

(1) A larger fraction of older water, coming from deeper karst, which had more time to become depleted in oxygen and enriched in dissolved P through the degradation of particulate or organic matter (for example, if the borehole tap “older” aquifer

waters deeper below the saline/fresh interface, Figure 24), or from the primary porosity.

(2) Different rates of oxygen consumption in the catchment and its aquifer in summer. During summer, the drier soil typically leads to larger respiration and degradation of organic matter in sediments, decreasing oxygen level in porewater. The lower recharge also plays a role, by favouring the presence of a larger fraction of older, oxygen-poor waters in the aquifer, by diminishing the inputs of oxygen-rich recharge water (Champ et al., 1979).

This observed change of dissolved oxygen may modify both the nitrogen and phosphorus cycles in the subterranean estuary around Kinvarra bay:

First, Ammonium-oxidizing microorganisms are less sensitive to reductions in dissolved oxygen (DO) content than nitrite-oxidizing ones (Anderson, 1982; Lipschultz et al., 1990). As a result, reduced O_2 levels may, in turn, lead to incomplete nitrification, due to lack of oxygen to complete the transformation of NH_4 in NO_3, leading to an increase of NO_2. In the marine environment, NO_2 peaks are generally associated with reduced DO (Gruber, 2008; Morrison et al., 1999). This can lead to a superposition of NO_2 formation by (aerobic) nitrification, and NO_2 formation by (anaerobic) denitrification (e.g. Yakushev and Neretin, 1997) both of which can co-occur at very low but non-zero DO. In coastal karst environment in which seawater intrusion occurs, on the other hand, increased NO_2 associated with decreased DO has been previously associated with the presence of deep karst conduits favouring the recirculation of seawater over large timescales (Garman and Garey, 2005). In such cases, nitrite levels are higher at the transition zone between low oxygen deep karst and surface karst waters (Garman and Garey, 2005).

Secondly, phosphorus desorption is dependent on oxidoreduction properties. Reducing conditions are more favourable for the presence of SRP in solution, as some P binding sites such as Fe or Mn (oxy)hydroxides are less stable under reducing condition (Colman and Holland, 2000; Paytan and Mclaughlin, 2007). Despite the different oxidoreduction properties, the increase of salinity and decrease of oxygen levels may also amplify the desorption of P and dissolution or transformation of phosphorus-containing minerals

(Price et al., 2010), releasing additional phosphorus to the system compared to what is typically present in the spring (Figure 24).

In Kinvarra catchment, a more marked changes of salinity (Figure 22a) and NO_2 (Figure 22b, c) was observed for the borehole than for the spring when groundwater level is low during spring tides. This difference suggests that the added saline discharge is coming from a deep conduit through a long pathway instead of coming from direct superficial salinity intrusions from a superficial karst network, as such superficial saline intrusion would most likely affect Kinvarra spring before the borehole.

The observations in the karst and Kinvarra spring show that recirculation of seawater occurring during low groundwater levels lead to larger dissolved phosphorus, radium and potentially other elements in the discharged waters to the bay. Conversely, only an increase of radium and no significant increase of dissolved SRP was visible in the bay water column. Moreover, there was no correlation between Ra level and SRP.

To find potential explanations for this trend we can first examine the sorption properties of Ra^{2+} and PO_4^{2-} ions. Ra^{2+} and PO_4^{2-} ions can potentially occupy sorption sites of similar sizes (their size are 221 pm and 238pm respectively) and tend to be both released following salinity increases (e.g. Price et al., 2010 ; Webster et al., 1995). Due to their opposite charge however, the mechanism for desorption is distinct. With increasing salinity, the competition with cations such as Na^+ (227 pm ion size) increase and lead to the release of cations (such as Ra^{2+}) previously occupying negatively charged sorption sites. In the case of phosphorus, the desorption occurring with increasing salinity, is a combined effect of (a) the dissolution of Ca-P compounds, (b) the substitution of positively charged ions (such as Ca^{2+}) by Na^+ on negatively charged sorption sites (Sharpley et al., 1988), reducing the ability of sorption sites to absorb negatively charged ions, and (c) the increasing competition with other anions in seawater for sorption sites.

Moreover, the sorption and desorption properties of soils are also a function of their oxidoreduction profiles. Under reducing conditions, oxic soils and marine sediments tend to retain the Mn, Fe (oxy)hydroxides, which are preferential sorption sites for both Ra and SRP. Under anoxic conditions, on the other hand, (oxy)hydroxides tend to be dissolved, releasing

elements adsorbed to them (Colman and Holland, 2000; Paytan and Mclaughlin, 2007). Thus, the increased salinity and reduced dissolved oxygen in porewater should be expected to lead to an increase of both SRP and Ra in bay water during periods of high saline SGD as it can lead sediment towards reducing conditions. Recirculated SGD would be then a source of added P to the bay (Figure 24).

However, here, no correlation is observed between Ra and SRP levels. This absence of correlation suggests that the added P inputs are rapidly consumed in the bay water column and superficial sediment layer, while Ra, as an element generally not used by the biological activity, remains. Phosphorus is a limiting nutrient for this system (Rocha et al., 2015), and added phosphorus would rapidly be transferred to organic matter and particulate form by the local biological activity, which is typically maximal during summer, low groundwater level periods when most of the saline SGD occurs. Such transfer to organic matter may occur within the water column, consumed by phytoplankton or macroalgae in the bay, and may provide in such areas less phosphorus limiting conditions than without saline SGD fluxes.

For example, a previous study showed that macroalgae types in Kinvarra were affected by the relative availability of phosphorus and nitrogen (Tara et al., 2018): sites with low N:P due to high fresh SGD were having more widespread species of *Fucus vesiculosus* and *Enteromorpha intestinalis* than *Ascophyllum nodosum* (Tara et al., 2018). Sites where saline SGD is present dominantly over fresh SGD may thus favour the survival of species requiring larger P availability such as *Ascophyllum nodosum*. This may be possible however only if the added P is not directly consumed by the local phytoplankton bloom, in which case the added inputs may have a negative effect on macroalgae in general by shading, unless the area considered is well flushed.

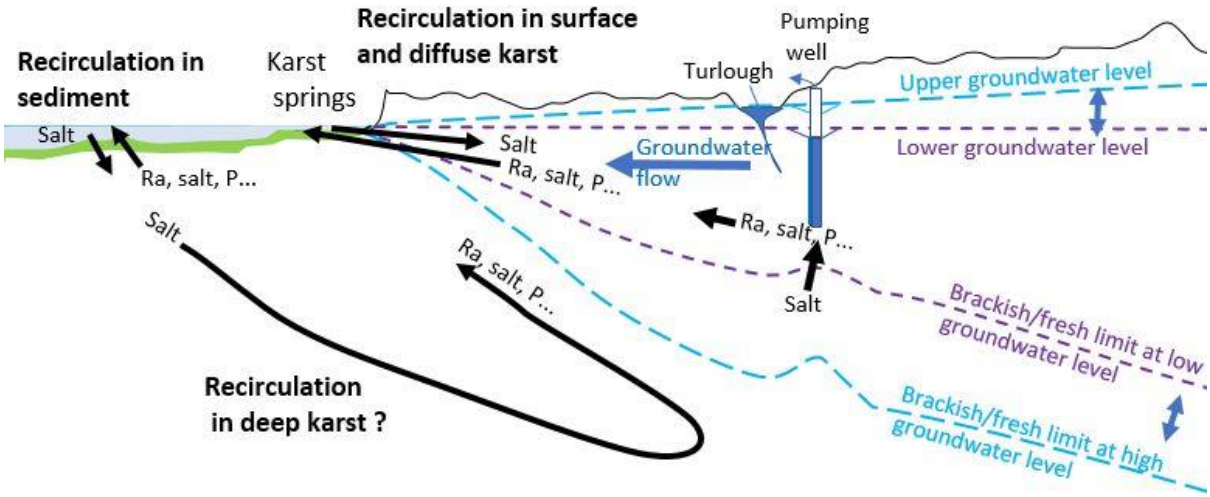

Figure 24: Conceptual model of the recirculated SGD in Kinvarra Bay. Brackish/fresh interfaces provided are theoretical interfaces if the karst network is sufficiently dense to allow deep recirculation of seawater. Actual brackish/fresh and groundwater level interfaces are likely to be modified by the deep structure of the karst, but would require a more accurate quantification of the karst system directly around Kinvarra Bay to be estimated.

4.5.4 Discussion on the representativeness of the transects analysed here for the annual variability

To determine to what extent the changes we observed in the freshwater end member and in Kinvarra Bay may be representative of the annual variability, we relate the survey in the current study to the annual changes of groundwater and tidal variability in Figure 25. Between 2016 and 2021, sea level at spring tides were closer to or higher than groundwater level around May-June-July-August or July-September (Figure 25). These periods can be subdivided in three to five smaller periods during which spring tides are the highest and are likely to lead to exceptionally high rates of saline SGD. The samples in the current study were taken close to spring tides, when sea-level fluctuations are the highest. These surveys are thus likely to represent the current mid-upper range of the effect of recirculation and seawater intrusion for the karst nutrient transformations. However, the maximum tidal level occurring during the surveys (2.3 m in Table 4), is still one meter lower than the maximum variability observed in the nearby Galway Bay (3.6 m), which suggests that periods of larger saline recirculation in the aquifer may be possible.

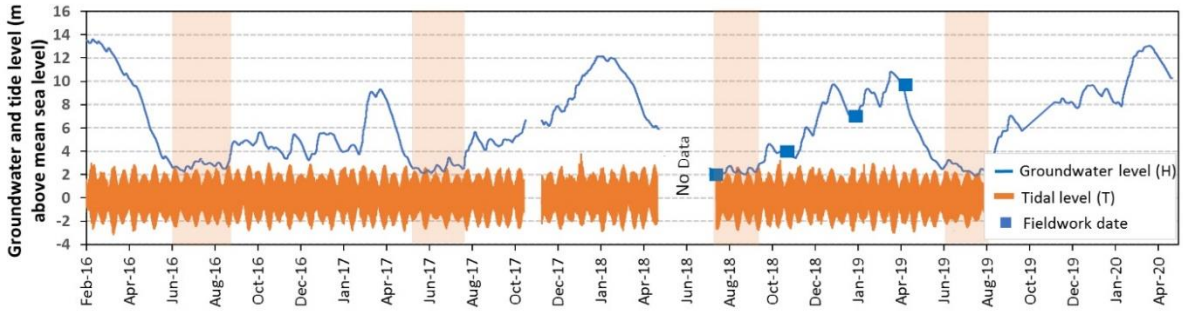

Figure 25: Groundwater and tidal variability between 2016 and 2020 compared to the conditions prevailing during the surveys in this work. Vertical colour zones highlight periods when the groundwater level measured at Killiny borehole is closer to or lower than the spring tide high tide sea level.

On the other hand, neap tides are likely to be less impacted by such seawater intrusion, unless by saline SGD due to the seaward movement of the saline-fresh interface (such as described in Kohout, 1965). As a result of this influence of tidal variability, the effect of groundwater level on dissolved oxygen, NO_2 and SRP observed here during spring tides (Figure 22) is not likely to appear as clearly in the EPA long term sampling in Kinvarra springs, which does not select specifically spring tides surveys. However, in the EPA dataset (2007-2015), dissolved oxygen in Kinvarra springs tend to be larger with increasing groundwater level, with values below 50% DO more frequent when groundwater level in Killiny Borehole was lower than 6m. Moreover, if we consider only the periods when the tidal variability and groundwater level variability is readily available (2010-2015), the maximum SRP level (24 µg/l) and NO_2 concentrations (10 µg/L) observed by the EPA long term monitoring of Kinvarra springs occurred during a survey when daily tidal variation was maximal, and groundwater level at Killiny was less than 3 m (2.41m). Thus, the trends observed in the EPA dataset do not contradict the evidence provided here.

To conclude, we show that a significant increase of SRP levels, increased NO_2 and reduced level of dissolved oxygen can occur in the discharged submarine groundwater discharge flux during such periods of spring tides occurring during droughts, creating potential ecosystem changes.

These periods coincide with periods during which Harmful Algae Bloom (HAB) are most common in Ireland (Figure 25). These are: Mid-March to early may for Amnesic Shellfish Poisoning events, April to December for Azaspiracid Shellfish Poisoning events, May to

December for Diarrhoeic Shellfish Poisoning events, June to mid-July and end September for Paralytic Shellfish Poisoning events (see Marine Institute, 2019b).

Low groundwater level conditions could thus amplify the intensity of blooms and play a role in the timing of HAB related closure of aquaculture activities, by driving additional inputs of solutes to the system (including limiting nutrients such as phosphorus) from sediment and section of karst previously not affected by salinity intrusion, during periods favourable for plankton growth.

On the other hand, the reduced dissolved oxygen in the discharged waters may increase the daily fluctuations of oxygen due to day-night cycle of primary production, amplifying P fluxes from the bay floor and increasing stress for marine organisms closest to the spring during such periods. The EPA long term sampling shows such oxygen fluctuations that are probably the result of the combined effect of reduced dissolved oxygen in the spring when groundwater level is low (Figure 22) and of the spatial and temporal changes of primary production-respiration.

Additional sampling of radium, nutrient and dissolved oxygen changes in Kinvarra spring along the tidal cycle during neap and spring tide surveys would allow to study further the effect of different rates of recirculation on dissolved oxygen and nutrient in karst springs and their linked bay, and validate which of the recirculation mechanisms listed in Table 6 is dominant for this system.

4.6 Conclusion of Chapter 4

Our combined method involving radium measurements, nutrient, dissolved oxygen and equations derived from Schneebeli (1986) allows studying the variability of the composition of SGD under different groundwater level conditions for a karst system and its effects on the bay chemistry. We demonstrate that the fraction between saline SGD and fresh SGD during spring tides is dependent on the hydraulic gradient in the regional aquifer (groundwater level-sea level). Furthermore, we give a preliminary assessment of saline SGD fluxes for this system during spring tides following five different hypotheses on the nature and location of the seawater recirculation affecting the bay. From this, we

derive the effect of these recirculation fluxes on nutrient transformations in the subterranean estuary. Saline SGD discharge estimated from the radium inventories in the bay represented between 0.2 $\times 10^5$ m^3 d^{-1} and 80 $\times 10^5$ m^3 d^{-1} (1-2 per cent to 80 times the fresh SGD discharge to this system) depending on the hypothesis on the dominant recirculation mechanism leading to the Ra increase (shallow, deep or a combination of both) and the method used to calculate the relative contribution to Ra fluxes from each bay floor type. The most likely hypothesis (hypothesis 3) considering that the added Ra comes from the increase of the volume of both deep and shallow recirculation cells lead to an intermediate range of 0.3-4.4 $\times 10^5$ m^3 d^{-1}. This is thus of a similar magnitude to the range for fresh SGD in the bay previously estimated. Equations derived from Schneebeli (1986), ignoring density and dispersion-driven recirculation led to a range of RSGD/FSGD ratio between 5% ±1 and 32% ±2, with the highest proportion observed for the lowest groundwater level. The added solute fluxes (here mainly radium and phosphorus) caused by saline SGD are the most significant during spring tides periods coinciding with low groundwater level (<6m here). This additional flux is likely to be created by bay water recirculation through the bay floor, releasing radium and other elements that tend to be released from particles under change of salinity and dissolved oxygen (such as phosphorus). The potential source for the observed increase would be either sediment, section of superficial karst aquifer typically saturated with freshwater, or changes of chemical conditions in deep karst networks. The SGD fluxes had reduced oxygen levels during low groundwater level periods. The combined effect of larger soil organic matter degradation and lower recharge in the catchment, and the additional dissolved oxygen consumption in the aquifer driven by the inputs of nutrient and dissolved organic carbon by seawater recirculation may explain this reduced oxygen levels. These combined effects were shown to be able to lead to greater availability in solution of P and NO_2 levels but may have effects on other elements sensitive to oxidoreduction conditions. In a context of global sea-level rise and increasing groundwater pumping for water supply, these combined trends are likely to lead to the release of solutes to coastal areas during drought periods coinciding with spring tides, and thus to play a role for the timing of blooms, reduced dissolved oxygens and other changes connected to land-derived solute fluxes in coastal areas.

4.7 Acknowledgements

This publication is a result of research supported in part by a research grant from Science Foundation Ireland (SFI) under Grant Number 13/RC/2092 and co-funded under the European Regional Development Fund and industry partners of the Irish Centre for Research in Applied Geosciences. Contribution was also made from an Irish Research Council and Environment Protection Agency funded project. Maxime Savatier was supported through an iCRAG PhD fellowship (ref TP GW3.2PhD5), co-funded by Science Foundation Ireland (SFI) and the European Union. We thank Dr Jan Scholten from Kiel University for his advice on radium analysis, Maria Teresa Guerra, Jennifer Murphy and Gennaro Scarselli, and Meabh Hughes for their assistance in fieldwork. We are also grateful towards Rainer Krause for his help during the transect surveys.

5 PAPER C: Radium isotope ratios as a tool to characterise nutrient dynamics in a variably stratified temperate fjord.

Keywords: Estuarine systems, Fjord, Stratification, Radium isotopes, Ecological Stoichiometry, Phytoplankton, Nutrients.

5.1 Abstract

The effect of freshwater discharge on solute vertical mixing and horizontal transfer rates is evaluated in a variably stratified temperate fjord (Killary Harbour, Ireland) using the activity ratios of ^{224}Ra and ^{223}Ra in the water column. With high river discharge (>1.7 $\times 10^6$ m^3 d^{-1}), surface $^{224}Ra/^{223}Ra$ activity ratios (ARs) decreased from 18.0 ±7.1 to 8.6 ±0.9 from the inner to the outer fjord and the system becomes stratified, resulting in clear differences of $^{224}Ra/^{223}Ra$ ARs between surface and bottom layers. When river discharge was low (<0.6 $\times 10^6$ m^3 d^{-1}), $^{224}Ra/^{223}Ra$ ARs dipped from 19.6 ±5.1 to 8.0 ±1.8 in the inner system before increasing again toward the outlet to the sea up to 11.3 ±3.6, and the water column was well mixed: the difference in $^{224}Ra/^{223}Ra$ ARs and salinity between surface and bottom layers was minimal. Longitudinal seaward decreases of surface water $^{224}Ra/^{223}Ra$ ARs within the inner fjord independently of river discharge suggested that the contribution of benthic-pelagic coupling to surface solute inventories is small in the inner section of the system. Conversely, the increase of $^{224}Ra/^{223}Ra$ ARs during low discharge conditions indicated that the slower flushing of the system, coupled with a well-mixed water column, facilitated solute transfers from deeper waters to the surface in the outer fjord. The effect of discharge on the residence time of water in the inner fjord was also determined using radium ages: longitudinal water flushing timescales are quickly reduced in the inner part of the bay with increasing discharge. We show that the degree of vertical mixing is an important driver of nutrient ratios in the system. Retention of soluble reactive phosphorus (SRP) and Ra in deep water and a higher molar N:P ratio in surface water were more likely under stratified conditions. Stratification may therefore amplify the effect of variable watershed inputs on the estuarine N:P ratio in Killary Harbour.

5.2 Introduction

Estuaries are key components of the land-ocean interface. They regulate watershed nutrient fluxes to the sea and contribute to the atmospheric CO_2 budget (Regnier et al., 2013), providing critical benefits to human society (Barbier et al., 2011; Costanza et al., 2014). Human activities have changed both the quantity and nature of terrestrial carbon and nutrient flowing into estuaries and the coastal ocean with likely consequences for global biogeochemical cycles and climate (Rabouille et al., 2001; Regnier et al., 2013; Ver et al., 1999). However, the role of estuaries as regulators of land-ocean nutrient fluxes is still poorly constrained (e.g. Borges, 2005; Mackenzie et al., 2005; Regnier and Steefel, 1999). This results mainly from the large spatial and temporal variability of the estuarine physicochemical environment.

Sediment-water fluxes and the reaction rates of elements within estuaries are significantly modified by the dynamics of stratification and flushing (e.g. Borges, 2005; Regnier and Steefel, 1999). Spatiotemporal changes of stratification in estuaries affect the transfer of solutes and nutrients between surface water, deep water and sediments. Furthermore, they impact the initiation of algal blooms, including harmful algal blooms (HABs) (Berdalet et al., 2017; Leming and Stuntz, 1984; Wyatt, 2014) and influence the makeup of phytoplankton communities in the water column (Frenette et al., 1996; Mena et al., 2019). Changes to flushing also affect chemical reactivity and solute concentrations (e.g. Andrews and Muller, 1983; Eshleman and Hemond, 1988; Boynton et al., 1995) with knock-on effects on the development of phytoplankton blooms (Tomasky-Holmes et al., 2013) or even on ecological succession, including the relative dominance of phytoplankton over macroalgae (Valiela et al., 1997).

In estuaries, timescales of water exchange with the sea can vary from a few to several hundred days, depending mainly on freshwater discharge (Alber and Sheldon, 1999). Moreover, the spatial variability of water exchange times in systems that are not well mixed, either laterally or vertically, can also vary across two orders of magnitude (Monsen et al., 2002; Webb and Marr, 2016). The complexity of real systems with regard to water renewal timescales is therefore not adequately represented by equations that assume complete mixing such as the flushing time (Geyer et al., 2000) or the tidal prism model (Dyer and

Taylor, 1973). To consider the spatial variability occurring in real-world systems, two timescales are necessary: the residence time, i.e. the time any water parcel takes to leave a coastal water body through its outlet to the sea from a given location (Dronkers and Zimmerman, 1982; Monsen et al., 2002), and the water age, i.e. the time a water parcel has spent within a water body since entering it (Zimmerman, 1988). Spatially variable water ages and residence times can be estimated with hydrodynamic models (Chen, 2007; Webb and Marr, 2016), or measured using radioactive tracers (Moore et al., 2006; Tomasky-Holmes et al., 2013). Estuarine circulation models still require a parametrisation of vertical mixing processes, on which questions of accuracy pend (Geyer and Ralston, 2011), and radioactive tracer methods were originally developed for coastal areas that were sufficiently far from the coast to have only one, dominant, radioisotope source (e.g. Moore, 2000). Estimating the spatial variability of water ages is more challenging in areas with multiple potential tracer sources such as estuaries, unless a unique source of constant radioisotope activity throughout the system is assumed (e.g. Moore et al., 2006). Nevertheless, radiotracers can help constrain sediment-water solute fluxes and the spatiotemporal variability of flushing in estuaries (e.g. Moore, 2000; Moore et al., 2006; Tomasky-Holmes et al., 2013). Thus, these techniques can validate modelling forecasts of residence time or water ages where other methods require the expensive collection of high-resolution temporal and spatial data (e.g. 400 drifters and 6000 driftcards in Pawlowicz et al., 2019). Ra isotope activity ratios determine both residence time and water age across a system (Moore, 2000; Moore et al., 2006). The four isotopes of radium (^{223}Ra, ^{224}Ra, ^{226} Ra, ^{228}Ra) have different half-lives, and the choice of isotope pairs to apply is determined by the timescale of interest (Moore, 2000).

Most importantly, radium isotope activities in a water sample integrate the short-term variability of stratification, sediment inputs, water mixing and renewal over the half-life of the isotope. For this reason, they provide time-averaged estimates of the magnitude of stratification, framing the conditions under which sediment-water fluxes are (or not) mixed throughout the water column. So far, however, very few studies have looked at the spatiotemporal variability of radium in estuaries in this way. As the natural processes leading to radium release in estuaries also lead to the release of key nutrients such as

phosphorus, grasping the dynamics of radium availability and mixing in estuaries is likely to improve the understanding of the estuarine biogeochemical and ecological functions.

Here radium isotopes were used to assess the spatiotemporal variability of estuarine flushing, and subsequently, the effect of water column stratification on the fluxes from bay floor sediments and on the nutrient resource-ratio availability in a variably stratified fjord. We used six longitudinal profiles of $^{224}Ra/^{223}Ra$ ages, nutrient concentration (N, P) and salinity, sampled at different times of the year in surface and deep waters from Killary Harbour in Western Ireland. We illustrate the combined effects of stratification, spatiotemporal changes to water ages and seasonal variability on elemental nitrogen: phosphorus (N:P) resource- ratio availability to the water column, demonstrating how this approach can provide insights into the biogeochemical functioning of estuarine ecosystems.

5.3 Materials and methods

5.3.1 Study Site - Killary Harbour

Killary Harbour is a fjord situated on the west coast of Ireland (Figure 26). On average, from 2015 to 2018, aquaculture activity in the bay produced 1035 tonnes of salmon (*Salmo salar*) and 866 tonnes of rope mussel (*Mytilus edulis*) annually - 7% and 10% respectively of the national production for these species (BIM, 2018a, 2018b). The fjord is 11 km long, 700 m wide and has a mean tide average depth of 12 m, with a maximum depth of 42 m near the mouth. The mean tide volume is 1.1×10^8 m^3, as determined using INFOMAR data (Geological Survey of Ireland/Marine Institute, 2019). The water column varies from well mixed to stratified, with the halocline developing between 3 and 10m depth (Keegan and Mercer, 1986). The system receives freshwater at a mean flow rate of 1.4×10^6 m^3 d^{-1} from a catchment area of ~260 km^2, delivered mainly by two rivers, the Bundorragha and Erriff, which drain respectively 19% and 63% of the catchment area (Figure 26). The catchment is mainly composed of sandstone and conglomerate, with tuffs and ignimbrites from the early Paleozoic, classified as a poorly permeable aquifer (GSI, 2020).

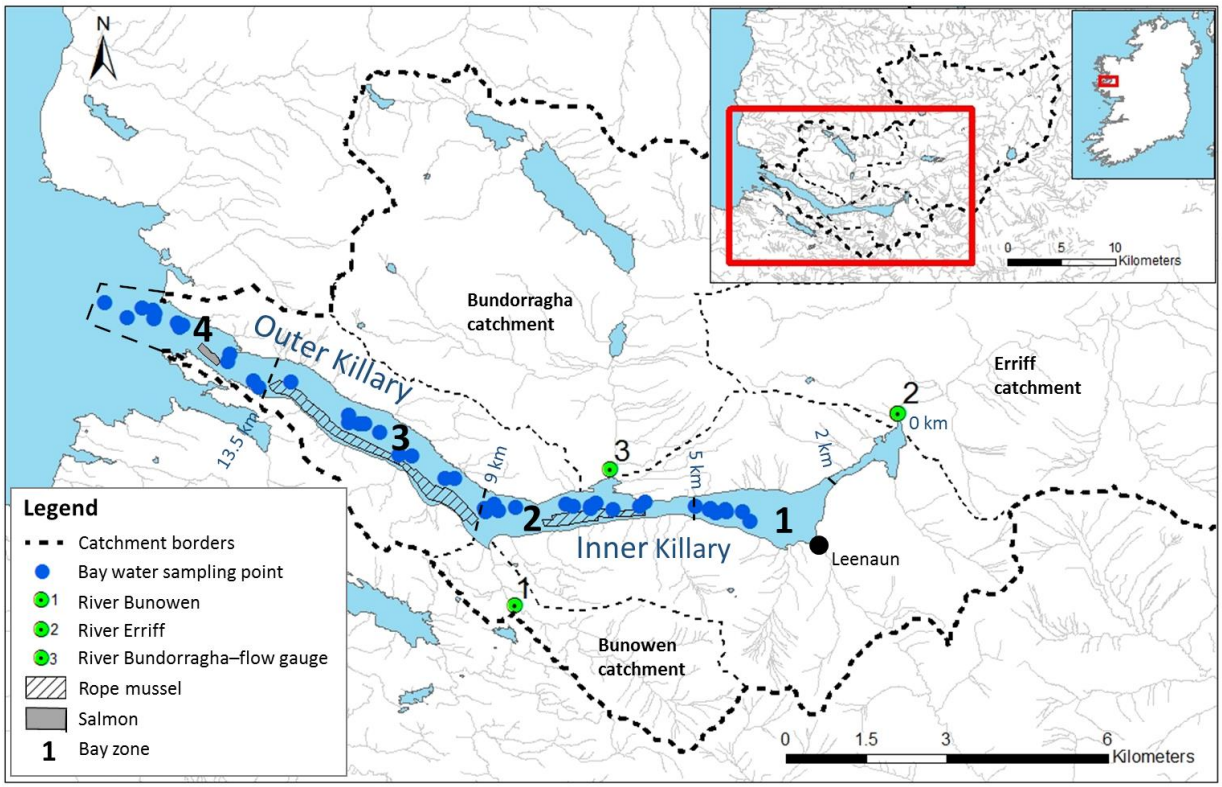

Figure 26. Bay and river water sampling locations (points 1-3) in Killary Harbour and its surrounding catchment. Rope mussel and salmon farms locations are shown with dashed and greyed symbols. The Environmental Protection Agency (EPA) monitors river flow rates of the Bundorragha River (upstream from sampling point 3). The four zones defined here are used later in the paper to analyse the potential Ra fluxes in each part of the bay.

5.3.2 Salinity and nutrient concentrations

Samples were collected during six longitudinal transects of Killary Harbour during the ebb tide on August 24, 2017; February 16-17, 2018; July 16, 2018; October 25, 2018; January 23, 2019; April 04, 2019, close to the spring tides on each occasion. The February 2018 survey also included transects during both ebb and flood to evaluate the effect of the tidal stage on the bay biogeochemistry. Samples were collected from the surface (0.5-1m) and at depth (~ 2 – 3 m above the bay floor) using a 5L Niskin bottle. River waters were also sampled during each survey in river Erriff, Bundorragha, and Bunowen (Figure 26). Each location was sampled in triplicate vials filtered separately, either before or after each survey, making sure that flow conditions during sampling were similar to condition prevailing during and before each transect. Salinity and turbidity were measured using a calibrated Aquaread® Aquaprobe 1000, with salinity values verified using a Carl Stuart Limited Cond197 i WTW electrical conductivity probe. Samples for dissolved nutrient

analysis were filtered using Rhizon membranes into vacutainers (J. S. P. Ibánhez and Rocha, 2014; Jiang et al., 2017), before analysis within 30 days for DIN, and 10 days for SRP (Jiang et al., 2017), using standard colorimetric methods (Grasshoff et al., 2009). DIN was analysed with a Lachat Quickchem 8500 FIA system, following manufacturer-adapted methods for sequential analysis (Lachat instruments, 2002, 2001). SRP was determined at 885 nm using a Hatch DR5000 spectrophotometer using standard colorimetric methods (Grasshoff et al., 2009).

5.3.3 River flow rates

Average flow rates of freshwater entering Killary Harbour in the period leading up to each sampling survey were estimated using 15 min resolution time series of flow rate measurements taken in Bundorragha River (EPA, 2019a), river stage measurements from the Erriff river, and river network and catchments maps (EPA, 2019b). The per cent contribution of each river to the total catchment freshwater flow was estimated from EPA sub-catchment limits of rivers connected to Killary Harbour (Figure 26). A power curve function and past unpublished measurement of stage and discharge provided by the Office of Public Works (OPW) was used to develop a stage-flow relationship for the River Erriff, following standard methods (Braca, 2008; ISO, 1998; Rantz, 1982). The stage flow relationship had a Nash-Sutcliffe Efficiency of 0.97 and included 14 points taken between 1987 and 2018. Total flow rates in the rivers Erriff and Bundorragha were then added and divided by the proportion of the catchment occupied by the two river sub-catchments (~82%), to correct for ungauged flow and determine the total flow rate to the bay at any given time. Finally, this flow rate time series was used to determine the average discharge rates affecting Killary Harbour during the ten days before each survey.

5.3.4 Radium analysis

Sampled on the same stations and dates as the nutrient's measurements, activities of ^{224}Ra and ^{223}Ra in the water column of Killary Harbour were used to assess the variability of estuarine flushing and evaluate vertical mixing. First, natural levels of ^{224}Ra and ^{223}Ra were preconcentrated on MnO_2 coated acrylic fibres (Moore, 1976). Two preconcentration methods were used and did not lead to significantly different results. In the first method, the fibres were attached to moorings, approximately 1 m below the surface and 1 m above the bay floor, and left for 24 hours to accumulate radium activity from the bay water (Rocha et al., 2015). In the second method, a water volume of between 60-100 L was pumped at a flow rate of less than 1 L min^{-1} through cartridges filled with MnO_2 coated acrylic fibres to adsorb the radium present (Moore and Arnold, 1996). In both cases, the fibres were then rinsed with Ra free water, dried until a water/Mn fibre ratio of approximately 0.4-1.1 was reached (Sun and Torgersen, 1998), and measured on a Radium Delayed Coincidence Counter (RaDeCC) (Moore and Arnold, 1996). To decrease the uncertainty of the final determination, at least three separate measurements were made on the same sample: after sampling, after 7-10 days (to improve the ^{223}Ra estimate), and after 25 days, to correct for ^{228}Th supported ^{224}Ra levels (Moore, 2007). ^{227}Ac supported activities for ^{223}Ra, determined after 80 days for selected samples, were within the uncertainty of measurement of ^{223}Ra.

5.3.5 Main radium sources into the system.

Source functions for Ra in an estuary may include riverine and oceanic inputs as well as estuarine sediments and groundwater (Swarzenski et al., 2003). To assess the contribution of sediments to the fjord Ra budgets, representative sediment types for the system were collected (Keegan and Mercer, 1986), both in intertidal (using a core sampler) and subtidal areas (using a grab sampler). The ^{223}Ra and ^{224}Ra that could be released from these samples were determined by resuspending these sediments in Ra-free artificial seawater and measuring the increase of ^{223}Ra and ^{224}Ra in solution. As benthic metal oxide levels regulate Ra released from sediment (Gonneea et al., 2008), and some sandy silt sediments in the bay had high oxide mineral content, sandy silts with high

and low oxide contents were differentiated in the analysis. The observed values were afterwards converted into equivalent activity per volume of pore space and per weight to determine the likely range of the different Ra sources within the system. Subsequently, these values were used to develop a first-order estimate of the magnitude of Ra fluxes to be expected from the seafloor, suspended sediments, direct inputs of suspended sediments from side streams or from resuspension events in the bay.

5.3.5.1 Benthic Ra fluxes due to diffusion and bioturbation

To determine an upper range value for diffusive Ra inputs from the seafloor, the water column in deep waters was assumed to be well mixed. Additionally, it was assumed that the radium activity gradient between bay water and porewater, estimated with resuspension experiments, occurs close to the sediment-water interface (SWI). The spatial scale for the Ra concentration gradient across the SWI was estimated from redox profiling of bay sediments (Keegan and Mercer, 1986). The bulk sediment diffusion coefficient for Ra was determined with the free solution coefficient following Ulman and Aller (1982) using the measurements of sediment porosity. Maximum values for the temperature dependence were taken from Li and Gregory (1973). Finally, the calculated fluxes were corrected for the potential effect of bioturbation following Hancock et al. (2000).

5.3.5.2 Ra release rates from suspended sediment in the bay water column

To evaluate the potential for Ra release by sediment in suspension, the amount of Ra desorbed in the sediment resuspension experiments was multiplied by the suspended particulate matter (SPM) amounts in the water column, estimated from the turbidity measurements following Jafar-Sidik et al. (2017). As the relationship between turbidity values in NTU and suspended solids can be site-dependent, the annual range of SPM calculated was then compared to maximum particulate organic carbon (POC) measured at Killary by McMahon and Patching (1984), converted into SPM using winter POC/SPM ratios in Winogradow et al. (2019).

5.3.5.3 Ra fluxes from resuspension/deposition of deep sediments

Keegan and Mercer (1986) cited resuspension due to tidal currents as a potential source of solutes in the bay. Sediment resuspension events occur when tidal, wind or wave-driven currents are above a shear limit (the critical current velocity) and cause an increase of suspended sediment in the water column. Critical current velocities in Killary Harbour were assessed from a previous study on sediment types similar to type 1 sediment (Niemistö and Lund-Hansen, 2019). They were compared with velocities in Killary Harbour's deep water (Keegan and Mercer, 1986) to assess the potential of sediment resuspension events to lead to Ra and phosphorus fluxes. Suspended sediment measurements and high-resolution bathymetry were then used to verify the observations and to identify the areas where resuspension was most likely during periods of high currents.

5.3.5.4 Ra release originating in river suspended sediment loading

The range of riverine SPM loads to Killary Harbour was assessed using freshwater POC data from the rivers Erriff and Bundorragha (Mcmahon and Patching, 1984) and a range of POC/SPM ratios in temperate river waters obtained by Abril et al. (2002). Riverine SPM loads were then multiplied by the maximum Ra activity measured in sediment.

5.3.5.5 Ra fluxes from potential submarine groundwater discharge.

The potential effect of submarine groundwater discharge (SGD) on the spatial variability of estuarine Ra ratios was assessed using three linked approaches.

Firstly, the local geology, sediment types in the bay and the bathymetry were examined to look for preferential pathways for fresh SGD, such as permeable rocks, faults, or for saline SGD, such as sandy intertidal areas.

Secondly, the relative ratio of fresh groundwater and river flux to the bay was assessed qualitatively from the Geological Survey of Ireland classification of aquifers (GSI, 2020) and from an examination of the density of river networks in the catchment.

Thirdly, radon in water, as a tracer for SGD (Burnett and Dulaiova, 2003) which might also comprise Ra fluxes, was measured in two surveys (August 24 to 26, 2017 and February 2018). This was done by continuously pumping bay water through gas exchange

membranes (Schmidt et al., 2008) using three Durridge RAD7 Rn monitors in parallel following Rocha et al. (2015). The first survey was conducted in the outer bay, the second in the inner bay. In addition to these surveys, radon levels were assessed in parallel with nutrient and Ra sampling transects for selected samples using a RAD7 and a modified WAT250 method (Durridge, 2015) for deep and surface samples. To extend the detection limit of the WAT250 method, the measurement period of the standard method was doubled or tripled, and triplicate samples were taken at each location.

5.3.6 Determination of uncertainty

When not specified, uncertainties associated with measurements or estimates are expressed as ± one standard deviation. For water and sediment samples, the uncertainty of analyte quantitation is determined from the standard deviation of replicate samples. When operations are used to derive values from these raw measurements, the standard propagation of uncertainty (JCGM, 2008) is applied.

5.4 Results

5.4.1 Effect of discharge on salinity structure and distribution of Ra ratios

River discharge strongly modifies the salinity structure of Killary Harbour. During the lowest discharge periods, most of the bay had salinities close to or above 30 in surface and deep waters (e.g. zones 2, 3, 4 in Figure 27a), with a range of salinity and distribution similar to prior observations by Keegan and Mercer (1986). During high discharge periods, the majority of the bay had reduced surface salinities between 0 and 25 (zone 1, 2 and 3 in Figure 27b). Deep water salinity generally remained above 30 for both periods (Figure 27b and Figure 28c).

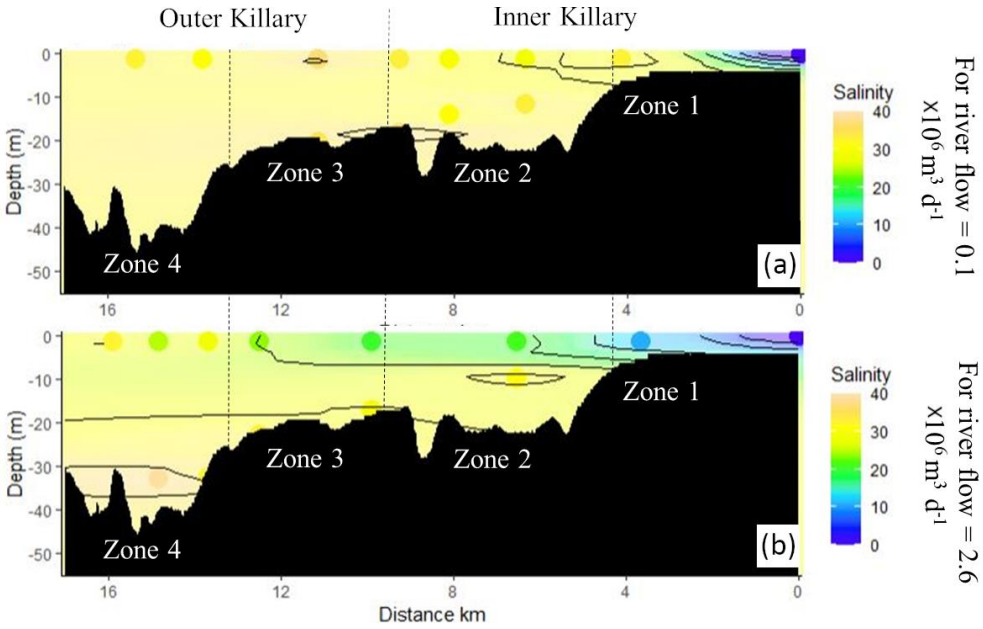

Figure 27: Effect of river discharge on the salinity structure in Killary Harbour. Inverse distance weighting interpolation (IDW) of salinity was performed using R software with a grid of 300 cells of 200 m length per 2m depth. Isohalines are shown for every 5 units of salinity, from 5 to 35. Depths shown are maximum depths, measured along the bay at high tide. Points show where data was collected.

Two zones can be distinguished regarding the influence of river discharge on the salinity structure of the fjord. The zone between the river Erriff and 10 km from the head of the estuary, inner Killary, is the most affected by river discharge and has reduced salinities even during low freshwater discharge (Figure 27). The rest of the bay, outer Killary, has more stable salinities, regardless of freshwater discharge levels, particularly in zone 4 (Figure 27). These two separate areas also have distinct distribution patterns of Ra ratios in surface water (Figure 28 e, f, g). Inner Killary (Km 0 to 9 from the River Erriff) generally

shows a steep decrease of Ra activity ratios from east to west. Meanwhile, outer Killary (>9 km, zone 3 and 4 in Figure 26) most often reveals a slight decrease of Ra activity ratios followed by an increase at the outermost part of the bay when low freshwater flow rates are measured.

The varying degrees of stratification caused by river discharge affect both the salinity structure of the water column and the distribution of Ra activity ratios (Figure 28). During low freshwater discharge (total river flow <1.2 $\times 10^6$ m^3 d^{-1}) salinity gradients between surface and deep waters are either low or insignificant (Figure 28a), while during high discharge periods salinity gradients fall between five and thirty units, and the degree of stratification is at its maximum observed level (Figure 28c). At discharge rates close to 1 $\times 10^6$ m^3 d^{-1}, the brackish water plume affects only inner Killary during spring tides, while the difference between surface and deep water in outer Killary is low (Figure 28b).

Similarly, the difference between $^{224}Ra/^{223}Ra$ activity ratios in surface and deep water is minimal under low discharge, well-mixed conditions ($\leq 1 \times 10^6$ m^3 d^{-1}, Figure 28d, e). Conversely, under high discharge conditions, deep water $^{224}Ra/^{223}Ra$ activity ratios are frequently different to surface values (Figure 28f).

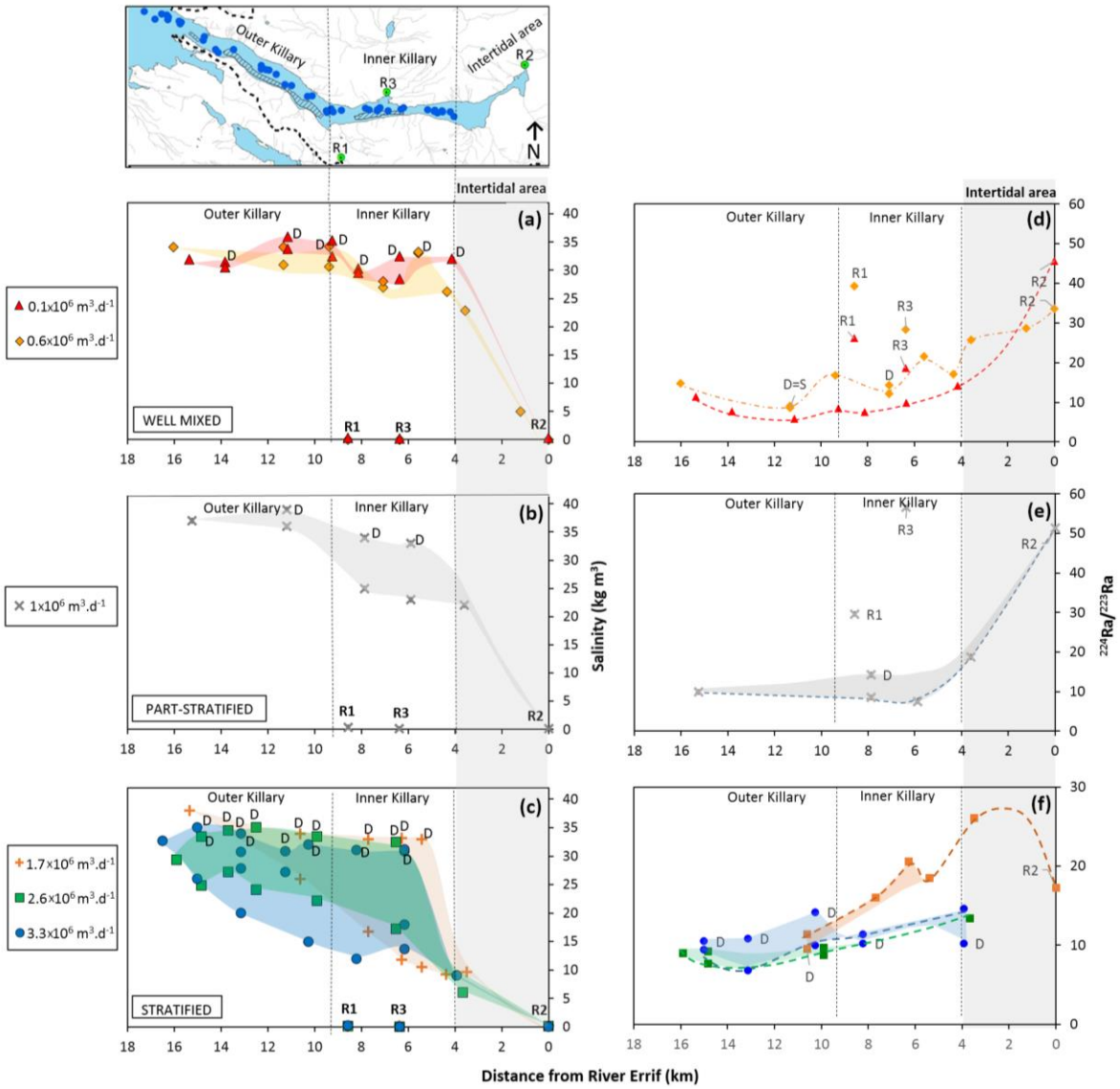

Figure 28: Surface and deep-water longitudinal profiles of salinity (a), (b), (c) and $^{224}Ra/^{223}Ra$ relative water ages (d), (e), (f) as a function of distance from the Erriff River mouth. The coloured areas highlight the difference between surface and deep waters. The dashed coloured lines in (d), (e) and (f), represent the surface distribution of Ra ratios. "D" highlights deep water samples. Points where the location of surface and deep water samples overlap are highlighted with "D=S". R1 to R3 points are river samples, with locations on the upper map. The longitudinal profiles are organised from top to bottom by increasing stratification states and increasing average freshwater discharge flowing to the bay over a period of ten days prior to each survey (legends to the left of the profiles).

5.4.2 Ra desorption experiments

Most of the subtidal bay floor is composed of clay sediments with variable silt content (type 1 in Keegan and Mercer, 1986). In contrast, intertidal sediments sampled in the upper bay (zone 1) were mainly either sand (type 3) or sandy silt (type 2a and type 2b). Sandy silt sediments had either low (type 2a), or high mineral oxide content (type 2b).

The finer sediments with low oxide content (type 1 and type 2a, Table 7) had the highest porewater Ra activities, as expected (Webster et al., 1995), and Ra activities similar to those found for fine sediment in the Bega estuary (4800±900 dpm $100L^{-1}$ for ^{224}Ra, Webster et al., 1995). Moreover, the more oxidised sandy silt sediment (2b, Table 7) had lower available Ra concentrations than sediments of similar grain size without oxides (2a, Table 7) in agreement with previous observations (Gonneea et al., 2008). The porewater Ra activities in the sandy type 3 sediment are within the range of previous observations for sediments of the same type elsewhere (10 to 506 dpm $100L^{-1}$ for ^{224}Ra and 0.5 to 30 dpm $100L^{-1}$ for ^{223}Ra, Gonneea et al., 2008). Type 1 and type 2b sediments had low Ra activity ratios (12.1±0.7 and 15.5±0.7, Table 7), similar to those measured in most of the water column (Figure 28). Types 2a and 3 sediments had higher Ra activity ratios of around 30 (Table 7), similar to the highest observed in the easternmost area of the fjord waters (1-4 km from the head of the estuary; Figure 28).

Table 7: Results of Ra desorption experiments for sediment taken in Killary Harbour. The first column relates the results to the sediment types as they were defined for the bay in Keegan and Mercer (1986), with additional subdivision of type 2 sediment, as one of the samples (2b) contained oxide rich layers, which are known to reduce the release of Ra from sediment (Gonneea et al., 2008). The sediment types are the following: 1* Clay, clayey silt with mm-scale shell debris and clast (1-2%), 2a** Sandy silt with mm-scale shell debris and mm-scale rock fragments 0.5%, 2b*** Sandy silt with oxides and shell debris (1-2%), 3**** Quartz sand with 5% of diverse rock fragments

Sediment Type	Porosity	Bulk density kg m^{-3}	Porewater Ra dpm $100L^{-1}$			Surface bound Ra dpm $100g^{-1}$		Estimated potential diffusion flux $\times10^{-9}$ dpm cm^{-2} s^{-1}		n
			^{224}Ra	^{223}Ra	$^{224}Ra/^{223}Ra$	^{224}Ra	^{223}Ra	^{224}Ra	^{223}Ra	
1*	0.75 ±0.03	526 ±30	3031 ±878	249 ±66	12.1 ±0.7	4.3 ±1.3	0.35 ±0.1	24 ±7	1.9 ±0.5	4
2a**	0.49 ±0.03	1280 ±30	3397 ±800	112 ±15	30.2 ±3.4	1.3 ±0.3	0.04 ±0.01	15 ±4	0.50 ±0.07	3
2b***	0.55 ±0.03	1153 ±30	1362 ±801	90 ±16	15.1 ±0.7	0.6 ±0.4	0.04 ±0.01	7.6 ±4.5	0.50 ±0.09	1
3****	0.35 ±0.03	1456 ±30	230 ±18	7 ±1	32.8 ±3.6	0.12 ±0.01	0.0017 ±0.0003	0.052 ±0.06	0.016 ±0.002	2

5.4.3 First-order estimate of potential Ra sources into outer Killary Harbour and the western part of inner Killary Harbour.

To assess the variability of flushing in an estuary using Ra isotopes, the different solute sources that would change water Ra activity ratios should be quantified. As we will show, Zone 1 is likely to receive most of the watershed-borne Ra inputs. The successive subsections investigate the processes that may contribute to potential Ra fluxes to the bay west of km 4 (zones 2, 3 and 4 in Figure 26), with results summarised in Table 8.

Table 8: Assessment of Ra potential fluxes in Killary Harbour west of km 4.

Potential fluxes	Likely effects on Ra fluxes	Argument
Fluxes from bottom sediment by diffusion and bioturbation	- Significant for deep water, particularly in Zone 2, see Table 7.	- Ra activities in porewater are sufficiently large to affect deep waters with diffusion and bioirrigation, but not surface waters.
Suspended sediment in the bay	- Not significant to the west of km 4 (except potential resuspension areas not yet identified).	- Surface bound Ra in analysed sediment is too low to lead to significant Ra increase at current suspended sediment levels.
Resuspension/deposition of sediments due to strong deep-water currents.	- Significant for deep waters (zone 3) and surface waters (mainly during well-mixed conditions, in zone 3 and 4).	- Deep water flow rates above critical flow value during mid-range tides. - Solute fluxes from resuspension can be one order of magnitude larger than diffusion fluxes.
Direct inputs of suspended sediment from rivers	- Not significant to the west of km 4 (except close to rivers).	- Surface bound Ra in analysed sediment, and the sediment loads are too low to result in significant Ra increase.
Advection from bay floor sediments (e.g. SGD)	- Small to the west of km 4.	- Low radon values in surface and deep waters in the locations sampled. - Steep bay margins, no intertidal areas to the west of km 4. - Poorly permeable bay floor sediment and bedrock.

5.4.3.1 Fluxes from bottom sediment by diffusion and bioturbation

The Ra fluxes due to diffusion and bioturbation from sediment west of km 4 and the increase of Ra activities in water they may create are estimated in Table 9. There are two distinct situations. When the bay is vertically well mixed, the Ra diffusing out of the sediment is distributed into the full water column. When the bay is stratified, radium inputs are held beneath the halocline, and only the lower box volume is used for calculations.

Under vertically well-mixed conditions, the sediment-water fluxes lead to a daily change of Ra activities below typical measurement uncertainty (Garcia-Solsona et al., 2007), except in the upper bay where it may have a second-order effect (Table 9, a). On the other hand,

when the bay is stratified (typically during high discharge surveys), these Ra inputs are concentrated in deep waters and can increase ^{224}Ra there at most by 2.6 dpm.100L^{-1} d^{-1} (Table 9, b). The largest effect of diffusion and bioturbation fluxes from sediment on water column solute levels is expected in the deep layers of inner Killary Harbour, where the volume of water in relation to sediment surface is the smallest (Zone 2, stratified bay deep water activities, Table 9).

Since typical ^{224}Ra activities in deep water during high discharge fall between 5 and 17 dpm 100L^{-1}, diffusion and bioturbation from the sediments can represent at most 15% to 50% of deep water ^{224}Ra activities. By contrast, ^{223}Ra activities fall between 0.4 and 1.2 dpm 100L^{-1} in deep water samples, and the maximum sediment contribution can thus represent between 10% and 150% of ^{223}Ra activities in deep water, depending on the zone of the bay. During high discharge periods, or periods of poor vertical mixing, this additional Ra is thus likely to accumulate and change the Ra activity ratios in deep waters significantly. However, the vertical stratification also limits the transfer to surface waters of Ra inputs from diffusion and bioturbation, and these fluxes will thus more rarely affect surface waters Ra ratios compared to when well-mixed conditions occur.

Table 9: Maximum contributions of benthic Ra fluxes due to diffusion and bioturbation to the water column Ra activities in the four zones of Killary Harbour. This table divides the bay into four surface and four deep segments, assumed to be well-mixed, with a stratification depth of 10 m. (a) estimate the increase of Ra in surface and deep waters due to benthic diffusive fluxes in each zone when water column is vertically mixed (b) gives the increase of activities in deep waters due to Ra fluxes from the bay floor, assuming that Ra fluxes from sediment remain in deep waters.

Bay zone	Volume 10^6 m^3		Bay floor area 10^6 m^2	Main sediment	Maximum inputs to the zone from the bay floor 10^6 dpm d^{-1}		Maximum activity increase due to bay floor fluxes dpm.100L^{-1} d^{-1}			
							(a) Well mixed		(b) Stratified	
	Surface layer	Deep layer			^{224}Ra	^{223}Ra	^{224}Ra	^{223}Ra	^{224}Ra	^{223}Ra
1	4.18	-	0.98	3-2a 2b	10.3	1.0	0.25	0.024	-	-
2	23.2	1.42	2.21	1	36.5	8.7	0.15	0.035	2.6	0.61
3	50.9	3.01	3.33	1	55.1	3.4	0.10	0.006	1.8	0.11
4	39.7	1.50	1.69	1	27.9	1.7	0.068	0.004	1.9	0.12

5.4.3.2 Suspended sediment measured in the bay

Turbidity levels for most surveys were close to zero in surface and deep-water samples, except for the highest discharge survey, when levels up to 10.1 NTU (18.7 mg L^{-1}) in deep waters and 4.8 NTU (8.9 mg L^{-1}) in surface waters were observed. Using the maximum suspended sediment value of 8.9 mg L^{-1} and the ^{224}Ra and ^{223}Ra levels recorded for the finer sediments (type 1 sediment, Table 7), the maximum contribution of Ra desorption from suspended sediment to the water column is thus 8 $\times 10^{-2}$ dpm $100L^{-1}$ and 7 $\times 10^{-3}$ dpm $100L^{-1}$. These values are several orders of magnitude lower than the uncertainty associated with the measurement of Ra activities. The potential desorption of Ra from SPM can thus be confidently discounted as a significant contributor to Ra activity ratios in the water column.

5.4.3.3 Suspended sediment load from rivers.

The rivers Erriff and Bundorragha are significant sources of POC to the system, with monthly inputs of POC of respectively up to 128 and 9 metric tonnes (Mcmahon and Patching, 1984). These translate into a suspended sediment load of 3 $\times 10^3$ kg d^{-1} to 147 $\times 10^3$ kg d^{-1} and 0.2 $\times 10^3$ to 11 $\times 10^3$ kg d^{-1} for the Erriff and Bundorragha rivers, respectively. These direct sediment inputs might provide a source of new radium by desorption at the upper end of the bay from the River Erriff and at around km 6 from the Bundorragha River. Again, assuming particles hold the maximum available Ra content observed in sediments (4.3±1.3 dpm $100g^{-1}$, type 1 sediment, Table 7), these rates may represent a load of added ^{224}Ra to the bay of up to 6.3 $\times 10^6$ ^{224}Ra dpm d^{-1} for the Erriff River and 5 $\times 10^5$ ^{224}Ra dpm d^{-1} for Bundorragha River. Most of Ra desorption from sediment typically occurs below salinity 7 (Webster et al., 1995). Salinity below 10 was only found in zone 1 (east of 4 km), suggesting that most of the Ra release into the water column by desorption occurs in this zone.

For sediment inputs from the Bundorragha River, a localized increase of Ra activities originating from desorption would also be possible in the vicinity of the freshwater plume associated with the small creek of approximately 1.05 $\times 10^5$ m^2, on the north shore of Killary Harbour. Considering the small size of the creek compared to the whole bay, a water residence time of one day in this area can be assumed as an overestimate. With the

creek having an average depth of 1-2m, the Ra desorption in the plume of suspended sediment coming from Bundorragha during high discharge conditions would increase ^{224}Ra levels in the creek by between 0.2 and 11 dpm 100L^{-1}. With a mixed layer of 8m, as typically observed during high discharge, the volume of the Killary Harbour's surface layer in the section outside the creek is 3.2 ×10^{6} m^{3} d^{-1}. Ra inputs from Bundorragha sediment loads in the creek are thus likely to be diluted within the main channel of Killary Harbour by a factor of thirty at least (e.g. 0.3 dpm L^{-1} for ^{224}Ra, consequently below detection limit). Ra release rates from sediment inputs from Bundorragha River would thus be dwarfed by the solute inputs coming from the River Erriff – 10 times the sediment loads of Bundorragha - and from the intertidal area east of km 4. Consequently, even if Bundorragha`s sediment discharge might decrease Ra ratios in direct proximity to its freshwater plume, outside this area this effect is likely to be small and not affect the Ra activity ratios measured in the bay, even during high discharge conditions.

5.4.3.4 Resuspension/deposition of sediments due to strong deep-water currents

Deep water current speeds in Killary Harbour vary between 0 at high or low tide to 20 cm.s^{-1} at mid-tide (Keegan and Mercer, 1986). Critical current velocities for another enclosed bay with similar sediment types (from silts to fine sands) are between 7.3 to 11.5 cm.s^{-1} (Niemistö and Lund-Hansen, 2019). Mid tide current velocities in Killary Harbour are thus double of the maximum critical shear velocity observed for similar sediment types by Niemistö and Lund-Hansen (2019). Cyclic sediment resuspension/deposition of fine sediment is thus likely to occur in deep waters, particularly in areas where the bay is shallower (zone 3, Figure 27). This could lead to localised resuspension/deposition of deep sediments and an added flux of SRP and radium from the bay floor. Some of this added P may be originally particulate P from feces from the salmon farm in zone 4, deposited and progressively degraded in dissolved P in sediment, then released during resuspension events. Indeed, the majority of P release for atlantic salmon farming occur as particulate P (Wang et al., 2012).

During the highest freshwater discharge survey, the highest turbidities (10.1NTU) were observed in zone 3, an area where the bay depth is restricted and may lead to increased flows. In contrast, maximum surface turbidity was lower, up to 4.8 NTU (Figure 29 a and

b). SRP concentrations in the deep waters of zone 3 were also higher than in other locations (Figure 29c). The other surveys had low turbidity values, generally close to zero.

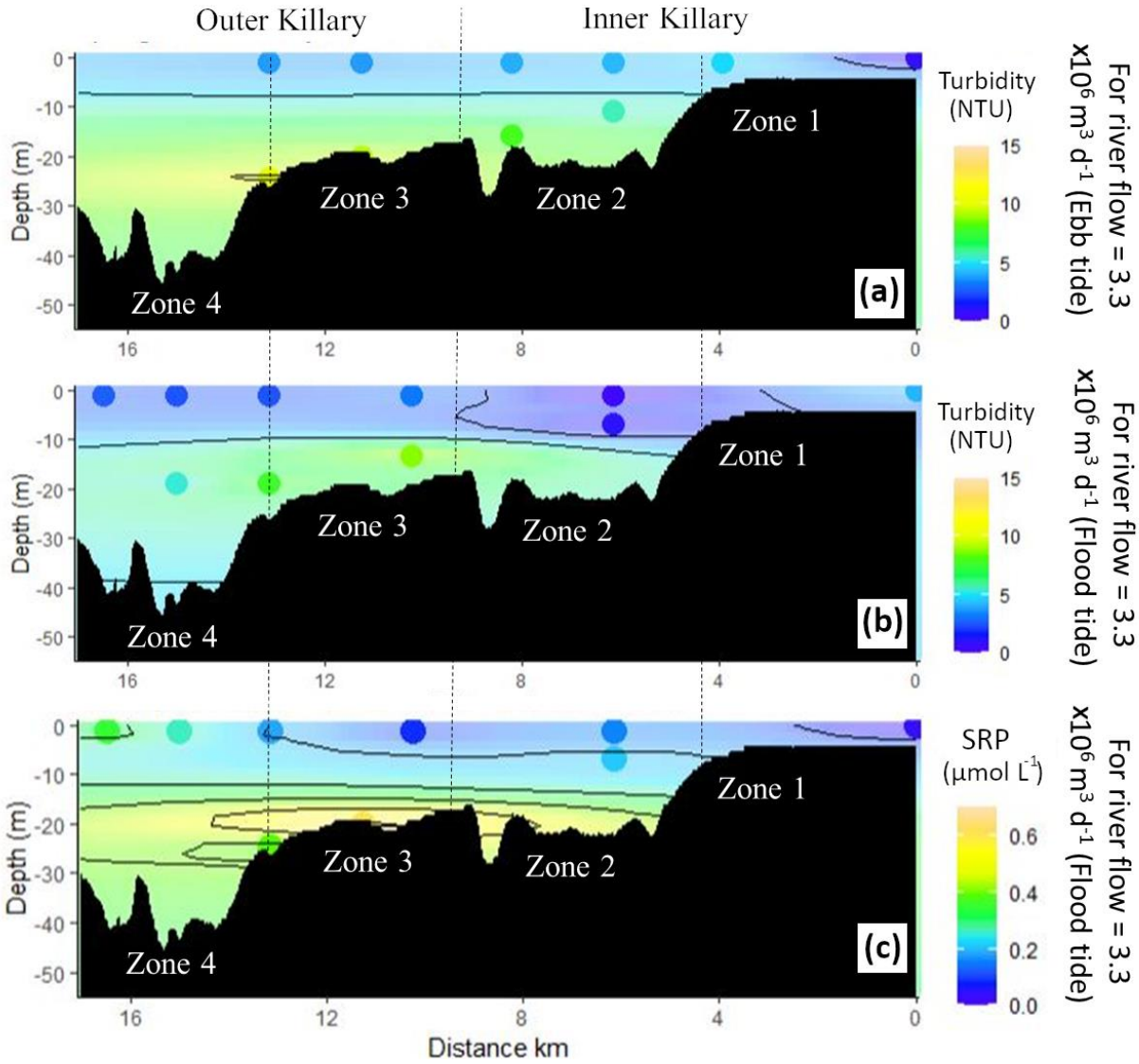

Figure 29: Increase of turbidity and SRP levels in Killary Harbour during the high discharge survey (3.3×10^6 m^3 d^{-1}), potentially an indication of flow-driven resuspension of sediment. In (a) and (b) contours are every 2.5 NTU, from 2.5 to 7.5. In (c), contours are every 0.1 µmol L^{-1}.

5.4.3.5 Advection from bottom sediment and bay floor (SGD)

While significant SGD fluxes might occur east of km 4, five pieces of evidence suggest that advected SGD is not likely to lead to significant changes of surface Ra activity ratios in Killary Harbour west of this point. Firstly, the low permeability of type 1 sediment composing most of the bay floor does not allow for large advection of porewater from sediment (e.g. SGD) over short timescales relevant for the short-lived Ra isotopes, ^{223}Ra and ^{224}Ra, which have half-lives of 11.4 days and 3.66 days, respectively. Secondly, the bay margins are steep, which does not favour the occurrence of large tidally driven fluxes of recirculated SGD. A significant intertidal area of permeable sediment (of type 2 and 3) is only present east of km 4, in zone 1. Thirdly, the catchment is mainly composed of poorly permeable sandstone and metasediment, pertaining to the less permeable classification of the Geological Survey of Ireland classification of aquifers, Pu, bedrock generally unproductive (GSI, 2020). Fourthly, a dense river network is present in the catchment, which suggests that direct fresh groundwater inputs are not likely to have a large effect on Ra mass balances in the bay compared to river inflows. Finally, the continuous radon measurements in surface water of outer Killary during the first survey showed very low values (3±2 Bq m^{-3}), similar to the ^{226}Ra supported activity previously measured by Schubert et al. (2015) in Kinvarra Bay (4 Bq m^{-3}). The second survey of radon levels in inner Killary (zone 2) was from the shore and led to higher radon levels of 34±3 Bq m^{-3}. This suggests that a small source of radon may be present in the inner bay, potentially from sediments in zone 1. Given the very low radon levels observed during the first survey in the outer bay (zone 3 and 4), SGD is not likely to affect Ra ratios beyond zone 1. During subsequent radon measurements with the modified WAT250 method, deep water at bay km 11 had a significant increase of radon levels when water was well mixed (385 ±184 Bq m^{-3} vs an average of 110 ±83 Bq m^{-3} observed in the three other deep locations sampled). For surface waters, radon levels were often not significant but tended to decrease with distance, from between 250 ±200 to 400 ±397 Bq m^{-3} in the River Erriff to between 278 ±250 and 105 ±150 Bq m^{-3} in zone 3 and 4. Consequently, Ra transport by advection may play a significant role over diffusion for surface waters only in the intertidal area (east of km 4), where sandy and silty sediments are present. However, the low radon levels in river waters and inner Killary waters do not suggest these advective inputs are

large compared to the river inputs. In any case, most of the water column radium data originate west of this area, which allows us to consider the area east of km 4 as the main Ra source for the bay.

5.4.4 Effect of stratification and changes of freshwater discharge on N:P ratios

The bay's N:P ratios, defined as the molar DIN: SRP ratio, are influenced by changes in both freshwater discharge and N:P solute ratios of river inputs. N:P ratios in the water column were higher during stratified surveys (surveys with discharge above 1.2×10^6 m^3 d^{-1} in Figure 30a) than in well-mixed conditions, except for one well-mixed survey (0.6×10^6 m^3 d^{-1}). The bay during this survey had higher N:P ratios than during other well-mixed surveys, with maximum levels comparable to high discharge periods (Figure 30a). N:P ratios in the River Erriff were larger during this period, of comparable magnitude (143) to those observed in river waters during the maximum discharge survey (166). With this exception, the difference in N:P ratios between surface and deep waters also tended to increase with increasing freshwater discharge (Figure 30b).

To highlight the effect of variable stratification on the N and P cycle, the observed DIN and SRP in Figure 30c and Figure 30d were expressed relative to the measured concentrations in the rivers during their respective surveys. Thus, the effect of changes in river N:P is removed. SRP concentrations in deep waters were generally higher than in river waters (Figure 30d). This suggests that a deep source of P may be present in the bay. The difference between surface and deep water SRP was higher during stratified periods than during mixed conditions (Figure 30b). Such a difference may be attributed to the benthic SRP efflux in the deep layer as well as to the net sinking of phosphorus bound to particles from the surface to the deep layer (Paytan and Mclaughlin, 2007; Smil, 2000); both are influenced by the pycnocline limiting the transfer of particles from the bottom to the surface layer. Comparatively, the effect of stratification on DIN was much smaller (Figure 30a), which corresponds to nitrogen and phosphorus's distinct properties (soluble vs particle reactive). Both DIN and SRP were generally lower in surface water than in deep water (Figure 30a and Figure 30b), probably due to the higher light availability for primary production in surface water.

As a result of nutrient advection driven by discharge and of stratification, stratified periods were likely to have higher surface N:P ratios than mixed periods (Figure 30c), except when river N:P ratios were exceptionally high (survey with a red rectangle in Figure 30c). Moreover, the vertical gradient in N:P ratio (Figure 30d) strongly increased with rising stratification.

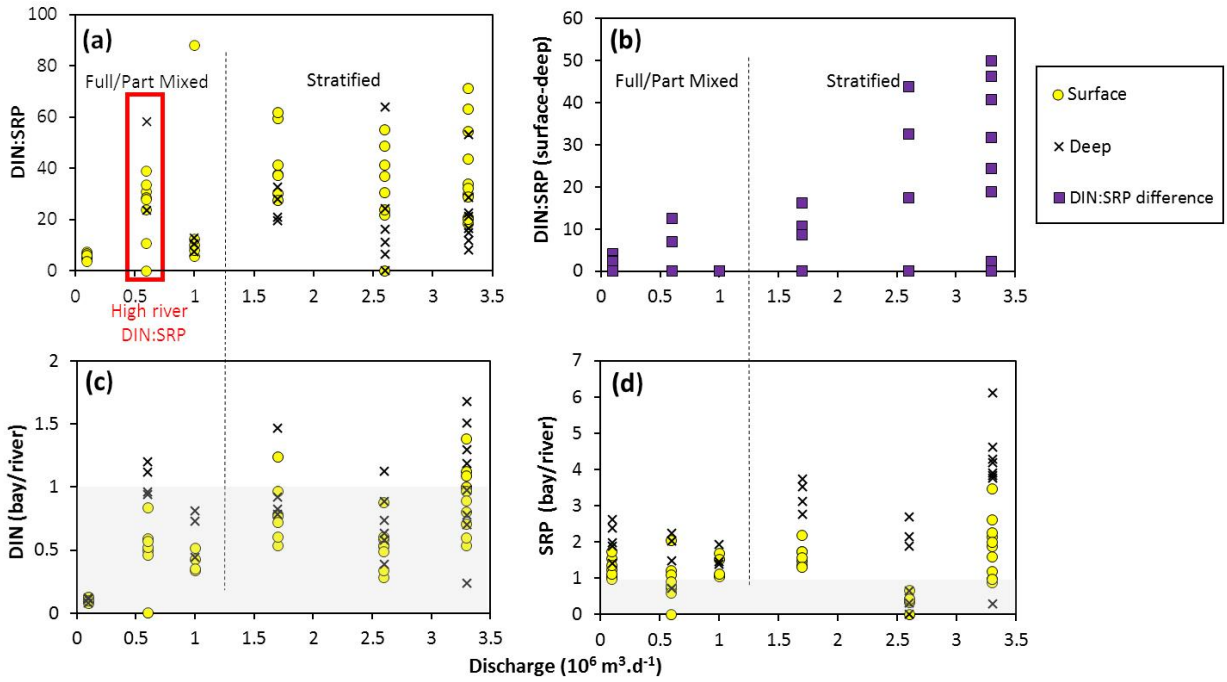

Figure 30: Effect of stratification and freshwater discharge on the nutrient availability and molar N:P ratios measured in the water column during bay transects. All data is expressed as a function of average river flow to Killary Harbour within the ten days preceding each survey (horizontal axis). Data on the vertical axis are as follows: (a) Surface and deep-water N:P ratios expressed as DIN:SRP quotients, with the red rectangle highlighting the survey for which DIN:SRP ratios in rivers were higher than expected for a similar range of flow rates; (b) The difference of N:P ratios between surface and deep waters; (c) Surface and deep water DIN normalised by river DIN; (d) Surface and deep water SRP normalised by river SRP. River DIN and SRP values used for normalisation are samples taken in triplicate in the river Erriff, Bundorragha and Bunowen, assuming that discharge, thus their relative contribution to the river end-member composition, is function of catchment size. River samples were taken in the same period than transect, under similar discharge conditions than during and before the transects. In (a), (b), (c) and (d) the vertical dashed lines show the flow threshold for this system between stratified and vertically well-mixed conditions, derived from the salinity observations in Figure 27 and Figure 28. In (a) and (b) the greyed area highlights the points that have lower SRP or DIN than the river concentrations during each period.

5.5 Discussion

5.5.1 Note on SPM values in this study

SPM values used here were assessed from turbidity measurements in Killary Harbour, converted using SPM/NTU ratios observed by Jafar-Sidik et al. (2017) and validated using both a historical dataset of POC in Killary Harbour from McMahon and Patching (1984) and a winter POC/SPM relationship from Winogradow et al. (2019). SPM/NTU relationships may be site dependent. SPM and POC loads from a catchment may also vary in time as a result of rainfall and changes of land use. Mussels can also amplify the transfer of suspended particulates from the water column to the benthos when feeding (Newell, 2004). However, SPM in water is expected to be a minor component of Ra inputs, and three lines of evidence suggest that this way to validate maximum SPM estimates is reasonable here. First, the rainfall levels, intensity and duration were similar in the 1983-1985 period and the 2017-2019 period. The long term average rainfall levels (Met Eireann, 2020) were 2468±325 mm in the 1983-1985 period and 2554±290 mm in the 2017-2019 period. The annual rainfall peaks varied between 73 and 86 mm/day during the 1994-1995 period and between 72 and 83 in the 2017-2019 period. We do not have data on storm duration during the 1983-1985 as the earliest hourly data readily available date back from 1991 in this area (Shannon airport). Nevertheless, there is no evidence of a change of storm duration for the two periods in the daily rainfall dataset. Secondly, changes of land use in the catchment between 1985 and 2019 were limited to the displacement of natural grassland and forest in some areas, while most of the catchment remains covered by peat bog, with no apparent acceleration of surface erosion (Copernicus, 1990, 2018). Finally, the maximum surface SPM levels estimated during the high freshwater discharge, winter survey was 8.8 mg L^{-1} in deep waters, a similar figure to the maximum turbidity of 8.7 mg L^{-1} in surface water estimated by McMahon and Patching (1984) in Killary Harbour. This similarity may be surprising as annual mussel production at present exceeds a thousand tonnes (BIM, 2018b), while it was 60 tonnes in 1981 (Cush and Varley, 2013). This currently larger mussel production is likely to decrease SPM in the surface water column compared to 1981. In this study, the maximum turbidity levels were observed one meter above the bay floor, thus below the depths reached by rope mussels, and during winter,

when mussel filtration rates are minimal as a result of lower food availability, temperature and salinity levels (Davenport, 1979; Jørgensen et al., 1990; Riisgård and Larsen, 2014).

5.5.2 Explaining the spatial variability of Ra ratios and estimating a younger limit of water ages

The diverse sediment types in Killary Harbour may provide Ra fluxes to deep waters with variable Ra ratios (Section 5.4.2 and Table 7). Moreover, the bay is variably stratified, and surface waters are not consistently affected by Ra fluxes from sediments (Section 5.4.1). These two observations suggest that the "continuous model" of Moore et al. (2006) is not applicable for this system to assess water ages from Ra ratios and that other methods must be applied. Most inputs of Ra to surface waters are likely to occur in zone 1, where the bay is shallow. Large inputs of suspended sediments are present there and an intertidal area of sandy sediments is also present (Section 5.4.3). In zones 2, 3 and 4, the effects of Ra sources on surface Ra ratios in the bay are likely to be distinct between stratified and well-mixed conditions (Section 5.4.3), and the changes of Ra ratios are interpreted accordingly below.

5.5.2.1 Well mixed conditions in zones 2, 3 and 4

At discharges below 1.2×10^6 m^3 d^{-1}, the bay is likely to be vertically mixed during spring tides, allowing inputs from deep sediments to reach surface waters. During these periods, outer Killary had an increase of Ra ratios, suggesting inputs of new Ra to surface waters (west of km 12, Figure 28d, 0.1×10^6 and 0.6×10^6 m^3 d^{-1} freshwater discharge surveys). A similar increase of Ra ratios was observed by Moore (2000) in proximity to the shelf break of the US coast and the Gulf Stream. Because it was associated with a slight decrease of salinity, this phenomenon was attributed to the fast advection of water from a nearby estuary, driven by upwelling-favourable conditions (Moore, 2000). In the current study, one of the surveys showed indeed a slight decrease of salinity (cf. salinity profiles when the flow was 0.1×10^6 m^3 d^{-1} in Figure 28a), but not the other (cf. salinity profiles when the flow was 0.6×10^6 m^3 d^{-1} in Figure 28a). Lamontagne and Webster (2019) demonstrated that when the vertical coefficient of solute dispersivity is above 10^{-4} m^2 s^{-1}, Ra ratios are likely to remain approximately constant vertically throughout the water column in a

coastal setting with Ra inputs from bottom sediments. To date, no similar modelling studies of Ra activity trends exist in an estuarine context, where the advection of Ra in deep waters due to the estuarine inflow (occurring to balance the surface inputs of freshwaters) adds complexity to the problem. Nonetheless, the close Ra ratios between surface and deep waters during these surveys (Figure 28d) can confidently be interpreted as a result of strong vertical mixing (advective + diffusive) relative to horizontal mixing during well-mixed periods, particularly as similar deep and surface salinities are also present.

Solute fluxes from bottom sediments can modify surface $^{224}Ra/^{223}Ra$ ratios when vertical mixing rates are faster than the rates of transfer of surface water towards the outer boundaries of the estuary, and faster than the decay rate of short-lived isotopes of radium. Internal gyres were identified previously in zone 3 and 4 (outer Killary) during low discharge periods (Keegan and Mercer, 1986), and may promote the vertical transfer of solutes from deep waters during such periods.

As Ra ratios in sediments are generally larger than water column ratios (Section 5.4.2), inputs from sediments are likely to increase Ra ratios and thus reduce water ages based on Ra ratio. For example, Ra ratios were higher in fine sediments (type 1) close to km 12 in deep waters than in the water column in this location ($^{224}Ra/^{223}Ra$ = 12.1, Table 7, box 4 compared to ≈10 in surface water).

Our review of potential Ra sources in the bay showed that diffusion, bioturbation of bottom sediment and resuspension/deposition of sediment due to deep currents in the bay were the most likely mechanism that could lead to a release of Ra to zone 2, 3 and 4 surface waters during well mixed periods. These Ra fluxes thus can increase Ra ratios in this location, and also affect surface waters west of km 12 during well mixed periods. However, the large volume of the bay compared to its bay floor surface area creates a strong dilution of the Ra fluxes originating from sediments during vertically mixed conditions. As a result, Ra fluxes from diffusion and bioturbation should have only a small effect on Ra activity ratios in surface water (Table 9).

Resuspension of fine sediment can increase fluxes from the sediment by one to two orders of magnitude compared to diffusion alone (Niemistö and Lund-Hansen, 2019), and

can be sometimes detected by a localised increase of turbidity close to the bay floor (e.g. Fig, 7, 8, 9 in Feely et al., 1979). During a period of low discharge, Keegan and Mercer (1986) observed an increase of SRP and NO_3^- in zone 3. These authors attributed this increase to mineralisation in the sediment and the disturbance of sediment by tidal currents.

Section 5.4.3.4 showed that deep currents observed during mean tides in Killary Harbour by Keegan and Mercer (1986) could be double of the critical currents above which resuspension of similar fine sediment is expected (Niemistö and Lund-Hansen, 2019). Increased suspended sediment levels were observed in deep water during the highest discharge survey, but not during others (section 5.4.3.4). The amplified surface and deep current flow in the fjord when discharge was high may have increased the resuspension of deep sediment during this period, making it observable in deep samples. As the deepest samples taken were at least 1 m above the bay floor, a cyclic increase-decrease of turbidity close to the bay floor might have also been present in other surveys during mid tides below this depth.

The Ra ratio increase observed in the outer bay during the low discharge surveys may therefore be due to Ra fluxes from deep sediment advected to surface water, most likely from diffusion and bioturbation, with larger fluxes happening during cyclic sediment resuspension events. This effect would be visible on surface waters only during low discharge periods when the surface advection rates are reduced, allowing Ra fluxes from resuspension in zone 3 to affect the Ra ratio in surface waters. As a net advection of surface water towards the mouth of the bay is present, this would then create a “plume” of increased Ra ratios and increased particulate and dissolved P between zone 3 and 4. Such transfer of solutes from deep to surface waters during vertically mixed conditions is likely to provide larger, additional nutrient inputs to surface waters compared to stratified conditions and to promote phytoplankton growth by providing limiting nutrients. An increase of SRP was frequently observed in zone 3 deep waters, which may support this hypothesis.

The model of Moore (2000), subsequently dubbed the “mummy” model (e.g. in Tomasky-Holmes et al., 2013), is an alternative to the “continuous” model to assess Ra

water ages. This model assumes that (1) there is a single and constant value of the ^{223}Ra and ^{224}Ra activity for the source region (2) no significant additions or losses of Ra except for mixing and radioactive decay occur after the water leaves the source area, and (3) the open ocean contains negligible excess ^{223}Ra or ^{224}Ra (Moore, 2000). As the Ra activity ratios in potential Ra sources to Killary Harbour are generally larger than the Ra activity ratios in the water column, Ra ages derived from Ra ratios are likely to underestimate water ages in parts of the bay where inputs of Ra other than those originating in zone 1 occur. For example, outer Killary deep waters contain multiple Ra sources with a larger Ra ratio than surface water, and Ra ages in surface water derived from Ra ratios are thus likely to underestimate water ages when the bay is vertically mixed. Conversely, the significant decrease of Ra ratios with distance between km 4 and 12 (inner Killary) suggests that Ra ratios east of km 12 are less affected by Ra fluxes from sediments. An underestimation of surface water ages may thus be calculated for these surveys using the "mummy" model of Moore (2000). If the inputs from sediments are sufficiently mixed vertically to generate no change at the measured location, deep water ages may also be determined by Ra ratios using the "mummy" model. On the other hand, if Ra release rates from sediments are larger than those calculated from diffusion and bioturbation, deep-water ages cannot be defined, as Ra ratios would be modified by multiple sources.

5.5.2.2 Stratified conditions in zones 2, 3 and 4

At freshwater discharge rising above 1.2×10^6 m^3 d^{-1}, the bay is likely to remain stratified during spring tides (Figure 28c), and solute inputs from sediments are concentrated in deep waters. In such conditions, changes of Ra ratios in surface waters in zones 2, 3 and 4 are mainly explained by the decay and mixing of Ra isotopes during their transfer from zone 1 to the open ocean. Ra ratios changes in these zones may be used to assess Ra relative water ages in the bay using the "mummy" model of Moore (2000). Ra ages in deep waters, on the other hand, cannot be calculated as Ra ratios are likely to be changed by fluxes from bottom sediment.

The faster decrease of surface Ra ratios with distance in inner Killary (zone 2) and the slower decrease in outer Killary (zone 3 and 4) suggest a faster flushing of surface waters in outer Killary than in inner Killary (Figure 28 and Figure 30). Hydrodynamic modelling

previously identified a specific retention zone at the limit between inner and outer Killary (Donohue, 2012), which may also explain the observed fast increase of Ra ratios westward.

5.5.2.3 Estimates of minimum water ages

Considering the above, a lower-end estimate of Ra water ages for the bay was determined using the "mummy model" method (Moore, 2000), using the Ra ratios at the divide between zone 1 and zone 2 (km 4, Figure 28) as a reference for age zero. With this method, relative ages decreased between km 12 and 16 during low discharge surveys (Figure 31a), a consequence of added Ra fluxes changing Ra ratios, potentially from deep sediments in this area. As a result, the peak water ages east of km 12 can be used to assess the minimum average time necessary for water to reach this point from the River Erriff, as an indicator of the variability of flushing between surveys. This time seems to decrease with increasing discharge: the time taken by surface water to be flushed from inner Killary to outer Killary during spring tide periods varied from 2 ±1 to 3.0 ±0.6 days under maximum discharge conditions (Figure 31c, 3.3 $\times 10^6$ m^3 d^{-1}) to 6.7 ±0.8 to 8.5 ±0.8 days during the lowest discharge periods (Figure 31a, 0.1 $\times 10^6$ m^3 d^{-1}). These values can be compared with a series of modelling approaches previously applied by Hartnett et al. (2011) to assess the flushing characteristics of Killary Harbour. The methods outlined by Ketchum (1951) and Edwards and Sharples (1986) as applied by Hartnett et al. (2011) are modified versions of the tidal prism method (Ketchum, 1951) to consider stratified systems. The Ketchum (1951) method gives a value of 2.6 days, and the Edwards and Sharples (1986) method yields water residence time values of 3.1 days for Killary Harbour surface waters (Hartnett et al., 2011). These values match the 2-3 days residence times observed here for high discharge, stratified conditions. On the other hand, the approach in Abdelrhman (2005), as applied by Hartnett et al. (2011), which assumes a vertically mixed water column and no inputs of freshwater, gives a value of 14.6 days for the water residence time in the system. The DIVAST and NEW methods in Hartnett et al. (2011), using 2D models and assuming tidally driven exchanges but no significant stratification, lead to values for the water residence time of 41.9 and 60.6 days. However, more recent studies involving the EFDC 3D model (Donohue, 2012) highlight the fact that river

discharge can significantly decrease residence time and lead to an average residence time of 15.9 days. All these values are higher than the low discharge estimate of maximum water ages of 8.5±0.8 days, which confirms that Ra water ages during low discharge, well mixed periods support the lower-end estimate of water ages for Killary Harbour arising from modelling studies.

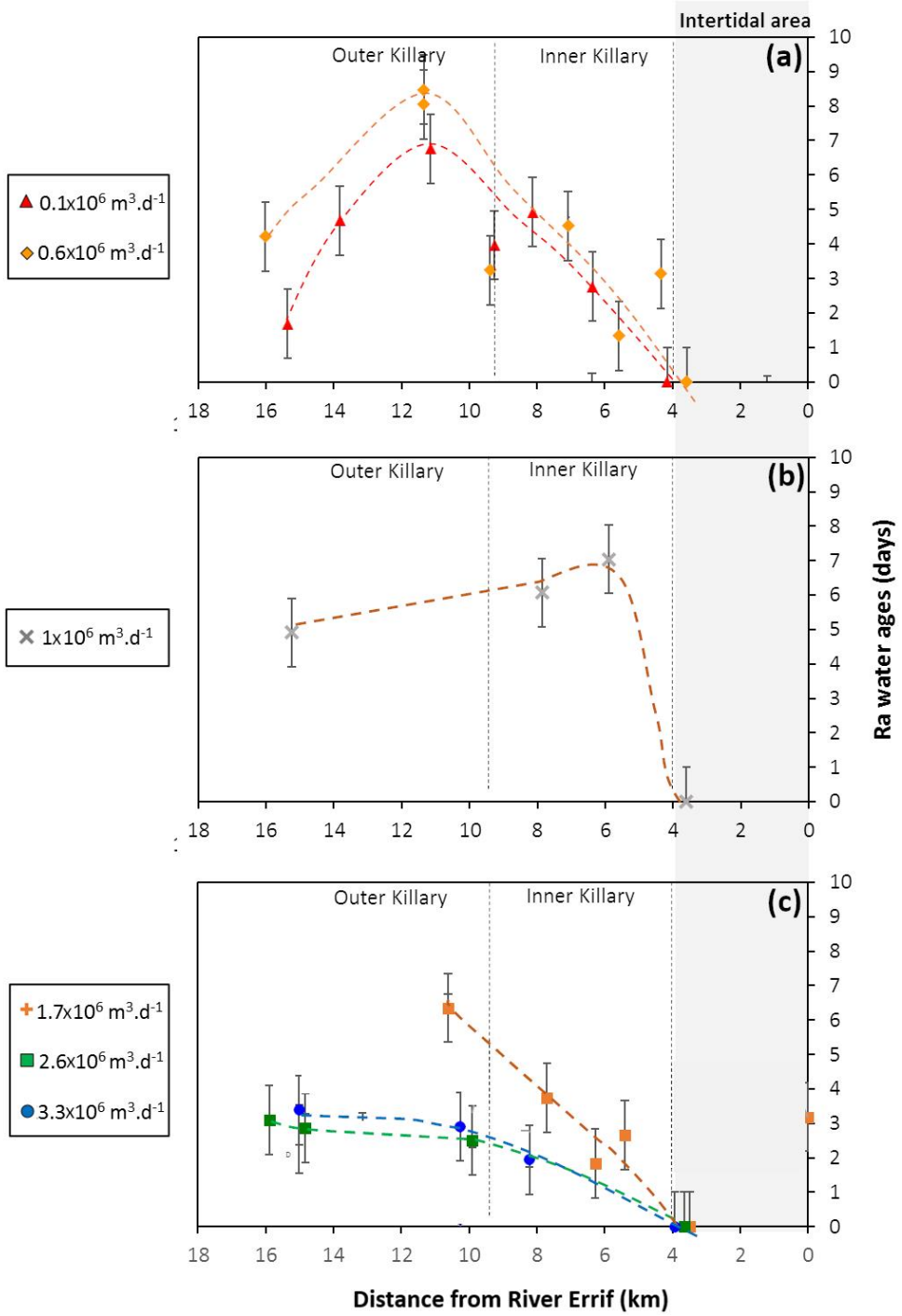

Figure 31: Apparent Ra water age profiles in Killary Harbour using the "mummy" model of Moore (2000) for a) vertically mixed surveys b) intermediate conditions c) stratified conditions.

5.5.3 Effects on phytoplankton growth and community composition

Estuarine stratification and the spatiotemporal variability of water ages may have three types of impacts on phytoplankton communities and aquaculture: (1) changes of water ages affect the spatial distribution on phytoplankton, (2) changes of discharge and stratification affect nutrient ratios available for phytoplankton growth and (3) the varying vertical mixing modifies phytoplankton species and timing of the blooms. These three aspects are summed up for Killary Harbour in a conceptual model in Figure 33.

Firstly, in estuaries, flushing rates and residence times strongly determine where and when the maximum amount of phytoplankton biomass occurs (Day et al., 2013; Liu and de Swart, 2018; Peierls et al., 2012; Tomasky-Holmes et al., 2013). Peak phytoplankton biomass frequently occur at a given range of residence times, for example at a residence time of around ten days in two North Carolina estuaries (Peierls et al., 2012) or for water ages between 8 and 10 days for two Massachusetts estuaries (Tomasky-Holmes et al., 2013). Neap and spring tide cycles affect water residence times and thus, phytoplankton biomass. Furthermore, maximum phytoplankton biomass tends to occur during low river flow and neap tides (e.g. Maier et al., 2012). Therefore, the effect of changing discharge and flushing on the distribution of phytoplankton biomass can be assessed with the spatial variability of water ages. Areas of high Ra water ages observed during low discharge, spring tide surveys (Figure 32 b, with conceptual model on the upper section of Figure 33) correspond to retention areas, favourable for summer phytoplankton growth, previously identified by either hydrodynamic or the Shellsim models as applied to the area (UISCE, 2010) (Figure 32 a). During high freshwater discharge surveys, on the other hand, the older waters are found further out in the bay and younger waters are more present throughout the bay (Figure 32 c, lower section of Figure 33). Increasing discharge of water from land (rivers or springs) reduce residence times, restricting phytoplankton growth and biomass build-up to the most downstream segments of estuaries (Day et al., 2013; Maier et al., 2012). This ‘rejuvenation’ of surface layers during high freshwater discharge events is thus likely to move the area of maximum phytoplankton density towards the estuary mouth. Indeed, an inverse correlation between primary production and the extent of the brackish/fresh layer in the bay was previously observed (Roden et al., 1987).

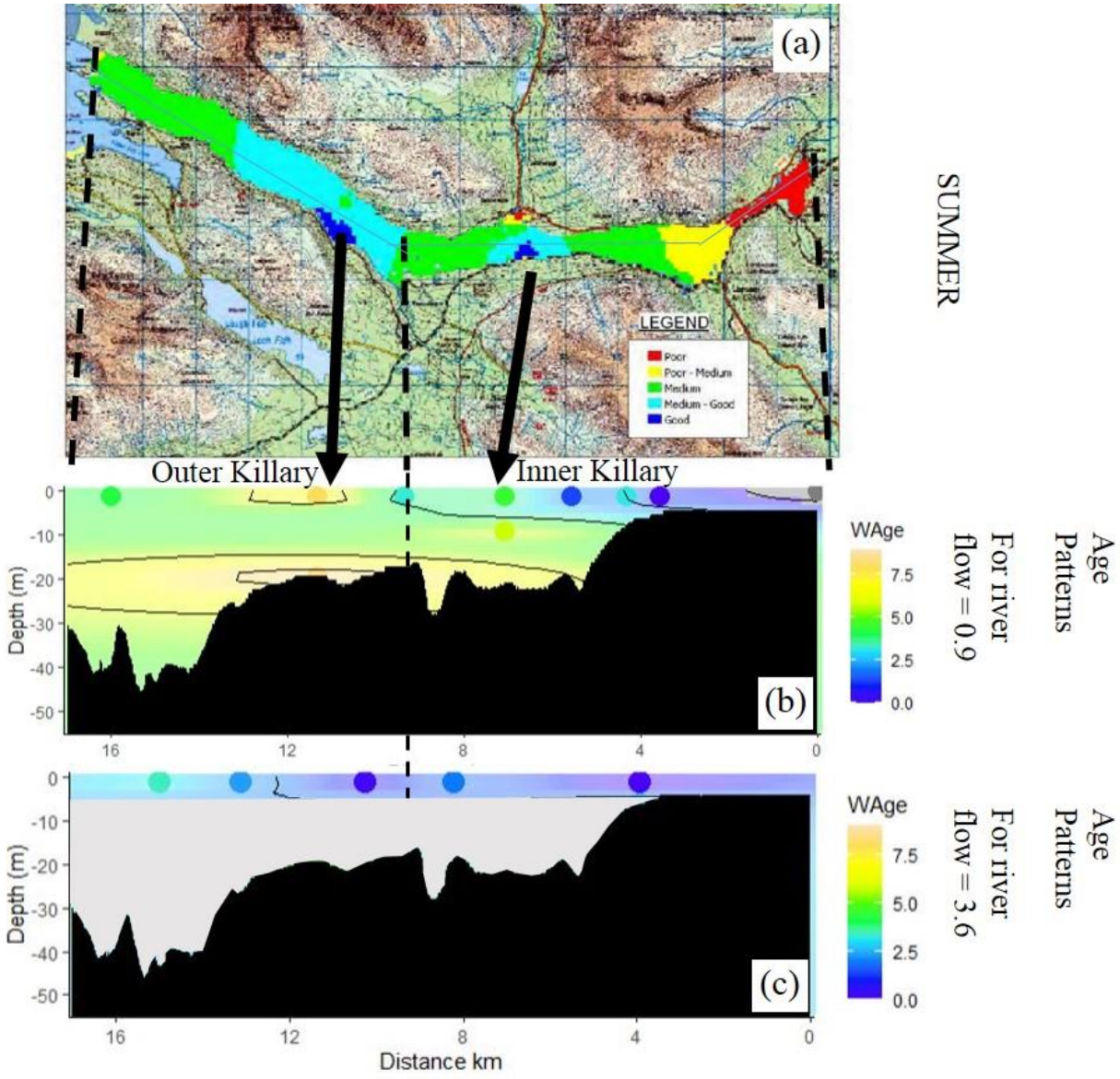

Figure 32: Comparison of predictions of surface phytoplankton growth potential from a previous study (a) *(UISCE, 2010)* with water age patterns observed in summer, low discharge surveys (b) and water ages patterns observed in high discharge surveys (c). (a) is reprinted from a previous report on Killary Harbour using hydrodynamic modelling and the Shellsim model to predict phytoplankton growth in the bay (AQUAFACT, 2013). (b) and (c) are derived from the current study. Arrows highlight points of high plankton growth potential in profile (a) that correspond to areas of high water age found during the low discharge surveys (b). In (c), deep water ages are not calculated, as Ra ratios were affected by multiple sources.

Secondly, variable river discharge and degree of stratification can modify absolute and relative nutrient availability (e.g. Sin et al., 1999), changes which affect phytoplankton composition and abundance. Under stratified conditions, SRP was relatively more enriched in deep water than in well mixed conditions (Figure 30b). This enrichment may be due to the combined effects of entrapment of P diffusing from deep sediments, P-bound particulates below the stratification boundary and lower primary production in

deep waters, compared to surface waters. These trends, combined with the inputs of DIN from surface freshwaters, led to higher N:P ratios in surface water during high discharge periods (Figure 30c and d). N:P ratios of surface waters were more likely to be above the Redfield ratio and to be closer to the high river N:P ratios at freshwater discharges above 1.4×10^6 - 1.5×10^6 m^3 d^{-1}. The lower salinity and P availability, as well as the faster transfer rates in surface waters during stratified, high discharge periods are likely to favour phytoplankton adapted to P limitation and potentially reduce phytoplankton biomass, compared to well-mixed, low discharge periods. A conceptual model illustrating this variability is provided Figure 33. As most species involved in harmful algae blooms (except diatoms and cyanobacteria) are or can become mixotrophs (Flynn et al., 2018), able to access nutrients directly from the ingestion of prey while using photosynthesis to grow, they may gain a competitive advantage over other species during such P limitation periods (Fischer et al., 2017). Particulate P and N may also provide limiting nutrients for phytoplankton in the system, but this role is likely to be restricted to the high turbidity sections observed in deep waters during high discharge and potentially in direct proximity to the river inputs, as most of the water column have generally close to zero turbidity. Particulate organic carbon and particulate organic nitrogen are supplied to the system by rivers and are then progressively consumed by the heterotrophic activity in Killary Harbour (Mcmahon and Patching, 1984). Particulate organic P is generally continuously remineralised within the water column in the euphotic zone (Paytan and Mclaughlin, 2007). As a result, an increase of particulate phosphorus levels likely leads to an increase of SRP, unless all the nutrient inputs are instantly consumed by primary production. As here particulate inputs are occurring in deep waters and driven by river water, the SRP produced by remineralisation is unlikely to be instantly consumed, and areas where inputs of particulate P are present should also show an increase of SRP. As P availability is driven by fluxes from sediment, and particulate P fluxes are continuously transformed in SRP, the DIN/SRP ratio is likely to be an acceptable proxy of the nutrient limitation affecting phytoplankton. However, the link between sediment fluxes, resuspension events in deep waters of Killary Harbour and dissolved P and N, may benefit from further investigation.

Thirdly, the intensity of stratification plays a major role in the initiation of phytoplankton blooms and in defining phytoplankton communities (Behrenfeld, 2010; Sverdrup, 1953). In Killary Harbour, a higher river discharge can increase the vertical salinity and the Ra activity ratios difference between surface and bottom waters (Figure 28, and conceptual model on Figure 33). Vernal blooms are generally triggered when vertical mixing falls below a certain threshold (Sverdrup, 1953). Conversely, vertical mixing during winter is essential for bloom formation, as it provides nutrients from deep waters and reduces predator-prey interactions, allowing phytoplankton growth to outrun grazing (Behrenfeld, 2010). Stratification can also favour phytoplankton capable of migrating vertically to position themselves actively at physically and chemically optimal depths (Paerl and Huisman, 2009). Examples would be the replacement of diatoms, which lack structures for motility such as cilia and flagella in their dominant vegetative stage (Gemmell et al., 2016), by cyanobacteria (Walsby et al., 1997) and dinoflagellates (Wyatt and Zingone, 2014). Consequently, the development of stratification can cause a shift in population dominance from diatoms to flagellates (Raine, 2014; Wyatt, 2014).

In situations when vertical mixing is low, such species would be able to position themselves at lower depths, with more favourable nutrient contents and N:P ratios, while benefitting from flushing slow enough to allow their development. When light is attenuated in surface water (e.g. due to high turbidity) phytoplankton may thus concentrate in thin layers close to the stratification boundary, where fluxes from deep sediment provide nutrients, but light availability is still sufficient (lower section of Figure 33). For this reason, salinity and water age gradients observed in stratified systems are also favourable to the concentration of blooms into thin layers along the halocline (Masunaga and Yamazaki, 2014). This phenomenon favours the concentration of an abundance of planktonic organisms and thus satisfies the growth requirements of fish and filter-feeding larvae during their reproductive periods (Berdalet et al., 2017). Conversely, it may also concentrate harmful microalgae within these thin layers (Berdalet et al., 2014; Gentien et al., 2005) and may thus increase the impact of HABs on adult filter feeders and other non-mobile species exposed to them.

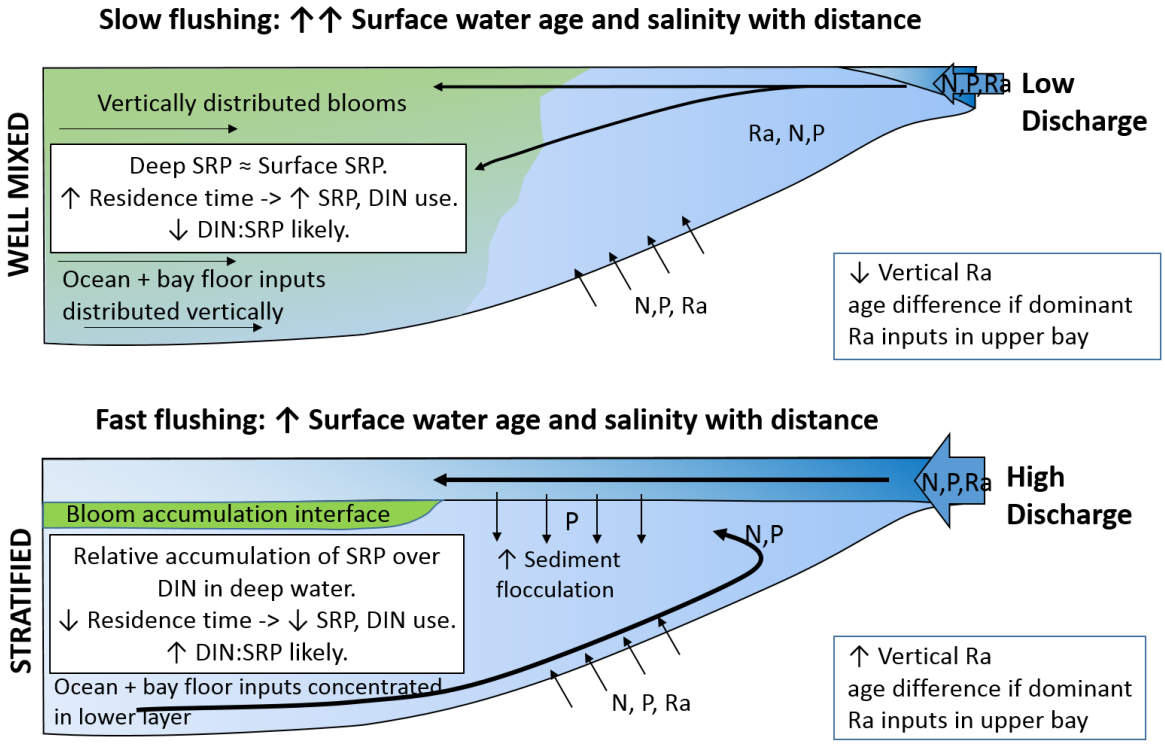

Figure 33: Conceptual model of the effect of variable stratification in Killary Harbour

5.6 Conclusions of Chapter 5

The measurements of $^{224}Ra/^{223}Ra$ activity ratios, salinity and nutrient concentrations along Killary Harbour show that the magnitude of stratification can be assessed using both the vertical gradients of salinity and Ra ratios. Once the different Ra sources are characterised, the effect of bay sediments as a source of solutes and a first-order estimate of the seasonality of the spatial distribution of water ages can also be determined. In Killary Harbour, an increase of both Ra and SRP in deep water suggested that deep sediment could provide significant solute inputs in the bay, increasing the availability of dissolved phosphorus in the bay. During well mixed periods, Ra ratios in surface waters decreased in inner Killary towards the west as a result of Ra decay, then increased in outer Killary, potentially as a result of new Ra fluxes from the bay floor to surface waters. Deep currents in the bay are large enough during neap tides to create cyclic resuspension/deposition of fine sediments, which may amplify solute fluxes from the bay floor, explaining part of the increase of Ra ratios. Conversely, during stratified periods, Ra

ratios in surface waters decreased towards the west in both inner and outer Killary, with a faster decrease in inner Killary. If this change is due mainly to Ra decay, it then indicates that surface waters are flushed faster in outer Killary than in inner Killary. The estimates of water residence time from Ra water ages are in the lower end of previous modelling studies of the water renewal timescale of Killary Harbour, except for stratified periods, when the two approaches concur. Increasing river discharge amplified the stratification of Killary Harbour during spring tides, leading to lower water ages and higher N:P ratios in surface waters. On the other hand, deep waters have lower N:P ratios than surface waters and are expected to have older water ages, conditions more favourable for phytoplankton growth. The effect of variable stratification, water ages and N:P ratios on phytoplankton biomass and community composition are likely to affect the timing of filter-feeder growth, mortality and/or of HAB related problems for aquaculture. In this context, Ra activity ratios combined with analyses of water chemistry can assess the magnitude of sediment fluxes and determine when fluxes from deep sediment are the most likely to provide solute and limiting nutrients to surface waters in estuaries. The seasonally and spatially variable effect of stratification on elemental cycling can be thus assessed, to better understand the timing of changes to ecosystem structure and services in a given estuary throughout the year, or to validate assumptions supporting transport and reaction models. The effect of sediment as a source of solute to the system should be investigated further, to further characterise the availability of phosphorus and other limiting nutrients to the bay.

Acknowledgment

This publication is a result of research supported in part by a research grant from Science Foundation Ireland (SFI) under Grant Number 13/RC/2092 and co-funded under the European Regional Development Fund and industry partners of the Irish Centre for Research in Applied Geosciences. Contributions were also made from an Irish Research Council and Environment Protection Agency funded project. Maxime Savatier and Maria Teresa Guerra were supported through an iCRAG PhD fellowship (ref TP GW3.2PhD5 and ref TP MG2.3PhD2), co-funded by Science Foundation Ireland (SFI) and the European Union. Jennifer Elaine Murphy was funded through an Irish Research Council/Environment Protection Agency PhD scholarship under grant number GOIPG/2016/1430. We thank Dr Jan Scholten from Kiel University for his advice on radium analysis, Mark Kavanagh from Trinity College Centre for the Environment for his technical support during nutrient analysis, Gennaro Scarselli and Meabh Hughes for assistance in fieldwork. We are also grateful towards Vincent Kane, Rainer Kraus and Simon Kennedy and his staff at Killary Fjord Shellfish, for providing their boat, and help during the transect surveys. Finally, we wish to thank J. Severino P. Ibánhez for providing comments on the text during the last phase of review, and the anonymous reviewers and the editor whose comments contributed to significant improvement of the original manuscript.

Note: The current version of this paper was accepted for publication to Marine Chemistry the 18/01/2021.

6 PAPER D: Effect of nutrient inputs from submarine groundwater discharge on primary production and aquaculture activities in an enclosed bay under changing climate.

6.1 Abstract

Nutrient fluxes from Submarine Groundwater Discharge (SGD) frequently modify the primary production of coastal ecosystems thus affecting aquaculture productivity. Here, the effect of SGD nutrient fluxes on phytoplankton biomass and aquaculture are investigated using previous SGD estimates, a ten-year nutrient and phytoplankton biomass dataset, a nutrient mass balance and a lower trophic model for a system receiving large SGD fluxes, Kinvarra bay. Nutrient inputs from SGD enhance phytoplankton growth in this bay, which directly benefit mussel growth in Kinvarra Bay. As only a fraction of the total nitrogen inputs from SGD are consumed inside Kinvarra Bay, it may also affect the aquaculture production in Galway Bay. Modelled dissolved nutrient and Chl-a were the highest around neap tides, when the bay was slowly flushed and retained solutes from SGD for a longer time period. Observed dissolved phosphorus in springs increased more frequently when groundwater levels were low during spring tides. Such periods can favour saline intrusions in coastal aquifers, increasing the magnitude of reactions leading to phosphorus release from the aquifer to coastal area, providing a net input of dissolved phosphorus and amplifying primary production. Between 2008 and 2018, the mussel production in Kinvarra Bay was the highest when May-July had a peak of fresh SGD followed by minimum fresh SGD flow rates during July-October. When higher fresh SGD fluxes occurred during July-October the next mussel harvest was lower, particularly when the next winter period had higher than average SGD fluxes and flooding. The effect of SGD on phytoplankton biomass and aquaculture thus strongly depends on the timing of the SGD flow and is not a linear function of discharge. The effect of rising water temperature and changes of annual rainfall patterns on fresh SGD discharge, Chl-a and aquaculture production in the system is also discussed using the lower trophic model and a recent assessment of the future rise of temperature and changes of rainfall frequency in Ireland. Both measured and modelled Chl-a levels were maximum during periods of low fresh SGD flux and high water temperature and were minimum during periods of high SGD flux and low water temperature. Considering here only the effect of temperature on

phytoplankton, likely to be influenced first by changes of temperature, an increase of sea water temperature by 1.7 degrees could increase the modelled Chl-a by up to 40 percent during spring or autumn but had less effect on modelled Chl-a levels during mid-summer. Other effects of temperature on nutrient cycles may however balance or amplify these changes and the effect of temperature on nutrient fluxes from and to sediments in SGD sites should be also investigated further.

6.2 Introduction

In recent years, submarine groundwater discharge (SGD) was shown to be potentially more important source of solutes for the global ocean than river flow (Cho et al., 2018; Moore, 2010). Coastlines and oceans supports a wide range of global ecosystems and human activities, besides contributing to the global economy by up to 60.5 trillion dollars per year (Costanza et al., 2014). Thus, an assessment of the effect of this flow on industries dependant on coastal ecosystem services is necessary to be prepared for the effects of these systems` changes. In coastal areas, aquaculture activities, such as shellfish production, are amongst the most sensitive to changes, as they depend on water quality and optimal phytoplankton availability to support production (Dame and Prins, 1998). The vast majority of marine aquaculture occurs along coastal areas. Nutrient inputs to coastlines from SGD, rivers or the open ocean affect phytoplankton growth rates and can lead either to positive or negative effects on aquaculture. Changes of water flow to and from coastal areas (river, springs, exchange with the open ocean) also modify the spatial variability of water ages, which affect phytoplankton biomass (Tomasky-Holmes et al., 2013) and the retention period of regenerated nutrient releases from aquaculture activities.

Due to their intrinsic permeability, coastal sands are locus of non-steady fluxes of fresh and saltwater across the sediment/water interface driven by seasonal differences of inland groundwater levels, tidal variability and other natural processes (Rocha, 2008; Santos et al., 2012). This variable water exchange provides both allochthonous and regenerated nutrients to coastal systems, supporting primary production and aquaculture. In some bays hosting aquaculture, SGD is the main nutrient source supporting the growth of the harvested organism, through the direct support for local

primary production it provides (e.g. Hwang et al., 2010; Wang et al., 2014). The nutrients added by SGD are either supplied by fresh SGD, composed of water initially infiltrated inland from net rainfall, flowing to the coast as groundwater, or by saline SGD, composed of water originally coming from the sea, infiltrated by tide, density difference or wave setup, and flowing back to the sea. The total SGD discharge is frequently a mix of the two, with relative proportion changing during the year, as a result of a combination of factors such as natural recharge or tidal variability.

Climate change is likely to modify the seasonal patterns of rainfall and temperature, and affect the annual patterns of water discharge to coastal areas, such as rivers (Hoegh-Guldberg et al., 2018). As fresh SGD is also fed by net rainfall, SGD fluxes are also likely to be modified, particularly for unconfined aquifers. Considering the current change of climate, the FAO identified the following priority research gap: "the implications of increasing droughts and changing precipitation patterns on aquaculture production need to be further contextualized (…) also in the light of competition between sectors for freshwater" (Anika and Cassandra De, 2016). The necessity to investigate changes of precipitation for aquaculture was also highlighted for Ireland and the UK by Callaway et al. (2012). The annual and interannual variability of SGD fluxes can be expected to vary as a result of climate change and changes of water use in catchments. As the primary production in some ecosystems and aquaculture sites rely in full or in part on nutrient fluxes from SGD, this is likely to affect aquaculture production and ecosystem functions significantly.

It can be expected that modifications of the annual variability of nutrient fluxes from SGD to a coastal bay as a result of climate change can create changes of the annual variability of nutrient levels and water chemistry parameters that may be sufficient to affect phytoplankton biomass and aquaculture production, even if annual averages remain similar. To determine how climate change could impact mussel production in the bay, and to investigate the effect of nutrient fluxes from SGD on phytoplankton and aquaculture in a coastal bay, we study a site where intense SGD fluxes are present, Kinvarra Bay, western Ireland. To estimate the effect of SGD on the annual and seasonal nutrient balance of coastal areas hosting aquaculture activities, we use three approaches: First, we analyse a ten-year surface water nutrient and chlorophyll-a dataset from

Kinvarra Bay (EPA, 2018a) and a groundwater quality dataset from its catchment (EPA, 2015), combined with new data collection to assess the effect of SGD fluxes over nutrient concentrations and phytoplankton biomass in the bay. Secondly, we use that dataset to build a nutrient mass balance of the system, based on the LOICZ guidelines (Gordon et al., 1996). With this balance, we assess the effect of nutrient inputs on the system during specific times of the year, and the variability of nutrient reactions occurring in the bay. Finally, we adapt an existing lower trophic ecosystem model (Cranford et al., 2007) to (1) model the variability of nutrient balance and tidal cycle between surveys (2) assess the effect of SGD on phytoplankton biomass in the bay and (3) test the effect on nutrient, primary production and aquaculture production of changes of climate, driving modifications of water and nutrient discharge to coastal areas. We conclude the analysis by discussing how this type of methods might allow to support and test potential policies and aquaculture management strategies to ensure the protection of SGD value for sites hosting aquaculture activities while considering the other water management problematics in the catchment (e.g. flood risk management, water supply fed by groundwater, discharge from sewage treatment plants).

6.3 Study site

Kinvarra Bay is a coastal embayment in the south of Galway Bay (Western Ireland), in which mussel aquaculture (150 tonnes in 2018) and oyster aquaculture (15 tonnes in 2018) are present. The local aquaculture benefits of nutrient fluxes coming from coastal springs fed by a catchment of 486 km^2 (Figure 34). The bay contains intertidal areas (Maritime wetlands in Figure 34) that can store, transform and release groundwater-fed nutrients in the area (Rocha et al., 2015). During low groundwater level periods, saline intrusion in the aquifer occurs (Petrunic et al., 2012) and leads to an increased content of phosphorus in the SGD fluxes (See Chapter 4).

The catchment from which the spring waters originate is composed of two parts of distinct geology and hydrology. The upper catchment is composed of poorly permeable sandstone, siltstone and mudstone, with a dense river network. The lower catchment is composed of limestones and dolomites, with little surface runoff and a well-developed karst network (Figure

34). The dense river network found in the upper catchment quickly infiltrates into the karst system in the lower catchment section and reappears in the coast as a series of springs, as identified by cave exploration and tracer tests (Figure 34). The two main springs present in the bay are Kinvarra East and West (KE and KW in Figure 34). The lower catchment contains a series of groundwater-fed lakes (turloughs) and inland marshes which flood when groundwater levels are high. Flooding periods during high groundwater level periods may drive increased nutrient fluxes to the bay.

The upper catchment is mainly composed of forests, peat bogs and transitional woodland shrubs (Figure 34), which likely provide some water storage and delay the flow of water from the upper catchment to the lower catchment, reducing peak discharge and flood risk in the areas downstream. On the other hand, most of the lower catchment has pastures, with little woodland cover. Moreover, the limestone aquifer in the western part of the catchment has little or no sediment coverage in some cases (e.g. bare rock in Figure 34) favouring quick groundwater recharge during rainfall events. However, the turlough in the lower catchment also can store large amounts of water which dampen the response time of the aquifer following rainfall periods in a more significant manner than the effect of soil and vegetation cover in the upper catchment. Gort and Kinvarra are the two main urban centres present in the catchment (Figure 34) and have reported floods during winter.

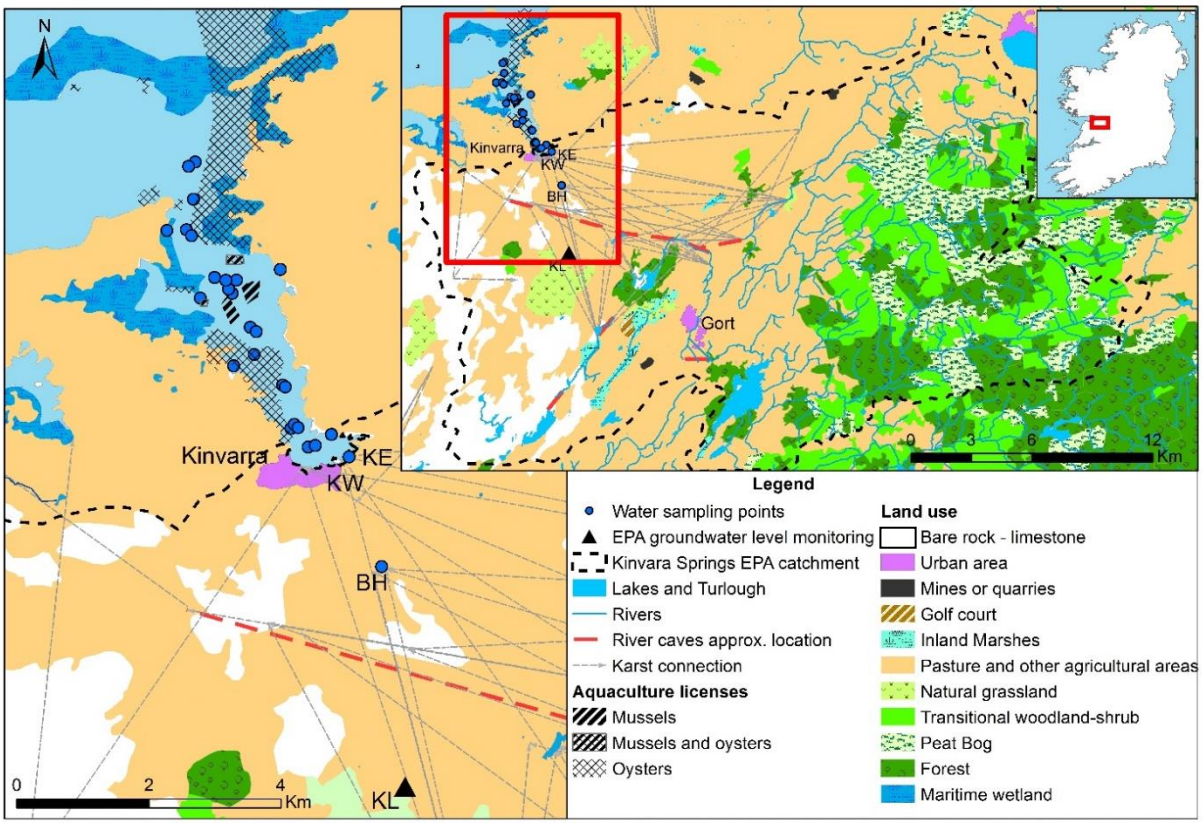

Figure 34: Kinvarra Bay's aquaculture activities and land use in the catchment from which Kinvarra spring waters originate. River networks are from EPA (2016), Karst connections are taken from Geological Survey, (2019) and the approximate locations of a network of caves carrying groundwater to the bay is shown with dashed lines and originally taken from Drew (2003). Land use shown is a reclassified Corine Land Cover data (EPA, 2018b). KE and KW are Kinvarra East and Kinvarra West, the two main springs providing fresh SGD to the bay. Groundwater level is recorded by the EPA at Killiny Borehole (KL) (EPA, 2020). BH is the approximate location of the borehole sampled in this work and Kinvarra Borehole, the borehole sampled by the EPA.

6.4 Methods

6.4.1 Data collection

Four surveys were performed in Kinvarra Bay under different discharge conditions, representative of the full annual variability of groundwater head in the main conduit network feeding Kinvarra spring, measured at Killiny Borehole (2m, 12-14 July 2018; 4m, 20-23 October 2018; 7.2m, 25-28 January 2019; 9.4m, 06-08 April 2019). Surveys were conducted during spring tides in order to have comparable results and to conservatively estimate the impact of SGD in this system. For each survey, we took surface water samples during boat transects at ebb tide using a Niskin bottle at 0.5-1m depth, except during the April 2019 when it was during flood tide. Additional samples were taken from Kinvarra spring during low tide and from a borehole connected to the main conduit feeding Kinvarra spring (Loughcurra) in the same day. Each sample was taken in triplicate and filtrated independently to account and correct for bias due to potential contaminations during filtration. Samples for dissolved nutrient analysis (NO_3^-, NH_4^+, NO_2^-, PO_4^{3-} as Soluble Reactive Phosphorus - SRP) were filtered into vacutainers with 0.15µm Rhizon membranes (Ibánhez and Rocha, 2014; Jiang et al., 2017). Samples for SRP determinations were stored at 4 degrees until analysis and analysed within 10 days after collection, while samples for dissolved inorganic nitrogen (DIN) determinations were analysed within 30 days after collection, following Jiang et al. (2017). DIN was analysed with a Lachat Quickchem 8500 flow injection analysis system, following manufacturer-adapted methods for sequential analysis (Lachat instruments, 2002, 2001). SRP was determined at 885 nm using a Hatch DR5000 spectrophotometer using standard colorimetric methods (Grasshoff et al., 2009). Total dissolved nitrogen was determined after conversion into nitrate through alkaline oxidation with potassium peroxodisulfate in an autoclave (Grasshoff et al., 2009), then analysed for nitrate using similar procedures than for DIN (Lachat instruments, 2002, 2001). DON was then calculated from the subtraction of DIN from the total dissolved nitrogen pool. Salinity and turbidity (in NTU) were measured using an Aquaread® Aquaprobe, calibrated according to standard manufacturer procedures (Aquaread, 2013). Salinity values were verified with a Carl Stuart Limited

Cond197 i WTW electrical conductivity probe. Finally, the Ra ages were determined from samples in these same surveys as described in Chapter 3.

In addition to these surveys, which provide "snapshots" of the bay biogeochemistry under specific conditions, the long term variability was estimated from a ten-year Environment Protection Agency dataset for transitional waters in Kinvarra Bay (EPA, 2018a) and for groundwater quality in Kinvarra springs and Kinvarra Borehole (EPA, 2015). These datasets include nutrient and ancillary water quality parameters taken by the EPA as part of the water framework directive, with four transects per year of ten samples each for Kinvarra bay water quality, and one to four samples per year for Kinvarra springs and Kinvarra borehole. The location of Kinvarra Borehole was selected as it is next to the main series of conduit bringing water from the rest of the catchment to Kinvarra springs and is thus thought to be representative of the water coming from the catchment through conduit flow.

6.4.2 Bay discretization for mass balances and box models

Inputs of freshwater such as fresh SGD or rivers to a bay and tides can create spatially and temporally variable stratification (Chapter 5). Kinvarra Bay is shallow, but can be variably stratified within spring/neap cycles and high/low tides (e.g. Figure 2 in Gregory et al., 2020). A surface plume of reduced salinity composed of water coming mainly from Kinvarra springs is present in the surface during neap low tide but dissipates at high tide with variable longitudinal extend depending on ebb or flood tide (Figure 2 in Gregory et al., 2020). Given this variable stratification, and the variable location of the brackish surface plume along the bay we cannot reasonably model Kinvarra Bay with multiple boxes at this stage, particularly as winter periods may be significantly different from what observed by Gregory et al. (2020) during summer. However, as previously shown in section 3.4.5, the bay can be approximated to be well mixed at the scale of one tidal cycle, to build mass balances for this system. In this study, Kinvarra Bay was thus modelled as a single box to assess the variability of nutrient and phytoplankton in the bay under the influence of SGD. This simplification allows to estimate relative changes in the bay under changes of SGD discharge, tide, light and temperature variability, while allowing a finer

analysis of the effect of different model parameters as we do not have the added complexity of considering multiple boxes.

The following method was applied to make spatially variable data collected during the surveys comparable with the outputs of the single box model: First, the EPA data was classified by date and depth. For each date, a representative concentration for the bay was calculated by doing a simplified 3D integration method described in Appendix 8. In short, the bay was divided in four sections with deep, surface and medium layer. Each sample was then grouped in each layer according to its location in the bay. Sections that did not had a sample within it were assumed to have values equal to the average of the surrounding boxes. The representative value for each date was then calculated using the volumes and concentrations of each boxes and layers. This value can be then compared with the outputs of a single box model to test its ability to model the overall annual changes of concentrations in bay waters or used for the LOICZ mass balance. This approach, while being a simplified 3D integration method, provide an estimate of the overall variability of parameters in the bay, while accounting for the bay asymmetric shape and true geometry. This method is thus preferred here to median and averages, as these can overestimate the effect of solute sources on the inventories of a tracer in aquatic bodies where these solute inputs occur in shallow areas (as previously shown for salinity in section 3.5.2).

6.4.3 LOICZ approach

To assess the effects of SGD discharge on net primary production and denitrification-nitrification rates in Kinvarra Bay, we closed nitrogen and phosphorus mass balances for the four surveys performed in the area, using the general LOICZ modelling approach (Gordon et al., 1996). This approach considers the bay to be well mixed at the scale of one tidal cycle, which is a reasonable first-order approximation for mass balances for this system during spring tide (as previously shown in Chapter 3, section 3.4.5). Furthermore, it assumes that the system is at steady state with respect to water, salt and nutrient balances (the sum of inputs and outputs of nutrient to the system is 0 for a given survey). For each survey, we considered groundwater inputs, exchange between the bay and the

open ocean, rainfall and evaporation in the system (Gordon et al., 1996). The retention of fluxes of N and P occurring in Kinvarra Bay were assessed based on the excess or loss of nutrient. The net molar retention of phosphorus was converted in stoichiometric carbon equivalents to assess the net primary production (primary production-respiration) occurring within the system. To assess the minimum /maximum net primary production, we considered two extremes: net primary production within the system is dominated by phytoplankton (C:P = 106) (Redfield, 1958) or by seagrasses or marine macroalgae (C:P=550) (Atkinson and Smith, 1970). The net N fixation-denitrification occurring in the system was assessed by closing mass balances for DIN and DON and determined the net gain or losses of N within the system. The net primary production in the system was assessed by closing mass balances of P for the system, following the LOICZ approach (Gordon et al., 1996) and the previous observation that P is a limiting nutrient in this bay (Rocha et al., 2015).

6.4.4 Lower trophic model

We used a modified version of the model of Cranford et al. (2007) to assess the effect of changes of nutrient and freshwater discharge from SGD on the nutrient mass balances and phytoplankton abundance across the year, while considering the effect of other seasonally variable drivers (temperature, light availability, day length). The model was initially developed as a carbon-based model by Dowd (2005) for a coastal system of a similar depth and shape to that of Kinvarra Bay and was adapted to model nitrogen fluxes in a system with mussel activities by Cranford et al. (2007). The initial purpose of the model was to assess the effects of aquaculture (mussel production) on nutrient or carbon mass balances. It had the advantage of explicitly including the variability of the main drivers of change of nutrient storage in the dissolved and particulate phases and in phytoplankton and sediments (i.e. inputs from land, exchange with the ocean, sediment, phytoplankton growth and decrease, mussels). A model map of the differential equations described in Cranford et al. (2007) and Dowd (2005) is shown in Figure 35.

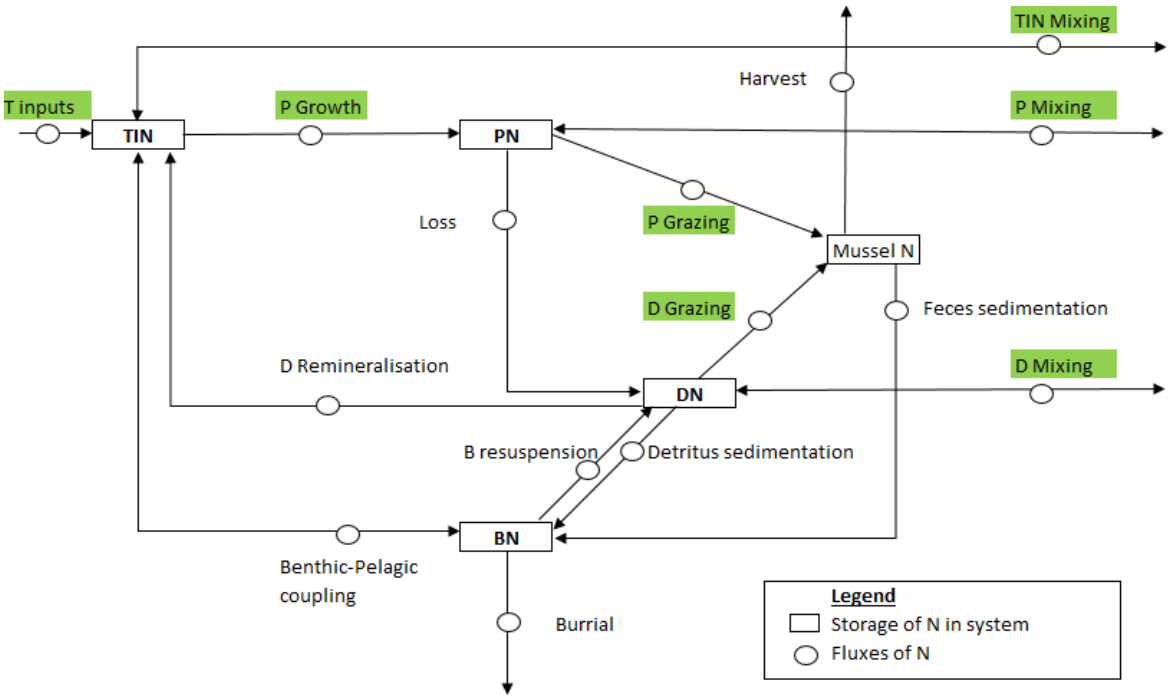

Figure 35: Model structure adapted from the model of Cranford et al., (2007) using the equations from Dowd (2005). TIN are dissolved inorganic nitrogen in the bay, PN is the nitrogen storage in phytoplankton, DN is the nitrogen storage in detritus or particulate N in the bay, BN is the Benthic N, stored in sediment. T inputs are the new dissolved inorganic nitrogen provided to the system by inputs from the land (here SGD). Dissolved nitrogen, Phytoplankton and Particulate nitrogen (Detritus, D) are exchanged with the outside of the system (Here Galway Bay), through the terms TIN mixing, P mixing, D mixing. The processes highlighted in green were updated in this study to account for the known characteristics of Kinvarra Bay.

We kept the parameters and expressions defined in Cranford et al. (2007), and Dowd (2005), unless for processes highlighted in green in Figure 35. This model was implemented using the Euler method, similarly to Dowd (2005). We made the following modifications to adapt the model to the specificity of SGD sites and to account for the evolution of knowledge since the study of Cranford et al., (2007):

1) A constant exchange rate K as in Dowd (2005) could not be assumed here because there is evidence that the spring/neap tide cycles in Kinvarra Bay strongly affected water exchanges with Galway Bay (Gregory et al., 2020). To account for the spring/neap tide cycle, we calculated the average tidal prism Pr for each day of the year, and determined the exchange rate K as a function of time, using the following equation (Sanford et al., 1992):

$$K = \frac{1-b}{V}\left(\frac{Pr(t)}{T} - \frac{I}{2}\right) \quad (5.1)$$

Where Pr(t) is the tidal prism as a function of time; b is the return flow factor, i.e. the quantity of water that has left on the ebb tide, returning on the next flood tide; V is the bay mean tide volume; T is the tidal period (in days); I is the volume of freshwater flowing into the system. We calculated Pr(t) for each timestep from the tidal variability in Galway Bay (Marine Institute, 2017) and the digital terrain model of Kinvarra Bay (GSI/MI, 2019).

2) Cranford et al. (2007) used shell size measurements in the bay from Waite et al. (2005) and an allometric equation from Smaal and Vonck, (1997) to assess clearance rates of mussels. We updated the values of Cranford et al. (2007) using information of mussel growth in Ireland as follows. The changes of mussel size were estimated as in Cranford et al. (2007), using a linear growth model from the mussel seed size to the commercial size (shell size of 50-70 mm BIM, (2019)). As it takes in average 18 months for mussels to reach marketable size in aquaculture sites in this part of Ireland (AQUAFACT, 2013; Rodhouse et al., 1984), Kinvarra Bay will contain mussels from at least two distinct settlement years. Furthermore, some mussels may be lost due to mussel mortality, drop-off or discarding of damaged mussels during harvest. Mortality in Ireland for mussel production is between 20 and 30 percent (BIM, 2019). To assess the number of mussels in Kinvarra Bay from the annual production dataset (BIM, 2018a), we thus assumed that the number of mussels in Kinvarra Bay was 2.3 times the annual production. This is similarly to what observed by Cranford et al., (2007) in Tracady Bay, where growth rates are similar to growth rates in this part of western Ireland (Rodhouse et al., 1984) . Finally, daily mussel filtration rates were then estimated from their shell size, using the equation of Riisgård et al., (2014) for a mussel with medium condition index. Taking the same expression as Cranford et al., (2007) and Dowd (2005), the value of the parameter I_m, the ingestion rate of all bivalves present in the bay (d^{-1}) is:

$$I_m = \frac{n*fr}{Vb} \quad (5.2)$$

Where *n* is the number of mussels in the bay, $f_r(t)$ the filtration rate of one individual (m^3 ind^{-1} d^{-1}) as a function of mussel size on a given day and the relationships of Riisgård et al. (2014), and V_b is the volume of the bay at mean tide (1.4×10^7 m^3).

3) We assessed nitrogen inputs into Kinvarra Bay (T inputs in Figure 35) in two steps. First the SGD flow rate was assessed using a relationship between groundwater levels and SGD flow rates determined for Kinvarra Bay in Chapter 3, relationship 1 in section 3.4.1 (Figure 13). Then, total nutrient discharge were estimated from

the SGD discharge and average nutrient content in the spring obtained from the EPA (EPA, 2015) and from the surveys carried out in this study. This simplification ignores the effect of variable N concentrations in groundwater due to reactions within the catchment, anthropogenic contamination of groundwater or flooding, and thus provides a minimum estimate of the effect of SGD on the nutrient mass balance variability. When testing the effect of a parameter on model outputs during a typical year, a representative annual cycle for the daily groundwater flow was estimated from the SGD flow between 2010 and 2013, classified by day number and averaged between years. This coincides with the period previously modelled by McCormack et al. (2016), and is well characterised for SGD flow rates to Kinvarra Bay. The SGD flow patterns vary from one year to another, and we also model the effect of the interannual variability using the daily averaged SGD flow between 2004 and 2019 as described in section 6.4.4.

4) We updated the phytoplankton growth calculations from Dowd (2005) and Cranford et al. (2007) by considering the effect of phosphorus limitation and light attenuation due to particulate matter and phytoplankton in the system (self-shading) on phytoplankton growth. To account for the seasonal variability of the chlorophyll-a: carbon ratio of phytoplankton (Geider et al., 1998; Jackson et al., 2017; Jakobsen and Markager, 2016), we used the estuarine formulation of Jakobsen and Markager (2016). The original equation from Dowd (2005) and Cranford et al. (2007) is:

$$P_{growth} = f\{X;\ k_x\} * yp(t, Temp) * P \quad (5.3)$$

Where P_{growth} is the phytoplankton growth (daily rate of N stored by phytoplankton); $f\{X; k_x\}$ is a saturation term to account for the reduction of growth due to the limitation of a nutrient X; $y_p(t,Temp)$ is the maximum growth rate of phytoplankton without nutrient limitation (day^{-1}); *P is* the total N level in phytoplankton of the bay.

Yp was calculated as in Dowd (2005) and Cranford et al. (2007) with minor adaptations (see Appendix 1 for details on the calculation method).

We updated the expression $f\{X; k_x\}$ to account for limitations due to both DIN and DIP, according to Michaelis-Menten kinetics (Caperon, 1967; Dugdale, 1967):

$$\mathrm{f\{X;\ k}_x\} = \frac{N}{N+K_n} * \frac{DIP}{DIP+K_{dip}} \quad (5.4)$$

Where K_n and K_{dip} are saturation constants for DIN and DIP concentration in the bay; and N is the concentration of DIN in the bay (mmol N m^{-3}) at a given timestep. K_n is taken from Cranford et al. (2007), K_{dip} is calculated from K_n using the average Redfield N:P ratios for phytoplankton from Garcia et al. (2018). As N:P in phytoplankton may be variable, the effect of variable N:P is then tested as described in section 6.5.4.4.2.

5) We included in the model variable water temperature calculation for each timestep, including the effect of groundwater inputs on temperature. Modelled water temperatures were calculated for each timestep of the model run following a similar method as Dowd (2005), with an added term to account for the effect of groundwater fluxes on the temperature in the bay. The temperature budget for the bay is then:

$$\frac{dTemp}{dt} = v + K[Temp_{\infty} - Temp_b] + H_{gw} \quad (5.11)$$

Where *v* is the heating rate of water due to solar radiation during the day considered; *K* is the exchange coefficient of the bay with the surrounding waters (calculated with equation 5.1); $Temp_{\infty}$ and $Temp_b$ are the average temperature outside and inside of the bay; H_{gw} is the heat flux due to the discharging groundwater (negative if the groundwater is colder than the bay). *V* was estimated as described in Appendix A in Dowd (2005). The net heat fluxes used to calculate *V* were estimated using a solar radiation dataset at Athenry (Met Eireann, 2020), a meteorological station 20 km from Kinvarra Bay.

6) Finally, a calculation of modelled residence time in Kinvarra Bay was included for each timestep to facilitate the validation of the model with Ra relative ages or outputs from hydrodynamic models. The modelled annual changes of relative water age were assessed with the modified version of equation 3 of Sanford, Boicourt and Rives (1992), and the return flow factor for Kinvarra Bay from Rocha et al. (2015). These were then compared with residence time values measured with $^{224}Ra/^{223}Ra$ during from four spring-tide surveys of water ages variability (data shown in Chapter 3).

6.4.5 Validation and sensitivity analysis of the lower trophic model

6.4.5.1 Validation

The lower trophic model outputs were validated using observed water temperature, salinity, residence time, Dissolved Inorganic Nitrogen, Chlorophyll-a in Kinvarra bay between 2007 and 2019 (EPA, 2018a). Furthermore, modelled net primary production and nutrient fluxes to the benthos were compared with estimates determined for summer by Rocha et al. (2015). The efficiency of the model for temperature, salinity, DIN and Chl-a was estimated from the Nash and Sutcliffe, (1970) model efficiency (ME). This parameter, estimated from modelled and observed values, is between -∞ and 1, and is positive when the relative performance of the model is better than the mean of observed values (Janssen and Heuberger, 1995; Nash and Sutcliffe, 1970).

Measured temperature, salinity, nutrients and Chl-a are generally spatially variable in Kinvarra Bay (EPA, 2018a). To allow the comparison between the output of our single box model and the values measured in Kinvarra Bay, temperature, salinity, nutrient and Chl-a measurements were integrated for the bay for each EPA surveys (EPA, 2018a), and averaged by volume as described in Appendix 8, following the justification previously described in section 6.4.2. These integrated concentrations estimates were then used to calculate the ME and visualise as a function of time the relative changes of water chemistry recorded across the bay. The changes of mussel N assimilation which are not known for this system were validated using the annual variability of mussel growth known for other systems in Ireland and in systems of similar latitude.

6.4.5.2 Sensitivity analysis

The sensitivity of each model output variable to the uncertainty of the model input parameters was assessed using a nominal range sensitivity analysis as in Morgan and Henrion, (1990). First, the range of possible values was assessed for all parameters of the model, based on earlier studies. When only one value was available without uncertainty or possible range given, a 50 % uncertainty of the value found in the literature was assumed (See Appendix 1, Appendix 2 for the list of parameters and the reference used). Then, all model parameters were changed from their minimum to their maximum possible values while keeping other stable, and sensitivity was assessed from the change of the

annual means of three selected modelled variables: DIN, phytoplankton biomass, and mussel N assimilation. For example, the sensitivity of the variable phytoplankton to changes of the parameter phosphorus concentration in the bay, is assessed by calculating the difference between the annual mean of the curves of phytoplankton biomass at high and low phosphorus concentrations.

The results of this analysis are shown in appendix 2. For each variable, the effect of the most sensitive parameters was then studied in more detail by incorporating them in different scenarios to illustrate the effect of modifications of these parameters on the model outputs and the ecosystem functioning (section 6.4.6).

6.4.6 Testing different scenarios for Kinvarra bay with the lower trophic model

As an attempt to identify the sensitivity of Kinvarra Bay to different changes, we considered five scenarios: changing mussel standing stock, modifications of the dissolved inorganic phosphorus concentrations in the bay, changes of water exchange with Galway Bay, changing phytoplankton types (through their nitrogen and phosphorus content, nutrient assimilation rate, Chl-a content, growth rate or grazing rates) and changing annual average water temperature and rainfall frequency (focusing on the effect on the bay water column). For each scenarios, the effect of these changes on average DIN and Chl-a during periods of low and high SGD flow are discussed. Where appropriate, the average difference and its 95% confidence interval is given for both periods.

6.4.6.1 Effect of changing mussel standing stock in the bay.

Between 2003 and 2018, the mussel production in Kinvarra Bay fluctuated between 110 and 200 tons, with an average of 159±28 tonnes (BIM, 2018a). To determine whether this variability could be expected to create a significant change of Chl-a in the bay we modelled the bay using these two extreme values and compared the outputs.

6.4.6.2 Warmest average temperature

Since 1980, a rise of sea water temperature of 0.3-0.4 °C per decade is observed in Ireland in satellite and in situ observations, generally following inland trends, and these trends are expected to continue over the coming decades (Dunne et al., 2007). Nolan and Flanagan, (2020) estimated the future changes of Irish climate for different path of future greenhouse gases emission emissions. They focused on the RCP4.5 and the RCP8.5. The RCP4.5 scenario consider a significant limitation of greenhouse gases emission leading to a radiative forcing stabilized at 4.5W/m^2 in 2100, or a CO_2-equivalent concentration of greenhouse gases of 650ppm. The RCP8.5 consider that emission of greenhouse gases keep increasing, leading to a radiative forcing above 8.5 W/m^2 in 2100, or a concentration of 1370 ppm CO_2 equivalent (IPCC, 2007). Under the RCP4.5 and RC8.5 scenarios, average temperatures in western Ireland where Kinvarra bay is located are expected to increase between 1 and 1.7 degrees for the 2041-2060 period compared to the 1980-2003 period (Nolan and Flanagan, 2020). The largest temperature increase is expected for the autumn period, leading to an increased length of the growth period of crops (Nolan and Flanagan, 2020). The expected increase of temperature due to climate change for this part of Ireland was assessed using the maps of the future climate of Ireland from a detailed climate modelling study (Nolan and Flanagan, 2020). As no similar long term record of groundwater temperature in karst could be found in Ireland during review, the potential increase of groundwater temperature was taken from long term measurements in another European karstic site at similar latitude (Jeannin et al., 2016).

Two model runs were made and compared: one at present temperature derived from EPA transitional water quality dataset (EPA, 2018a) and one at future temperatures for the 2040-2060 period (increase between 1 and 1.7 degrees of seawater temperature), and the modelled chlorophyll-a values were compared.

6.4.6.3 Changes of patterns of SGD discharge

In the part of Ireland where Kinvarra Bay is located, the number of days with precipitation above 40 mm per day is expected to increase by 10-40%, while the number of extended dry periods (precipitation below 1 mm) will increase by 10-40% (Nolan and Flanagan, 2020). Moreover, summer precipitation is expected to decrease by 0-12% in this region of Ireland (Nolan and Flanagan, 2020). These changes are likely to lead to a larger annual and interannual variability of fresh SGD rates, and frequency of flooding, particularly in aquifers responding quickly to rainfall events such as karsts.

As an attempt to estimate the potential effect of these increasingly frequent flood and drought periods for SGD sites, we first run the lower trophic model for the 2005-2019 period. We then examined whether current drought or flood period were followed by specific patterns of modelled Chl-a levels and of observed annual mussel production (BIM, 2018a). Finally the observed trends were related to the results of Nolan and Flanagan (2020) to discuss the potential impact of changes of rainfall frequency due to climate change on the biogeochemistry of Kinvarra Bay and its aquaculture activities through changes of SGD patterns.

6.4.6.4 Change of SRP availability in the bay

The effect of a change of SRP availability on DIN levels and phytoplankton biomass was assessed by comparing the modelled Chl-a for SRP fixed at the minimum, median and maximum SRP values observed in the EPA dataset (EPA, 2018a).

Maximum, medium and minimum SRP concentrations used for these model runs were taken from the EPA transitional water quality dataset for Kinvarra Bay (EPA, 2018a) and our own data collection in Kinvarra Bay. Combined runs of the models were made with or without nitrogen inputs from SGD and at high and low SRP concentrations to assess (1) the impact of the range of SRP availability within the bay and (2) the effect of DIN inputs from SGD on ecosystem primary production.

6.4.6.5 Change of marine currents in Galway bay, modifying the return flow to the bay.

Marine currents in Galway Bay may be modified by climate change, or other influences, which would then modify during the rising tide the return of water that left the bay during the previous ebb tide, thus the flushing time of water in Kinvarra bay. This influence of returning water on the flushing time of a bay is typically accounted for by introducing a return flow factor to the flushing time equations (Sanford et al., 1992). We thus tested the effect of changes of marine currents in Galway bay by assessing the sensibility of model outputs to the value of the return flow factor, taking a value between 0.7-0.94 (range previously estimated for Kinvarra Bay by Rocha et al., 2015 ±2σ).

6.4.6.6 Change of phytoplankton communities

Phytoplankton communities can vary as a result of a change of limiting nutrient (Fischer et al., 2017) or climate (Guinder and Molinero, 2013; Murphy et al., 2020). Carbon : nutrient ratios in phytoplankton communities are likely to increase as a result of the increased CO_2 in the atmosphere and the increased thermal stratification of surface waters (Guinder and Molinero, 2013). We tested the effect of changing C:N:P nutrient ratios of phytoplankton in the model from their lower end to upper end values given in Garcia et al. (2018). We also tested the impact of a change of phytoplankton grazing on model Chl-a and DIN outputs. Finally, we estimated the effect of the presence of phytoplankton communities with

different half saturation levels for dissolved inorganic phosphorus (K_{dip}) as follows. First, a range of potential values for the N saturation parameter (K_n) were taken from Cranford et al. (2007). Then, these values were converted in a range for the P half saturation parameter using the range of N:P ratios for phytoplankton in estuaries from Garcia et al. (2018) (see Appendix 2 for values).

6.5 Results

6.5.1 The seasonal variability of nutrient inputs and its effect on nutrient levels in Kinvarra

6.5.1.1 Variability of nutrient levels in Kinvarra springs and Kinvarra Borehole

During the period recorded the range of variability of DIN and Si in the borehole and the spring appears similar between different years (Figure 36a, c). For TP, it is not possible to determine whether there is or not a pluriannual trend of concentration in the aquifer or the spring, as only five years of data are available, and the concentrations are too variable within each year (Figure 36b). For DIN, most concentrations measured are between 0.5 and 2mg L^{-1} (Figure 36a). Values at 2 mg L^{-1} or above occur in Kinvarra spring mainly during periods when groundwater level is rising or is above 4.8m (Figure 36a, Figure 37a). This translates in the more frequent occurrence of larger peak DIN concentrations during these periods of high groundwater level (Figure 37a). The averages DIN concentrations in Kinvarra spring are larger at groundwater level above 4.8m (1.94±0.98 mg N L^{-1}) than at groundwater level below 4.8m (1.2 ±0.64 mg N L^{-1}), with a statistically significant difference between the two periods ($t(20) = 2.3$, $p= 0.03$). Borehole DIN concentrations are also likely to be higher during periods of high groundwater level ($t(32) = 2.09$, $p= 0.04$), with averages going from 0.85±0.37 mg N L^{-1} to 1.14±0.46 mg N L^{-1} at groundwater level above 4.8m (Figure 37a). Similarly, average DRSi concentrations in the borehole are more likely to be significantly larger ($t(14.5) = 2.4$, $p= 0.03$) with groundwater level above 4.8m (3.9±1.1 mg Si L^{-1}) than at groundwater level below 4.8m (3.1±0.5 mg Si L^{-1}). Conversely, spring DRSi concentrations are significantly larger (t(9.64)

= 2.98, p =0.01) for groundwater level between 3.5-5.5 m (4.0±0.5 mg Si L^{-1}) than in other conditions (3.2±0.5 mg Si L^{-1}, Figure 37 b).

Secondly, at groundwater level below 3.5m, the Kinvarra Springs are more likely to contain higher total phosphorus levels (p=0.04) (Figure 37 b, c). Averages concentrations at groundwater level below 3.5 m reach 30±10 µg P L^{-1} for TP while they are 10±10 µg P L^{-1} at groundwater above 3.5 m. Moreover, DRSi levels in the spring are also more frequently low when groundwater levels are below 3.5m (2.9±0.3 mg Si L^{-1}) than in other situations (4.0±1.0 mg Si L^{-1}) , with a significant difference between the two averages (t(15) = 3.5, p =0.003 Figure 37 c). These observations suggest that groundwater table height plays a significant role in the nutrient composition of spring waters flowing into the bay.

Generally, DIN and Total Phosphorus (TP) concentrations are more variable in the spring than in the borehole (95 confidence interval of the ratio of the variance between the borehole and the spring DIN concentration: 6.1±3.9 mg N L^{-1}; p value for the F test: p= 2 10^{-5}, Figure 37a, b). SRP fluctuate vastly between 5 and 35 µg P L^{-1}, with larger fluctuations in Kinvarra spring than in Kinvarra Borehole. Kinvarra springs DIN concentrations are either within a similar range to the borehole DIN concentration or up to 3 times larger (Figure 36a). TP concentrations in the spring, are frequently larger than the borehole TP concentration (Figure 36 b), in particular, when groundwater level is below 3.5m. During such periods, peak values in the spring can be more than the double of the borehole typical concentrations (Figure 36b, Figure 37 b).

Conversely, DRSi remains similar between the borehole and the spring (3.52±0.96 mg Si L^{-1} vs 3.51±0.62 mg Si L^{-1}), with concentrations either slightly higher or lower in Kinvarra Borehole than in Kinvarra Springs (Figure 36c, Figure 37 c). DRSi is more stable than DIN with time, with most values at 2.5-5 mg Si L^{-1} (Figure 36c).

As both Kinvarra springs and Kinvarra Borehole are connected to the same karst network, the difference between them for DIN and TP suggests that variable DIN and TP sources are present in the catchment between the borehole and the spring. These sources would provide dissolved phosphorus and nitrogen, but few Si as boreholes and spring DRSi are frequently similar.

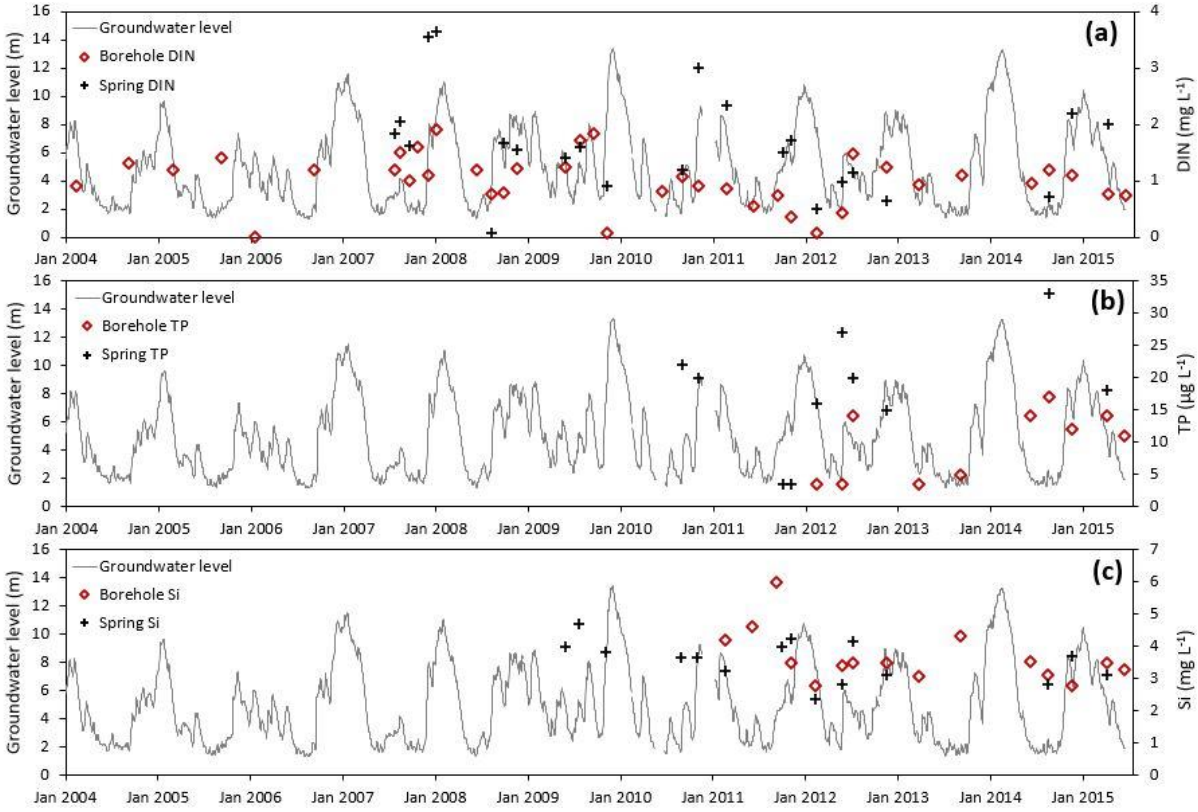

Figure 36: Dissolved Inorganic Nitrogen (a), Total Phosphorus (b) and Dissolved Reactive Silica concentration (c) in Kinvarra borehole (2004-2015) and Kinvarra springs (2007-2015) taken from the EPA groundwater quality dataset (EPA, 2015); compared to the groundwater level variability measured in Killiny Borehole (EPA, 2020). DIN is mainly NO_3 in both spring and borehole.

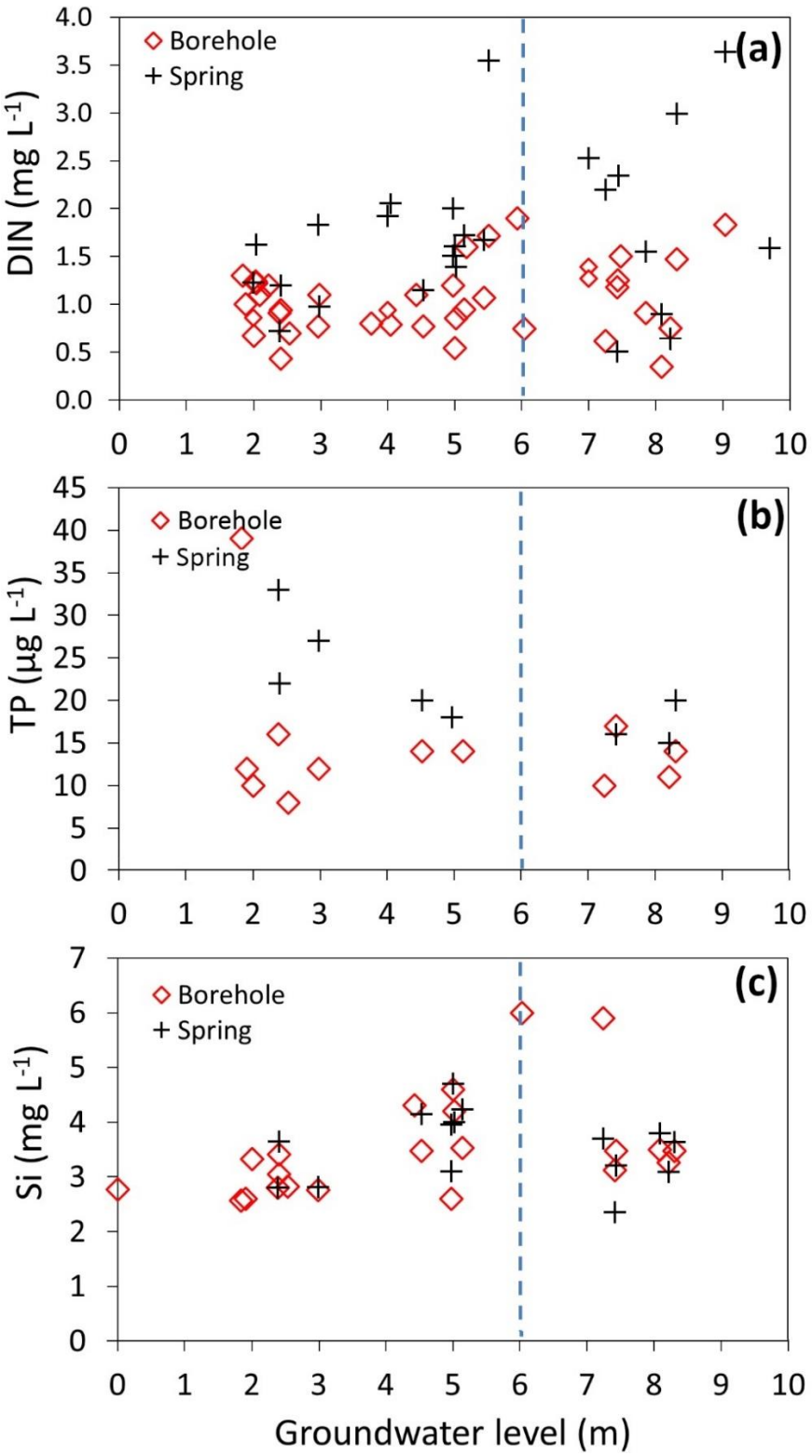

Figure 37: Dissolved Inorganic Nitrogen (a), Total Phosphorus (b) and Dissolved Reactive Silica concentration (c) in Kinvarra borehole (2004-2015) and Kinvarra springs (2007-2015) as a function of groundwater level during the day sampled, taken from the EPA groundwater quality dataset (EPA, 2015). The rectangles highlight the apparent changes of the range of concentrations with groundwater level measured at Killiny Borehole EPA, (2020). DIN is mainly NO_3 in both spring and borehole.

6.5.1.2 Variability of nutrient levels in Kinvarra bay

The slopes between DIN and salinity (Figure 38a) and between DRSi concentrations and salinity (Figure 38b) in Kinvarra Bay are higher when groundwater levels were high (DIN/Salinity slope: -0.023±0.001, DRSI/Salinity slope: -48.5±2.7, $p< 10^{-6}$ for groundwater above 6m) than when groundwater levels are low (DIN/Salinity slope: -0.013±0.0005, DRSI/Salinity slope: -37.7±1.2, $p< 10^{-6}$ at groundwater below 6m, measured at Killiny borehole). Both the difference in slope and intersect with groundwater level are highly significant (for the intersect Z score = -14.2, p value = 10^{-46} , for the slope Z score = 7.21, , p value = 10^{-13}, with number of observations much greater than 30 -above 260 for each series- and most data following normality).

A non-linear trend with salinity is generally expected for non-conservative elements within an estuary (Officer, 1979). Here, however, we see significant linear trends between DIN and salinity (r^2= 0.58, $p<2\ 10^{-16}$) and between DRSi and salinity in Kinvarra Bay (r^2 = 0.5, $p<2\ 10^{-16}$) (Figure 38). The presence of linear trends suggests that the DIN and DRSi inputs from fresh SGD are so large compared to the amount consumed by net primary production that the effect of net primary production on DIN levels in the bay often remain small compared to mixing. Alternatively, the net effect of primary production could be too variable from a year to another to show as a constant nonlinear trend.

As primary production typically consumes DIN and DRSi at different rates, a significant effect of primary production on DIN or DRSi levels should lead to changes of DIN/Si ratio. For salinity below 25, the DIN/DRSi ratio in the bay is stable, with an average of 1.7±3.1 (Figure 38c) and does not become larger than the ratios in the spring and the borehole, between 0.5 and 4.2. Conversely, at salinity above 25, some DIN/DRSi ratios in the water column are larger than DIN/DRSi ratios in the freshwater end-member (Figure 38c). These larger DIN/DRSi suggest a preferential DIN loss over Si in the water column at high salinities at least part of the time. This preferential loss of DIN over Si may be due to the seasonal variability of sediment-water fluxes, or changes of exchange with the open ocean. However, most of the DIN:DRSI ratio in the water column are within the range of borehole and spring DIN:DRSI ratio. Consumption of nutrients by primary production or other sinks within the system are thus not likely to explain a large fraction of the change

of the slope between DIN and salinity seen between high and low groundwater level (Figure 38). The variability of nutrient inputs from SGD seems to thus dominate the variability of the concentrations of DIN and DRSi in Kinvarra bay, with a potential minor effect of nutrient loss in the system, particularly at high salinities and during warm, low groundwater level periods.

SRP, on the other hand, has no relationship with salinity (Figure 39), suggesting that fresh SGD fluxes are not leading to a significant increase of P availability in the bay compared to Galway Bay values. Other processes than fresh SGD inputs are thus likely to dominate the P availability (e.g. sorption, desorption from sediment within the bay), and SRP is rapidly cycled along the path from Kinvarra spring to Galway Bay. SRP values are more frequently large when groundwater level is high, with average values at 15.9±6.7 at groundwater level above 6m compared to 7.1±6.0 at low groundwater level below 6m. This trend is statistically significant ($t(470) = 18.16$, $p < 10^{-16}$) and is potentially a result of a lower SRP loss within the bay during these periods, or larger SRP fluxes within the bay, for example due to larger inputs from sediment (Figure 39). Such larger inputs from sediment may occur through increased sediment load from surface sources, or more frequent release from bottom sediment during these periods (e.g. due to sediment resuspension events or increased bioturbation amplifying solute exchanges with sediments). Despite the change of total phosphorus concentration in Kinvarra Springs with groundwater level, no significant changes of the range of SRP values are observed in Kinvarra Bay (Figure 39).

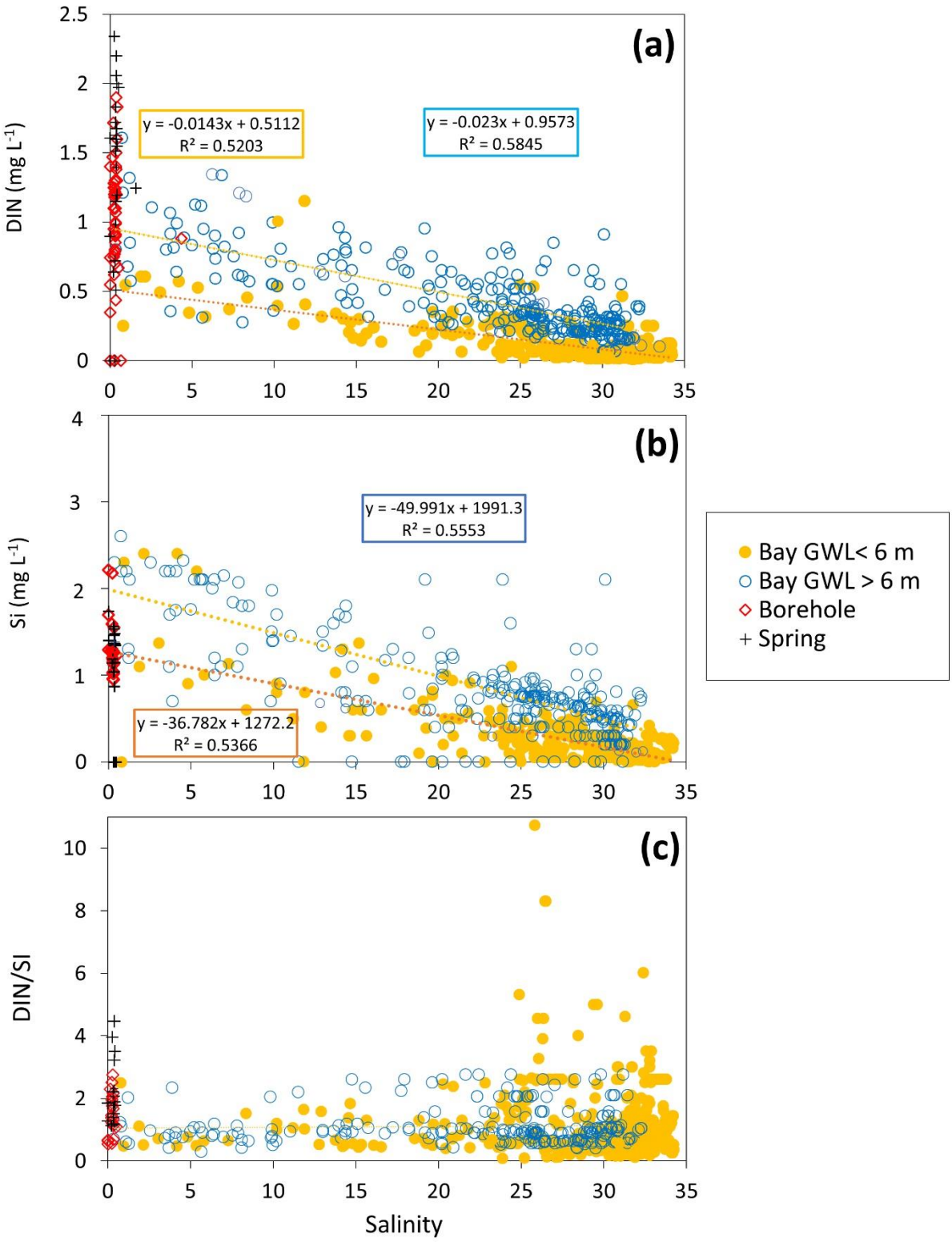

Figure 38: Effect of groundwater level on the relationship between nutrient and salinity for the water columns of Kinvarra Bay. Values for Kinvarra bay are taken from the EPA transitional water quality dataset (EPA, 2018a), classified according to the groundwater level in Killiny Borehole, EPA, (2020). Borehole and spring values are taken from the values at Kinvarra Borehole and Kinvarra springs (locations on Figure 34) from the groundwater quality dataset (EPA, 2015).

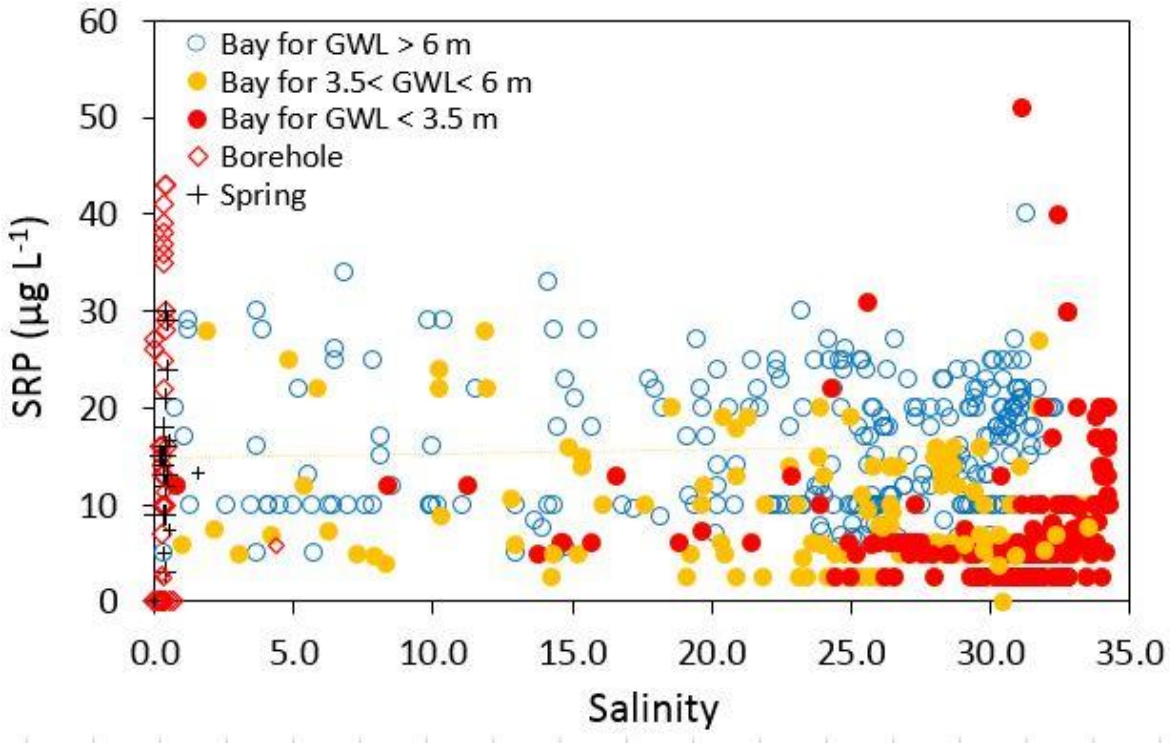

Figure 39: Comparison between bay concentrations of Soluble Reactive Phosphorus (SRP) in Kinvarra Bay (EPA, 2018a) and freshwater end member concentrations (borehole, spring) as a function of salinity (EPA, 2015). Bay values are classified according to the groundwater level in Killiny Borehole, EPA, (2020). Borehole and spring values are taken from the values at Kinvarra Borehole and Kinvarra springs (locations on Figure 34) from the groundwater quality dataset (EPA, 2015). The limit of detection in the EPA dataset was variable with time between 12, 10 and 5 µg.l^{-1}, with most LOD reported 10 and 5 µg.l^{-1}, which explains the aberrant horizontal lines at and below 10 µg l^{-1}. Values below 12 µg.L^{-1} are shown to give a sense of the relative frequency of low SRP values but should not be interpreted in term of trend against salinity.

6.5.2 Effects of SGD on nutrient balance and phytoplankton biomass

Summer chlorophyll-a in Kinvarra Bay can be up to ten times higher than the maximum values observed in the nearby Galway Bay (Figure 40). As we showed in section 6.5.1, SGD brings to the system nutrients with variable rates and concentration depending on the time of the year.

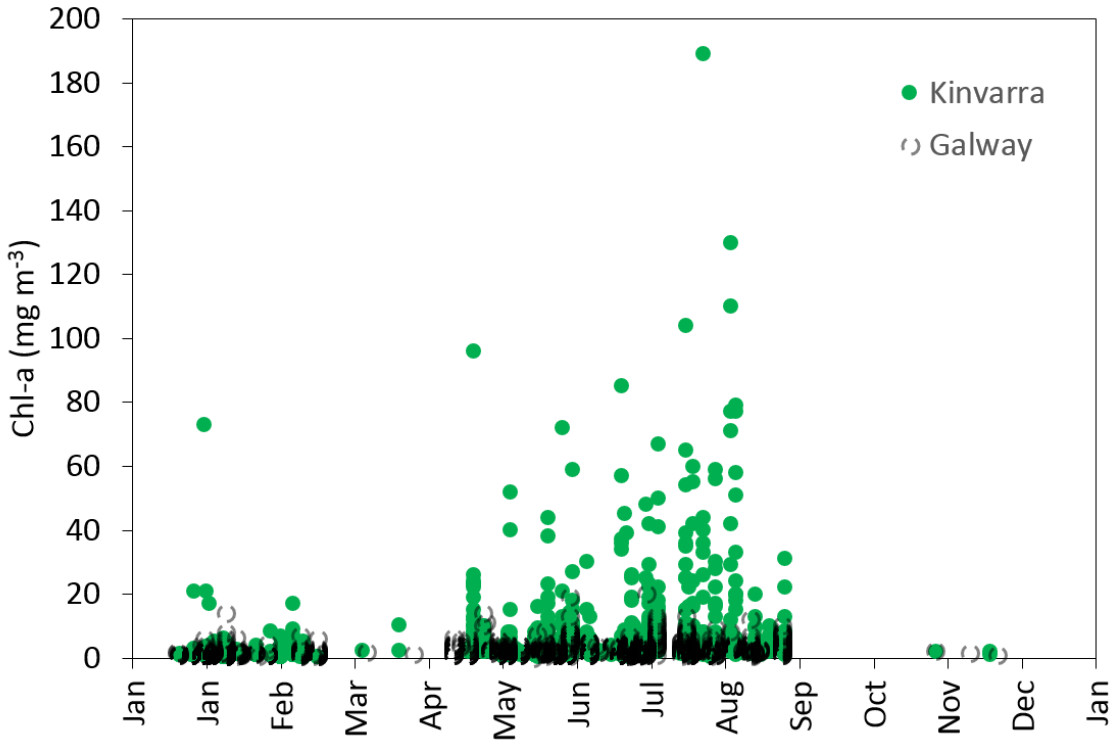

Figure 40: Range of chlorophyll-a values in Kinvarra and Inner Galway Bay classified by day number between 2007 and 2018 (All values, ICES, 2019).

Sea surface temperature (SST) and chlorophyll-a (Chl-a) are often linked (Behrenfeld et al., 2001, 2006; Chavez, Messié and Pennington, 2011; Behrenfeld, 2014). Here, the peaks of chlorophyll-a are observed more frequently when the water temperature in Galway Bay is the highest (Figure 41). However, during warm periods with high light irradiation values, low chlorophyll-a values similar to the ones typical of cold periods with low irradiation values can also be observed (Figure 41). While high Chl-a is more likely during summer (June-August) than during winter (December-February), the measured Chl-a can be as different between two summer days as the difference between an average summer day and an average winter day (Figure 41). Moreover, the periods of maximum chlorophyll-a are not coinciding with periods of maximum temperature, when growth rate should be expected to be the highest. These non-coinciding trends suggest that drivers

other than temperature and light changes are also explaining the variability of Chl-a levels for a given season.

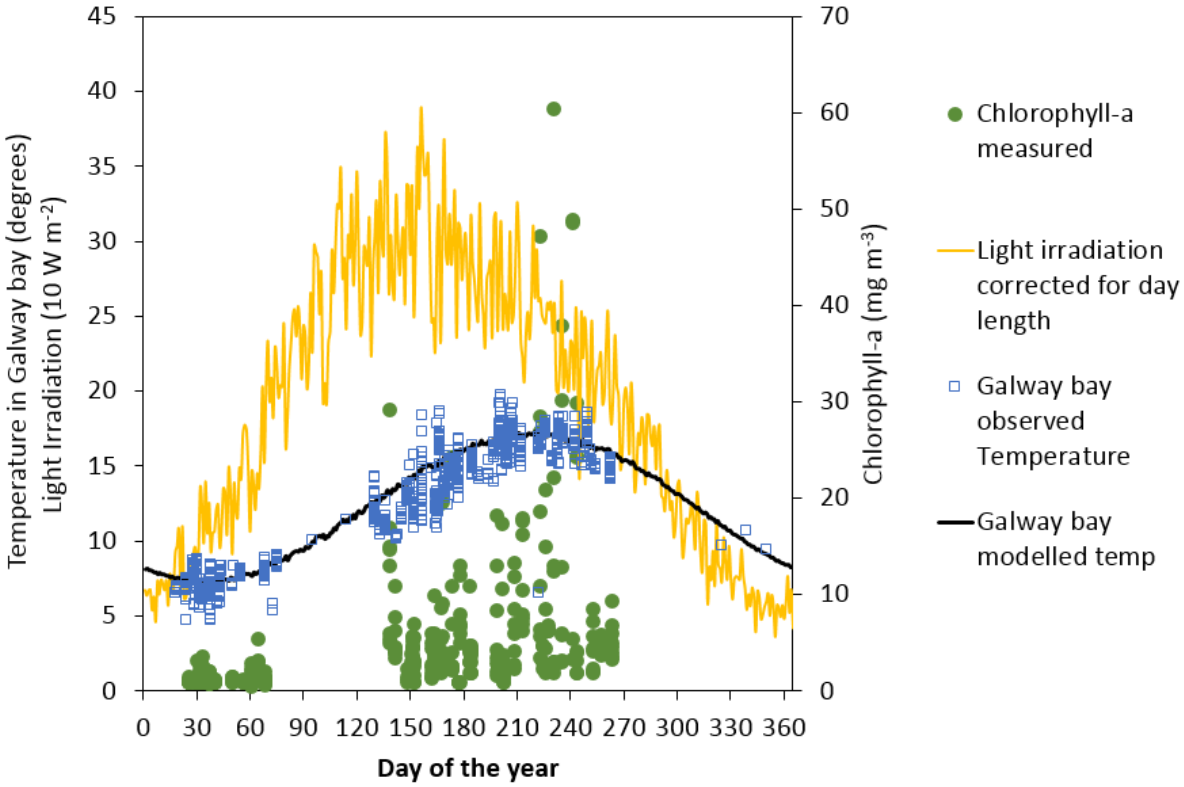

Figure 41: Changes of daily averaged Chl-a values in Kinvarra Bay between 2007 and 2018, averaged by day number and surveys (EPA, 2018a), related to the variability of daily averaged water temperature in Galway bay (ICES, 2019) and light availability (Met Eireann, 2020). Temperatures shown are the CTD values observed in Galway Bay between 2007 and 2018 in the ICES database.

The closure of nutrient mass balances for four spring tide surveys under different groundwater levels and water temperatures showed that regardless of the groundwater level, a net retention of Nitrogen is occurring in the bay (Net DIN is negative in Table 10). This net retention of DIN tended to be larger with increasing groundwater level and at a lower temperature. Two potential paths are possible to explain this net loss: storage of nitrogen in the benthos or consumption by the biological activity in the bay water column, as shown previously by Rocha et al., (2015).

A net loss of SRP was only present under low groundwater level and high-temperature conditions. A gain of SRP occurred under high groundwater level and low-temperature conditions (Table 10). Net primary production (p-r) was negative during high groundwater level and low-temperature conditions and positive during low groundwater level and

high-temperature conditions (Table 10). Periods of high temperature and low groundwater level coincide with positive net primary production (primary production > respiration) and higher chlorophyll-a concentration in the bay (Figure 42). The bay is thus a sink of carbon and P during the productive months as the net phytoplankton growth is consuming CO_2 and P through photosynthesis. On the other hand, periods of lower temperature and high groundwater level (>6m) coincide with periods of negative net primary production (primary production < respiration) and lower chlorophyll-a levels (Figure 42). This suggests that the bay is a source of CO_2 and P during the winter period when organic matter provided by SGD and freshwater sources or by sediments are consumed by respiration in the bay. Kinvarra Bay is thus likely to alternate between being a source of CO_2 during high SGD periods and a sink of CO_2 during low fresh SGD periods. The fact that net primary production is negative for the periods when the net DIN balance is the most negative (Table 10) suggests that N consumption by primary production is not the only mechanism explaining this net DIN loss, but a large part of the DIN is likely to be stored in sediment and the benthos, or denitrified.

Table 10: Results of the LOICZ mass balance. The balance of DIN and DON are derived from a LOICZ mass balance of DON and DIN (Gordon et al., 1996). P-r is the primary production minus respiration per area of the bay estimated from the SRP balance. The SRP balance is converted to p-r using two sets of C:P ratios to assess the maximum and minimum p-r. Minimum p-r assumes that most primary production is carried out by phytoplankton (C:P = 106) (Redfield, 1958). Maximum p-r assumes that most of the primary production is done by seagrasses or marine macroalgae (C:P=550) (Atkinson and Smith, 1970). Groundwater levels are the averages in the 10 days leading to each surveys in Kinvarra bay, measured at Killiny Borehole, and taken from EPA, (2020).

Survey	Groundwater level	Average bay temperature	Average bay salinity	DIN balance	DON balance	SRP balance	Equivalent (p-r) mmol C m^{-2} d^{-1}	
	m	°C		mmol N m^{-2} d^{-1}	mmol N m^{-2} d^{-1}	µmol P m^{-2} d^{-1}	Minimum	Maximum
201807	2.17	19.4	34	-0.86	-	47	5	26
201810	4.1	14.4	30	-5.36	-	5	0.5	3
201901	7.25	10.7	16	-27	-36	-85	-9.0	-47
201904	9.75	11.4	16	-23	-1	-15	-1.6	-8

While water temperature and groundwater level are negatively linearly correlated (Pearson correlation= -0.82, $p<0.001$, n= 919), peak Chl-a occur at minimum groundwater level, but not at maximum temperature as would be expected (Figure 42). There is a significant non-linear monotonic negative relationship (Figure 42), between groundwater level and Chl-a (Rho = -0.45) and a positive relationship between temperature and Chl-a (Rho = 0.41). The unsigned correlation between Chl-a and groundwater level is larger than the unsigned correlation between Chl-a and temperature. However, we cannot be 95% confident that the difference between the two correlated Spearman correlations coefficients (Rho) is not due to random variation in sampling ($t(1213,1134)= -1.01$, $p=0.16$). Thus both graphical observation and a weak statistical evidence suggest that the groundwater level (an indicator of the likelihood of large fresh SGD fluxes to Kinvarra bay, see Chapter 3) may be a more appropriate predictor of chlorophyll-a levels than temperature in Kinvarra Bay (Figure 42). Bay averaged maximum chlorophyll-a levels decrease quickly when groundwater levels increase from 2m to 6 m, while the change is less clear when considering decreasing temperature (Figure 42). Moreover, all bay averaged chlorophyll-a levels above 60mg l^{-1} between 2007 and 2018 were recorded during periods of lowest groundwater level (<4m, Figure 42).

The net ecosystem production obtained with the LOICZ model seems also to be significantly different with changing groundwater level (Figure 42), which implies that the trophic status of this SGD dominated system is affected by the changing water chemistry not only due to seasonal variability but also linked to the magnitude of the SGD discharge coming to this bay. The next section will investigate further the drivers of the variability of Chl-a and DIN levels in Kinvarra Bay using the lower trophic model.

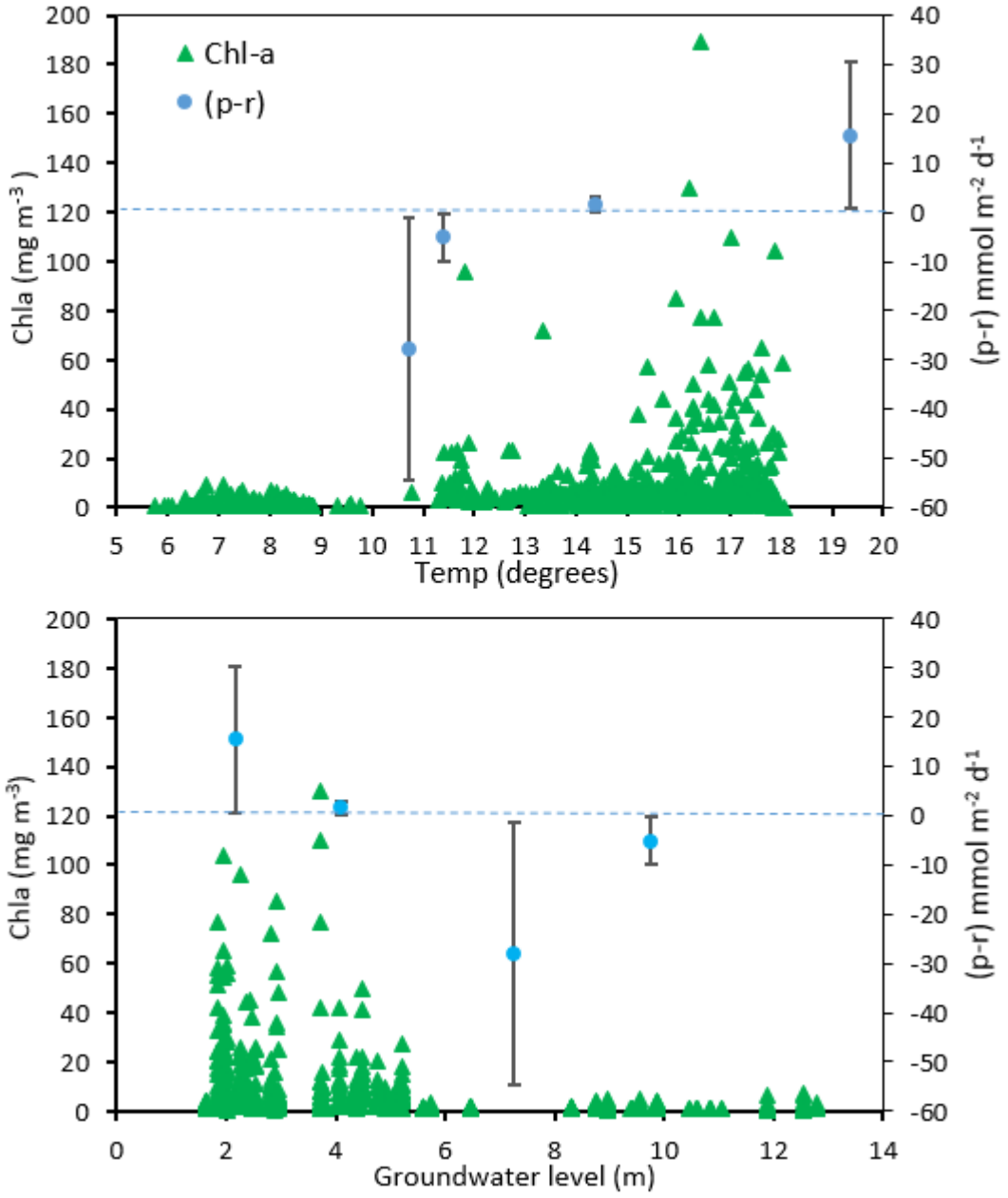

Figure 42: Net ecosystem production (p-r) in Kinvarra determined from the LOICZ approach from the nutrient data collected in this study, and chlorophyll-a level observed by the EPA between 2007 and 2018 (EPA, 2018a) as a function of water temperature (EPA, 2018a) and groundwater level on the day of sampling, measured at Killiny Borehole (EPA, 2020).

6.5.3 Lower trophic model sensitivity analysis and validation

6.5.3.1 Sensitivity analysis and lessons learnt on Kinvarra Bay

The sensitivity analysis of the lower trophic model (Appendix 1 to 5) identified three parameters with the highest impact on the modelled phytoplankton biomass and DIN levels in the bay: the return flow factor as a driver of exchange between Kinvarra Bay and Galway Bay, b (ΔDIN=21, ΔChl=12, ΔNmussel=0.1; Appendix 2); the dissolved phosphorus levels in the bay as a limiting nutrient for phytoplankton growth (ΔDIN=-5.8, ΔChl=17, ΔNmussel=0.09; Appendix 2); and the loss of phytoplankton by grazing of other organisms than mussels, λ_p (ΔDIN=5.3, ΔChl=-54, ΔNmussel=-0.07; Appendix 2), as a limiting factor for phytoplankton growth in the system.

The lower trophic model illustrated the strong effect of new/spring tidal cycles on the variability in Kinvarra Bay. The modification of the K exchange factor in the lower trophic model to account for neap/spring tidal cycles (section 6.4.4) led to a fluctuation of modelled DIN, phytoplankton biomass, salinity and residence time with a 15 days period (Figure 43).

Concentrations of elements provided by SGD, such as DIN, increased during neap tides and had their largest modelled values at the end of neap tide periods and decreased during spring tides (Figure 43). Chlorophyll-a concentrations, increased during neap tide periods and decreased during spring tides (Figure 43).

Spring tides, on the other hand, showed a decrease of DIN and Chl-a, and the lowest modelled DIN and Chl-a frequently occurred at the end of periods of spring tides, except when SGD fluxes were strongly increasing during the spring tide periods (e.g. second spring tide period highlighted in Figure 43).

These fluctuations are also visible in other modelled parameters e.g. peaks of water residence times and decrease of modelled salinity were also present during neap tides. Modelled water temperature in comparison was not affected significantly by spring/neap cycles and was mainly seasonal (Figure 45 a). This is mainly because groundwater temperatures (3-18 degrees) are of similar range to sea water temperature in Galway Bay (5-18 degrees).

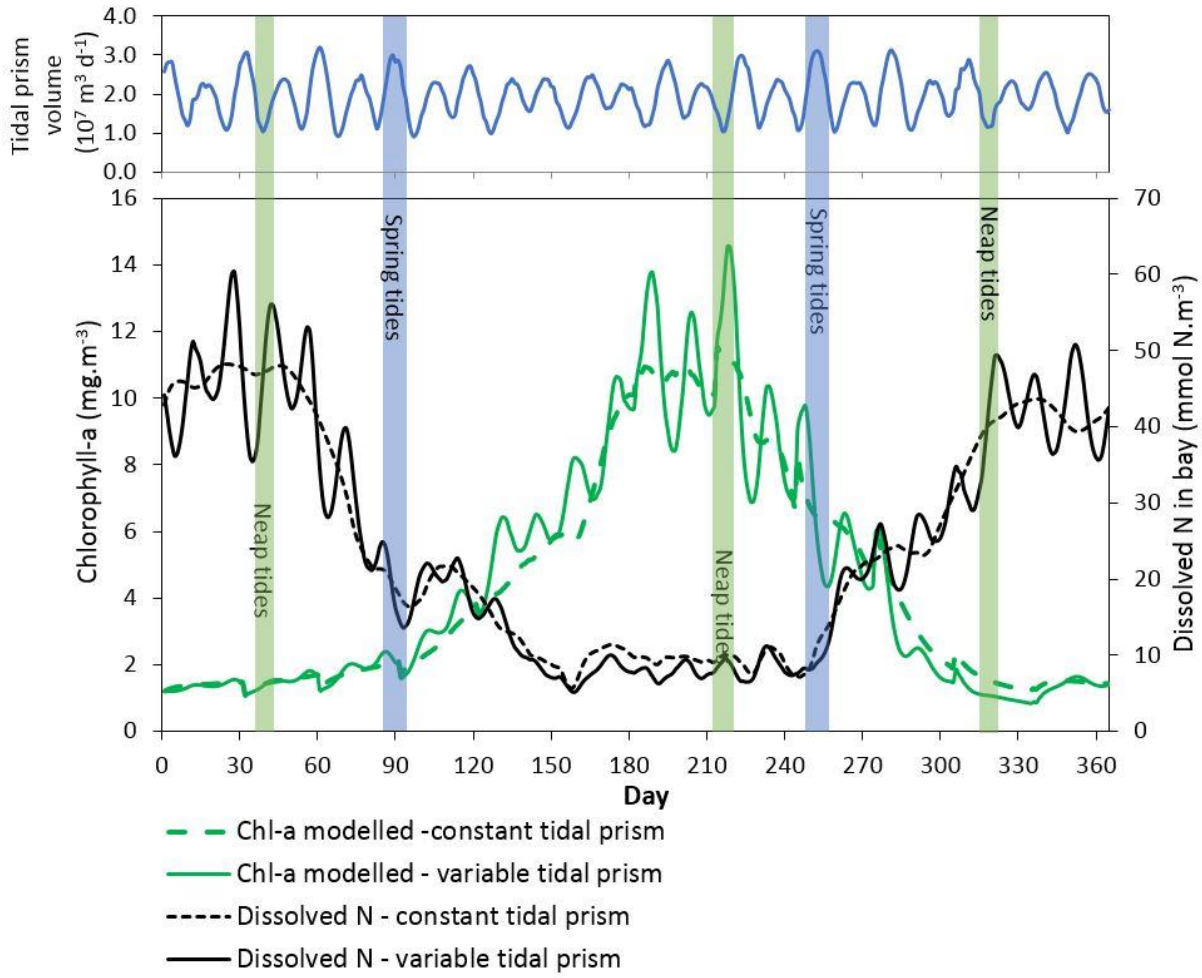

Figure 43: Effect of considering a variable tidal prism during neap/spring tidal cycles on model outputs from the lower trophic model of Cranford et al. (2007). The modelled outputs with constant tidal prism use the yearly mean tidal fluctuations to assess the tidal prism value used in the K calculations. Modelled outputs with variable tidal prism value use the tidal range on each day of an average year to calculate the value of the tidal prism for each day, to assess the effect of neap/spring tidal cycles on the modelled outputs. The dashed lines show the DIN and Chl-a outputs for a constant tidal prism value (no neap or spring tides considered). Plain lines show the DIN and Chl-a outputs for a variable tidal prism value (neap or spring tides are present). The daily changes of the tidal prism volume as a result of neap/spring tidal cycles for Kinvarra bay are shown in the upper chart.

A second trend in Kinvarra Bay illustrated by the lower trophic model is the weak influence of the yearly variability of aquaculture standing stock on the bay dissolved nitrogen and chlorophyll balance. Increasing mussel standing crop in Kinvarra Bay from its minimum to maximum estimated value between 2005 and 2018 (BIM, 2018a) led to a decrease of modelled DIN by between 0.3 to 3.5 mmol N m^{-3} and Chl-a levels in the bay by between 0.2 to 5 mg m^{-3}. The effect of mussel standing crop on Chl-a levels increased during the growth season, and was the largest during the autumn, when phytoplankton growth decreased as a result of light availability, and mussel feeding is more likely to outrun phytoplankton growth (Figure 44).

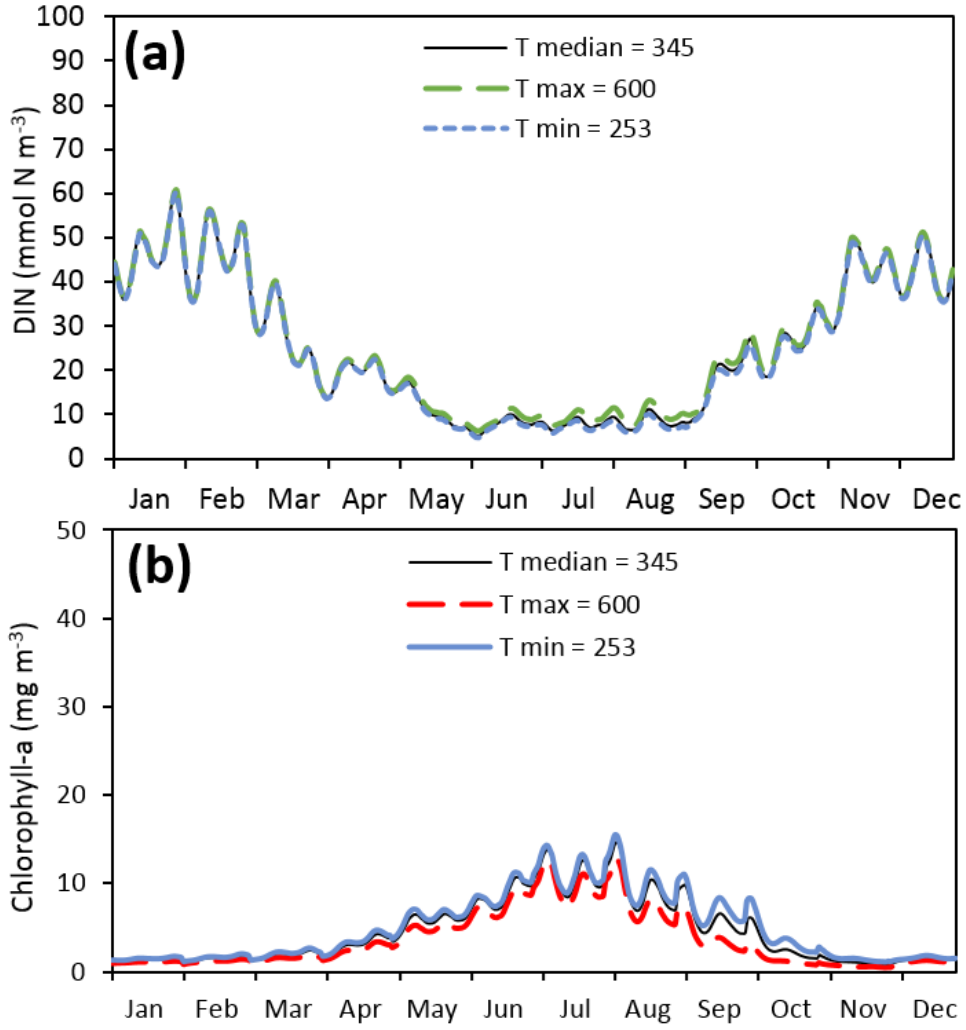

Figure 44: Effect of mussel standing crop (T) on model output, values are in metric tonnes, equal to the median, minimum and maximum production in the bay multiplied by 2.3 (BIM, 2018a).

As will be shown in the next sections, the effect of modifications of mussel standing crop on modelled Chl-a and DIN is however small compared to the effect of other parameters such as the return flow factor (Figure 50), the grazing rate (Figure 51), or parameters describing phytoplankton growth and nutrient contents (Figure 51 to Figure 54). As a result, mussel production can be fixed at its median value to further study the effect of other changes on the system.

6.5.3.2 Model validation

Modelled temperatures follow the observed values in the bay with a model efficiency (ME) of 0.95 (Figure 45a). Similarly, modelled salinities expected for a range of return flow factor of $0.78<b<0.94$ ($b \pm 2\sigma$ from Rocha et al., 2015) include most of the observed values of salinities in Kinvarra Bay, with only two point above the curve during mid-summer (Figure 45b). If b is fixed a 0.89, the model efficiency is 0.4 for salinity (Figure 45b), and the modelled variability of residence time is close to the observed values estimated from $^{224}Ra/^{223}Ra$ profiles (difference less than one day in Figure 45c).

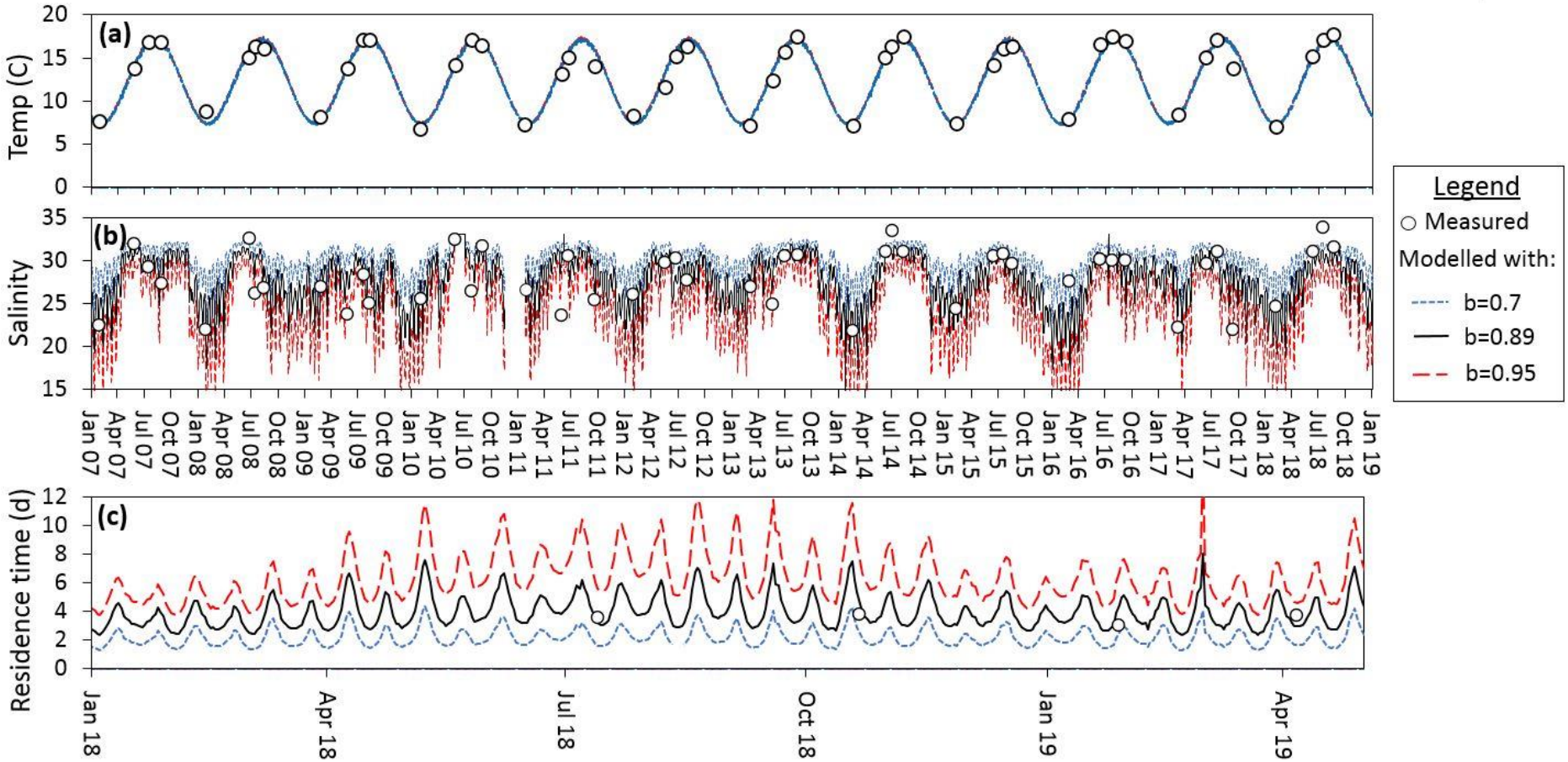

Figure 45: Validation of modelled flushing characteristics of Kinvarra Bay by comparing model outputs with observed values in the bay for: (a) temperature, (b) salinity and (c) residence time. In (c), the observed values are estimated from a Ra ages model during spring tides (See Chapter 3 for more detail). Modelled values in (c) are determined using changes of tidal range across the year as observed in the nearby Galway Bay, using the equation of Sanford et al. (1992), assuming a return flow factor of b=0.86±0.04 (from previous findings by Rocha et al., 2015) and considering the variations of the tidal prism across a typical year. In (a), (b) and (c), the three curves illustrate the effect of the uncertainty of return flow factor on the model results. In (a) and (b) observed values are calculated from the 3D integration of ten samples in average in surface and deep waters (Data from EPA, 2018b).

Similarly, modelled DIN and chlorophyll-a when DIP is fixed in the observed range of bay-integrated values in Kinvarra Bay (from below EPA detection limit, represented by the 0.02 run, to 0.8) correspond acceptably well with the observed variability between 2007 and 2018 in Kinvarra Bay (Figure 46a, b). The modelled DIN variability matches the observed seasonal trends in the bay. Some higher Chl-a values are observed during August and may be due to larger than averages import of Chl-a from Galway Bay or variable SRP inputs for example. If b is fixed to 0.89 and DIP to its minimum value (0.08), which is the most likely when high phytoplankton biomass are present, the model efficiency is 0.51 for DIN and 0.55 for Chl-a.

The model thus performs significantly better than the mean of the observed values, but there is room for improvements. One way to improve the efficiency of the model would be to account for variable P availability in the bay, based on additional data collection and characterisation of the drivers of variability of dissolved P in the bay. Indeed, most of the observed data is included within the range of potential values expected when SRP is between 0.02 and 0.8 (Figure 46).

Previous studies made in this area on the reproduction periods of mussels showed that the main reproduction periods of naturally occurring mussels in Galway Bay were in March/April and July/August, followed by settlements in June and August-September (King et al., 1989). The two modelled N assimilation peaks in June-July and September-October (Figure 46c) follow immediately the reported periods of mussel reproduction, and thus correspond to settlement periods in this part of Ireland. If we consider that mussels adapt their reproduction behaviour to ensure an exposure to optimum food availability, the modelled trends are thus corresponding to the observed variability in natural mussel population in this area. Without the measurements of actual growth rates of cultured mussels in Kinvarra Bay, however, the modelled changes of N assimilation can only be interpreted in terms of relative changes.

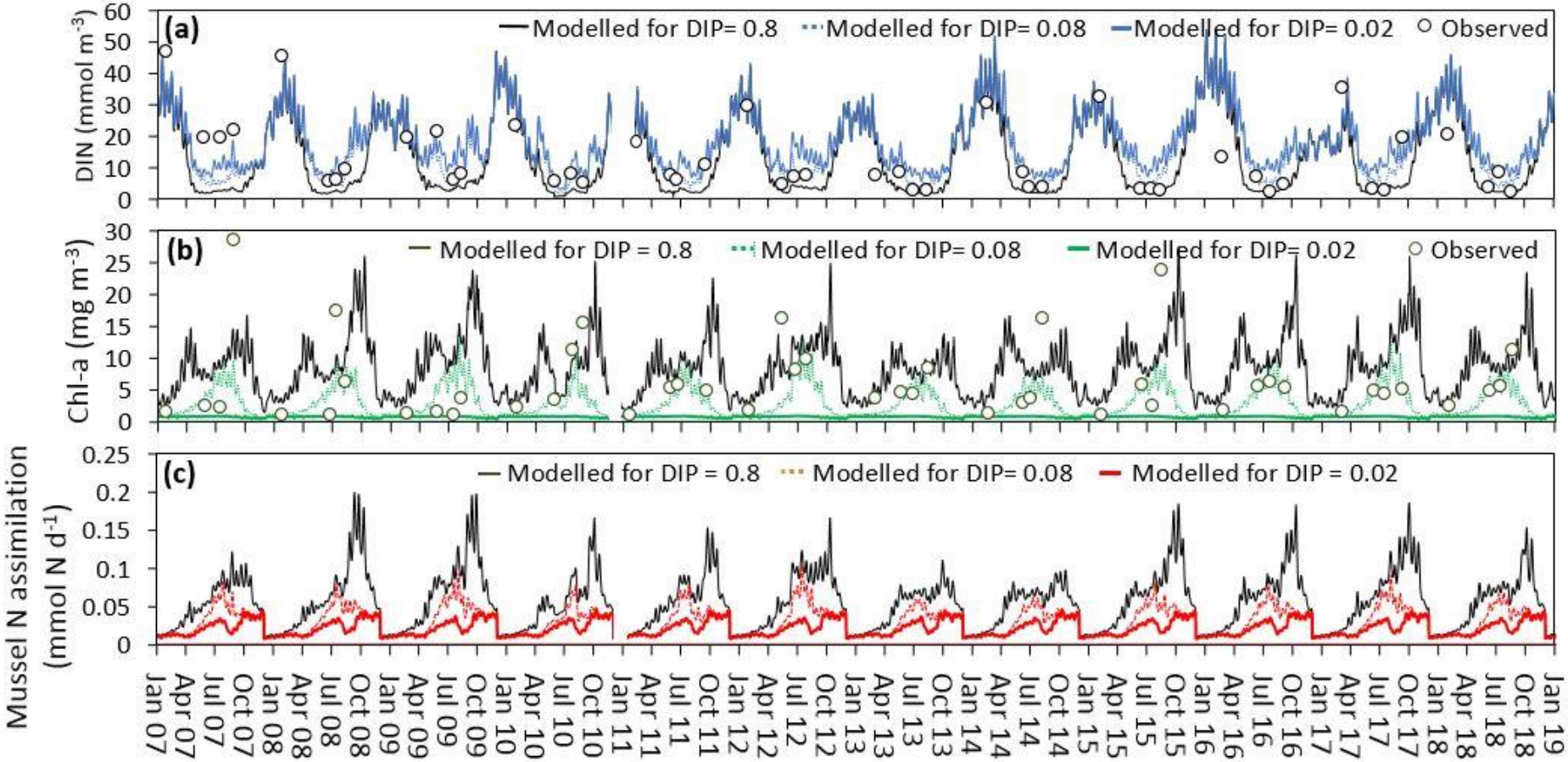

Figure 46: Comparison of model predictions for average DIN (a) and chlorophyll-a (b) with observed values in the bay. The effect of different concentrations of Dissolved Inorganic Phosphorus in the bay is shown by three different runs of the model, using different DIP in water as input (mmol m^{-3} or µmol L^{-1}). The range of value tested for DIP correspond to the maximum (0.8), and minimum DIP level (0.08) observed in the bay between 2007 and 2018 by the EPA (2018b), after integration of the values observed in transects following the procedure in Appendix 8. During summer, some of the SRP level observed by the EPA were below detection limit, and the bay minimum integrated averages may be overestimates. Consequently, we add a model run for very low SRP values (0.02), to illustrate the effect of very low P availability.

The modelled total N transfer to the benthos corresponds to the range cited previously for the bay ($3.7\pm2.6\times10^3$ mol d^{-1}, Rocha et al., 2015), if P is maintained at its low value (DIP= 0.08). On the other hand, the peak N consumption by phytoplankton, is larger than the DIN consumption ($1.15\pm0.94\times10^4$ mol d^{-1}, Figure 47). Rocha et al., (2015a) showed that a large part of the N requirement of phytoplankton growth is provided by a quick cycling of N in the bay via DON ($1.08 \pm0.87\times10^4$ mol d^{-1}, Rocha et al., 2015). The model of Cranford et al. (2007) does not differentiate DIN and DON but include the cycling of N via particulate organic matter. The sum of the DIN consumption by phytoplankton and DON loop correspond to the lower mid-range of the peak modelled DIN consumption here for the summer period when DIP is fixed at 0.08 (Figure 47).

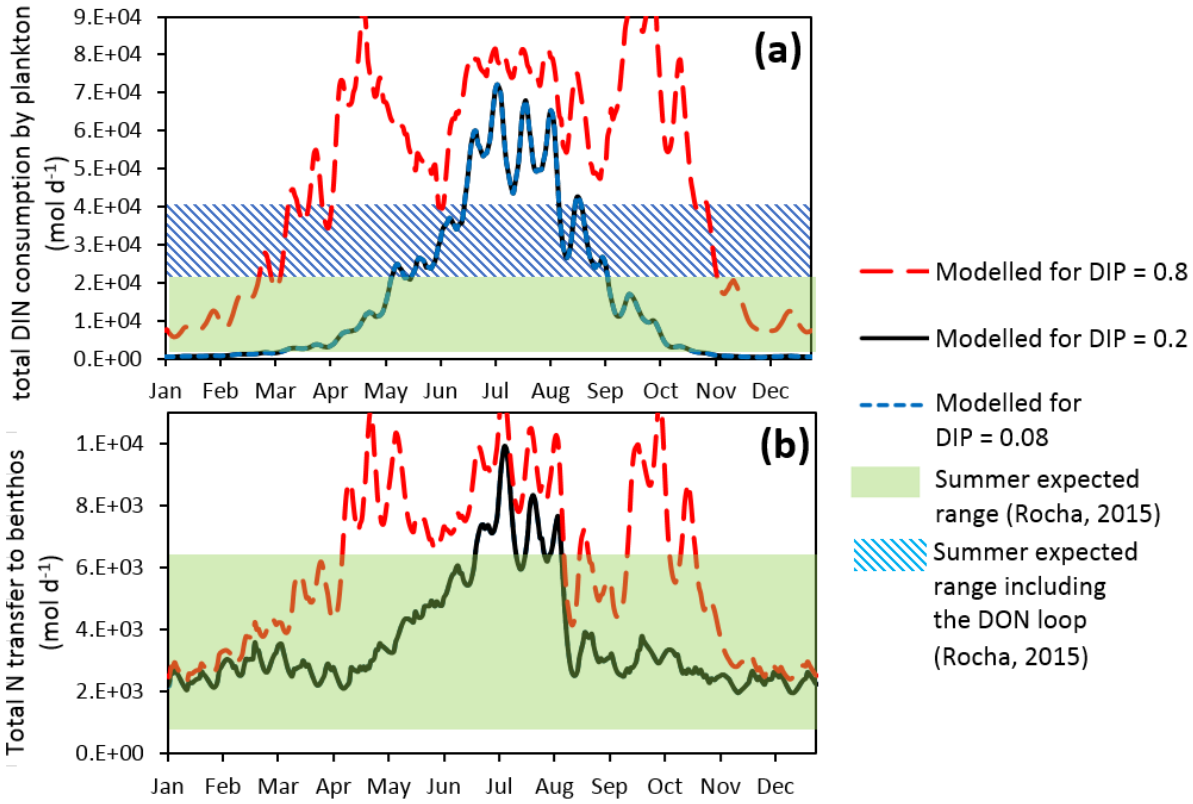

Figure 47: Comparison of key N reaction rates predicted by the model with previous estimates for summer from Rocha (2015). (a) for plankton total DIN consumption by phytoplankton (b) for total N transfer to the benthos. The area highlighted in green are the values from Rocha (2015). Dashed blue areas are the N consumption values by phytoplankton accounting for the cycling of DON in the bay (Rocha, 2015).

6.5.4 Scenario testing for the lower trophic model

6.5.4.1 Modelled effect of temperature changes on Chl-a levels

The average temperature in the part of western Ireland where Kinvarra Bay is located is expected to be larger by between 1 and 1.7 degrees for the 2041-2060 period compared to the 1980-2003 period under the scenarios of representative concentration pathway RCP4.5 and RCP8.5 (Nolan and Flanagan, 2020). The largest increase of temperature is expected for the autumn period, leading to an increased length of the growth period of crops (Nolan and Flanagan, 2020) and of the bloom period for phytoplankton (Marine Institute, 2009). Karst groundwater temperature may also increase, although less than air and sea water temperature. We considered a groundwater temperature at +0.2 degrees for the 2041-2060, assuming a similar rise of temperature that observed in another European karst system: + 0.003 degrees per year (Jeannin et al., 2016).

Changes of temperature of +1.7 degrees in sea water and +0.2 degrees for Karst groundwater temperature could increase modelled Chl-a levels by 0 to 40% on an average year if temperature was the only variable modified by the change of climate. Under this scenario, Chl-a levels during mid-winter were the least modified (+0.1mg m^{-3}), while modelled Chl-a level were larger in spring to autumn, particularly following neap tides (+2.4 to +3.5 mg m^{-3}, Figure 48). The largest increase was observed during neap tides in late summer-autumn (+3.5 mg m^{-3}, Figure 48). The extension of the growth period expected by Nolan and Flanagan, (2020) for land-based plants in Ireland may thus also affect phytoplankton growth in enclosed bays such as Kinvarra bay if other parameters of the system are not also affected by temperature changes.

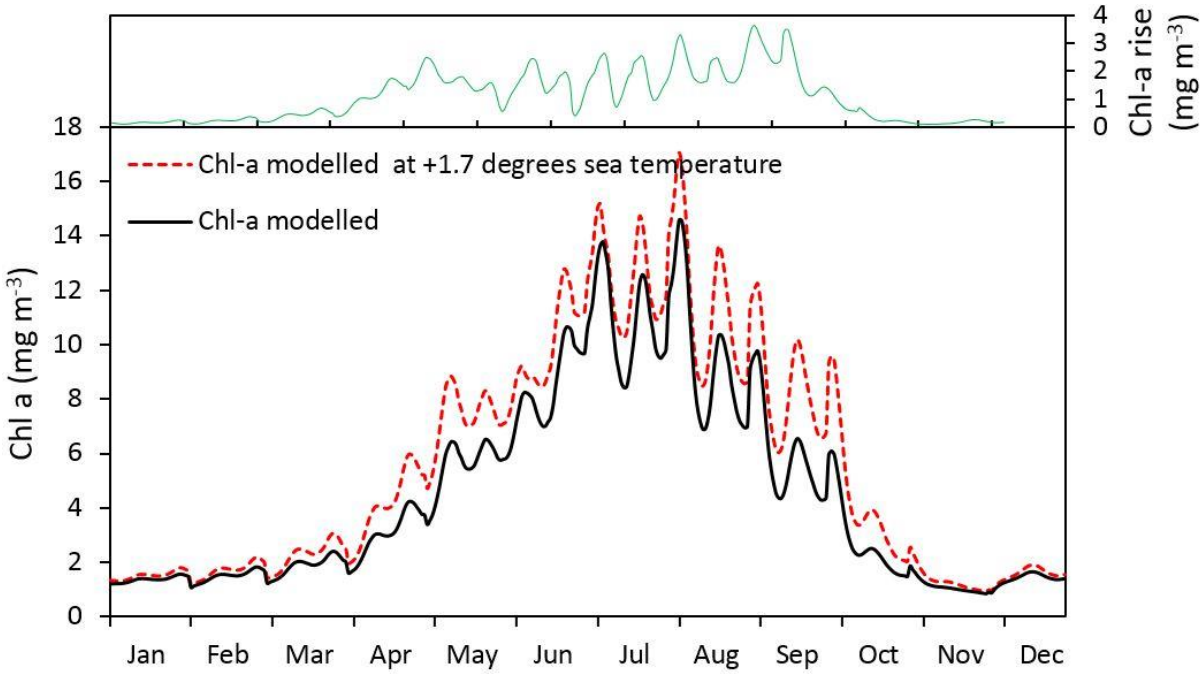

Figure 48: Effect of a rise of sea temperature of +1.7 degrees on the modelled Chl-a values for an average year in Kinvarra bay for a standing stock of mussel of 345 tonnes.

6.5.4.2 The combined effect of nitrogen inputs from SGD flow and phosphorus limitation

Both the N inputs from SGD and the availability of P in the water column affected the modelled nitrogen storage in the different nitrogen reservoirs in Kinvarra Bay (Chl-a modelled, dissolved N, particulate N, benthic N, Figure 49). The difference between the scenario with and without SGD depends on SRP levels within the bay (Figure 49a). At P levels set to the upper range seen in Kinvarra Bay, the presence of SGD lead to an increase of Chl-a of 8.5±0.3 mg m^{-3} during summer (Figure 49 a, c), At P levels set to the lower range seen in Kinvarra Bay, the presence of SGD lead to an increase of the averaged modelled Chl-a of 6.1±0.4 mg m^{-3} during summer (Figure 49 b, d). In the absence of N inputs from SGD, Chl-a modelled values were only 33±5 % of Chl-a levels modelled with SGD and high P levels; and 33±3 % of Chl-a levels modelled for scenarios with SGD and low P level. These results suggest that N inputs from SGD have a direct amplifying influence of Chl-a within the bay, and that 67±5 % of average Chl-a levels within the bay may be attributed to the N inputs from SGD, the rest being imported from Galway Bay regardless of the SGD input occurring.

Moreover, modelled N transfer to sediment was enhanced by both increased SGD fluxes and increased SRP availability. This enhancement was the result of a stronger

transfer of dissolved N to particulate N and phytoplankton, then deposited in larger fraction to sediment as organic nitrogen (particulate or dissolved). Consequently, modelled N storage in sediment increased during summer and were maximum in late summer/fall, with the largest storage occurring under a scenario of N inputs from SGD and high P in the bay (Figure 49a).

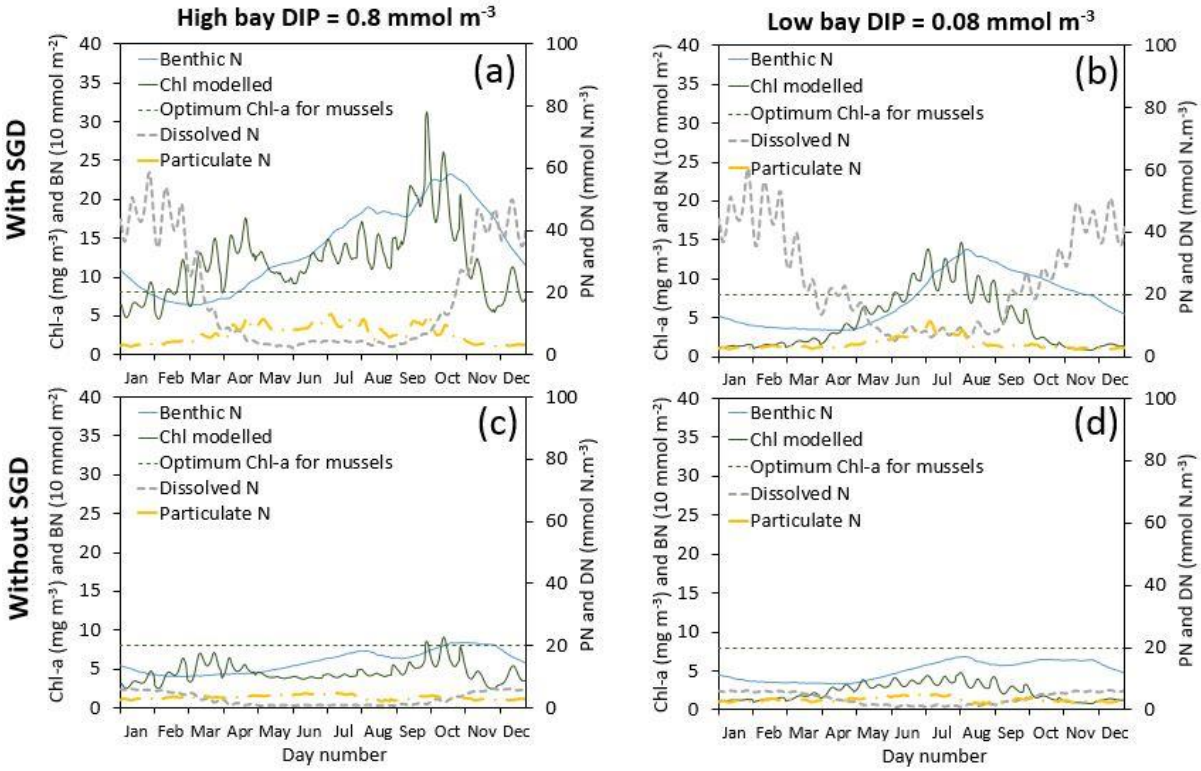

Figure 49: Effect of phosphorus availability and SGD presence/absence on modelled DIN (DN), Phytoplankton, particulate N (PN), and N storage in sediment (BN) in Kinvarra Bay for an annual production in Kinvarra Bay of 165 tonnes (standing stock of mussel of 345 tonnes).

Other changes than water temperature and SGD rates may also occur simultaneously. For example: changes of marine current and change of phytoplankton communities. The next section highlight the effect of these potential changes, starting from the parameters of the lower trophic model to then show graphically to which extent a physical change of marine current, phytoplankton communities may amplify or reduce changes of nutrient balance or primary production due to temperature changes or SGD discharges.

6.5.4.3 Change of marine currents in Galway bay, modifying the return flow to the bay.

According to Sanford et al. (1992), the value of b is influenced by three processes: "the phase of the tidal flow in the channel relative to the flow along the coast", "the strength of the channel flow relative to the strength of the coastal flow", and "the amount of mixing that occur once the basin water has been ejected into coastal water". Thus, if the phase or the strength of marine currents in Galway bay is modified, this may affect the return flow factor of Kinvarra Bay. A more frequent thermal stratification of Galway Bay could also affect this parameter, by modifying the frequency of mixing of freshwaters from Kinvarra Bay within Galway Bay.

A change of return flow factor from 0.7 to 0.85, corresponding for example to an decrease of cross shore currents within Galway bay in the proximity to the mouth of Kinvarra Bay relative to currents within Kinvarra bay, could strongly increase the modelled averaged dissolved N in Kinvarra Bay during periods of high discharge (average difference for October-March: 47±1 mmol N m^{-3}), and to a smaller extent, phytoplankton concentrations (average difference: 0.9±0.1 mg m^{-3} , Figure 50 a, b). Changing return flow factor during summer led to small changes of modelled dissolved nitrogen (average difference: 0.5±0.3 mmol N m^{-3} during June-August, Figure 50 a), but large changes of phytoplankton biomass with changing values of return flow factor (difference: 9.2±0.4 mg m^{-3} for June-August, Figure 50 b). This can be expected as modelled fresh SGD is low and primary production is high during these periods. The value of the return flow factor also had a small effect by comparison on modelled Chl-a during mid-November to January (Figure 50 b).

Modification of marine currents within Galway Bay, the relative tidal phase between Kinvarra and Galway Bay, or of the amount of mixing outside of Kinvarra Bay, if leading to a change of return flow, can be thus expected to have a large effect on both dissolved nutrient and phytoplankton in the system, affecting aquaculture activities.

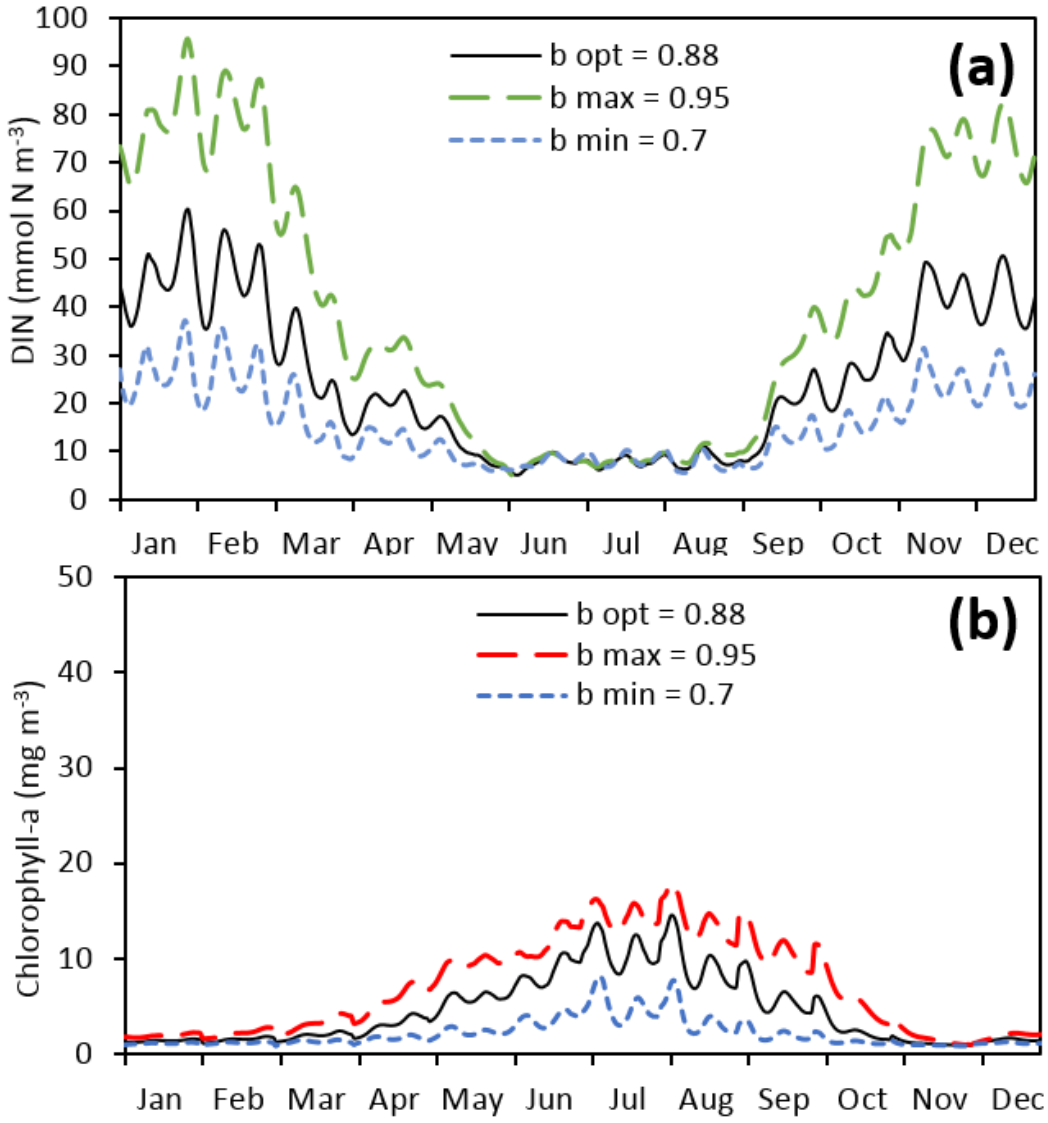

Figure 50: Effect of changes of return flow factor (used in equation 5.1) on (a) modelled Dissolved Nitrogen and (b) Chl-a in Kinvarra bay

6.5.4.4 Change of phytoplankton communities

6.5.4.4.1 Sensitivity to the grazing rate in the bay or the growth rate of phytoplankton

A larger grazing rate led to a large decrease on average modelled Chl-a level during the peak growth period (average change for June-August : -19.2±0.8 mg m^{-3}). Conversely it had only small effects on modelled Chl-a during winter (average change for December-February: -0.6±0.1 mg m^{-3}), when little modelled phytoplankton net growth occurred in the system (Figure 51b). As a result, modelled dissolved N levels were significantly modified by changes of grazing rates during the growth season of phytoplankton (average change: +9.3±0.4 mmol N m^{-3}, Figure 51a), but were not significantly modified during the high discharge periods (-0.2±1.4 mmol N m^{-3}).

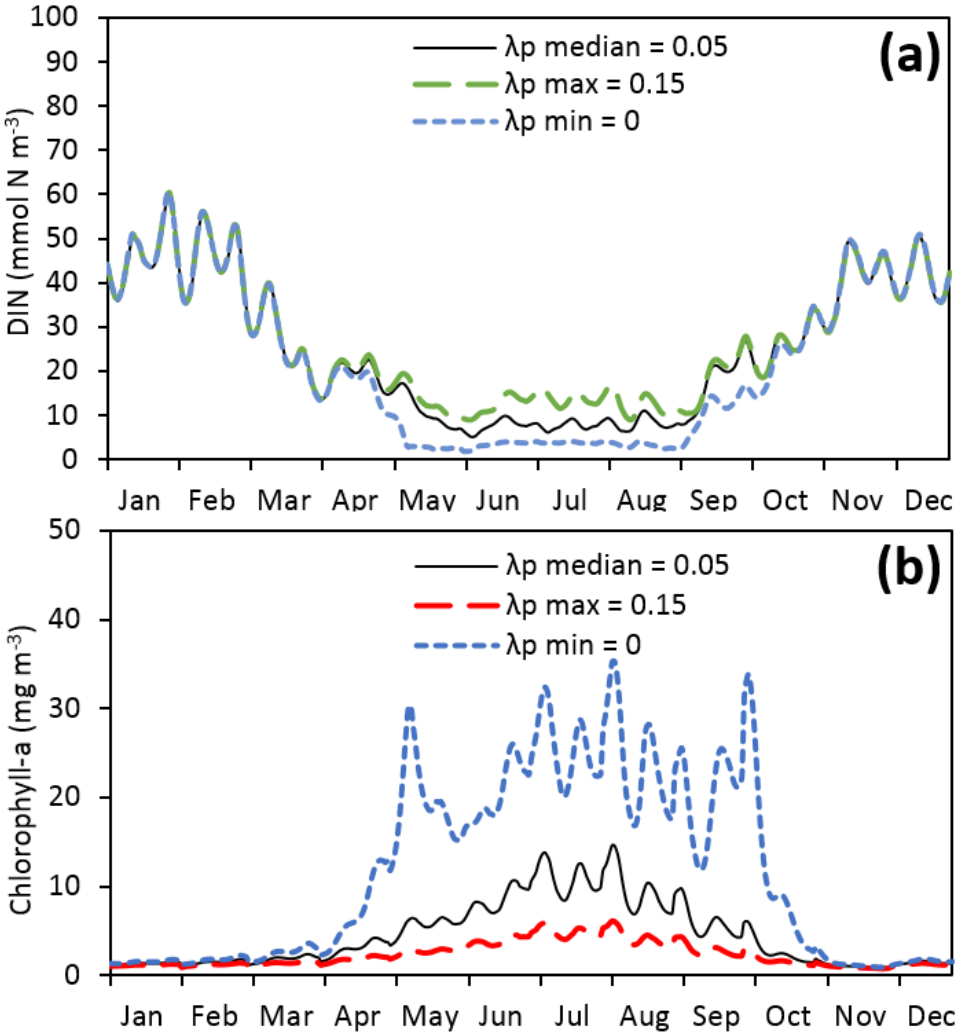

Figure 51: Effect of modification of grazing rates on the model outputs of (a) dissolved nutrients (b) modelled Chl-a levels for a standing stock of mussel of 345 tonnes.

Similarly, a change of the specific growth rate of phytoplankton (α) led to similar annual patterns changes of modelled DIN and Chl-a than grazing rates, but with a smaller amplitude of changes for the range of α tested (Figure 52). Modelled Chl-a during low discharge periods increased with increasing alpha (average change for June-August: +3.4±0.4 mg m^{-3}) but was less modified during high discharge periods (+0.1±0.04 mg m^{-3}). As a result, DIN decreased significantly during low discharge periods with increasing alpha (-5.4±0.5 mmol N m^{-3}) but close to no change of average values was forecasted during winter (-1.0±1.3 mmol N m^{-3}).

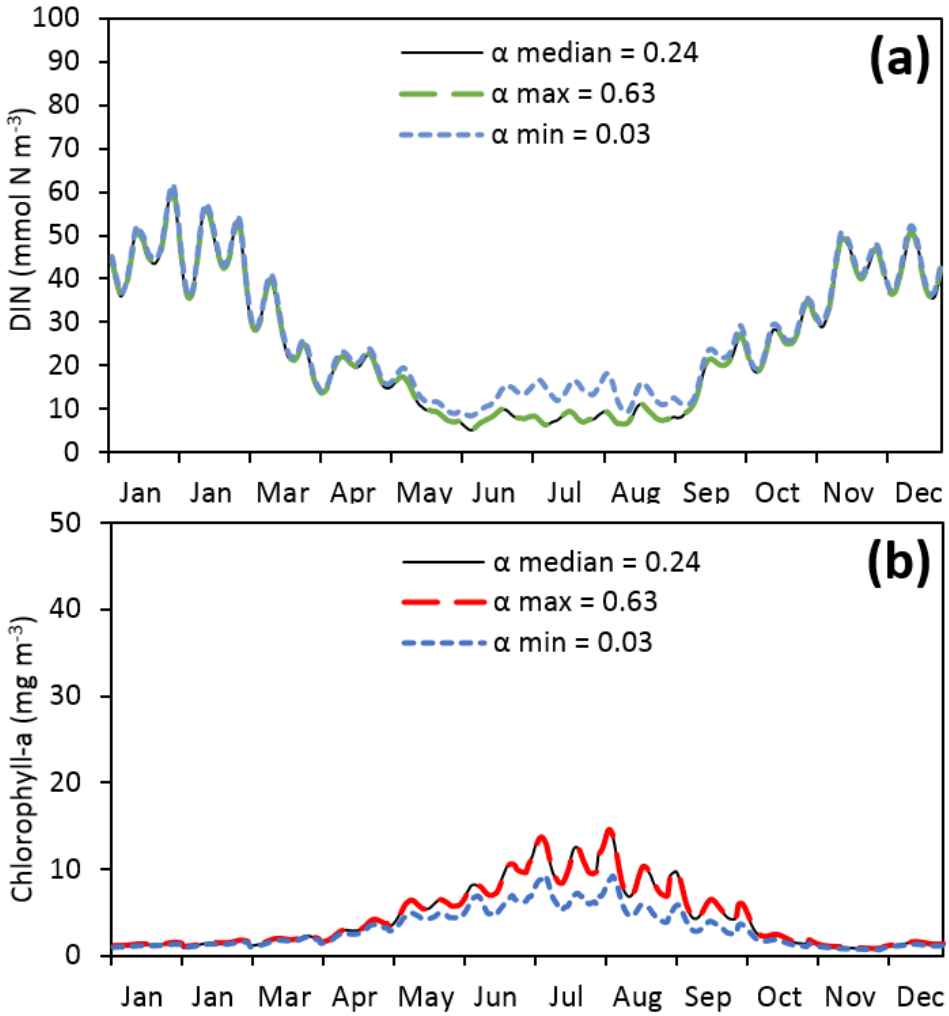

Figure 52: Sensitivity to α, the initial slope of the growth rate of phytoplankton in the phytoplankton growth equation (Equation 5.6) of (a) dissolved N and (b) Chl-a for a standing stock of mussel of 345 tonnes.

6.5.4.4.2 Effect of changes in the nutrient ratios of phytoplankton and in their sensitivity to nutrient limitation

Reductions of C:N in phytoplankton decreased modelled phytoplankton biomass levels during both periods of low discharge (-6.0±0.5 mg m^{-3} for June-August) and high discharge (-0.10±0.04 mg m^{-3} for November to February). However this was not affecting N levels in the bay significantly (-0.28±0.31 mmol N m^{-3} and -0.05±1.2 mmol N m^{-3} for the same periods) (Appendix 2, Figure 53).

Increases of MaxC:Chl ratios also decreased modelled phytoplankton biomass levels (-4.2±0.6 mg m^{-3} during summer, -0.01±0.05 mg m^{-3} during high discharge periods), without affecting N levels in the bay significantly (-0.2±0.3 mmol N m^{-3} and 0±1 mmol N m^{-3} for the same periods). Change of MinC:Chl ratio for the range tested had small to no significant effect on both Chl-a and DIN during both summer (Chl-a change: 0.3±0.5 mg m^{-3}, DIN change: 0.0±0.3 mmol N m^{-3}) and winter (Chl change: 0.05±0.05 mg m^{-3}, DIN change: 0±1 mmol N m^{-3}). Increase of K_{dip} to simulate the presence of phytoplankton adapted to P limitation increased phytoplankton biomass levels during summer (+9.9+0.4 mg m^{-3}) and decreased DIN in the bay (-12±0.5 mmol N m^{-3}, Figure 54). Changes of nutrient availability may thus have no effect on Chl-a if nutrient ratios of phytoplankton or their sensitivity to nutrient limitation changes to adapt to it, for example following changes of phytoplankton species type in the bay.

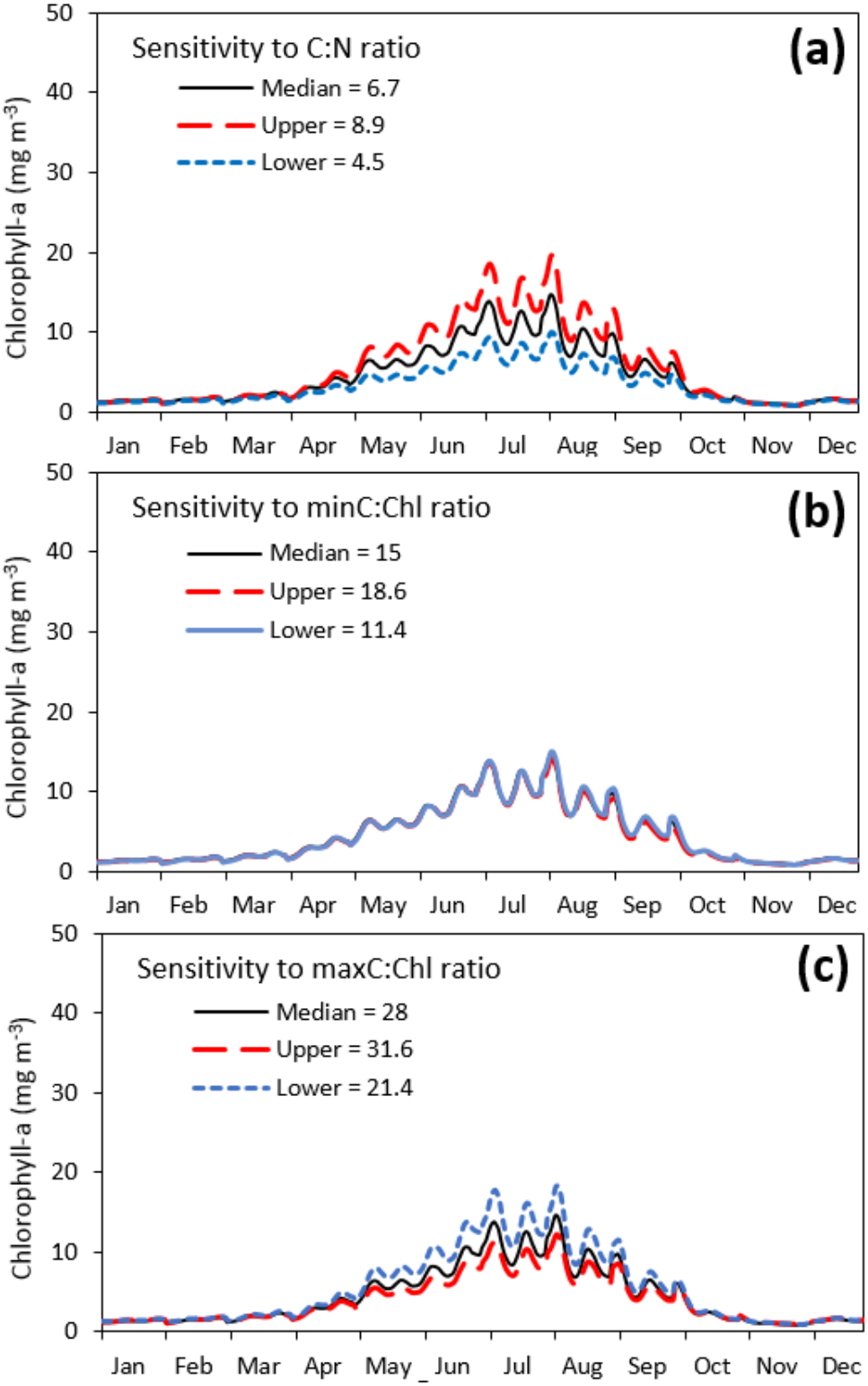

Figure 53: Effect of changes of nutrients ratios of phytoplankton on modelled Chl-a levels for a standing stock of mussel of 345 tonnes.

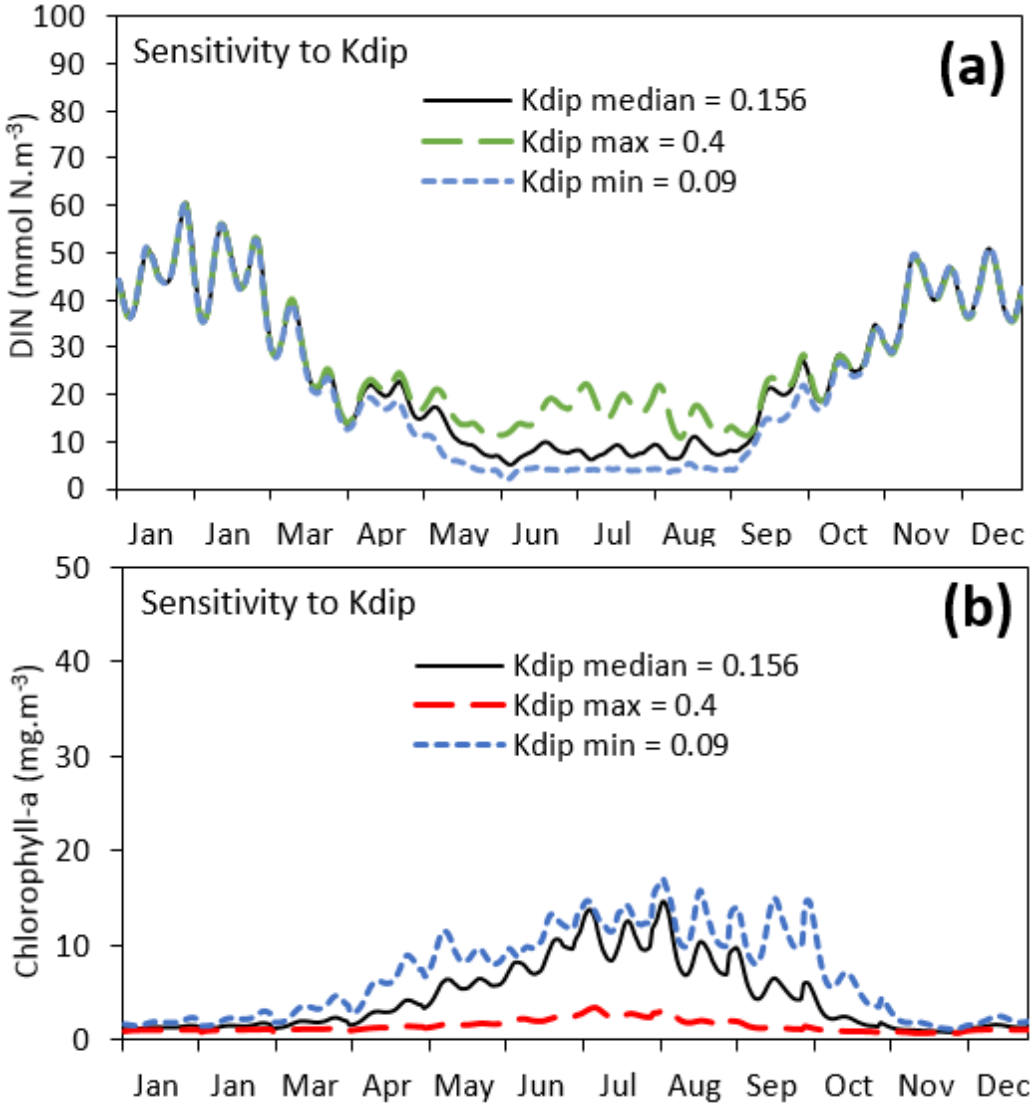

Figure 54: Effect of changes of Phosphorus saturation constant K_{dip} on (a) modelled DIN and (b) modelled Chl-a in Kinvarra Bay.

6.5.4.5 Effect of changes of the annual variability of SGD flow rates on Chl-a levels and mussel production.

Modelled Chl-a levels in Kinvarra Bay had variable peak values depending on the year considered. Modelled Chl-a concentrations were the largest between 2005 and 2019 when continuous modelled SGD flow was occurring during the growth period of phytoplankton (e.g. April-October 2019, Figure 55). The Chl-a concentrations were the lowest when the modelled SGD flow was minimum during most of the growth period of

phytoplankton (red circles, Figure 55), with bay averaged Chl-a close to 8 mg m^{-3} during most days.

Observed mussel production were also highly variable from a year to another. The two lowest production periods in Kinvarra Bay (2015 and 2016 in Figure 56) were reported following winter 2015-2016, when groundwater level was particularly high and flooding of large section of the catchment occurred around turlough (see maps in Figure 2 in Morrissey et al., 2020). However, winter 2013-2014 also had similarly large fresh SGD flow to the bay (Figure 55) and reported flooding in Kinvarra (Siggins, 2016), but aquaculture production was maximum during this period (Figure 56).

When SGD rates where present throughout the growing season, modelled Chl-a levels were more frequently above 8 mg m^{-3} (Figure 56). On the other hand, when a peak of SGD occurred at the beginning of the growing season, followed by a period of minimal SGD rates (red circles, Figure 55), the modelled Chl-a level was more frequently close or below 8 mg m^{-3} (green areas in 2005, 2006, 2013, 2014, in Figure 56). Between 2006 and 2019, the largest harvest of mussels, 200 tonnes, always occurred following periods of modelled Chl-a levels around 8 mg m^{-3} (2006, 2013 and 2014, in Figure 56).

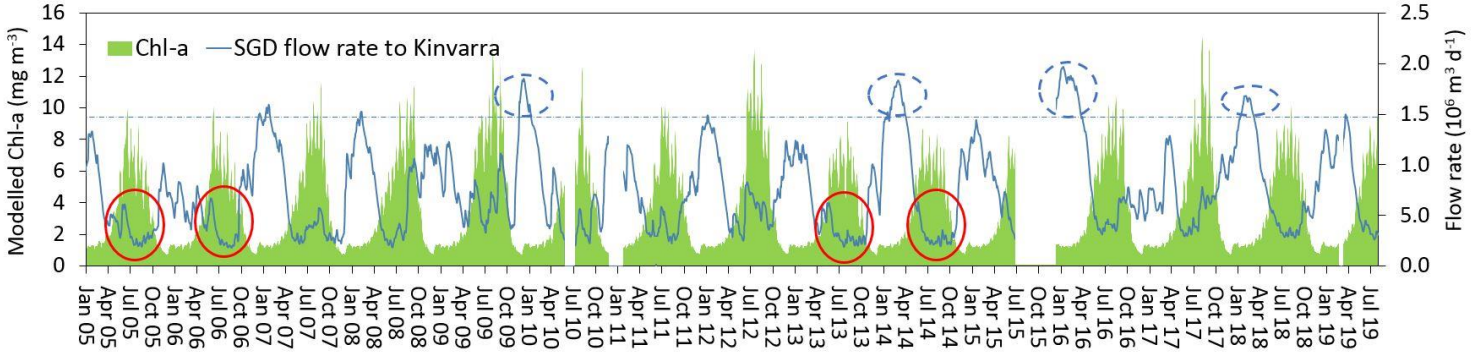

Figure 55: Compared modelled Chl-a levels and patterns of SGD flow rates to Kinvarra Bay between 2005 and 2019. Periods when a peak SGD occurred at the beginning of the growth season, followed by a low SGD flow rate to the bay are highlighted with red circles. Periods when a particularly high fresh SGD rate occurred during winter (>1.5 10^6 m^3 d^{-1}) are highlighted with blue dashed circles. These periods had flooding in the catchment (reported either for Kinvarra town or Gort). White vertical zones are periods when the likely range of SGD flow could not be estimated due to missing data on groundwater level.

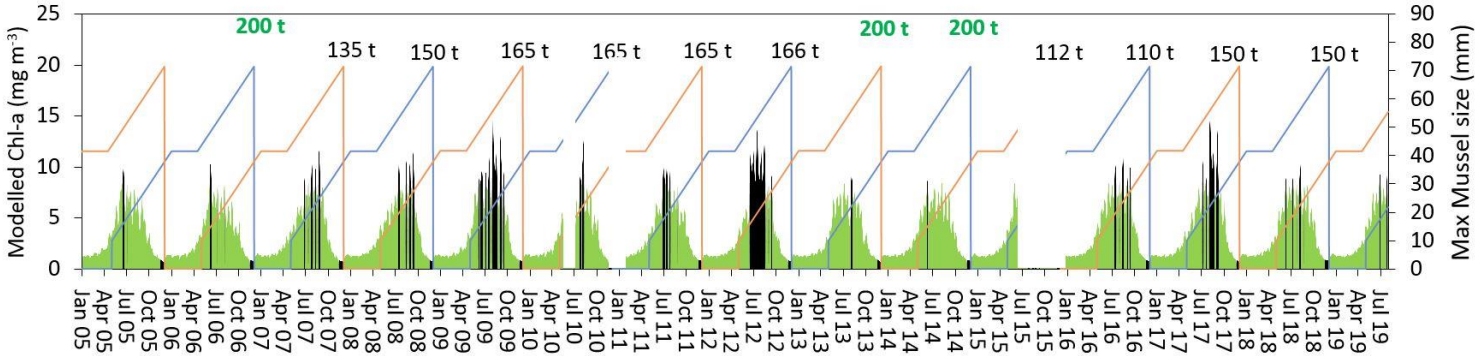

Figure 56: Modelled changes of chlorophyll-a level between 2005 and 2019, using the SGD patterns shown in Figure 55. The sections of the Chl-a curves at the expected change of shell size under optimum Chl-a level for mussel growth (2-8.5 mg m-3 according to Larsen et al., 2018) are shown in green, sections outside of these optimum growth conditions are shown in black. Numbers are the corresponding harvest production reported for the bay for each year (BIM, 2018a). Curves of mussel shell size under optimum growth conditions highlight the periods during which the growth of the harvested mussel took place. (the rates are only indicative of the period when growth of a harvest is likely to have taken place, as the actual growth curves are variable from year to year). White vertical zones are periods when the likely range of SGD flow could not be estimated due to missing data on groundwater level.

6.6 Discussion

6.6.1 Drivers of the changes of nutrient composition of the SGD end member in Kinvarra bay

Groundwater level measured at Killiny Borehole modified the nutrient levels in groundwater and SGD discharge coming to Kinvarra Bay. High DIN concentrations in Kinvarra Spring occurred more frequently during periods of groundwater level above 4.8m. Similarly, peak DRSi concentrations in the spring occurred more frequently when groundwater level was above 5.5m. Moreover, high TP level in the spring occurred more frequently when groundwater level was below 3.5m (Section 6.5.1.1).

As shown in Chapter 4, when groundwater level is close to or lower than high tide sea level, seawater recirculation is likely to lead to the intrusion of some seawater in the aquifer, releasing additional solutes (Ra, DIN, DRSi) by desorption and mineral dissolution. The maximum high tide level recorded in Galway bay during spring tide is between 3.1m to 3.5m (Marine Institute, 2020b). The 3.5m limit below which a significant increase of the average TP and a slight decrease of DRSI in the spring was observed, thus correspond to a level close from the highest tide in Kinvarra Bay, for which maximum saline intrusion is expected. The substantial increase of phosphorus concentration in the spring, coupled with a slight -but significant- decrease of DRSi may be caused by an increasing fraction of recirculated sea water in the aquifer, explaining the first 3.5m limit identified (Figure 37 b).

On the other hand, turloughs in the area flood if groundwater levels are sufficiently high (e.g. Morrissey et al., 2020). Such a flooding situation is likely to release added DIN to the turlough and then to the karst. The catchment contains numerous turloughs (Figure 34). The nearest one from Kinvarra spring and the Kinvarra borehole sampled by EPA, at Loughcurra South has its lowest altitude at 5m, and most of the surrounding land has an altitude of between 7 and 12m. Although Killiny Borehole, where the EPA records groundwater level is 3 km south from this location, and although we can consider that the level in the turlough might be lower compared to Killiny Borehole, this altitude range seems to correspond to the 5-6m transition observed in the spring concentration. It is likely that when the recorded groundwater level is above 5-6 m, the water table is

sufficiently close to the ground surface for significant flooding to occur in the land surrounding the turlough. Such flooding was observed here during the high groundwater level surveys. This flooding would then accelerate the release of nutrients from the surrounding lands to groundwater if the local biological activity within the turlough and the karst are not high enough to consume the added nutrients. McCormack et al., (2016) observed peak nutrient levels in turlough in the catchment in early winter, periods of maximum or near maximum turlough level, followed by reductions of concentrations during spring and summer, linked to reactions within the turlough consuming nutrients (e.g. denitrification). This is consistent with the higher DIN and DRSi concentrations peaks observed here when groundwater levels were above 6m at Killiny borehole (Figure 37 a, c), with peak values most likely corresponding to the early winter peaks previously observed by McCormack et al., (2016). The observation of McCormack et al., (2016), show however that the variability of nutrient concentration in the aquifer may also depends on which stage of the groundwater level rise and fall cycle we are at. Larger concentrations are more likely to occur at the beginning of the high groundwater level periods, while may decrease afterwards, following the consumption of the added nutrient by biological activity in the aquifers and or the turloughs.

Temperature variability may also affect nutrient concentrations in the groundwater itself. A previous study showed that denitrification could be present in deep parts of flooded turloughs, leading to a consumption of nutrient in the turlough when conditions were favourable in the catchment (McCormack et al., 2016). Rising temperatures can lower oxygen concentrations by reducing oxygen solubility and enhancing respiration rates relative to photosynthesis (Allen et al., 2005; Boulêtreau et al., 2012; Hanke et al., 2016; Yvon-Durocher et al., 2010). Diffusion rates of oxygen into sediment can also decrease with rising temperature (Elberling and Damgaard, 2001). As a result of these combined factors, nitrogen consumption in soils tend to increase with temperature (Saad and Conrad, 1993). Potential maximum NO_3^- reduction rate in saline sediment can be multiplied by 3.5±0.2 when temperature rise by ten degrees (Ibánhez and Rocha, 2017). In freshwater sediment, denitrification rates can increase tenfold when the temperature increases from 10 to 25 degrees (de Klein et al., 2017). The observed difference may be thus due to the combined effect of low temperature reducing N consumption by

denitrification in the catchment and added nutrient inputs to groundwater from the flooding of turloughs.

This effect of biological activity in sediments and soils, turlough and the karst network would then explain why low nutrient concentrations may be seen in both Kinvarra borehole and Kinvarra spring even during groundwater levels high enough to flood the surrounding land.

The nutrient levels in the discharged water are thus not constant but depend on the nutrient sinks and sources in the subterranean estuaries and catchments. Here, we showed that this led to variable nutrient levels in the SGD waters, as a function of the rise and fall of groundwater level. If these nutrients are not consumed within the catchment and the karst system by biological activity, these nutrients are then brought to coastal springs as an added nutrient load to coastal areas, feeding phytoplankton growth and changes of N:P ratios.

6.6.2 Effect of SGD variability on modelled chlorophyl-a and observed aquaculture production

Section 6.5.4.5 identified that years of minimum mussel production frequently followed one or several periods of maximum modelled fresh SGD discharge during winter. Winter floods and periods of particularly large freshwater fluxes discharge or storms affecting bays containing aquaculture (e.g. may lead to fluctuations of water chemistry parameters (e.g. salinity), and may increase mussel mortality (Callaway et al., 2012; Harger and Landenberger, 1971; Hastie et al., 2001; Nehls and Thiel, 1993). Exceptions were also present however, for example in winter 2013-2014 when mussel production was maintained at high level the following harvest. This suggests that mussel metabolic stress during periods of high freshwater discharge to Kinvarra Bay is not the only driver of the increased mussel winter mortality during or following floods.

From August to October energy reserves are built up in the mantle of mussels, which will fuel gametogenesis during the winter (Seed and Suchanek, 1992). Thus, the feeding conditions of mussels during the growing season are likely to impact the mussel mortality during the winter, when mussel use their reserves to fuel gametogenesis and sustain their metabolism. Larsen et al. (2018) showed that Chl-a levels above 8 mg m^{-3} can slow down the

growth of mussels as they are not physiologically adapted to such conditions. The period for which mussel production were not reduced following a flood during winter 2013-2014 followed a summer for which modelled phytoplankton biomass were around or below 8mg/l Chl-a. Moreover, maximum annual production for mussel frequently followed periods for which the model predicted phytoplankton biomass around or below 8mg/L Chl-a.

The joint occurrence of (1) optimum feeding condition during the growth period of mussel and (2) low stress during the winter period may thus explain in part the variability of mussel production from year to year. Such effect is likely to be visible on aquaculture production if other parameters affecting mussel mortality (e.g. predation, mussel density; Davenport, 1979; Gruffydd et al., 1984; Larsen et al., 2018; Seed, 1969) are otherwise maintained at a relatively constant level between years through aquaculture practices.

6.6.3 A distinct effect of SGD on phytoplankton biomass, and N level in Kinvarra Bay depending on seasons, tidal variability and SRP availability.

Section 6.5.2 identified a significant negative correlation between groundwater level (here an indicator of the likeliness of high fresh SGD flow) and observed Chl-a, with maximum Chl-a levels occurring at minimum groundwater level periods. SGD sites, frequently have reduced water temperatures during summer, and increased water temperature during winter which allows identification by remote sensing (e.g. Wilson and Rocha, 2012). Colder temperatures during summer can reduce primary production rates (Eppley, 1972), and increased rates of freshwater inputs can accelerate the flushing of bays (Alber and Sheldon, 1999; Sanford et al., 1992), which is known to be able to reduce primary production with respect to respiration (Lucas et al., 1999). The variability of Chl-a and net primary production is thus likely to be strongly modified by changes of SGD rates in addition to light and temperature variability. Phytoplankton production is generally the highest in coastal systems that have the longest flushing times and that retain nutrients and phytoplankton biomass (Gilmartin and Revelante, 1978). This supply of nutrients from SGD, as well as the longer retention of water in Kinvarra Bay, may thus explain the larger Chl-a levels in Kinvarra Bay compared to Galway Bay.

The seasonal variations of light and temperature also play an important role on the effect of SGD on a given system. The results from the lower trophic model suggest that a substantial

SGD-derived nutrient load to a coastal bay during a period of low light availability and temperature may not have a significant effect on the phytoplankton biomass (here assessed with modelled chlorophyll-a level), as the low-temperature and light availability limit growth. As a result, during such periods a larger fraction of the nutrient loads from SGD are exported to the outside of the bay without being consumed within the bay by primary production. On the other hand, a small nutrient load from SGD during a period of high light availability and high temperature can lead to significant increases of phytoplankton biomass, particularly if limiting nutrients are supplied. Consequently, small inputs of limiting nutrients such as phosphorus by recirculated SGD (Chapter 4) may affect the growth rates of phytoplankton in coastal systems, even when the net inputs are small.

The effect of SGD on the water composition and nutrient content of a bay will also depend on how quickly freshwater discharge and tide flush the system. Neap tide periods are the most favourable for lower flushing rates of coastal systems, leading to a more frequent accumulation of SGD waters close to their discharge points compared to spring tide periods. This effect of tides was recently demonstrated for Kinvarra Bay (Gregory et al., 2020) and the modelling in this work confirmed that this was likely to impact residence time and phytoplankton biomass levels in the bay (e.g. Figure 45c, Figure 46b). Modelled peaks of phytoplankton biomass, dissolved N and residence time of the systems happened during neap tides. The variability observed may be the result of a balance between nutrient inputs from SGD and accelerated flushing due to SGD, mediated by the spring/neap tide variability.

6.6.3.1 Effect of SRP availability in the bay on the long-term variability of nutrient, primary production and mussel N assimilation

Section 6.5.4.2 showed that without sufficient available limiting nutrients, an increase of nitrogen loads from SGD does not necessarily affect chlorophyll-a levels and mussel nitrogen assimilation. Increased modelled chlorophyll-a levels in the bay could occur as a result of increasing DIN loads from SGD only if sufficiently high phosphorus levels were present in the bay to allow growth, in addition to the other parameters previously discussed. The storage of N in sediment was also reduced when SRP levels in the bay were lower, because of the reduced settlement of particulate matter (e.g. dead phytoplankton and pseudofeces from mussels) when blooms were less frequent.

Before 2015, Kinvarra Bay received an average of 343.7 m^3 d^{-1} untreated sewage with a mean concentration of 14.79 mg L^{-1} Total Phosphorus and 72.11 mg L^{-1} Total Nitrogen (UISCE Eirean Irish Water, 2016), giving a daily input to the bay of 5.132 kg d^{-1} for P and 24.78 kg d^{-1} for N. By comparison, the discharge from SGD is between 10^5 and 10^6 m^3 d^{-1}, with a concentration of SRP of 15 µg L^{-1} and of 0.5 mg L^{-1} for DIN, giving a daily flux to the bay of 1.5-15 kg d^{-1} for P and 50-500 kg d^{-1}. These figures are consistent with the previous estimates by McCormack et al., (2016) who estimated the average load of Total Phosphorus from Kinvarra spring to be 17.3 kg d^{-1} and 788 kg day^{-1} for Total nitrogen. The discharge of sewage to the bay was thus sufficiently high compared to SGD discharge to increase the P levels, in particular during low SGD discharge periods. By contrast, the N loads from sewage are too small compared to the N load provided by SGD to change the N concentration in the bay significantly during winter, but not during summer. In 2015-2017, a new treatment plant was installed (UISCE Eirean Irish Water, 2016). It was suggested that this could reduce the phosphorus availability in the bay, driving the system further towards P limitation (Rocha et al., 2015). After 2015 a reduction of SRP levels was observed in the bay (Figure 57). We can expect the reduction of phosphorus concentration to reduce phytoplankton growth, as limiting nutrients become less available. However, so far, no significant decrease in the annual average of Chl-a level was observed (Figure 57). Four explanations are possible:

(1) the phytoplankton assemblage changed, favouring species adapted to P limitation, with a different nutrient ratio than that considered here, for example mixotrophic species with a larger N:P ratio

(2) a significant part of the growth occurs outside of Kinvarra Bay

(3) the phosphorus available is still sufficiently high to feed primary production as before and is not the limiting nutrient

(4) other processes provide the missing phosphorus directly to phytoplankton, without releasing dissolved phosphorus to the water column, for example through a faster internal cycling of P in the bay or the release of legacy P from sediment (e.g. such as in Conley et al., 2002). For example, the slow release of P that was previously discharged to the bay by sewage and stored in sediment may provide such additional P inputs.

The observed Chl-a in Kinvarra Bay is generally much larger than the observed Chl-a levels in Galway Bay, and the lower trophic model suggested that most of phytoplankton biomass in Kinvarra Bay is generally due to growth *within* the bay. Thus (2) is unlikely. It was already determined that the system is phosphorus limited during summer (Rocha, 2015), and the modelled patterns of Chl-a correspond better to the observed seasonal Chl-a variability when P limitation is accounted for, thus (3) is also unlikely.

Section 6.5.4.4.2 showed that a change of nutrient ratio and Chl-a nutrient ratio of phytoplankton could reduce or increase the apparent Chl-a levels in the bay. A change of the phytoplankton communities could thus counterbalance the effect of SRP on Chl-a, which makes (1) thus possible.

Observations of phytoplankton assemblage in the bay would allow to confirm whether mixotrophic species and other species adapted to P limitations are more frequently present in the bay. If so, hypothesis 1 would be validated. Fluxes from sediment, from recirculated SGD and from particulate matter already present in the bay that supply phosphorus to sustain phytoplankton growth (Hypothesis 4) may also provide additional P to limit the shift of species present in the bay. In such a context, we suggest investigating further the phosphorus cycles and the shifts of phytoplankton species to assess why there is no apparent effect of reduced P concentration in the bay on Chl-a concentrations.

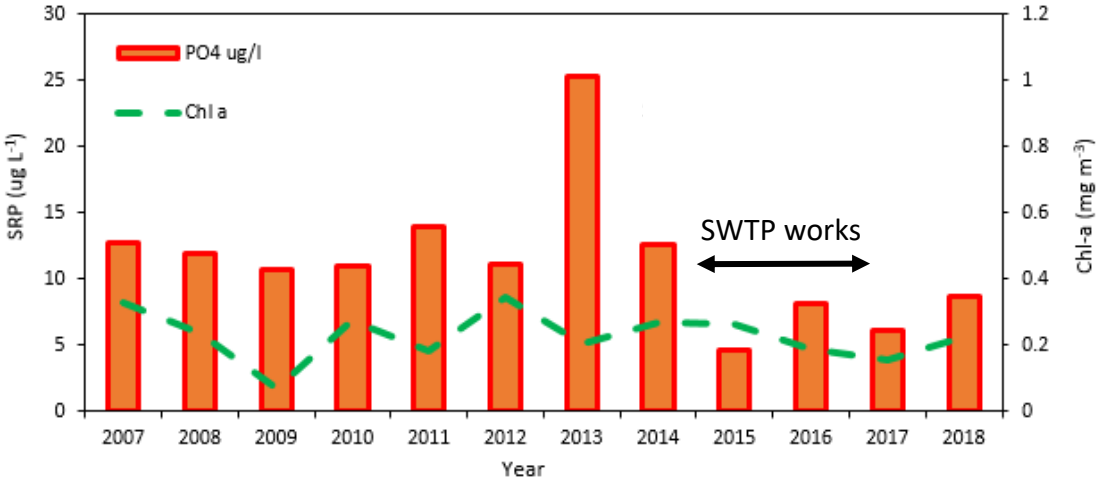

Figure 57: Effect of the sewage treatment plant (SWTP) put in place in 2015-2017 for Kinvarra Bay annual average Soluble Reactive Phosphorus and Chl-a levels (EPA, 2018a). The arrow show the period of construction of the SWTP according to UISCE Eirean Irish Water, (2016).

6.6.4 Limitations of the lower trophic model and knowledge gap on Kinvarra Bay.

The model used here is a single box model, which allows to visualise with a small number of graphs the relative effect of changes of nutrient inputs from SGD on nutrient balances, and the associated effect on primary production in enclosed bays hosting aquaculture activities. The model can be implemented with limited computational power, either in professional modelling software, coding or even in a spreadsheet. Thus, it can be of value to investigate in an accessible manner the effect of potential changes on enclosed bay hosting mussel aquaculture and receiving SGD. This accessibility makes improvements easier to implement.

Fresh Submarine groundwater discharge inputs to the bay are estimated using a site-specific linear relationship between groundwater level and flow rate, previously developed in Chapter 3. This first order relationship was derived from observed correlation between groundwater level measured close to the main phreatic conduit feeding Kinvarra springs and flow rates estimated from multiple methods involving modelling, water balances and SGD tracers. This approximation works best for mid groundwater level but is likely to overestimate SGD flow rates at high and low groundwater levels, where turbulent flow may be present in larger section of the karst system and create significant reductions of flows. We can also note that while such linear relationship may work for a range of groundwater level conditions in phreatic conduit, epikarst conduit may be more strongly non-linear (e.g. as highlighted by Jeannin, 2001). An intercalibration paper is currently under preparation looking at different alternative relationships between groundwater level and fresh SGD discharge for Kinvarra Bay, and may be used in a later date to update the current groundwater-discharge relationship.

In its current single box version, the model does not assess the spatial variability of the bay composition. Dividing the bay in several boxes may be a first approach typically applied to consider spatial variability. However, Gregory et al., (2020) observed a variable spatial change of salinity in Kinvarra Bay between and within tidal cycles. This fast variability does not allow to define stable multiple boxes for the bay. Consequently, we use here a single box model to study conceptually the overall seasonal variability of the bay, and facilitate the comprehension of the key drivers of variability with a limited

number of graphs. A spatially distributed hydraulic model for the system could be also applied for a more accurate modelling of the bay. However, to properly characterise the variability of surface stratification in the bay, such model would require more extensive data collection based on multiple continuous sensors in surface and deep waters in several points of the bay. This dataset should also include data during neap and spring tidal cycles and during high and low SGD discharge periods. Before such data is available, the current single box model gives an acceptable approximation to study conceptually the general changes in the system. Indeed, the model reproduce the general seasonal changes present in the EPA dataset, as suggested by the fair model efficiency (between 0.95 for temperature to above 0.5 for DIN and Chl-a, before an in-depth calibration of the parameters, and without accounting yet for the effect of variable DIP in the bay).

The model in its current version allowed to identify graphically several knowledge gaps in Kinvarra Bay. First, the conceptual modelling allowed to identify the importance of a series of parameters which variability is currently virtually unknown in the system. We observed in the EPA dataset peak values of Chl-a for low groundwater level period (section 6.5.2). On the other hand, the lower trophic model predicted minimum Chl-a levels when nutrient inputs from SGD were reduced during summer. This seems in part inconsistent with the observed maximum phytoplankton biomass during low groundwater level periods (section 6.5.2). As demonstrated by the sensitivity analysis of the model, other parameters which were kept stable in the current run of this model, may affect Chl-a levels in Kinvarra Bay. These parameters may include: a change of nutrient ratios in phytoplankton, changes of grazing loss of phytoplankton, change of the saturation constant to SRP of phytoplankton, or a seasonal variability of SRP availability in the bay (such as due to saline SGD).

Successive runs of the models allowed to identify the potential effect of such parameters. Changes of nutrient ratios in phytoplankton could lead to an upper range of modelled changes of 10 mg Chl-a m^{-3} (section 6.5.4.4.2). The changes of grazing for the range tested could lead to a maximum change of 30 mg Chl-a m^{-3}, and of 20 mg Chl-a m^{-3} for the range of P saturation constant tested (section 6.5.4.4.1). Finally, increasing SRP availability in the bay from its upper to lower range observed in the EPA data for the bay, could lead to a change of 20 mg Chl-a m^{-3} (section 6.5.4.2). The current poor

characterisation of the variability of these parameters thus limits our ability to forecast the impact of changes in the system. By comparison, the maximum observed Chl-a modelled could rise by 40 mg m^{-3} when groundwater decreased from 5m to 2m (Figure 42).

From the previous results, the observed increase of maximum Chl-a with decreasing groundwater level could have several explanations. Fist, a decrease of grazing constant with decreasing groundwater level during summer larger than tested here, could explain the observed increase of maximum Chl-a with decreasing groundwater level. Overall however, warmer temperature are expected to lead to increased grazing rates (Guinder and Molinero, 2013), thus such a decrease of grazing rate constant coincident with decreasing groundwater level seems unlikely. Alternatively, a combined change of SRP saturation constant in phytoplankton and an increase of SRP availability during summer could explain the observed Chl-a change when groundwater level is lower, as modelled in section 6.5.4.4.2. As pointed out in Chapter 3, saline SGD (or recirculated SGD) may supply added P during low groundwater level periods. Other processes leading to fluxes from sediment may also play this role, for example through a seasonal release iron bound P and degrading organic matter (Van Helmond et al., 2020). Future studies should thus investigate in priority the P cycling in SGD sites hosting aquaculture activities, particularly where P is the limiting nutrient.

Another knowledge gap identified is the fact that the effect of grazing on N and C cycles in Kinvarra Bay has not been yet determined though measurements in this system. However, several studies in mussel aquaculture sites in shallow bays showed that mussels tend to dominate the grazing of phytoplankton over zooplankton, and thus zooplankton grazing plays a minor role on the phytoplankton biomass (e.g. Cranford et al., 2007; Grant et al., 2007). Cranford et al. (2007) applied his model for a similarly shallow temperate bay, and the value for grazing loss the authors used is also suggested to model ecosystems in Jorgensen et al., (1991). As a starting point to model the system, their value for this parameter was kept. To illustrate the effect on model results of this choice, we tested the effect of different values of the grazing loss of phytoplankton on the system in Appendix 4. Moreover, we discussed the effect of changing rates of grazing in our scenario testing, section 6.5.4.

Finally, the model of Cranford et al. (2007) also does not include at this stage the contribution of DON for the local primary production and N cycling in the bay, while Rocha et al. (2015) showed that it can amplify the N cycling in the bay during summer. A new component for DON cycling may need to be included, but this would require more investigations on the variability and cycling of DON in SGD dominated sites to determine which model structure may be the most appropriate to do so, or to add equations including DON to the current model. Similarly, more data collection on particulate N would allow a fine tuning of this model.

6.6.5 Potential effects of climate change on nutrient levels and phytoplankton biomass

Section 6.5.4.1 showed that changes of yearly average temperatures could have a significant effect on modelled Chl-a levels in Kinvarra bay. An increase of average Chl-a in the bay is expected if other variables (exchange with Galway Bay, nutrient ratio of phytoplankton, grazing rate and growth rates of mussels) remain constant.

This estimation does not include the effect of variable temperature on fluxes from sediments (e.g. desorption, diffusion of degradation of organic matter or nutrients) which were not yet included in the model, as we lack information on the effect of temperature on fluxes from sediment in this bay. As temperature in sediment is more stable than the overlaying water column, particularly as a result of SGD inputs this effect is likely to be smaller than the ones due to rising air temperatures. Moreover, turbidity in the bay is generally close to zero, suggesting that fluxes to and from suspended sediments are negligeable for most of the water column.

Moreover, the effect of other variables may lead to Chl-a changes which may balance the effect of temperature increase in the system. Most phytoplankton parameters in the Cranford model can be dependent on species assemblage and may vary spatially (Garcia et al., 2018; Jakobsen and Markager, 2016; Platt and Jassby, 1976). An increase of C:N ratio or the specific growth rate of phytoplankton (α) could increase modelled Chl-a levels and the modelled DIN consumption within the bay, while an increase of grazing (λp), max C:Chl-a ratio or K_{dip} could decrease the modelled Chl-a level and modelled DIN

consumption within the bay (section 6.5.4.4). Thus, the amplifying effect of an increase of water temperature on Chl-a level may be balanced if associated by specific changes of phytoplankton types in the bay. For example, an increase of the grazing rate of phytoplankton, or the predominance of species with lower specific growth rate (alpha), lower C:N ratio, or higher C:Chl-a ratio during summer (MaxC:Chl) could counter the effect of increasing temperature. The predominance of new species of phytoplankton less sensitive to limiting nutrients such as here phosphorus, represented here by an increase of K_{dip} could also balance the phytoplankton biomass increase due to increasing water temperature. Alternatively if increase of temperature are associated with other phytoplankton changes also leading to an amplification of phytoplankton biomass, such a decrease of Kp, MaxC:Chl-a ratio, λp or an increase of C:N ratio in phytoplankton or of their specific growth rate (α) , the result of a rise of temperature may be higher than described in section 6.5.4.1.

The consequences of increase of the bay water temperature on the phytoplankton biomass and nutrient concentrations are thus strongly dependant on future changes of phytoplankton assemblage. Climate change is expected to lead to a reduction of C:N ratios and increase the prevalence of mixotrophs in phytoplankton. As shown by the lower trophic model, these changes alone may reduce Chl-a levels and balance thus potentially temperature increases.

6.6.6 Economic impact of SGD on coastal ecosystems

Considering the previously discussed points, estimating the economic effect of SGD on coastal systems requires a detailed characterisation of the biogeochemistry of coastal systems and their catchment. In most cases, the effect of SGD on aquaculture is not linearly dependant as a function of the inputs from groundwater flow. Bivalve growth rates may be affected by food availability, competition for space, wave exposure, light, pH, temperature, and salinity (Malone and Dodd, 1967; Bayne and Worrall, 1980; Kautsky, 1981; Wai and Levinton, 2004;), and most of these parameters are modified in different ways by SGD.

During the winter season, high fresh SGD discharge may lead to reduced phytoplankton biomass, salinity and temperature, as they supply the system with new cold (during

summer), fresh waters, initially low in phytoplankton and can accelerate the flushing of coastal systems. If phytoplankton biomass, salinity, temperature, or pH are reduced below the optimal level for filter feeder growth, the effect of SGD can be damaging for mussel growth. On the other hand, during warm periods, SGD discharge may reduce water ages and temperatures in the bay, and prevent phytoplankton from reaching levels that reduce mussel growth (e.g. above 8.1 µg Chl-a L^{-1}, according to Larsen et al. (2018).

On the other hand, under low groundwater levels (ex: summer periods), some solutes previously stored in sediment and in the karst system are more likely to be released as a result of saline intrusion (See Chapter 4 on recirculation). In such warm conditions, SGD can thus provide a source of food for filter feeders growth, unless the nutrient availability is already sufficiently large to lead to phytoplankton biomass beyond the optimum level for mussel growth, in which case increasing SGD discharge may lead to a negative effect on aquaculture.

The lower trophic model suggests that without DIN inputs from SGD, Kinvarra Bay would be mainly dependent on phytoplankton biomass from Galway Bay and peak Chl-a values in Kinvarra Bay would be between 50 percent to 15 percent of current levels, with the lowest reduction occurring if phosphorus availability in the bay is also at its minimum level. Section 6.5.4.2 determined that 67±3% of modelled Chl-a level in the bay could be attributed to be a result of the amplification of primary production linked to N inputs from SGD. As phytoplankton is often the main source of food for cultured mussels (Rodhouse et al., 1984), and also indirectly increases the particulate nutrient availability in the water column, SGD thus control the majority of the mussel aquaculture production in Kinvarra Bay. At current market price of mussels (646 euros per ton, BIM, 2019), the median production in Kinvarra Bay, 150 tonnes represent a value of 96 900 euros per year. Oyster production in the bay is also likely to benefit from phytoplankton growth in the system induced by SGD. At current market price, 2200-6000 euros per ton (BIM, 2019), the 15 tonnes of annual oyster production in the system may represent a value of between 33 000 and 90 000 euros per year. Considering that the input of SGD lead to an increase of phytoplankton biomass by 67%, as suggested by our lower trophic model, we can estimate the economic value of SGD flow to Kinvarra bay mussel and oyster aquaculture only to be between 86 400 and 121 200 Euro per year.

6.7 Conclusion of Chapter 6

Our combined use of EPA long term datasets for transitional water and groundwater quality, new nutrient data collection, LOICZ mass balances and lower trophic models illustrated the seasonal variability of the effect of SGD discharge on phytoplankton and nutrient levels in a coastal bay. This variability is a function of (1) the variability of the nutrient composition of the SGD fluxes (2) the seasonal variations of light availability and temperature in the bay (3) system flushing rates (or residence times), which fluctuate between neap and spring tides and change with fresh SGD fluxes (4) the availability of the limiting nutrients in the bay (such as phosphorus). Other potential effects not estimated in this study include the effect of SGD driven changes of water chemistry on filter feeder's growth. As a result of these combined drivers, the effects of SGD discharge on a coastal ecosystem is not likely to increase linearly as a function of SGD discharge. This contrast what was previously assumed to develop optimum groundwater management strategies in order to preserve the value of SGD for algae harvesting (ex: Pongkijvorasin et al., 2010). Mussel production in Kinvarra Bay in strongly dependant on phytoplankton growth within the system, fed mainly by nutrients inputs from SGD. In the current mussel and oyster production, the presence of SGD in Kinvarra Bay allows the local aquaculture to create an estimated economic direct value of between 86 400 and 121 200 euros per year. SGD may also have further indirect economic impacts on other activities in the bay and outside of the bay (e.g. Galway Bay aquaculture, through the nutrient exported, in particular during winter periods). We showed that increases of water temperature linked to climate change on this system may be expected to extend the growth period of phytoplankton as a result of increased average temperature. The modification of rainfall patterns predicted by current climate models under scenario RCP4.5 and RCP8.5 will not necessarily modify the annual average of phytoplankton biomass in the bay, but may affect the time of exposure of filter feeders to optimum Chl-a levels for their growth and the type of phytoplankton species. We identified correlations between the patterns of SGD flow and aquaculture productions from the observed variations of mussel production in the bay and the comparison with modelled outputs for the same periods. The highest mussel production occurred when modelled Chl-a were at optimum levels for mussel growth, as a result of

peaks of SGD during early summer followed by a low SGD fluxes during most of the growth season. On the other hand, the lowest mussel production occurred following large fresh SGD fluxes during winter, but only if the previous growth period did not have optimum modelled Chl-a levels. If climate change leads to increased frequency of drought during summer, this may thus positively affect aquaculture, if a peak SGD flow is still occurring in early spring. This positive impact may be however balanced by the effect of increased floods and high SGD discharge during winter.

Several limitations in this work can be highlighted and should be investigated in future studies to assess more assertively the effect of climate change on coastal systems receiving SGD inputs and hosting aquaculture activities. Further studies should aim at (a) measuring of mussel growth variability in SGD dominated systems to assess the effect of changes of physical parameters on mussel growth and reproduction periods, (b) further characterising the main sources and sinks of phosphorus in SGD dominated sites, including the role of particulate P and its transfer to and from sediments, due to the fact that P can control the effect of SGD N load on primary production, (c) including in modelling efforts of SGD dominated sites the role of dissolved organic nitrogen for the recycling of nutrient in the bay in addition to particulate N considered in the Cranford model (d) estimating the variability of nutrient ratios, Chl-a and nutrient/Chl ratio of phytoplankton communities along the year in SGD dominated sites to better assess the effect of climate change and other anthropogenic changes on nutrient cycling.

Appendix of chapter 6.

Appendix 1: Parameters chosen for the application of the adapted version of the model of Cranford et al. (2007); Dowd (2005).

Parameter	Unit	Value	Description	Reference for the seleced value
α	mgC (mg.chl)$^{-1}$ hr^{-1} (W)$^{-1}$	0.24	Initial slope of phytoplankton growth curve	Platt and Jassby (1976) between 1-5 m phytoplankton assemblage
Min C:Chl	gC gChl^{-1}	15	Carbon:Chlorophyll-a minimum value of P	Values for annual variability of estuaries of C:Chl ratio in Jakobsen and Markager (2016).
amp C:Ch	gC gChl^{-2}	28	Carbon:Chlorophyll-a amplitude of P	
month	month	-0.2	Month after July when peaks occur	
N:P	-	16	Nitrogen:Phosphorus ratio of P	Variability of the Redfield ratio in phytoplankton Garcia et al. (2018). Mean ±2σ
C: N	-	6.6	Carbon:Nitrogen ratio of P	
Kn	mmol N m^{-3}	2.5	Half saturation for DIN for P growth	Cranford (2007)
K_{dip}	mmol DIP m^{-3}	0.156	Half saturation for DIP for P growth	$K_{dip} = K_n$/N:P
K_{bg}	m^{-1}	0.095	Light attenuation by seawater	(Pennock, 1985)
K_c	m^{-} .kg^{-1}	50	Light attenuation by sediment	(Pennock 1985; Banas et al. 2009)
K_p	m^2 mol^{-1} N	18	Light attenuation phytoplankton	
λ_p	mmol N m^{-3}	0.05	Grazing loss of P	Cranford (2007)
ϕd(T)	d^{-1}	0.1	Remineralisation rate of D to TIN	
λd	d^{-1}	0.05	Sinking rate for D	
ϕ_b(T)	d^{-1}	0.01	Remineralisation rate of B to TIN	
α	-	0.01	Burial fraction	
ε	-	0.065	Assimilated fraction for bivalves	
βm	-	0.11	Excreted fraction for bivalve	
N_{bm}	nb ind kg^{-1}	84.74	Number of mussels per kg	
Bay_ m_stock	tonnes	345	Tonnes of mussels present in the bay	Median mussel production between 2005 and 2018 ×2.3 (BIM, 2018a)
Bay MTL vol	10^7 m^3	1.80	Bay mean tide volume	From bay characteristics and tidal data
η	m	2.5	Bay depth	
T	d tide^{-1}	0.52	Tidal period	
b	-	0.89	Return flow factor	Chosen value fitting best salinity and res. time data, in the range given by Rocha (2015)
DIP level	mmol P m^{-3}	0.08	Dissolved Inorganic Phosphorus levels	Lowest integrated value in bay

Appendix 2: Sensitivity analysis for the parameters of the nutrient model used here, based on a modified version of the model of Cranford et al. (2007); Dowd (2005). Positive and negative sensitivity values are respectively the observed net increase and decrease of the annual peak of the modelled variable, when going from lower to upper range of a given parameter. Values in bold are above 10% of the average observed values for the annual variability in model runs.

Parameter	Unit	Sensitivity analysis range	Range based on	Max sensitivity of DIN (mmol N m^{-3})	Max sensitivity of Chl a (mmol N m^{-3})	Max sensitivity of Mussel N assimilation (mmol N m^{-3})
α	mgC $(mg.chl)^{-1}$ hr^{-1} $(W)^{-1}$	0.03 - 0.63	Platt and Jassby (1976)	**-2.36**	**5.3**	**0.036**
Min C:Chl	$gC.gChl^{-1}$	11.4 - 18.6	Values for estuaries Jakobsen and Markager (2016).	-0.04	**-0.9**	0.000
amp C:Ch	$gC.gChl^{-1}$	21.4 - 34.6		-0.14	**-6.1**	0.001
month	month	0.48 - 0.08		-0.01	**0.8**	0.000
N:P	-	6.2 - 26.2	Garcia et al. (2018) Mean ±2σ			
C:N	-	4.5 - 8.9		0.26	**9.4**	-0.002
K_n	mmol N m^{-3}	1.25 - 3.75	±50%	1.24	**-3.4**	**-0.024**
$K_{dip} = K_n/N:P$	mmol P m^{-3}	0.048 - 0.60	±50%	**6.63**	**-21.4**	**-0.111**
K_{bg}	m^{-1}	0.0475 - 0.143	±50%	0.05	-0.1	-0.001
K_c	m^{-2} kg^{-1}	25 - 75	±50%	0.00	0.0	0.000
K_p	m^2 mol^{-1} N	9 - 27	±50%	0.04	-0.1	-0.001
λ_p	mmol N m^{-3}	0 - 0.55	±50%	**5.17**	**-33.3**	**-0.081**
$\phi_d(T)$	d^{-1}	0 - 0.6	±50%	1.76	1.6	**-0.017**
λ_d	d^{-1}	0 - 0.51	±50%	0.77	0.5	**-0.045**
$\phi_b(T)$	d^{-1}	0 - 0.51	±50%	**2.00**	**2.5**	**0.020**
α	-	0 - 0.51	±50%	**-2.19**	**-1.4**	**-0.008**
ε	-	0 - 0.565	±50%	-0.55	-0.5	**0.863**
β_m	-	0 - 0.61	±50%	0.51	0.9	**0.008**
ind	nb ind kg^{-1}	42.37 - 127.1	±50%	1.49	**-3.0**	**0.077**
Bay_ m_stock	tonnes	253 - 600	Range of mussel production between 2005 and 2018 ×2.3	1.31	**-2.8**	**0.064**
Bay MTV	10^7 m^3	0.9 - 3	±50%	-4.47	**6.8**	**-0.034**
η	m	1.25 - 3.75	±50%	-0.41	-0.7	0.003
T	d $tide^{-1}$	0.262 - 0.786	±50%	**18.76**	**8.9**	**0.076**
b		0.78 - 0.94	±2σ Rocha (2015)	**24.49**	**9.8**	**0.093**
DIP level	mmol P m^{-3}	0.08 - 0.8	bay range seen	**-5.79**	**16.7**	**0.092**

Appendix 3: Effect of modifications of the four most sensitive parameters of Cranford Model on the modelled dissolved inorganic nitrogen level in the bay.

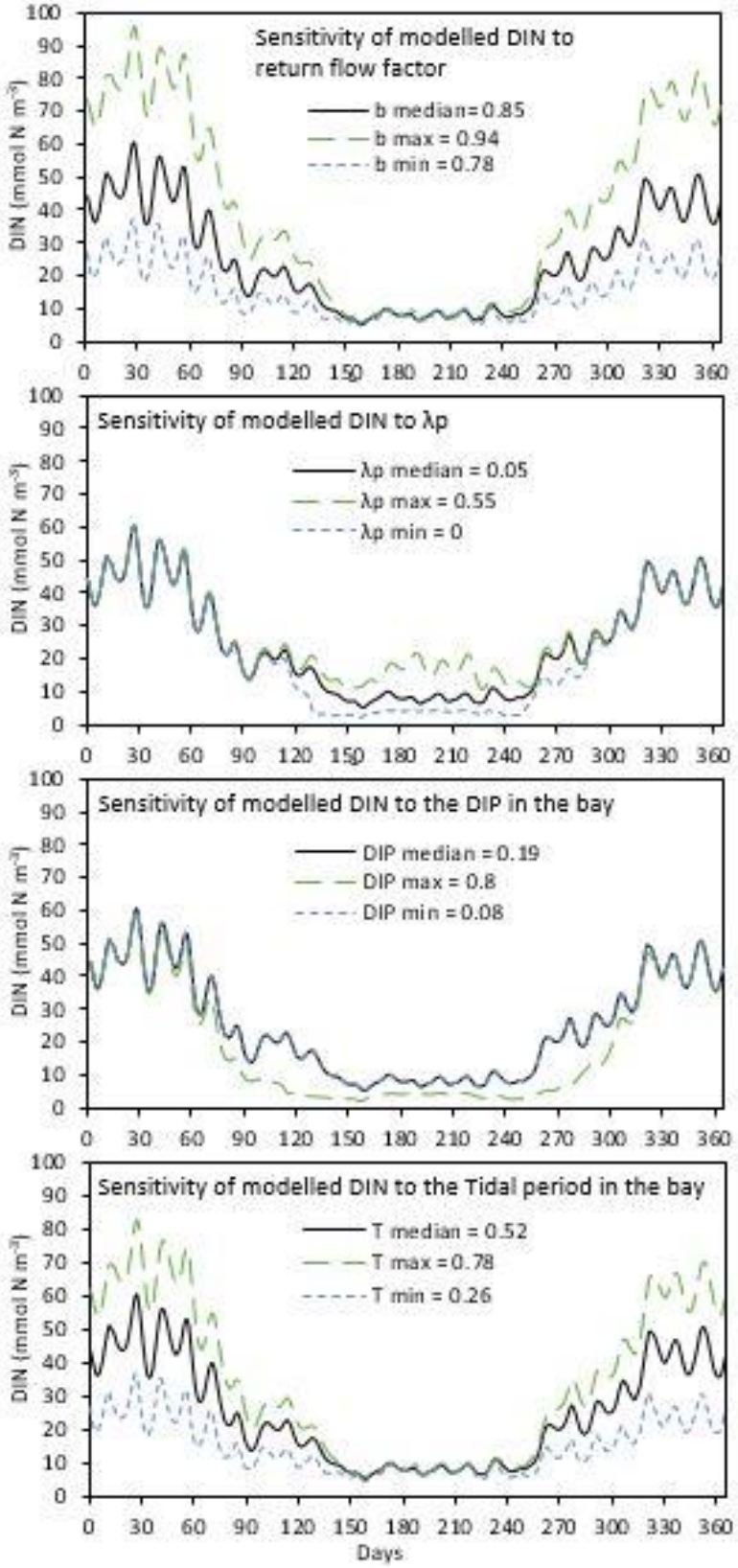

Appendix 4: Effect of modifications of the four most sensitive parameters of Cranford Model on the modelled chlorophyll a.

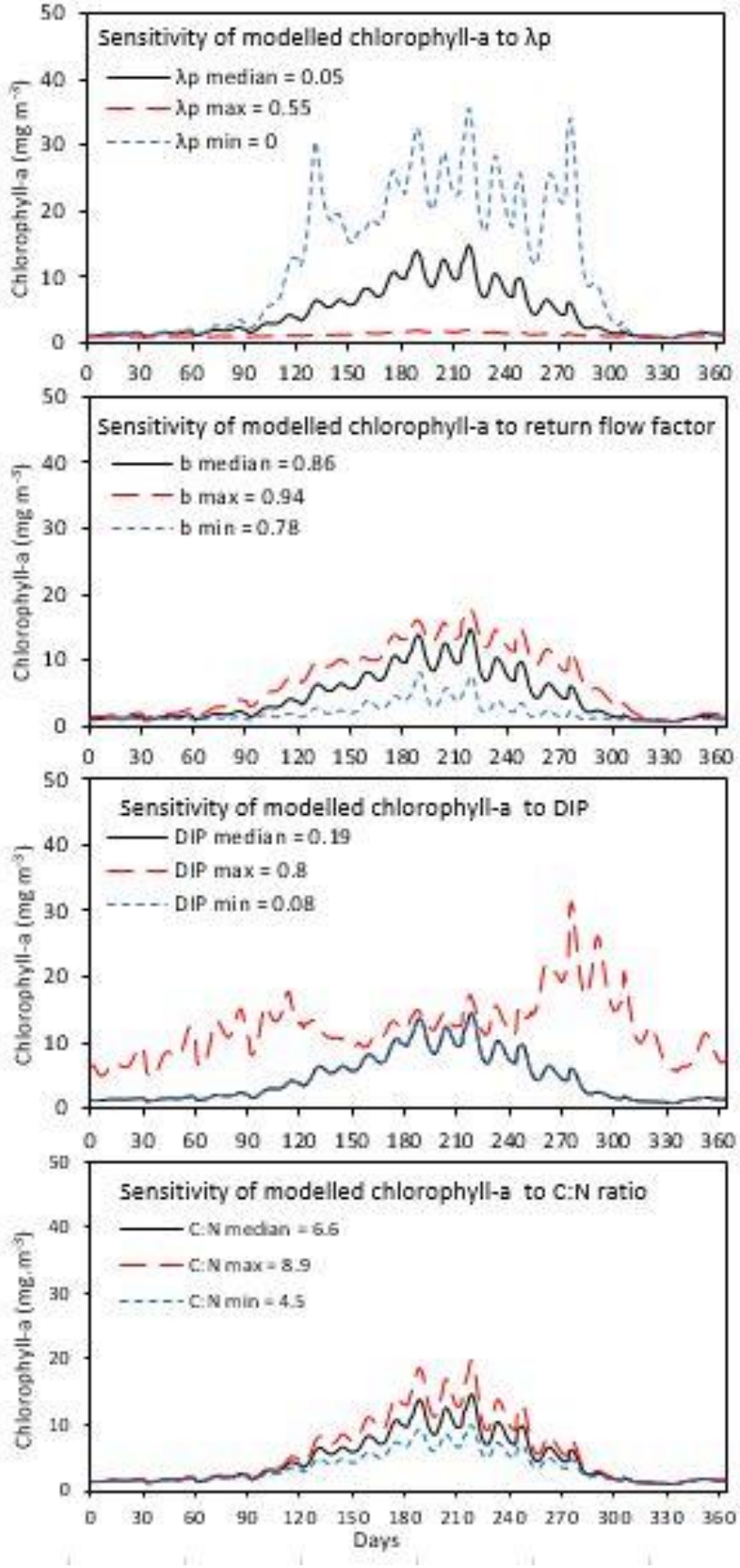

Appendix 5: Effect of modifications of the four most sensitive parameters of Cranford Model on the modelled mussel nitrogen assimilation in the bay.

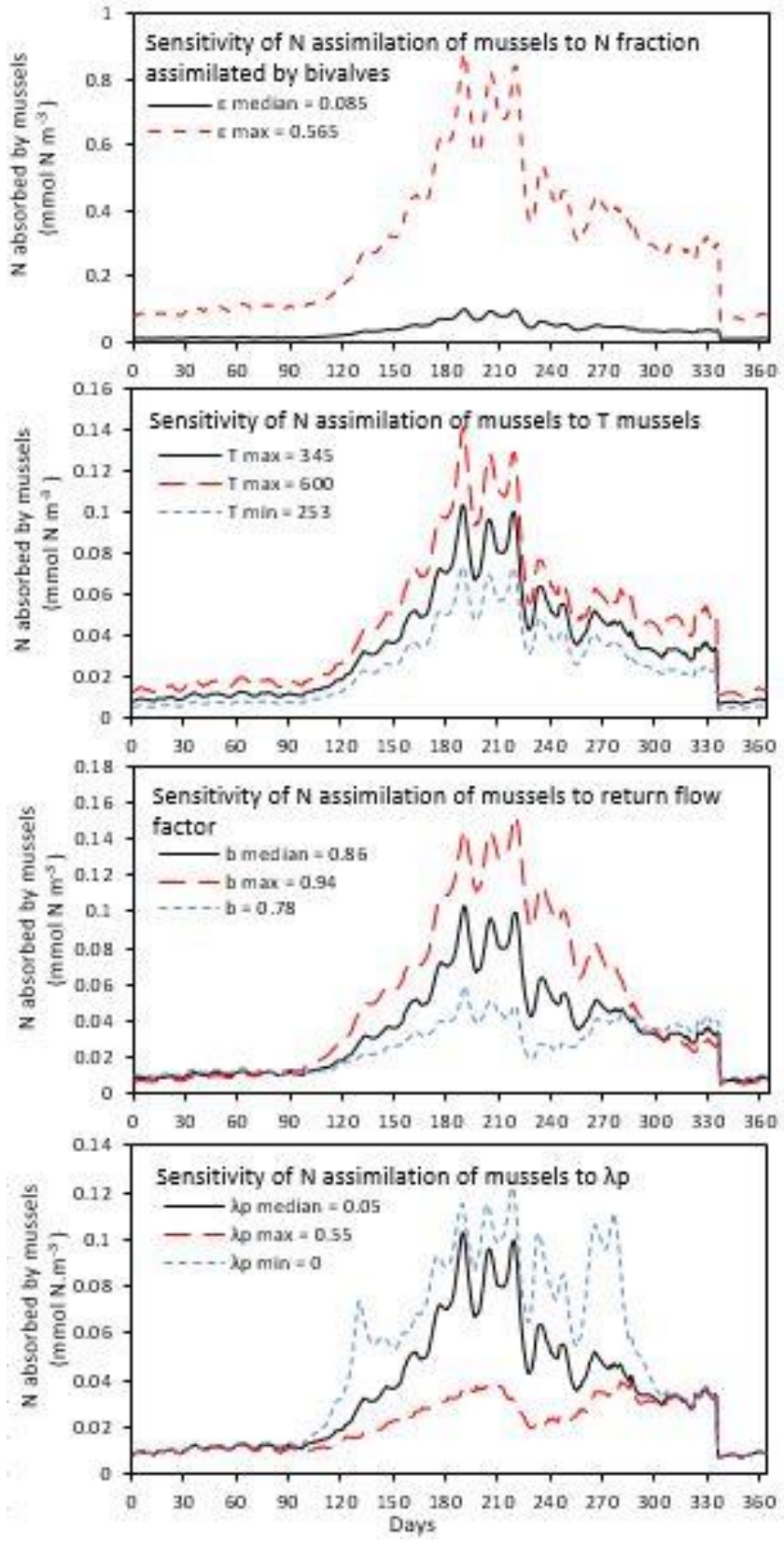

.

Appendix 6: Calculation of yp.

The expression of y_p in Dowd (2005) and Cranford et al. (2007) is:

$$y_p(t, Temp) = \frac{Chl}{C} \frac{1}{nT} \int_0^T \int_0^n g\{I(z,t); \theta(Temp)\} dz dt \quad \text{(A6.5)}$$

Where z is the water depth, t is the time, *T* is the number of hours of light in one day; *η* is the total depth of the water column; *Chl/C* is the chlorophyll-a to carbon ratio of the phytoplankton; and *g* is the growth irradiance curve as a function of light intensity *I(z,t)* and θ is the phytoplankton growth parameter, calculated using the expression of Platt et al. (1980), here using the modelled bay temperature for each timestep.

According to Platt et al. (1980), phytoplankton growth (P^B) in the absence of light saturation (*g*) is:

$$P^B = P_m^B * (1 - e^{-\frac{\propto I}{P_m^B}}) \quad \text{(A6.6)}$$

Where $P^B{}_m$ is the specific production rate at optimal light intensity (mgC (mg Chl a)$^{-1}$ hr^{-1}); $\propto$ is the initial slope of the growth curve (mgC (mg Chl a)$^{-1}$ hr^{-1} W^{-1} m^2) taken from Platt and Jassby (1976); I is the photosynthetically active radiation (PAR).

Thus:

$$yp(t, Temp) = \frac{Chl}{C} \frac{1}{nT} \int_0^T \int_0^n P_m^B * (1 - e^{-\frac{\propto I(z)}{P_m^B}}) dz dt \quad \text{(A6.7)}$$

As this model is a simplified box model for a shallow system, light attenuation in the water column is small compared to other variables, and we can approximate changes of light as a function of depth *I(z)* to a constant I_{int} in equation A6.7. I_{int} will be then the integral of *I(z)* as a function of depth, averaged by the total depth. Similarly to Jackson et al. (2017), this approximation leads to:

$$I_{int} = \frac{1}{Z_m} \int_0^Z I_0 e^{-K_d * Z_m} dz = \frac{I_0}{K_d * Z_m} (1 - e^{-K_d * Z_m}) \quad \text{(A6.8)}$$

Where I_0 is the daily (24 h) average PAR at the sea-surface and Z_m is the mixed-layer depth (Platt et al., 1991; Cloern et al., 1995), here equal to the total water depth m as Kinvarra Bay is shallow and solutes inputs are assumed to be vertically mixed at a timescale of one day.

The value of K_d was calculated as a function of the light attenuation by (1) seawater, (2) particulate concentrations and (3) phytoplankton concentration present on a given day (self-shading), following Dijkstra, et al. (2019).

$$K_d = k_{bg} + k_c\, c + k_p\, P \quad \text{(A6.9)}$$

Where K_d is the attenuation coefficient of light in the water column, k_{bg} the background light attenuation parameter for seawater (m^{-1}); k_c is the light attenuation of sediment (m^2 kg^{-1}); k_c is the light attenuation of phytoplankton (m^2 mol^{-1} N).

We can then simplify the integral in equation A6.7 using the approximation of a constant depth-averaged light field $I(z) \approx I_{int}$:

$$yp(t, Temp) = \frac{Chl}{C}\, T_{dayligh}\, P_m^B * \left(1 - e^{-\frac{\propto I_{int}}{P_m^B}}\right) \quad \text{(A6.10)}$$

Where $T_{daylight}$ is the approximate length of daylight for a given day (hours); $\propto$ is the initial slope of growth, taken from parameters of Platt and Jassby (1976) (parameter listed in Appendix 1); $P^B{}_m$ is the maximum specific production rate at optimal light intensity (mgC $mgChl^{-1}$ h^{-1}).

$P^B{}_m$ was calculated using the temperature-dependent relationship of Eppley (1972), converted from doubling/day^{-1} to mgC $mgChl^{-1}$ h^{-1} using equation 5 in Eppley (1972) and variable carbon:chlorophyll-a ratio determined from the equations and parameters for estuaries taken from Jakobsen and Markager (2016).

Appendix 7: Note on mussel growth.

Cultured mussels generally take 18 months (Rodhouse et al., 1984) to 24 month (Nunes et al., 2011) to reach marketable size, around 50-70 cm shell length in Ireland. Along the west coast of Ireland, the rope growth method is preferred, where mussels is packed into "stockings" that are suspended in the water from longlines (Maguire et al., 2007). In the lower trophic model, we considered that mussel seeds were introduced in April, similarly as done by Nunes et al. (2011) for another sheltered bay in western Ireland.

Appendix 8: 3D integration of values in Kinvarra bay.

As shown previously in section 3.5.2, median and averages can overestimate the effect of solute inputs coming from land in bays where water inputs occur in shallow areas. To allow a comparison of the relative changes of spatially variable DIN, Temperature, Salinity and Chl-a values observed for Kinvarra Bay and spatially lumped outputs given by our lower trophic model, a 3D integration of these parameter was carried out (following the recommendation from our findings in section 3.5.2).

First the EPA samples were grouped in four geographical areas, including the inner Kinvarra Bay where freshwater inputs from Kinvarra springs occur, the outer Kinvarra Bay where exchange with Galway bay occur and two intermediate boxes were mixing between. Within each of these areas, surface (depth<1 m), and deep samples were distinguished (depth>3m), to better account for mixing between these two layers, an intermediate layer was also included (1<depth<3m). The volumes of these 16 boxes at mean tide was then calculated in QGIS using a 30m bathymetry raster of the bay, considering a mean tide level at +3.377m above lowest astronomical tide (Marine Institute, 2020b). An average DIN, salinity, temperature, and Chl-a value for each box was then calculated from the EPA samples, and then multiplied by the volume of the box. Finally, all values were summed and divided by the total mean tide volume of the bay to provide units comparable with the lower trophic model.

7 Comparison of Killary harbour and Kinvarra Bay water, salt and nutrient mass balance and how it relates to previous findings in paper A to D.

In this section, mass balances of water, salt and nutrients (dissolved inorganic N and P) are built and compared for high and low discharge surveys in a bay receiving dominant SGD inputs, Kinvarra bay, and a bay receiving dominant river inputs, Killary Harbour. This approach aims to examine the effect of (a) the nature (river inputs or groundwater inputs) and (b) the quantity of water inputs from land on the balance of dissolved nutrients in enclosed bays, using the findings discussed in previous chapters.

7.1 Method used.

The water sampling surveys, and the river and SGD discharge estimates carried out in Killary Harbour and Kinvarra Bay (as described in the previous chapters) are used to build mass balances following the LOICZ approach (Gordon et al., 1996). Kinvarra Bay is shallow and does not generally have a stratification stable for a full tidal cycle, so the bay is treated as a single box for mass balance purposes at the daily timescale (following the reasons previously developed in section 6.4.2). Conversely, Killary Harbour has a depth much larger than the range of the tidal variability, and a frequent water stratification. Consequently, mass balances in the bay are made by defining two boxes (surface and deep), with a stratification limit at 10m depth, corresponding to the lower depth of the transition layer between surface and deep waters in previous surveys (Keegan and Mercer, 1986). This simplified approach allows a direct comparison between the two system, to highlight the differences between sites with and without large SGD discharge. To facilitate the comparison, only the mass balances built for surveys carried out during the periods of highest and lowest freshwater discharge (river in Killary Harbour, and fresh SGD for Kinvarra Bay) are presented here. Observed trends are put in perspective and interpreted further using the findings of the previous chapters.

7.2 Results: compared water salt and nutrient mass balance.

7.2.1 Compared water balance.

In Killary harbour, daily water discharge from land (River waters, Vq, Figure 58) during the two high and low discharge surveys are thirty to hundred times smaller than the volume of the bay (Vsys). By comparison, the daily volumes exchanged with the open ocean (Vsurf and Vd) are larger, but still more than nine times smaller than the volume of the bay. Conversely in Kinvarra bay, water inputs from land (SGD) are in the same order than the volume exchanged with the open ocean (Figure 59), 0.04-1.6*$10^6 m^3$ d^{-1} for the first, around 0.03 to 1.6 $10^6 m^3$ d^{-1} for the second, to be compared with the smaller volume of the bay of 21 $10^6 m^3$. This, salinity in Kinvarra Bay (Ss, Figure 58) tend to be lower than salinity in Killary Harbour (Ss, Figure 59). Kinvarra Bay has a hydraulic flushing time calculated with the LOICZ of between 3 and 18 days, with the larger value observed during low discharge periods (Tsys, Figure 59), while Killary Harbour has a hydraulic flushing time more stable with discharge at around 5 to 6 days (Tsys, Figure 58).

7.2.2 Compared DIP balance.

The first difference between Kinvarra Bay and Killary Harbour DIP balance is that DIP fluxes in Kinvarra Bay are accounted in mol d^{-1} while DIP fluxes in Killary Harbour in 10^2 mol d^{-1}. The fluxes of DIP provided by land derived inputs (river or SGD) and leaving the bay are lower in Kinvarra bay than in Killary Harbour, suggesting a lower P availability. P levels in Killary Harbour rivers are generally lower than in Kinvarra springs (less than or equal to 0.1 µM in Killary Harbour rivers vs. 0.2 to 0.4µM during droughts in Kinvarra spring). Despite these lower inputs, the concentrations of DIP in the two bays are similar (0.2 µM Figure 58, Figure 59, DIP budgets). The water exchange with the open ocean is transporting more P in Killary Harbour (20-30 10^2 mol d^{-1}, Figure 58) than in Kinvarra Bay (-1.4 to 3 10^2 mol d^{-1}, Figure 59).

There is a net DIP gain in deep waters and a loss in surface waters in Killary Harbour for both the high and the low discharge surveys (Figure 58). The loss of DIP in surface waters and the gain of DIP in deep waters is larger during the high discharge survey than during

the low discharge survey (Figure 58). The surface water loss in Killary Harbour increases more significantly between the low and high discharge survey than the deep-water net DIP. Consequently, the net DIP for the entire Killary Harbour is positive to balanced during the low discharge surveys and negative during the high discharge survey. This suggest an effect of temperature and light availability for surface waters net nutrient cycles, comparable at times to the effect of discharge and variable stratification.

Similarly, in Kinvarra Bay, during the low discharge surveys the DIP is positive and negative during the high discharge survey (Figure 59).

7.2.3 Compared DIN balance.

Killary Harbour had a net gain of DIN during the low discharge survey, and a net loss during the high discharge survey (Figure 58). During the low discharge survey in Killary Harbour, deep waters act as a net source of DIN while surface water act as a sink. During the high discharge survey both surface and deep waters are a sink of DIN (Figure 58). In Kinvarra Bay, there is a net loss of DIN during both the high and low discharge period, which is larger during the high discharge survey (Figure 59).

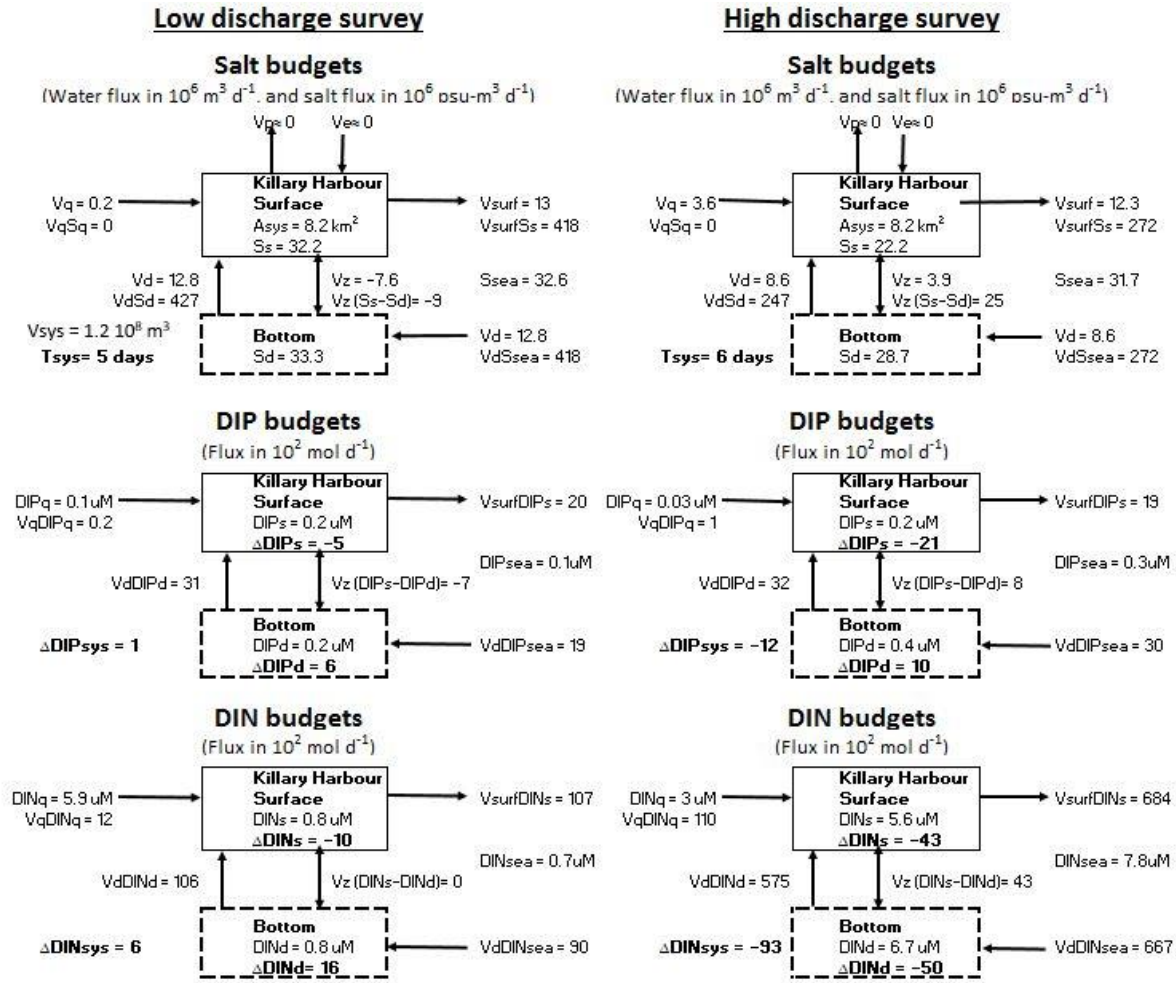

Figure 58: Budgets for water, salt, Dissolved Inorganic Nitrogen (DIN), and Soluble Reactive Phosphorus (SRP) for Killary Harbour during spring tides periods of low (2 10^5 m^3 d^{-1}, July 2018) and high river flow (3.6 10^6 m^3 d^{-1}, February 2018) .

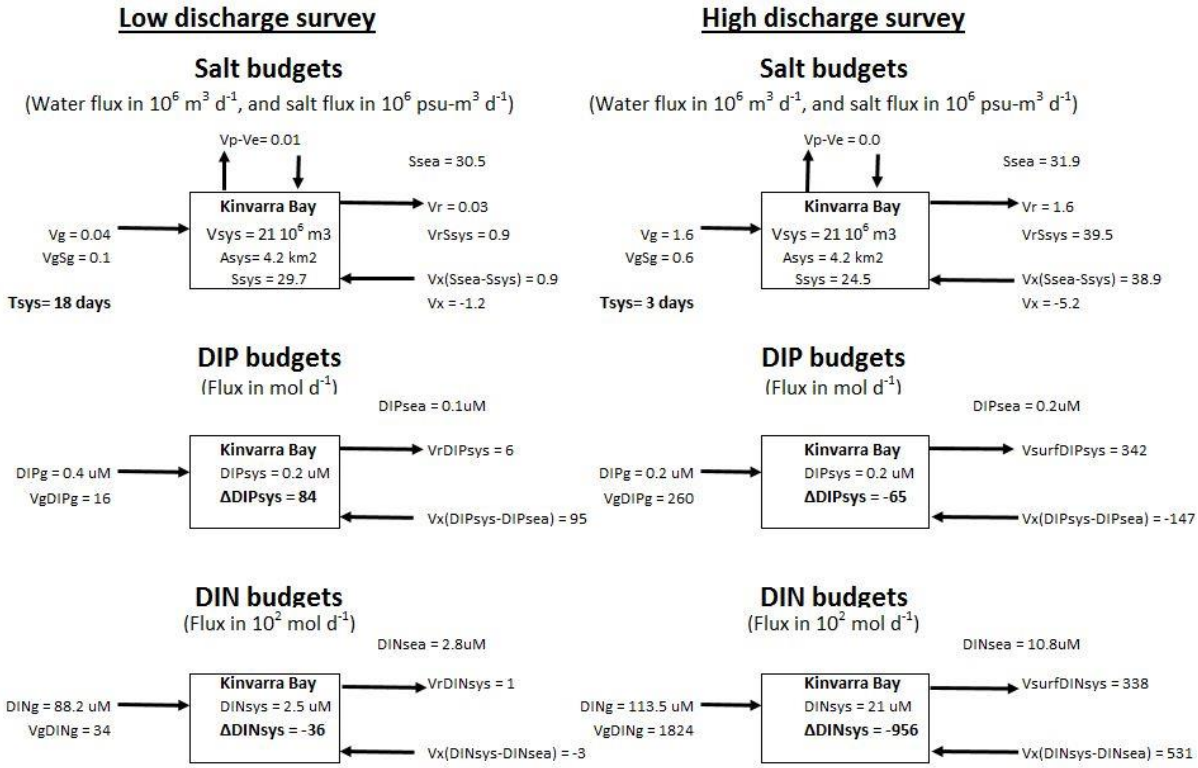

Figure 59: Budgets for water, salt, Dissolved Inorganic Nitrogen (DIN), and Soluble Reactive Phosphorus (SRP) for Kinvarra Bay during spring tides periods of low (4 10^4 m^3 d^{-1}, July 2018) and high groundwater discharge (1.6 10^6 m^3 d^{-1}, April 2018). Vg is the volume of fresh SGD coming to the bay, Vp is the rainfall, Ve is the evaporation in the system, Vr is the net exchange of water with the nearby Galway Bay, Vx is the exchange of salt occurring by diffusion to balance the salt budget.

7.3 Discussion on the water balances differences and on the trend explaining the DIN and DIP changes.

Kinvarra bay and Killary Harbour had similar ranges of hydraulic flushing times with the LOICZ approach (3-18 days for Kinvarra, 5-6 days for Killary Harbour). Chapter 3 and 5 previously showed that the two bays had similar water ages using Ra water ages. Water ages ranged between 0 and 7.5 days in Killary Harbour, and between 0 and 7.1 days in Kinvarra Bay. Section 7.2.1 showed that freshwater inputs from SGD in Kinvarra Bay are large compared to the volume of the bay and the water exchange with the outside of bay, while this is not the case in Killary Harbour which have a greater volume compared to the water inputs it receives. Consequently, the hydraulic flushing time derived from the LOICZ water balance was reduced significantly in Kinvarra Bay with decreasing discharge, but not in Killary Harbour, where exchange with the open ocean played a greater role in the renewal of the bay. For the selected surveys, the volume of the bay relative to the amount

of water it receives from groundwater, river discharge or the open ocean is thus an important element to consider, regardless of the nature of the discharge received. Another consequence of the volume difference between Kinvarra Bay an Killary Harbour was previously shown in the previous sections. Neap/spring tidal cycles, which can modify the volume of water exchanged with the open ocean have a strong effect on residence time in Kinvarra Bay (section 6) while this variability does not have such a large effect in Killary Harbour (section 5).

In Kinvarra Bay, the DIP gain of 84 mol d^{-1} observed suggest inputs of DIP to deep waters other than provided by fresh SGD and exchange with Galway Bay waters (Figure 59). This may occur, for example through fluxes from the bay floor such as coming from recirculated SGD, as suggested by the increase of Ra activities in the bay when groundwater level is low (chapter 4).

In Killary Harbour, a net gain of SRP in deep waters regardless of the discharge was observed in section 7.2.2 (Figure 58). This trend may be explained in light of the results of section 5. During spring tide periods of high discharge, when both surface and deep currents are the fastest, this section identified a change of Ra ratio, associated with larger SRP. During the highest discharge periods, turbidity also increased in deep waters at more than 1 m above bay floor. These changes were attributed to solute inputs from sediments, amplified by the cyclic resuspension deposition of bottom sediments by deep currents. These fluxes may explain part of the gain of DIP in deep waters in Killary Harbour in section 7.2.2 (Figure 58). Another influence on this trend is seasonal variability, with lower temperature and light availability favouring a lower consumption of DIP in the bay, by decreasing primary production, for which phosphorus is a limiting nutrient in this bay. The larger loss of DIP in surface water when discharge is low may be also attributed to seasonal variability of light availability and temperature, driving the variability of phosphorus cycles in surface waters by decreasing or increasing the magnitude of primary production relative to respiration/organic matter decomposition.

In the two bays, some of the dissolved P coming from the bay floor may originate from the degradation of particulate and organic P in sediment, later released from the porewater as dissolved P. As shown previously, the mechanism leading to periods of larger

P release is however different: in Killary Harbour release of porewater from bottom sediments during resuspension events could amplify the P fluxes, while in Kinvarra Bay, saline SGD during spring tides periods occurring during droughts could play a similar role. Particulate phosphorus inputs as suspended particulate matter and feces or pseudofeces from the aquaculture activities in the bays and other particulate waste may provide some of the original sources of particulate P if quickly deposited to sediment before degradation in the water column.

In Kinvarra Bay, the net losses of DIN (Figure 59) could be linked to the consumption of N by biological activity in the bay, including phytoplankton growth and the subsequent use of the N stored in phytoplankton by mussels and oysters in the bay and other organisms relying on phytoplankton as a source of food. N and P losses in surface waters in Killary Harbour surface waters (Figure 58) and Kinvarra Bay waters (Figure 59) are likely to be due to primary production and the transfer of dissolved nutrient to dissolved organic and particulate phase by other biological activity in the bay.

The net N gain in deep water during the low discharge survey in Killary Harbour (Figure 58) could be explained through the degradation of organic N to DIN in sediment, when catchment N inputs are lower and the temperature is warmer, favouring the faster degradation of DON and particulate N.

7.4 Transferable findings in other systems.

While the results of the LOICZ approach seems consistent with the other evidence provided in other chapters using radium isotopes and other tools, it is a simplified approach which require to determine inventories of nutrient and salts in the studied coastal systems. As shown previously in section 3, when the method used to calculate inventories is not accounting for the true distribution of depths (such as median or averages), inventories of a solute in a system can overestimate the effect of water inputs occurring in shallow areas. This should be kept in mind when interpreting such results. Where possible 3D integrations methods such as described in section 6.4.2 and Appendix 8 should be preferred to avoid this bias. An alternative could be also to test in a site-by-site basis if the effect of the method chosen to calculate inventories is significant.

Another challenge is the definition of stable boxes in system where the stratifications layers are not stable. This limitation has been previously discussed in section 6.6.4 for the case of the lower trophic model, which has a similar limitation than the LOICZ, but allows however to better consider the temporal variability.

The last problematic aspect of the LOICZ is when this approach is applied using averages across several survey at the same season, where conditions are assumed to be “the same”. In coastal systems, and particularly in systems receiving groundwater discharge, the variability is most frequently occurring at greater frequency than seasonal, as both tide, groundwater storage (for example) at the moment of the survey strongly influence the results (as shown for example using both observed data and modelling results in section 6). A list of other drivers of variability for SGD discharge is shown in section 2.4.2.2. As a consequence it seems preferable to apply the LOICZ only in dataset from a series of “snapshot” surveys as done in the current chapter, and then if sufficient data is available and it is not feasible to develop a full spatially distributed model for the system, use a single or multiple box model such as illustrated in section 6 to better account for the temporal variability due to the natural variability (tide, groundwater storage, temperature) between these snapshot surveys.

The effect of a given flux of water from land is much different in Kinvarra Bay, a shallow bay and in Killary Harbour, a deep bay. In Killary Harbour, the large depth favours a more frequent stratification (see paper C), and exchanges with the open ocean are generally larger than the inputs from rivers. Conversely, in Kinvarra bay, depths are in the similar order of scale than the tidal range, and exchanges with the open ocean are in similar scales than what is provided by fresh SGD. Depth is thus a critical factor to consider when estimating the effect of a given flux of water (river or SGD). Larger depths allows a greater dilution with open ocean waters of the solutes provided by the land-derived inputs at the scale of the systems. However, stratifications can also concentrate the effect of solutes in surface or deep waters as highlighted in Killary Harbour. This occurs as (1) the faster flushing of surface waters limits the effect of transfers from deep to surface waters on the concentrations of elements in surface waters and (2) the density difference between surface and deep waters limits the transfer of water and particles from bottom to surface waters, thus the effect of deep water composition on surface waters. Studies aiming at estimating the impact of SGD fluxes should thus concentrate first on shallow areas or sheltered areas with restricted exchanges with the open ocean, which are the most likely to be impacted first by solute inputs from SGD.

Both river and fresh SGD inputs provide significant N inputs that support primary production of aquatic ecosystems and aquaculture activities which depends on it. Net N loss significantly increased with rising fresh SGD/river inputs in both Kinvarra Bay and Killary Harbour. The results from modelling confirm that larger SGD fluxes tends to amplify primary production. However, once again this effect of discharge is likely to be visible only when comparing similar seasons and (for shallow sites) similar tidal stage, as illustrated by the modelling results of the lower trophic model in chapter 6. A large change of SGD inputs during winter may have a negligeable effect on primary production, compared to a small change of SGD inputs occurring during summer.

As Irish springs generally have low particulate P, and as dissolved P tends to be retained in the aquifer, fresh SGD is likely to provide less phosphorus than what a similar discharge of river water would provide. When estuarine circulation occurs in deep systems, it may provide nutrient from the outside of the system. The associated deep currents may also favour the release of solute from sediments: in Killary Harbour and Kinvarra Bay, exchange

with the outside of the bay (which are greater in Killary Harbour as a result of its greater depth) could provide larger fluxes of DIP than rivers and SGD discharge, but those were not necessarily consumed within the bay. These two combined effects may explain the much lower DIP concentrations and DIP fluxes in the LOICZ of Kinvarra Bay (DIP units in mol d^{-1} in Figure 59) compared with Killary Harbour (units in 10^2 mol d^{-1} in Figure 58), which is deeper. However, in some case, recirculated SGD can provide added dissolved P following periods of extended drought, when larger saline intrusion occurs, amplifying reactions in the aquifer leading to Ra release and P release (Paper B).

The observed solute concentrations in Killary Harbour also showed that even when groundwater-surface interactions are not important, sediment and the bay floor could still be significant sources of dissolved nutrients and solute. The LOICZ nutrient balance of Killary Harbour highlighted an apparent net gain of dissolved P in deep waters (Figure 58). As shown in Chapter 5, resuspension of sediment during periods of strong current (here during mid tides) can provide limiting nutrient such as phosphorus in this bay. Such periods can be detected through modifications of the $^{224}Ra/^{223}Ra$ activity ratios in deep waters, which become closer to Ra ratio in sediments than to Ra ratio in surface waters (generally an increase of Ra ratio but the reverse might also occur locally). When the nutrients provided to the water columns are not rapidly consumed in the bay, these events can be detected through an increase of nutrient levels in deep waters, as we did during winter in Killary Harbour in paper C. In this sense, increase of radium isotopes activities in bay water allows to identify periods when the increase of a reactive solute concentration is linked to sediment sources, either from resuspension, or SGD for example, and differentiate it from a seasonal or spatial change of reactions of the solute of interest in the water body.

8 General conclusion.

The study of Kinvarra bay illustrated that fresh SGD from karst aquifers can significantly amplify primary production in coastal areas and gave a first estimate of its effect on the local aquaculture. Saline SGD can also play an important role for this coastal ecosystem connected to a limestone karst aquifer, by providing limiting nutrients following specific periods of the year when saline intrusion is maximal. In Kinvarra Bay, these periods were deemed to be the most likely following spring tides occurring during droughts. Moreover, the findings in Killary Harbour illustrated that even in sites where SGD is not significant, solute fluxes from the bay floor can still play an important role for solute mass balances, as fine sediments are more prone to events amplifying fluxes, such as current-induced sediment resuspension. Such solute fluxes from bottom sediment or from SGD can be detected using Ra isotopes as they are frequently releasing these elements, leading to a change of activities and/or ratios.

The literature review and modelling effort illustrated that the effect of SGD on the nutrient balance of coastal systems is a non-linear function of multiple natural drivers. The flow of nutrients from SGD is dependent on sources and sinks of nutrients in catchments and aquifers, including in the subterranean estuary, but also vary with SGD flow rates. Flow rates vary broadly within a season and between years for the same period as they are the results of multiple natural drivers (in Kinvarra Bay, groundwater storage, and tide level). While the effect of tides is particularly high in shallow bays, the effect of groundwater storage on discharge is particularly high for coastlines containing karsts and is also likely in other aquifers that have (a) an inland seasonal change of groundwater level of similar or larger magnitude than tidal variability, and (b) a groundwater head close to the high tide mark during droughts. As a result, studies planning to estimate the role of SGD discharge for the annual changes in a system should consider how each survey relate to the key drivers of SGD variability, such as sea level variability and groundwater storage variability.

The two bays studied in this work had a distinct role for coastal nutrient balances during spring tides. The bay with major SGD inputs studied here, Kinvarra Bay, was generally a

sink of DIN for the spring tide surveys carried out, more significantly so during periods of high fresh SGD discharge, and either a sink (when high fresh SGD discharge occurred) or a source of SRP (during spring tides with low groundwater storage). Saline SGD could provide part of the SRP sources during these periods. Conversely, the bay with major river inputs studied here, Killary Harbour was either a net source or a sink of DIN and SRP depending on the relative magnitude of nutrient sources in deep waters and nutrient losses in surface waters. Greater SRP inputs occurred in deep waters during high discharge periods in Killary Harbour, and could be in part due to fluxes from deep sediment, amplified by resuspension/deposition of sediment.

In Kinvarra Bay, maximum flow rates for fresh SGD generally occur during low tide, high groundwater level periods (Chapter 3). Minimum fresh SGD occurs during dry periods and high tides (Chapter 3). Maximum saline SGD occurs most frequently during springs tides periods coinciding with low groundwater level, which favour saline intrusion in the aquifer (Chapter 4). This increased fraction of saline SGD could lead to periods of phosphorus enrichments in coastal waters by releasing P previously sorbed in the aquifer, thus reducing the N:P ratio of total SGD discharge and providing critical limiting nutrient for primary production in coastal areas (Chapter 4 and 6). Periods of increased saline intrusion in coastal aquifers (e.g. dry periods during spring tides) may be thus followed by enhanced primary production in coastal areas, potentially during the next groundwater recharge period, when the saline/fresh interface in the subterranean estuary moves seawards (Chapter 2 and 4), contributing to a net SRP source in the bay (section 7).

However, the effect of SGD on coastal systems is not only dependent on SGD composition but also on the time SGD waters stay within coastal ecosystems. Specific zones in coastal bays store the solute inputs from sediments and SGD preferentially. Stratification (e.g. in Killary Harbour in Chapter 5) favours the retention of solutes coming from submarine fluxes in deep or surface waters, while areas where natural barriers or enclosed bays restrict the tidal exchange (e.g. Kinvarra Bay in Chapter 3) also concentrate SGD fluxes coming to them for several tidal cycles. Such areas concentrating SGD fluxes will be the first modified by changes of SGD discharge and should be accounted for and surveyed in priority to determine the variable effect of SGD on the ecosystems that they contain.

Another finding was that the progressive mixing of SGD waters with ocean water along estuaries can potentially bias estimates of SGD flow to coastal areas based on conservative or non-conservative tracers (Chapter 3). Mass balances approaches to assess SGD typically use system averaged values to compute inventories of ^{222}radon or ^{223}Ra, ^{224}Ra. These tracers may have decayed (and for radon, degassed) in an exponential manner when getting farther from a point that is source of the tracer, such as a coastal spring. In such conditions, averages are likely to underestimate the inventory of the SGD tracer, unless the spatial variability of flushing is corrected for. Chapter 3 demonstrates so by comparing the SGD estimates from non-conservative tracers with SGD estimates using conservative tracers and modelling. The results suggest that this issue may be addressed by correcting for decay and degassing of the tracer in a location-specific manner using water ages values, estimated from modelling or ^{224}Ra/^{223}Ra. The correction using radium ratios leads to ranges of SGD rates more compatible with other methods. Models or experiments using drifters may also help getting estimates of water ages for doing such corrections (See section 2.4.3.2 for references on the available methods). Even after this correction was carried out, the discharge estimates derived from radon during one of the high groundwater levels was lower than the estimated fresh discharge during this survey. Groundwater-surface interactions, such as those occurring in turlough may also lead to greater losses of radon from groundwater to the atmosphere, thus lower radon levels in SGD discharge. If springs are fed by water coming from distinct pathways, this could lead to radon activities lower than equilibrium activities in SGD discharge points connected to conduits with fast flow linked with turlough, and radon activities at or close to equilibrium in others. When this occur and if these springs are not included in the spring end member radon activity due to lack of accessibility or non-identification of the springs, this could lead to underestimation of SGD discharge. A similar difference could derive from a greater discharge of groundwater through springs above sea level during high discharge surveys, leading to additional inputs of radon depleted groundwater to the bay.

SGD estimates based on conservative tracers on the other hand (e.g. salinity for fresh SGD or ^{226}Ra), can vary significantly depending on the method chosen to integrate the values across the system, which create a significant bias derived not from the dataset, but from the choice of the method to integrate the inventory. Comparing different methods

is a way to assess the effect of this bias on the final SGD estimate. Where sufficient data is available, the 3D shape of the bay or coastal system should be accounted for to compute more accurate inventories through a 3D integration of interpolated values (e.g. IDW method or kriging) or dividing the bay in several boxes with limits based on the knowledge of the system variability of stratification and mixing. When these steps cannot be applied due to lack of data or resources, the uncertainty due to the integration step should be kept in mind and where possible, assessed or discussed to allow more robust estimates of SGD.

In chapter 6, the observations on the variability of nutrient fluxes from SGD and flushing are used to build a model of the effect of SGD on Kinvarra Bay, a coastal bay receiving large SGD fluxes. The analysis of the variability of mussel production, nutrient levels and chlorophyll-a level in Kinvarra Bay and the application of a lower trophic model for the system suggest that SGD amplifies the chlorophyll-a concentrations in the bay and directly benefits the local mussel aquaculture during the growing season. Phosphorus availability in the bay is also critical to allow phytoplankton to absorb a greater fraction of the nitrogen provided by SGD and benefit mussel growth in the bay, as the groundwater flowing to Kinvarra Bay provides only small quantities of it compared to nitrogen. Outside of the main growing season, the effect of SGD on modelled chlorophyll-a and mussels N assimilation was small, and most provided nutrients were either stored in sediment or exported to the outside of the bay. At a modelled phosphorus level in the lower end of the annual variability in the bay (0.08 mmol m^{-3}), the effect of SGD on phytoplankton was much lower than at higher phosphorus level, corresponding to the upper end of the annual variability in the bay (0.8 mmol m^{-3}). Neap/spring tides cycles led to changes in modelled residence time, chlorophyll-a levels and DIN with 25 days periods. The effect of SGD on shallow systems similar to Kinvarra Bay, where the tidal prism volume is large compared to the total bay volume, is thus likely to be variable, with larger effects during neap tides.

Finally, the model results are used to test the effect of current fluctuation of fresh SGD discharge (estimated through a groundwater discharge relationship using the previous SGD discharge data) and future temperature rise on the bay primary production and mussel production. Increase of average sea water temperature could amplify the

modelled phytoplankton biomass in the bay during spring and autumn but had less effect on phytoplankton biomass during mid-summer. This agrees with previous studies which predicted an extension of the growth period of phytoplankton as a result of climate change in Ireland. During the 2006 and 2018 period modelled Chl-a at levels were optimum for mussel growths when a peak of SGD occurred at the beginning of the growth season, followed by low fresh SGD during summer. During these periods, mussel production in the bay was maximal. Conversely, when SGD rates were larger during the growth period of phytoplankton, leading to modelled Chl-a outside of the optimum level for mussel growth, and the next winter had peak fresh SGD rates and flood in the catchment, the next mussel harvest was in the lower end of the interannual variability. This suggest that the timing of SGD rates have a significant impact on phytoplankton blooms and thus may affect mussel growth and mortality rates. As climate change in this part of Ireland is likely to increase the frequency of dry periods during summer and large rainfall events during winter, creating a modification of the patterns of SGD rates during the year, the impact of these changes deserves further research to determine whether positive (through increased primary production during summer) or negative changes (metabolic stress during peak SGD fluxes) may be expected.

It is likely however, that the changes of phytoplankton communities in the bay, and the phosphorus cycling in the system not fully accounted for in this model also play an important role and should be assessed in further studies. Our scenario testing section estimate the potential effect of phytoplankton changes on the model output (section 6.5.4.4), and changes of phosphorus availability (Section 6.5.4.2) and may serve as a base of thought to develop further research to assess the effect of potential effect of phytoplankton changes and phosphorus cycling on the primary production of the system.

In either case, taking early preventive measure aimed at reducing potential negative impacts on coastal ecosystems with extensive groundwater/surface interactions are likely to be beneficial. These are discussed in the next section.

9 Water management in the catchment of bays receiving large fresh SGD discharge.

Considering the impact of SGD on aquaculture, management strategies in a coastal system should account for the effect of groundwater/surface interactions. For example, in coastal ecosystems hosting aquaculture activities, the development of management strategies should account for the additional fluxes of nutrient provided by SGD. This would be important for instance to adapt aquaculture to the amount of nutrient available for primary production in the coastal ecosystem, so as to avoid detrimental effects on the ecosystem.

Another example may involve maintaining the exposure of filter feeders to optimum levels of SGD fed blooms for their growth requirements, while limiting the contact with "pure " SGD water, where the physicochemical characteristics could be potentially stressful for filter feeder growth (e.g. quick salinity fluctuations, in some cases reduced DO). This last strategy may be applied, for example, by choosing locations for aquaculture that are close enough to an SGD site in order to have optimum phytoplankton biomass during summer low SGD discharge periods. At the same time, they should be sufficiently far from fresh SGD sources to be exposed to minimum fresh water related stress during winter high SGD discharge periods. As SGD rates and composition vary seasonally, the optimum location for aquaculture in an SGD site may vary as a function of groundwater level and nutrient levels in the discharged waters, for example. This strategy is currently applied by aquaculture farmers in Kinvarra Bay, who chose the location of the raft such as to be close to a spring, but in a section of the bay with sufficient depth to have less salinity fluctuations. While this solution may be best in terms of aquaculture production, adopting such measures may not be always practical and resource optimal in environment with water chemistry and volume which are quickly changing, particularly if the variations are large enough to require the movement of the aquaculture rafts or lines.

An alternative and potentially complementary solution is to consider the presence of an ecosystem influenced by SGD downstream during the development of catchment and groundwater management policy such as to ensure the SGD flow have (or keep having)

desirable effect on the ecosystem and on the local aquaculture. In sites with dominant SGD inputs, if phytoplankton biomass above optimum levels are observed during low groundwater periods, limiting saline intrusion in the aquifer during drought through appropriate water management should help to limit the added P load from recirculated SGD due to saline intrusion in the aquifer. This could contribute to optimise the value of SGD discharge for aquaculture. For example in Kinvarra bay, groundwater pumping for water supply could be reduced when spring tide periods coincide with low groundwater levels (e.g. level in close to the main conduit feeding Kinvarra spring close to the high tide marks during drought period). This measure is already in place to limit salt contaminations in Kinvarra water supply during spring tides occurring during droughts (Irish Water, personal communication), and its benefit for aquaculture in the bay may merit further investigation. These previous observations suggest that such a measure might also limit the release into the system by seawater recirculation of solutes stored previously in sediment and the aquifer.

During high groundwater level periods, on the other hand, the higher fresh SGD fluxes coupled with stratification might create stressful conditions for marine organism (including thus aquaculture activities) that are the closest to the SGD spring, particularly during neap tides periods when the flushing of the system is lower. In such a context, reducing or limiting the discharge of fresh water to the system during neap tide periods is likely to reduce the stress of filter feeders and other fixed organisms during high discharge periods (where such stress is present). In reality, however, land-use practices in a catchment often vary with time. Land artificialisation and modification of the drainage network can lead to modifications of the timing of the peak flow rate of freshwater, which could affect positively or negatively filter feeder's mortality rates, when combined with other drivers already at play (food availability, predations, environmental stress etc..). In Kinvarra Bay, a project is in place to favour the discharge to the bay as surface flow to divert part of the groundwater flow accumulating in the catchment turloughs and creating flood risk in the surrounding lands (e.g. in Morrissey et al., 2020). This measure, while likely contributing to solve the flood risk problem in the area, raise concerns of aquaculture stakeholders that it might affect salinity and other water chemistry parameters in the bay, reducing the growth of filter feeders in Kinvarra Bay. A study

showed that the effect of this added flow on salinity was not likely to be significant if the bay was fully mixed (Morrissey et al., 2020). However, another recent study showed that, under low flow conditions, the bay was not likely to be fully mixed during neap tide and was stratified, being more vertically mixed during spring tides (Gregory et al., 2020). This observation of significant neap tide stratification in Kinvarra Bay suggests that this added water will have the largest effect on Kinvarra Bay solute level and salinity during neap tide periods. Our modelling results accounting for changes of the tidal prism due to neap/spring tide cycles confirm this previous finding.

Following this observation, if the discharge considered allows it, a different flow rate could be allowed to flow to the bay during neap and spring tide, as a precaution measure, for example through the use of a weir of adaptable level. If, as a precautionary measure, the flow is reduced during neap tides, periods when the bay is most likely to become and remain stratified (Gregory et al., 2020), this should limit the potential effect on aquaculture activities of the discharge from the turloughs waters diverted as surface flow to the bay. This stored flow might be then released at a higher rate during spring tides, when the bay is more likely to be flushed more efficiently, to reduce to the maximum the effect of the added flow to the local aquaculture. The benefit of such measure on the bay biogeochemistry could be checked by several surveys of the salinity, nutrient and phytoplankton structure during neap and spring tides when groundwater level measured at Killiny borehole is above 7 m before and after implementation.

In the longer term, and in particular in a context of climate change, an alternative path to reduce the effect of flood from turlough while limiting the peak discharge to the bay (thus winter stress for filter feeders in the bay) may be to act further on the natural water storage in the catchment. This may be done by favouring passive management flood risk strategies in the upper catchment (a review is given in Dadson et al., 2017). Natural Flood Management (NFM) describes the restoration of natural hydrological functions in systems to reduce downstream flood risk. Peat bog, transitional woodland shrubs and forests cover most of the upper Kinvarra catchment (Figure 34). Restoration and preservation measure of peat bogs can reduce peak discharge and increase lag times significantly

(Shuttleworth et al., 2019). Afforestation and limiting soil impermeabilization is another potential measure (Dittrich et al., 2019). Favouring such measure, or making sure that they keep being applied, might, in turn, affect the aquaculture positively by reducing the winter nutrient load and the stress to filter feeder due to salinity and other parameter fluctuations related to peak winter fresh SGD.

10 Further developments to assess and manage the effect of SGD in coastal Irish sites.

Considering the significant impact of SGD nutrient loads and of the timing of SGD rates for nutrient concentration, Chl-a levels and mussel production in coastal bays, assessing the impact of SGD for more sites in Ireland would benefit the preservation of coastal ecosystems and aquaculture activities. However, this work identifies three mains obstacles to assess the impact of SGD at country scale, using the example of Ireland.

First, the effect of variable tide and water inputs from land on the variability of flushing and stratification of transitional waters and estuaries has been assessed for only a few systems in Ireland. This lack of knowledge is an obstacle for an accurate estimation of the environmental effects of water inputs from rivers or SGD on aquaculture. The effect of a given water input on the nutrient ratios and primary production of coastal ecosystems depends on its residence time and stratification (Chapter 2, Chapter 54, Chapter 6).

The second knowledge gap is the lack of measurements of SGD tracers at sufficient spatial and temporal resolution representative of the short-term variability of SGD in Ireland. Existing equipment to measure tracers of SGD are appropriate for surveys of length of a week or less but less so for annual continuous surveys, as they have a large volume and are humidity sensitive. The further development of affordable, compact sensors (e.g. for radon) and use of existing methods to detect SGD in more sites would allow measuring the annual variability of SGD without having to assume stable SGD fluxes between repeated surveys or to relate them to groundwater level recorded along preferential pathways for groundwater flow as done in this work. SGD fluxes are the results of multiple drivers at annual, daily and hourly scales. The measurement timescale allowed by the current technologies and previous studies are appropriate to assess during field surveys the effect of groundwater level variability and tidal variability on SGD flow, but other influences may be less predictable and difficult to capture with sampling restricted in time or space (Chapter 2, Table 1).

Finally, this work confirmed that the effect of SGD on primary production on coastal ecosystems is not a linear function of the amount of SGD discharged to coastal areas. This finding contradicts the assumption taken by Pongkijvorasin et al. (2010) of algae growth

being a linear function of salinity to develop an optimum strategy to manage groundwater abstraction value while preserving the value of algae growth. Given the observed non-linearity, a detailed assessment of the biogeochemical changes occurring when groundwater level (or SGD discharge) varies is likely to be more helpful for the preservation of marine ecosystem affected by SGD than a model assuming that effect of SGD is linearly related to discharge rates.

A first step to develop this understanding at country scale could be to monitor on more sites changes of nutrient concentrations in intertidal springs and inland boreholes around Irish aquaculture sites on similar days than bay water samples and under different groundwater level conditions. If included in environmental monitoring, this data collection, coupled with appropriate mass balances (e.g. as in Chapter 7) or models (from box model as used in Chapter 6 to spatially distributed model including time variable nutrient balances for example) should help the development of an understanding of the range of the different dynamics of subterranean estuaries across Ireland. These are among the conditions to help to achieve the protection of Irish coastal ecosystems under a changing climate while allowing the growth of the aquaculture sector. Further coordination between the EPA sampling campaigns and the Marine Institute may help to provide the data necessary to achieve this goal.

Another aspect is the effect of climate change and SGD variability on phytoplankton communities, their nutrient ratio and growth rates. Depending on the changes occurring in phytoplankton communities, the cycling of nutrient is likely to be modified, and may change the effect of other drivers (e.g. changes of phosphorus availability, temperature, rainfall patterns) on primary production and on the organisms depending on it, thus affecting aquaculture growth. Developing the understanding of these effects would provide information to improve forecast models of the changes to be expected (or already occurring) in aquatic ecosystem, including those influenced by groundwater/surface interactions. If we consider the lower trophic model used in this work (Chapter 6), improvements could include more accurate estimates of the variability of SGD discharge, coupled with an inventory of the seasonal variability of nutrient ratio and Chl-a nutrient ratio in phytoplankton and of the seasonal variability of particulate organic matter and phosphorus cycling.

11 References

Abdelrhman, M.A., 2005. Simplified modeling of flushing and residence times in 42 embayments in New England, USA, with special attention to Greenwich Bay, Rhode Island. Estuar. Coast. Shelf Sci.

Abril, G., Nogueira, M., Etcheber, H., Cabeçadas, G., Lemaire, E., Brogueira, M.J., 2002. Behaviour of organic carbon in nine contrasting European estuaries. Estuar. Coast. Shelf Sci. 54, 241–262.

Alber, M., Sheldon, J.E., 1999. Use of a date-specific method to examine variability in the flushing times of Georgia estuaries. Estuar. Coast. Shelf Sci. 49, 469–482.

Allen, A., 1976. Outline of the hydrogeology of the superficial formations of the Swan Coastal Plain. West. Aust. Geol Surv Ann Rep 31–42.

Allen, A.P., Gillooly, J.F., Brown, J.H., 2005. Linking the global carbon cycle to individual metabolism. Funct. Ecol. 19, 202–213.

Altieri, A.H., Gedan, K.B., 2015. Climate change and dead zones. Glob. Chang. Biol. 21, 1395–1406.

Anderson, D.M., Hoagland, P., Kaoru, Y., White, A.W., 2000. Economic impacts from harmful algal blooms (HABs) in the United States. Natl. Ocean. Atmos. Adm. Norman OK Natl. Sev. Storms Lab No. WHOI-2000-11.

Anderson, J.J., 1982. The nitrite-oxygen interface at the top of the oxygen minimum zone in the eastern tropical North Pacific. Deep Sea Res. Part A, Oceanogr. Res. Pap. 29, 1193–1201.

Andrews, J.C., Muller, H., 1983. Space-time variability of nutrients in a lagoonal patch reef. Limnol. Oceanogr. 28, 215–227.

Anika, S., Cassandra De, Y., 2016. Climate Change Implications for Fisheries and Aquaculture. Summary of the findings of the IPCC Fifth Assessment Report, FAO Fisheries and Aquaculture Circular.

Appelo, C.A.J., Postma, D., 1993. Geochemistry, groundwater and pollution. Geochemistry, Groundw. Pollut.

AQUAFACT International Services Ltd, 2013. Killary Mussel Licence Renewal Appeal.

AQUAFACT International Services Ltd, 2012. Subtidal Benthic Investigations in Galway Bay.

Aquaread, 2013. Instruction Manual for the Aquaprobe® AP.

Arfib, B., de Marsily, G., Ganoulis, J., 2007. Locating the Zone of Saline Intrusion in a Coastal Karst Aquifer Using Springflow Data. Ground Water 45, 28–35.

Atkinson, M.J., Smith, S. V., 1970. C : N : P ratios of benthic marine plants. Limnology 28, 568–574.

Barbier, E., Hacker, S., Kennedy, C., Koch, E., Stier, A., Silliman, B., 2011. The value of estuarine and coastal ecosystem services. Ecol. Monogr. 81(2), 169–193.

Barwell, V.K., Lee, D.R., 1981. Determination of horizontal-to-vertical hydraulic conductivity ratios from seepage measurements on lake beds. Water Resour. Res.

Basterretxea, G., Tovar-Sanchez, A., Beck, A.J., Masqué, P., Bokuniewicz, H.J., Coffey, R., Duarte, C.M., Garcia-Orellana, J., Garcia-Solsona, E., Martinez-Ribes, L., Vaquer-Sunyer, R., 2010. Submarine Groundwater Discharge to the Coastal Environment of a Mediterranean Island (Majorca, Spain): Ecosystem and Biogeochemical Significance. Ecosystems 13, 629–643.

Bates, S., Garrison, D., Horner, R., 1998. Bloom Dynamics and Physiology Producing Pseudo-nitzschia Species. NATO ASI Ser. G Ecol. … 267–292.

Bayne, B., Worrall, C., 1980. Growth and Production of Mussels Mytilus edulis from Two Populations. Mar. Ecol. Prog. Ser. 3, 317–328.

BBC news, 2009. BBC NEWS | Europe | Seaweed suspected in French death [WWW Document]. Bbc. URL http://news.bbc.co.uk/2/hi/8242649.stm (accessed 12.23.17).

Bear, J., 1979. Hydraulics of groundwater.

Bear, J., Cheng, A.H.-D., Sorek, S., Ouazar, D., Herrera, I., 1999. Seawater Intrusion in Coastal Aquifers - concepts, methods and practises. Geophys. Investig. pp 9-50.

Beck, A.J., Tsukamoto, Y., Tovar-Sanchez, A., Huerta-Diaz, M., Bokuniewicz, H.J., Sañudo-Wilhelmy, S.A., 2007. Importance of geochemical transformations in determining submarine groundwater discharge-derived trace metal and nutrient fluxes. Appl. Geochemistry 22, 477–490.

Behrenfeld, M.J., 2014. Climate-mediated dance of the plankton. Nat. Clim. Chang.

Behrenfeld, M.J., 2010. Abandoning sverdrup's critical depth hypothesis on phytoplankton blooms. Ecology 91, 977–989.

Behrenfeld, M.J., O'Malley, R.T., Siegel, D.A., McClain, C.R., Sarmiento, J.L., Feldman, G.C., Milligan, A.J., Falkowski, P.G., Letelier, R.M., Boss, E.S., 2006. Climate-driven trends in contemporary ocean productivity. Nature 444, 752–755.

Behrenfeld, M.J., Randerson, J.T., McClain, C.R., Feldman, G.C., Los, S.O., Tucker, C.J., Falkowski, P.G., Field, C.B., Frouin, R., Esaias, W.E., Kolber, D.D., Pollack, N.H., 2001. Biospheric primary production during an ENSO transition. Science (80-.). 291, 2594–2597.

Berdalet, E., McManus, M.A., Ross, O.N., Burchard, H., Chavez, F.P., Jaffe, J.S., Jenkinson, I.R., Kudela, R., Lips, I., Lips, U., Lucas, A., Rivas, D., Ruiz-de la Torre, M.C., Ryan, J., Sullivan, J.M., Yamazaki, H., 2014. Understanding harmful algae in stratified systems: Review of progress and future directions. Deep. Res. Part II Top. Stud. Oceanogr. 101, 4–20.

Berdalet, E., Montresor, M., Reguera, B., Roy, S., Yamazaki, H., Cembella, A., Raine, R., 2017. Harmful Algal Blooms in Fjords, Coastal Embayments, and Stratified Systems: Recent Progress and Future Research. Oceanography 30, 46–57.

Berge, J., Johnsen, G., Nilsen, F., Gulliksen, B., Slagstad, D., Pampanin, D.M., 2006. The Mytilus edulis population in Svalbard: How and why. Mar. Ecol. Prog. Ser. 309, 305–306.

Billerbeck, M., Werner, U., Polerecky, L., Walpersdorf, E., DeBeer, D., Huettel, M., 2006. Surficial and deep pore water circulation governs spatial and temporal scales of nutrient recycling in intertidal sand flat sediment. Mar. Ecol. Prog. Ser. 326, 61–76.

BIM, 2019. Aquaculture Report 2019. Natl. Seaf. Surv. Aquac. Rep. 2019 National Seaffod Survey Aquaculture report 2019.

BIM, 2018a. Kinvarra Bay aquaculture production dataset.

BIM, 2018b. Ireland aquaculture National production trends dataset.

BIM, 2018c. Killary Harbour aquaculture production dataset.

Bogli, A., 1964. Corrosion par melange des eaux. Int. J. Speleol. 61–70.

Bokuniewicz, H.J., 1992. Analytical descriptions of subaqueous groundwater seepage. Estuaries 15, 458–464.

Boldovski, N., 1996. Groundwater flow in the coastal zone of the east Sikhote-Alin' volcanogenic belt. Proc. Int. Symp. Groundw. Disch. Coast. Zo. Land–Ocean Interact. Coast. Zo. (LOICZ), Moscow, July 6–10 8–15.

Bollinger, M.S., Moore, W.S., 1993. Evaluation of salt marsh hydrology using radium as a tracer. Geochemica Cosmochim. Acta 57, 2203–2212.

Bonacci, O., 1987. Karst Hydrology : With Special Reference to the Dinaric Karst. Springer Berlin Heidelberg.

Borges, A. V., 2005. Do we have enough pieces of the jigsaw to integrate CO2 fluxes in the coastal ocean? Estuaries 28, 3–27.

Bosch-Belmar, M., Azzurro, E., Pulis, K., Milisenda, G., Fuentes, V., Kéfi-Daly Yahia, O., Micallef, A., Deidun, A., Piraino, S., 2017. Jellyfish blooms perception in Mediterranean finfish aquaculture. Mar. Policy 76, 1–7.

Boudreau, B.P., Huettel, M., Forster, S., Jahnke, R.A., McLachlan, A., Middelburg, J.J., Nielsen, P., Sansone, F., Taghon, G., Van Raaphorst, W., Webster, I., Weslawski, J.M., Wiberg, P., Sundby, B., 2001. Permeable marine sediments: Overturning an old paradigm. Eos (Washington. DC). 82, 133–136.

Boulêtreau, S., Salvo, E., Lyautey, E., Mastrorillo, S., Garabetian, F., 2012. Temperature dependence of denitrification in phototrophic river biofilms. Sci. Total Environ. 416, 323–328.

Boycott, T., Bunce, C., Cronin, P., Drew, D., Farrant, A., Hobbs, S., Mullan, G., Self, C., Simms, M., Wilson, L., 2003. Caves of County Clare and South Galway.

Boynton, W.R., Garber, J.H., Summers, R., Kemp, W.M., 1995. Inputs, Transformations, and Transport of Nitrogen and Phosphorus in Chesapeake Bay and Selected Tributaries. Estuaries 18, 285–314.

Braca, G., 2008. Stage – Discharge Relationships in Open Channels : Practices and Problems, Agency for Environmental Protection and Technical Services, Rome, Italy.

Bratton, J.F., 2010. The Three Scales of Submarine Groundwater Flow and Discharge across Passive Continental Margins. J. Geol. 118, 565–575.

Buddemeier, R.E., 1996. Groundwater discharge in the coastal zone: proceedings of an international symposium, Texel, The Netherlands. LOICZ/R and S/96-8, iv+179 pp. LOICZ.

Burnett, W.C., Aggarwal, P.K., Aureli, A., Bokuniewicz, H., Cable, J.E., Charette, M.A.,

Kontar, E., Krupa, S., Kulkarni, K.M., Loveless, A., Moore, W.S., Oberdorfer, J.A., Oliveira, J., Ozyurt, N., Povinec, P., Privitera, A.M.G., Rajar, R., Ramessur, R.T., Scholten, J., Stieglitz, T., Taniguchi, M., Turner, J.V., 2006. Quantifying submarine groundwater discharge in the coastal zone via multiple methods. Sci. Total Environ. 367, 498–543.

Burnett, W.C., Bokuniewicz, H., Huettel, M., Moore, W.S., Taniguchi, M., 2003. Groundwater and pore water inputs to the coastal zone. Biogeochemistry 66, 3–33.

Burnett, W.C., Dulaiova, H., 2003. Estimating the dynamics of groundwater input into the coastal zone via continuous radon-222 measurements. J. Environ. Radioact. 69, 21–35.

Burnett, W.C., Kim, G., Lane-Smith, D., 2001a. A continuous monitor for assessment of 222 Rn in the coastal ocean. J. Radioanal. Nucl. Chem. 249, 167–172.

Burnett, W.C., Peterson, R., Moore, W.S., de Oliveira, J., 2008. Radon and radium isotopes as tracers of submarine groundwater discharge - Results from the Ubatuba, Brazil SGD assessment intercomparison. Estuar. Coast. Shelf Sci. 76, 501–511.

Burnett, W.C., Taniguchi, M., Oberdorfer, J., 2001b. Measurement and significance of the direct discharge of groundwater into the coastal zone. J. Sea Res. 46, 109–116.

Callaway, R., Shinn, A.P., Grenfell, S.E., Bron, J.E., Burnell, G., Cook, E.J., Crumlish, M., Culloty, S., Davidson, K., Ellis, R.P., Flynn, K.J., Fox, C., Green, D.M., Hays, G.C., Hughes, A.D., Johnston, E., Lowe, C.D., Lupatsch, I., Malham, S., Mendzil, A.F., Nickell, T., Pickerell, T., Rowley, A.F., Stanley, M.S., Tocher, D.R., Turnbull, J.F., Webb, G., Wootton, E., Shields, R.J., 2012. Review of climate change impacts on marine aquaculture in the UK and Ireland. Aquat. Conserv. Mar. Freshw. Ecosyst. 22, 389–421.

Carmichael, S.K., Zorn, B.T., Santelli, C.M., Roble, L.A., Carmichael, M.J., Bräuer, S.L., 2015. Nutrient input influences fungal community composition and size and can stimulate manganese (II) oxidation in caves. Environ. Microbiol. Rep. 7, 592–605.

Carpenter, S.R., Caraco, N.F., Correll, D.L., Howarth, R.W., Sharpley, A.N., Smith, V.H., 1998. Nonpoint pollution of surface waters with phosphorus and nitrogen. Ecol. Appl. 8, 559–568.

Cave, R.R., Henry, T., 2011. Intertidal and submarine groundwater discharge on the west coast of Ireland. Estuar. Coast. Shelf Sci. 92, 415–423.

Champ, D.R., Gulens, J., Jackson, R.E., 1979. Oxidation-reduction sequences in ground water flow systems. Can. J. Earth Sci. 1.

Charbonnier, C., Anschutz, P., Poirier, D., Bujan, S., Lecroart, P., 2013. Aerobic respiration in a high-energy sandy beach. Mar. Chem. 155, 10–21.

Charette, M.A., Henderson, P.B., Breier, C.F., Liu, Q., 2013. Submarine groundwater discharge in a river-dominated Florida estuary. Mar. Chem. 156, 3–17.

Chavez, F.P., Messié, M., Pennington, J.T., 2011. Marine primary production in relation to climate variability and change. Ann. Rev. Mar. Sci. 3, 227–260.

Chen, X., 2007. A laterally averaged two-dimensional trajectory model for estimating transport time scales in the Alafia River estuary , Florida. Estuarine, Coast. shelf Sci.

75, 358–370.

Cheng, K.H., Luo, X., Jiao, J.J., 2020. Two-decade variations of fresh submarine groundwater discharge to Tolo Harbour and their ecological significance by coupled remote sensing and radon-222 model. Water Res. 178.

Cho, H.M., Kim, G., Kwon, E.Y., Moosdorf, N., Garcia-Orellana, J., Santos, I.R., 2018. Radium tracing nutrient inputs through submarine groundwater discharge in the global ocean. Sci. Rep. 8, 4–10.

Church, T.M., 1996. An underground route for the water cycle. Nature.

Clare, C., Mcnamara, M.E., 2009. The geology of the Burren region.

Cloern, J.E., Alpine, A.E., Cole, B.E., Wong, R.L.J., Arthur, J.F., Ball, M.D., 1983. River discharge controls phytoplankton dynamics in the northern San Francisco Bay estuary. Estuar. Coast. Shelf Sci.

Colman, A.S., Holland, H.D., 2000. the Global Diagenetic Flux of Phosphorus From Marine Sediments To the Oceans: Redox Sensitivity and the Control of Atmospheric Oxygen Levels. Mar. Authigenes. From Glob. to Microbial, SEPM Spec. Publ. No. 66 53–75.

Condon, R.H., Graham, W.M., Duarte, C.M., Pitt, K.A., Lucas, C.H., Haddock, S.H.D., Sutherland, K.R., Robinson, K.L., Dawson, M.N., Beth, M., 2012. Questioning the Rise of Gelatinous Zooplankton in the World's Oceans. Bioscience 62, 160–169.

Conley, D.J., Humborg, C., Rahm, L., Savchuk, O.P., Wulff, F., 2002. Hypoxia in the baltic sea and basin-scale changes in phosphorus biogeochemistry. Environ. Sci. Technol. 36, 5315–5320.

Cooper, H.H.J., 1965. A hypothesis concerning the dynamic balance of fresh water and salt water in a coastal aquifer. Geol. Surv. water-supply Pap.

Copernicus, 2018. Corine Land Cover 2018 maps. [WWW Document]. URL https://land.copernicus.eu/pan-european/corine-land-cover

Copernicus, 1990. Corine Land Cover 1990 map. [WWW Document]. URL https://land.copernicus.eu/pan-european/corine-land-cover

Costanza, R., D'Arge, R., de Groot, R., Farber, S., Grasso, M., Hannon, B., Limburg, K., Naeem, S., O'Neill, R. V., Paruelo, J., Raskin, R.G., Sutton, P., van den Belt, M., 1998. The value of the world's ecosystem services and natural capital. Nature 387, 253–260.

Costanza, R., de Groot, R., Sutton, P., van der Ploeg, S., Anderson, S.J., Kubiszewski, I., Farber, S., Turner, R.K., 2014. Changes in the global value of ecosystem services. Glob. Environ. Chang. 26, 152–158.

Coxon, C., Drew, D., 2000. Interdependence of groundwater and surface water in lowland karst areas of western Ireland: Management issues arising from water contaminant transfers, in: ROBINS, N. S. & MISSTEAR, B. D. R. (Eds) Groundwater in the Celtic Regions." Studies in Hard Rock and Quaternary Hydrogeology. Geological Society, London, Special Publications, 182, 81 88. The Geological Society of London 2000. pp. 81–88.

Cranford, P.J., Strain, P.M., Dowd, M., Hargrave, B.T., Grant, J., Archambault, M., 2007.

Influence of mussel aquaculture on nitrogen dynamics in a nutrient enriched coastal embayment. Mar. Ecol. Prog. Ser. 347, 61–78.

Cush, P., Varley, T., 2013. Cooperation as a survival strategy among west of Ireland small-scale mussel farmers. Marit. Stud. 12, 1–17.

Dadson, S.J., Hall, J.W., Murgatroyd, A., Acreman, M., Bates, P., Beven, K., Heathwaite, L., Holden, J., Holman, I.P., Lane, S.N., O'Connell, E., Penning-Rowsell, E., Reynard, N., Sear, D., Thorne, C., Wilby, R., 2017. A restatement of the natural science evidence concerning catchment-based "natural" flood management in the UK. Proc. R. Soc. A Math. Phys. Eng. Sci. 473.

Dame, R.F., Prins, T.C., 1998. Bivalve carrying capacity in coastal ecosystems. Aquat. Ecol. 31, 409–421.

Dangendorf, S., Marcos, M., Wöppelmann, G., Conrad, C.P., Frederikse, T., Riva, R., 2017. Reassessment of 20th century global mean sea level rise. Proc. Natl. Acad. Sci. U. S. A. 114, 5946–5951.

Darcy, H., 1856. Les Fontaines Publique de la Ville de Dijon [The public fountains of the city of Dijon]: Paris, Victor Dalmont.

Davenport, J., 1979. The Isolation Response of Mussels (Mytilus Edulis l.) Exposed to Galling Sea-Water Concentrations. J. Mar. Biol. Assoc. United Kingdom 59, 123–132.

Day, J.W., Crump, B.C., Kemp, W.M., Yañez-Arancibia, A., 2013. Estuarine Ecology.

de Klein, J.J.M., Overbeek, C.C., Juncher Jørgensen, C., Veraart, A.J., 2017. Effect of Temperature on Oxygen Profiles and Denitrification Rates in Freshwater Sediments. Wetlands 37, 975–983.

Debieche, T.H., Guglielmi, Y., Mudry, J., 2002. Modeling the hydraulical behavior of a fissured-karstic aquifer in exploitation conditions. J. Hydrol. 257, 247–255.

Deirmendjian, L., Loustau, D., Augusto, L., Lafont, S., Chipeaux, C., Poirier, D., Abril, G., 2018. Hydro-ecological controls on dissolved carbon dynamics in groundwater and export to streams in a temperate pine forest. Biogeosciences 15, 669–691.

Deleersnijder, E., Campin, J.M., Delhez, E.J.M., 2001. The concept of age in marine modelling I. Theory and preliminary model results. J. Mar. Syst. 28, 229–267.

Delhez, É.J.M., Deleersnijder, É., Mouchet, A., Beckers, J.M., 2003. A note on the age of radioactive tracers. J. Mar. Syst. 38, 277–286.

Diersch, H.J.G., 1992. Interactive, graphics-based finite element simulation of groundwater contamination processes. Adv. Eng. Softw. 15, 1–13.

Dijkstra, Y.M., Chant, R.J., Reinfelder, J.R., 2019. Factors Controlling Seasonal Phytoplankton Dynamics in the Delaware River Estuary : an Idealized Model Study. Estuaries and Coasts (2019) 1839–1857.

Dittrich, R., Butler, A., Ball, T., Wreford, A., Moran, D., 2019. Making real options analysis more accessible for climate change adaptation. An application to afforestation as a flood management measure in the Scottish Borders. J. Environ. Manage. 245, 338–347.

Dong, Z., Liu, D., Keesing, J.K., 2010. Jellyfish blooms in China: Dominant species, causes

and consequences. Mar. Pollut. Bull. 60, 954–963.

Donohue, F.O., 2012. Physical and numerical modelling of impeded tidal flows: Effects of aquaculture structures on hydrodynamics and material transport.

Dowd, M., 2005. A bio-physical coastal ecosystem model for assessing environmental effects of marine bivalve aquaculture. Ecol. Modell. 183, 323–346.

Drew, D., 2003. The hydrology of the Burren and of the Clare and Galway Lowlands., in: Mullan G, Caves of County Clare and South Galway. University of Bristol Spelaeological Society.

Drew, D.P., 2008. Hydrogeology of lowland karst in Ireland. Q. J. Eng. Geol. Hydrogeol. 41, 61–72.

Drew, D.P., 1991. Karstification during the Holocene., in: The Post- Glacial Period, Fresh Perspectives, Irish Quaternary Association Symposium, November 1991, Dublin. pp. 14–16.

Drew, D.P., Daly, D., 1993. Groundwater and karstification in Mid-Galway, South Mayo and North Clare. Rep. Ser. 93/3.

Drew, D.P., Jones, G.L., 2000. Post-Carboniferous pre-Quaternary karstification in Ireland. Proc. Geol. Assoc. 111, 345–353.

Dronkers, J., Zimmerman, J.T.F., 1982. Some principles of mixing in tidal lagoons. Oceanol. acta. 107–117.

Dulai, H., Kamenik, J., Waters, C.A., Kennedy, J., Babinec, J., Jolly, J., Williamson, M., 2016. Autonomous long-term gamma-spectrometric monitoring of submarine groundwater discharge trends in Hawaii. J. Radioanal. Nucl. Chem. 307, 1865–1870.

Dulaiova, H., Camilli, R., Henderson, P.B., Charette, M.A., 2010. Coupled radon, methane and nitrate sensors for large-scale assessment of groundwater discharge and non-point source pollution to coastal waters. J. Environ. Radioact. 101, 553–563.

Dulaiova, H., Peterson, R., Burnett, W.C., Lane-Smith, D., 2005. A multi-detector continuous monitor for assessment of 222Rn in the coastal ocean. J. Radioanal. Nucl. Chem. 263, 361–363.

Dunne, S., Hanafin, J., Lynch, P., McGrath, R., Nishimura, E., Nolan, P., Ratnam, J.V., Semmler, T., Sweeney, C., Varghese, S., Wang, S., 2007. Report Series No . 27 Ireland in a Warmer World - Scientific Predictions of the Irish Climate in the Twenty-First Century, Environment Protection Agency.

Durridge, 2015. Rad7 Radon Detector User Manual. DURRIDGE Co. Inc 1–81.

Dyer, K.R. (Keith R.., 1973. Estuaries: a physical introduction. John Wiley, [Chichester] :

Dyer, K.R., Taylor, P.A., 1973. A simple, segmented prism model of tidal mixing in well-mixed estuaries. Estuar. Coast. Mar. Sci. 1, 411–418.

Edmunds, W.M., 2003. Renewable and non-renewable groundwater in semi-arid and arid regions. Dev. Water Sci. 50, 265–280.

Edwards, A., Sharples, F., 1986. Scottish Sea-Lochs - A Catalogue., Scottish Marine Biological Association, Oban, Scotland.

Edwards, M., 2000. Large-scale temporal and spatial patterns of marine phytoplankton in the north-east Atlantic.

Einsiedl, F., 2012. Sea-water/groundwater interactions along a small catchment of the European Atlantic coast. Appl. Geochemistry 27, 73–80.

Einsiedl, F., Schubert, M., Knöller, K., Cave, R., 2009. Application of Environmental Tracers for assessing groundwater discharge into Galway Bay, Ireland, in: Paper Presented at HydroEco 2009, Vienna, 20th–23th, April 2009.

Elberling, B., Damgaard, L.R., 2001. Microscale measurements of oxygen diffusion and consumption in subaqueous sulfide tailings. Geochim. Cosmochim. Acta 65, 1897–1905.

Eleftheriou, G., Tsabaris, C., Patiris, D.L., Androulakaki, E.G., Vlastou, R., 2017. Estimation of coastal residence time of submarine groundwater discharge using radium progenies. Appl. Radiat. Isot. 121, 44–50.

EPA, 2020. Killiny Borehole water level- EPAHydronet, All data 15min TS and All data DayMean TS [WWW Document]. URL http://www.epa.ie/hydronet/#IE_WE_G_0002_1200_0013 (accessed 1.25.18).

EPA, 2019a. Bundorragha flow data, Hydronet Website (Ireland). http://www.epa.ie/hydronet/#32026 [WWW Document]. EPA HydroNet Website.

EPA, 2019b. WFD_SubCatchments (NEW)-Subcatchments for use in River Basin Management planning, 2015 - 2021, Catchment Data Package. http://gis.epa.ie/GetData/Download [WWW Document].

EPA, 2018a. Water quality dataset in Kinvarra bay between 2007 and 2018 (On request from EPA).

EPA, 2018b. Corine Land Cover 2018 - National (ING) [WWW Document]. URL http://gis.epa.ie/GetData/Download

EPA, 2016. OSI River and Lakes [WWW Document]. URL http://gis.epa.ie/GetData/Download

EPA, 2015. Groundwater quality dataset - Kinvarra springs 2007-2015.

EPA, 2004. EU Water Framework Directive Monitoring Programme - Appendix 7.1 and 10.4.

Eppley, R., 1972. Temperature and phytoplankton growth in the sea. Fish. Bull. 70, 1063–85.

Erler, D. V., Santos, I.R., Eyre, B.D., 2014. Inorganic nitrogen transformations within permeable carbonate sands. Cont. Shelf Res. 77, 69–80.

Eshleman, K.N., Hemond, H.F., 1988. Alkalinity and major ion budgets for a Massachusetts reservoir and watershed. Limnol. Oceanogr. 33, 174–185.

Fairbanks, R.G., 1989. A 17,000-year glacio-eustatic sea level record: influence of glacial melting rates on the Younger Dryas event and deep-ocean circulation. Nature 342, 637–642.

Feely, R.A., Baker, E.T., Schumacher, J.D., Massoth, G.J., Landing, W.M., 1979. Processes affecting the distribution and transport of suspended matter in the northeast Gulf of

Alaska. Deep Sea Res. Part A, Oceanogr. Res. Pap. 26.

Ferris, J.G., 1952. Cyclic fluctuations of water level as a basis for determining aquifer transmissibility, U.S. Geological Survey Water Ressource Division, Groundwater Branch.

Fischer, R., Giebel, H.A., Ptacnik, R., 2017. Identity of the limiting nutrient (N vs. P) affects the competitive success of mixotrophs. Mar. Ecol. Prog. Ser. 563, 51–63.

Fleury, P., Bakalowicz, M., de Marsily, G., 2007. Submarine springs and coastal karst aquifers: A review. J. Hydrol. 339, 79–92.

Flynn, K.J., Mitra, A., Glibert, P., Burkholder, M.J., 2018. Mixotrophy in Harmful Algal Blooms: By Whom, on Whom, When, Why, and What Next, in: Global Ecology and Oceanography of Harmful Algal Blooms. pp. 113–132.

Freeze, A.R., Cherry, J.A., 1979. Groundwater.

Frenette, J., Demers, S., Legendre, L., Boule, M., 1996. Size-related photosynthetic characteristics of phytoplankton during periods of seasonal mixing and stratification in an oligotrophic multibasin lake system. J. Plankton Res. 18, 45–61.

Frierdich, A.J., Hasenmueller, E.A., Catalano, J.G., 2011. Composition and structure of nanocrystalline Fe and Mn oxide cave deposits: Implications for trace element mobility in karst systems. Chem. Geol. 284, 82–96.

Fukuo, Y., Kaihotsu, I., 1988. A theoretical analysis of seepage flow of the confined groundwater into the lake bottom with a gentle slope. Water Resour. Res.

Garcia-Solsona, E., Garcia-Orellana, J., Masqué, P., Dulaiova, H., 2007. Uncertainties associated with 223 Ra and 224 Ra measurements in water via a Delayed Coincidence Counter (RaDeCC).

Garcia, N.S., Sexton, J., Riggins, T., Brown, J., Lomas, M.W., Martiny, A.C., 2018. High variability in cellular stoichiometry of carbon, nitrogen, and phosphorus within classes of marine eukaryotic phytoplankton under sufficient nutrient conditions. Front. Microbiol. 9, 1–10.

Garman, K.M., Garey, J.R., 2005. The transition of a freshwater karst aquifer to an anoxic marine system. Estuaries 28, 686–693.

Geider, R.J., Maclntyre, H.L., Kana, T.M., 1998. A dynamic regulatory model of phytoplanktonic temperature acclimation to light , nutrients , and temperature. Limnol. Oceanogr. 43, 679–694.

Gemmell, B.J., Oh, G., Buskey, E.J., Villareal, T.A., 2016. Dynamic sinking behaviour in marine phytoplankton: Rapid changes in buoyancy may aid in nutrient uptake. Proc. R. Soc. B Biol. Sci. 283.

Gentien, P., Donaghay, P., Yamazaki, H., Raine, R., Reguera, B., Osborn, T., 2005. Harmful algal blooms in stratified environments. Oceanography 18, 172–183.

Geological Survey, 2019. Bedrock Geology 100K and Traced Underground Connections datasets. Contains Irish Public Sector Data (Geological Survey) licensed under a Creative Commons Attribution 4.0 International (CC BY 4.0) licence. [WWW Document]. URL https://data.gov.ie/dataset/gsi-bedrock-geology-100k-series-

1100000

Geological Survey, 1965. Sea water in coastal aquifers-relation of salt water to fresh ground water. Geol. Surv. water-supply Pap. 12, 574–575.

Geological Survey of Ireland/Marine Institute, 2019. Bathymetry - bathymetry_lidar_inshore_30m_wgs84. Data request on GSI Jetstream Website. Irish Public Sector Data (Geological Survey) licensed under a Creative Commons Attribution 4.0 International (CC BY 4.0) licence. [WWW Document]. URL https://www.infomar.ie/data

Gerssen, A., Pol-Hofstad, I.E., Poelman, M., Mulder, P.P.J., van den Top, H.J., Dde Boer, J., 2010. Marine toxins: Chemistry, toxicity, occurrence and detection, with special reference to the dutch situation. Toxins (Basel). 2, 878–904.

Geyer, W.R., MacCready, P., 2014. The Estuarine Circulation. Annu. Rev. Fluid Mech. 46, 175–197.

Geyer, W.R., Morris, J.T., Pahl, F.G., Jay, D.A., 2000. Interaction between physical processes and ecosystem structure: A comparative approach, in: J. E. Hobbie [Island Press], Estuarine Science: A Synthetic Approach to Research and Practice. pp. 177–206.

Geyer, W.R., Ralston, D.K., 2011. The Dynamics of Strongly Stratified Estuaries, in: Treatise on Estuarine and Coastal Science. Elsevier Inc., pp. 37–51.

Gill, L.W., Naughton, O., Johnston, P.M., Basu, B., Ghosh, B., 2013. Characterisation of hydrogeological connections in a lowland karst network using time series analysis of water levels in ephemeral groundwater-fed lakes (turloughs). J. Hydrol. 499, 289–302.

Gilmartin, M., Revelante, N., 1978. The phytoplankton characteristics of the barrier island lagoons of the Gulf of California. Estuar. Coast. Mar. Sci.

Gonneea, M.E., Morris, P.J., Dulaiova, H., Charette, M.A., 2008. New perspectives on radium behavior within a subterranean estuary. Mar. Chem. 109, 250–267.

Gordon, J.D.C., Boudreau, P.R., Mann, K.H., Ong, J.-E., Silvert, W.L., Smith, S.V., Wattayakorn, G., Wulff, F., Yanagi, T., 1996. LOICZ BIOGEOCHEMICAL Modelling Guidelines D.C. Loicz report series no 5.

Grant, J., Curran, K.J., Guyondet, T.L., Tita, G., Bacher, C., Koutitonsky, V., Dowd, M., 2007. A box model of carrying capacity for suspended mussel aquaculture in Lagune de la Grande-Entrée, Iles-de-la-Madeleine, Québec. Ecol. Modell. 200, 193–206.

Grasshoff, K., Kremling, K., Ehrhardt, M., 2009. Methods of seawater analysis., Wiley, Hoboken.

Great Britain. Environment Agency., 2009. The potential risks to human health posed by living, attached seaweeds and dead, beach-cast material associated with sand beaches : a preliminary report. Environment Agency, Bristol :

Green, L., Sutula, M., Fong, P., Fong1, P., 2014. How much is too much? Identifying benchmarks of adverse effects of macroalgae on the macrofauna in intertidal flats. Source Ecol. Appl. Ecol. Appl. 24, 300–314.

Gregory, C., Cave, R.R., Raine, R., Mcdermott, G., O'Flynn, L., 2020. The interaction of retention areas and submarine ground water (SGD) in small bays : implications for phytoplankton growth. Estuar. Coast. Shelf Sci. 106681.

Gruber, N., 2008. The Marine Nitrogen Cycle: Overview and Challenges, in: The Marine Nitrogen Cycle: Overview and Challenges.

Gruffydd, L.D., Huxley, R., Crisp, D.J., 1984. The reduction in growth of mytilus edulis in fluctuating salinity regimes measured using laser diffraction patterns and the exaggeration of this effect by using tap water as the diluting medium. J. Mar. Biol. Assoc. U. K. 64, 401–409.

GSI, 2020. Geological Survey Ireland Spatial Ressources - Bedrock aquifer. [WWW Document]. URL https://dcenr.maps.arcgis.com/apps/MapSeries/index.html?appid=a30af518e87a4c0ab2fbde2aaac3c228

Guerra, M.T., Lefèvre, N., Savatier, M., Murphy, J.E., Rocha, C., n.d. Magnitude and typology of freshwater input as a driver of carbonate system variability in Irish coastal systems.

Guinder, V.A., Molinero, J.C., 2013. Climate change effects on marine phytoplankton. Mar. Ecol. a Chang. World 68–90.

Guo, W., Bennett, G.D., 1998. Simulation of saline/fresh water flows using MODFLOW. Proc. MODFLOW'98 Conf., Oct. 4-8, 1998, Golden, Color. USA 267–274.

Hallegraeff, G.M., 1993. A review of harmful algal blooms and their apparent global increase*. Phycologia 32, 79–99.

Hancock, G.J., Webster, I.T., Ford, P.W., Moore, W.S., 2000. Using Ra isotopes to examine transport processes controlling benthic fluxes into a shallow estuarine lagoon. Geochim. Cosmochim. Acta 64, 3685–3699.

Hanke, A., Berg, J., Hargesheimer, T., Tegetmeyer, H.E., Sharp, C.E., Strous, M., 2016. Selective pressure of temperature on competition and cross-feeding within denitrifying and fermentative microbial communities. Front. Microbiol. 6, 1–14.

Hansell, D.A., Follows, M.J., 2008. Nitrogen in the Atlantic Ocean.

Hansen, L.K., Jakobsen, R., Postma, D., 2001. Methagnogenesis in a shallow sandy aquifer, Rømø, Denmark. Geochim. Cosmochim. Acta 65, 2925–2935.

Harger, J.R.E., Landenberger, D.E., 1971. The effect of storms as a density dependent mortality factor on populations of sea mussels. The Veliger 14, 195–201.

Hartmann, A., Liu, Y., Olarinoye, T., Berthelin, R., Marx, V., 2021. Integrating field work and large-scale modeling to improve assessment of karst water resources. Hydrogeol. J. 29, 315–329.

Hartnett, M., Dabrowski, T., Olbert, A.I., 2011. A new formula to calculate residence times of tidal waterbodies. Proc. Inst. Civ. Eng. - Water Manag. 164, 243–256.

Hastie, L.C., Boon, P.J., Young, M.R., Way, S., 2001. The effects of a major flood on an endangered freshwater mussel population. Biol. Conserv. 98, 107–115.

Hatta, M., Zhang, J., 2013. Temporal changes and impacts of submarine fresh

groundwater discharge to the coastal environment: A decadal case study in Toyama Bay, Japan. J. Geophys. Res. Ocean. 118, 2610–2622.

Hay, C.C., Morrow, E., Kopp, R.E., Mitrovica, J.X., 2015. Probabilistic reanalysis of twentieth-century sea-level rise. Nature 517, 481–484.

Hill, C., Forti, P., 1997. Cave Minerals of the World., National Speleological Society, Inc., Huntsville, Alabama.

Hoefel, F.G., Evans, R.L., 2001. Impact of low salinity porewater on seafloor electromagnetic data: A means of detecting submarine groundwater discharge? Estuar. Coast. Shelf Sci. 52, 179–189.

Hoegh-Guldberg, Jacob, O.D., Taylor, M., Bindi, M., Brown, S., Camilloni, I., Diedhiou, A., Djalante, R., Ebi, K.L., Engelbrecht, F., J.Guiot, Hijioka, Y., Mehrotra, S., Payne, A., Seneviratne, S.I., Thomas, A., Warren, R., Zhou, G., 2018. IPCC Special Report 2018 - Chapter 3 - Impacts of 1.5°C of Global Warming on Natural and Human Systems, in: Global Warming of 1.5°C. An IPCC Special Report on the Impacts of Global Warming of 1.5°C above Pre-Industrial Levels and Related Global Greenhouse Gas Emission Pathways, in the Context of Strengthening the Global Response to the Threat of Climate Change,. pp. 175–311.

Honda, H., Sugimoto, R., Kobayashi, S., 2018. Submarine Groundwater Discharge and its Influence on Primary Production in Japanese Coasts: Case Study in Obama Bay, in: Endo A., Oh T. (Eds) The Water-Energy-Food Nexus. Global Environmental Studies. Springer, Singapore.

Hsu, F.H., Su, C.C., Wang, P.L., Lin, I.T., 2020. Temporal variations of submarine groundwater discharge into a tide-dominated coastalwetland (Gaomei Wetland, Western Taiwan) indicated by radon and radium isotopes. Water (Switzerland) 12.

Hwang, D.W., Kim, G., Lee, W.C., Oh, H.T., 2010. The role of submarine groundwater discharge (SGD) in nutrient budgets of Gamak Bay, a shellfish farming bay, in Korea. J. Sea Res. 64, 224–230.

Ibánhez, J.S.P., Rocha, C., 2017. Kinetics of inorganic nitrogen turnover in a sandy seepage face on a subterranean estuary. Appl. Geochemistry 87, 108–121.

Ibánhez, J.S.P., Rocha, C., 2016. Oxygen transport and reactivity within a sandy seepage face in a mesotidal lagoon (Ria Formosa, Southwestern Iberia). Limnol. Oceanogr. 61, 61–77.

Ibánhez, J. Severino P., Rocha, C., 2014. Effects of recirculation of seawater enriched in inorganic nitrogen on dissolved organic carbon processing in sandy seepage face sediments. Mar. Chem. 166, 48–58.

Ibánhez, J. S. P., Rocha, C., 2014. Porewater sampling for NH 4 + with Rhizon Soil Moisture Samplers (SMS): potential artifacts induced by NH 4 + sorption. Freshw. Sci. 33, 1195–1203.

ICES, 2019. CTD and Bottle Data for all ships in ireland, geographical selection for Galway bay for 2007-2018. [WWW Document]. URL https://ocean.ices.dk/HydChem/HydChem.aspx?plot=yes

INFOMAR, GSI, 2019. bathymetry_lidar_inshore_30m_wgs84.ers Available at:

https://jetstream.gsi.ie/iwdds/map.jsp [WWW Document].

International Atomic Energy Agency (IAEA), 2014. The environmental behaviour of radium: revised edition. Tech. Reports Ser. No. 476 44–51.

IPCC, 2007. Towards New Scenarios for Analysis of Emissions, Climate Change, Impacts and Response Strategies, IPCC Expert Meeting Report.

ISO, 1998. 1100-2, Measurement of liquid flow in open channels - Part 2: Determination of the stage-discharge relation.

Jackson, T., Sathyendranath, S., Platt, T., 2017. An Exact Solution For Modeling Photoacclimation of the Carbon-to-Chlorophyll Ratio in Phytoplankton. Front. Mar. Sci. 4, 1–10.

Jafar-Sidik, M., Gohin, F., Bowers, D., Howarth, J., Hull, T., 2017. The relationship between Suspended Particulate Matter and Turbidity at a mooring station in a coastal environment: consequences for satellite-derived products. Oceanologia 59, 365–378.

Jakobsen, H.H., Markager, S., 2016. Carbon-to-chlorophyll ratio for phytoplankton in temperate coastal waters: Seasonal patterns and relationship to nutrients. Limnol. Oceanogr. 61, 1853–1868.

Jakobsen, R., Postma, D., 1999. Redox zoning, rates of sulfate reduction and interactions with Fe-reduction and methanogenesis in a shallow sandy aquifer, Romo, Denmark. Geochim. Cosmochim. Acta.

Janssen, P.H.M., Heuberger, P.S.C., 1995. Calibration of process-oriented models. Ecol. Modell. 83, 55–66.

Jarvie, H.P., Sharpley, A.N., Brahana, V., Simmons, T., Price, A., Neal, C., Lawlor, A.J., Sleep, D., Thacker, S., Haggard, B.E., 2014. Phosphorus retention and remobilization along hydrological pathways in karst terrain. Environ. Sci. Technol. 48, 4860–4868.

JCGM, 2008. JCGM 100:2008, Evaluation of measurement data — Guide to the expression of uncertainty in measurement, Joint Committee For Guides In Metrology.

Jeannin, P.Y., 2001. Modeling flow in phreatic and epiphreatic karst conduits in the Hölloch cave (Muotatal, Switzerland). Water Resour. Res. 37, 191–200.

Jeannin, P.Y., Hessenauer, M., Malard, A., Chapuis, V., 2016. Impact of global change on karst groundwater mineralization in the Jura Mountains. Sci. Total Environ. 541, 1208–1221.

Jerome Morrissey, P., McCormack, T., Naughton, O., Meredith Johnston, P., William Gill, L., 2020. Modelling groundwater flooding in a lowland karst catchment. J. Hydrol. 580, 124361.

Jiang, S., Kavanagh, M., Rocha, C., 2017. Evaluation of the suitability of vacutainers for storage of nutrient and dissolved organic carbon analytes in water samples. Biol. Environ. Proc. R. Irish Acad. 117B, 33.

Jordan, T.E., Correll, D.L., Weller, D.E., 1997. Relating nutrient discharges from watersheds to land use and streamflow variability. Water Ressour. Res. 33, 2579–2590.

Jørgensen, C., Larsen, P., Riisgård, H., 1990. Effects of temperature on the mussel pump.

Mar. Ecol. Prog. Ser. 64, 89–97.

Jorgensen, S.E., Nielsen, S.N., Jorgensen, L.A., 1991. Handbook of ecological parameters and ecotoxicology. Handb. Ecol. parameters Ecotoxicol.

Kautsky, N., 1981. On the trophic role of the blue mussel (Mytilus edulis L.) in the Baltic coastal ecosystem and the fate of the organic matter produced by the mussels. Kieler Meeresforsch 5, 454–461.

Keegan, B.F., Mercer, J.P., 1986. An Oceanographical Survey of Killary Harbour on the West Coast of Ireland. Source Proc. R. Irish Acad. Sect. B Biol. Geol. Chem. Sci. Proc.R.Ir.Acad 86, 1–70.

Kelly, C., Hunter Williams, T., Misstear, B.M., Motherway, K., 2015. Irish Aquifer Properties – a Reference Manual and Guide Version 1 March 2015.

Ketchum, B., 1951. The flushing of tidal estuaries. Sewage Ind. Waste. 23, 198–209.

Ketchum, B.H., 1951. The exchanges of fresh and saltwaters in tidal estuaries. J. Mar. Res. 0–44.

Khosrow Badiozamani, 1973. The Dorag Dolomitization Model--Application to the Middle Ordovician of Wisconsin. SEPM J. Sediment. Res. 43, 965–984.

Kilroy, G., Coxon, C., 2005. Temporal variability of phosphorus fractions in Irish karst springs. Environ. Geol. 47.

King, P.A., McGrath, D., Gosling, E.M., 1989. Reproduction and settlement of mytilus edulis on an exposed rocky shore in galway bay, west coast of ireland. J. Mar. Biol. Assoc. United Kingdom 69, 355–365.

Knee, K., Paytan, A., 2011. Submarine Groundwater Discharge: A Source of Nutrients, Metals, and Pollutants to the Coastal Ocean. Treatise Estuar. Coast. Sci. 4, 205–234.

Kohout, F.A., 1965. The flow of fresh water and salt water in the Biscayne aquifer of the Miami area, Florida. Geol. Surv. water-supply Pap. 12, C12–C20.

Korom, S.F., 1992. Natural denitrification in the saturated zone: A review. Water Resour. Res. 28, 1657–1668.

Kresic, N., Panday, S., 2021. Modeling of groundwater flow and transport in coastal karst aquifers. Hydrogeol. J. 29, 249–258.

Krest, J.M., Moore, W.S., Gardner, L.R., Morris, J.T., 2000. Marsh nutrient export supplied by groundwater discharge: Evidence from radium measurements. Global Biogeochem. Cycles.

Krest, J.M., Moore, W.S., Rama, 1999. 226Ra and 228Ra in the mixing zones of the Mississippi and Atchafalaya rivers: Indicators of groundwater input. Mar. Chem. 64, 129–152.

Kwon, E.Y., Kim, G., Primeau, F., Moore, W.S., Cho, H.-M., DeVries, T., Sarmiento, J.L., Charette, M.A., Cho, Y.-K., 2014. Global estimate of submarine groundwater discharge based on an observationally constrained radium isotope model. Geophys. Res. Lett. 1–7.

Lachat instruments, 2002. QuikChem® Method 31-107-06-1-B, determination of Ammonia in Brackish or Seawater by flow injection analysis.

Lachat instruments, 2001. QuikChem® Method 31-107-04-1-E, determination of Nitrate and/or Nitrite in Brackish or Seawater by Flow Injection Analysis Colorimetry.

Lagos, N., 1998. Microalgal blooms: A global issue with negative impact in Chile. Biol. Res. 31, 375–386.

Lambeck, K., Chappell, J., 2001. Sea level change through the last glacial cycle. Science (80-.). 292, 679–686.

Lamontagne, S., Cosme, F., Minard, A., Holloway, A., 2018. Nitrogen attenuation, dilution and recycling in the intertidal hyporheic zone of a subtropical estuary. Hydrol. Earth Syst. Sci. 22, 4083–4096.

Lamontagne, S., Webster, I.T., 2019. Cross-Shelf Transport of Submarine Groundwater Discharge Tracers: A Sensitivity Analysis. J. Geophys. Res. Ocean. 124, 453–469.

Lamontagne, Sébastien, Webster, I.T., 2019. Theoretical assessment of the effect of vertical dispersivity on coastal seawater radium distribution. Front. Mar. Sci. 6, 1–10.

Langevin, C.D., 2003. Simulation of Submarine Ground Water Discharge to a Marine Estuary: Biscayne Bay, Florida. Ground Water 41, 758–771.

Laroche, J., Nuzzi, R., Waters, R., Wyman, K., Falkowski, P.G., Wallace, D.W.R., 1997. Brown Tide blooms in Long Island's coastal waters linked to interannual variability in groundwater flow. Glob. Chang. Biol. 3, 397–410.

Larsen, P.S., Lüskow, F., Riisgård, H.U., 2018. Too much food may cause reduced growth of blue mussels (Mytilus edulis) – Test of hypothesis and new 'high Chl a BEG-model.' J. Mar. Syst. 180, 299–306.

Lauber, U., Goldscheider, N., 2014. Utilisation des traceurs naturels et artificiels pour estimer la distribution des temps de transit et les systèmes d'écoulement dans un système karstique alpin d'altitude (Montagnes Wetterstein, Allemagne). Hydrogeol. J. 22, 1807–1824.

Lecher, A.L., Chien, C.-T., Paytan, A., 2016. Submarine groundwater discharge as a source of nutrients to the North Pacific and Arctic coastal ocean. Mar. Chem. 186, 167–177.

Lecher, A.L., Mackey, K., Kudela, R., Ryan, J., Fisher, A., Murray, J., Paytan, A., 2015. Nutrient loading through submarine groundwater discharge and phytoplankton growth in Monterey bay, CA. Environ. Sci. Technol. 49, 6665–6673.

Lecher, A.L., Mackey, K.R.M., 2018. Synthesizing the effects of submarine groundwater discharge on Marine Biota. Hydrology 5, 1–21.

Lee, D.R., 1977. A Device for Measuring Seepage Flux in Lakes and Estuaries. Limnol. Oceanogr. 22, 140–147.

Leming, T.D., Stuntz, W.E., 1984. Zones of coastal hypoxia revealed by satellite scanning have implications for strategic fishing. Nature 310, 136–138.

Li, H., Zhang, Y., Tang, H., Shi, X., Rivkin, R.B., Legendre, L., 2017. Spatiotemporal variations of inorganic nutrients along the Jiangsu coast, China, and the occurrence of macroalgal blooms (green tides) in the southern Yellow Sea.

Li, L., Barry, D.A., Stagnitti, F., Parlange, J.Y., 1999. Submarine groundwater discharge and associated chemical input to a coastal sea. Water Resour. Res. 35, 3253–3259.

Li, L., Barry, D.A., Stagnitti, F., Parlange, J.Y., Jeng, D.S., 2000. Beach water table fluctuations due to spring-neap tides: Moving boundary effects. Adv. Water Resour. 23, 817–824.

Li, Y.-H., Gregory, S., 1973. Diffusion of ions in seawater and deep sea sediments. Geochemica Cosmochim. Acta 38, 703–714.

Liefer, J.D., MacIntyre, H.L., Novoveská, L., Smith, W.L., Dorsey, C.P., 2009. Temporal and spatial variability in Pseudo-nitzschia spp. in Alabama coastal waters: A “hot spot” linked to submarine groundwater discharge? Harmful Algae 8, 706–714.

Lipschultz, F., Wofsy, S.C., Ward, B.B., Codispoti, L.A., Friedrich, G., Elkins, J.W., 1990. Bacterial transformations of inorganic nitrogen in the oxygen-deficient waters of the Eastern Tropical South Pacific Ocean. Deep Sea Res. Part A, Oceanogr. Res. Pap. 37, 1513–1541.

Liu, B., de Swart, H.E., 2018. Quantifying the Effect of Salinity Stratification on Phytoplankton Density Patterns in Estuaries. Estuaries and Coasts 41, 453–470.

Liu, F., Pang, S., Chopin, T., Gao, S., Shan, T., Zhao, X., Li, J., 2013. Understanding the recurrent large-scale green tide in the Yellow Sea: Temporal and spatial correlations between multiple geographical, aquacultural and biological factors. Mar. Environ. Res. 83, 38–47.

Ló Pez-Rivera, A., O ’callaghan, K., Moriarty, M., O ’driscoll, D., Hamilton, B., Lehane, M., James, K.J., Furey, A., 2009. First evidence of azaspiracids (AZAs): A family of lipophilic polyether marine toxins in scallops (Argopecten purpuratus) and mussels (Mytilus chilensis) collected in two regions of Chile.

Loveless, A.M., Oldham, C.E., 2010. Natural attenuation of nitrogen in groundwater discharging through a sandy beach. Biogeochemistry 98, 75–87.

Lovley, D.R., Chapelle, F.H., 1995. Deep subsurface microbial processes. Rev. Geophys.

Lucas, L. V., Koseff, J.R., Monismith, S.G., Cloern, J.E., Thompson, J.K., 1999. Processes governing phytoplankton blooms in estuaries. II: The role of horizontal transport. Mar. Ecol. Prog. Ser. 187, 17–30.

Luczaj, J.A., 2006. Evidence against the Dorag (mixing-zone) model for dolomitization along the Wisconsin arch - A case for hydrothermal diagenesis. Am. Assoc. Pet. Geol. Bull.

Luijendijk, E., Gleeson, T., Moosdorf, N., 2020. Fresh groundwater discharge insignificant for the world’s oceans but important for coastal ecosystems. Nat. Commun. 11.

Luijendijk, E., Gleeson, T., Moosdorf, N., 2019. The flow of fresh groundwater and solutes to the world’s oceans and coastal ecosystems.

Luketina, D., 1998. Simple tidal prism models revisited. Estuar. Coast. Shelf Sci. 46, 77–84.

Macintyre, S., R., W., Chanton, J.P., 1995. Trace gas exchange across the air-sea interface in freshwater and coastal marine environments, in: P. A. Matson and R. C. Harris [Eds.], Biogenic Trace Gases: Measuring Emissions from Soil and Water. Blackwell Science Ltd. pp. 52–97.

Mackenzie, F.T., Andersson, A., Lerman, A., Ver, L.M., 2005. Boundary exchanges in the

global coastal margin: implications for the organic and inorganic carbon cycles. Glob. Coast. Ocean multiscale Interdiscip. Process. Univ. Press 193–225.

Maguire, J., Knights, T., Burnell, G., Crowe, T., O'Beirn, F., McGrath, D., Ferns, M., McDonough, N., McQuaid, N., O'Connor, B., Doyle, R., Newell, C., Seed, R., Smaal, A., O'Carroll, T., Watson, L., Dennis, J., Ó Cinneide, M., 2007. Management recommendations for the sustainable exploitation of mussel seed in the Irish Sea.

Maier, G., Glegg, G.A., Tappin, A.D., Worsfold, P.J., 2012. A high resolution temporal study of phytoplankton bloom dynamics in the eutrophic Taw Estuary (SW England). Sci. Total Environ. 434, 228–239.

Mallast, U., Siebert, C., Wagner, B., Sauter, M., Gloaguen, R., Geyer, S., Merz, R., 2013. Localisation and temporal variability of groundwater discharge into the Dead Sea using thermal satellite data. Environ. Earth Sci. 69, 587–603.

Malone, P.G., Dodd, J.R., 1967. Temperature and Salinity Effects on Calcification Rate in Mytilus Edulis and Its Paleoecological Implicatons. Limnol. Oceanogr. 12, 432–436.

Maramathas, A.J., Boudouvis, A.G., 2010. A "fractal" modification of Torricelli's formula. Hydrogeol. J. 18, 311–316.

Marine institute, 2017. Tidal Observations | Marine Institute [WWW Document]. URL http://www.marine.ie/Home/site-area/data-services/real-time-observations/tidal-observations-0?instrumentname=Galway Port (accessed 1.20.18).

Marine Institute, 2020a. Digital Ocean flow rate model [WWW Document]. URL http://www.digitalocean.ie/Home/ConnemaraModel

Marine Institute, 2020b. Galway bay tide data [WWW Document]. Digit. Ocean. URL http://www.digitalocean.ie/Data/DownloadTideData/Galway Port

Marine Institute, 2019a. Kinvarra tidal observation [WWW Document]. URL http://www.marine.ie/Home/site-area/data-services/real-time-observations/tidal-observations-0?instrumentname=Galway Port

Marine Institute, 2019b. Weekly HAB Bulletin [WWW Document]. URL https://www.marine.ie/Home/site-area/data-services/interactive-maps/weekly-hab-bulletin

Marine Institute, 2009. Irish Ocean Climate and Ecosystem Status Report Summary 2009.

Marine Institute, Food Safety Authority of Ireland, Bord Iascaigh Mhara, 2005. Proceedings of the 6 th Irish Shellfish Safety Scientific Workshop, in: Marine Environment and Health Series.

Masunaga, E., Yamazaki, H., 2014. A new tow-yo instrument to observe high-resolution coastal phenomena. J. Mar. Syst. 129, 425–436.

McBride, M.S., Pfannkuch, H.O., 1975. The distribution of seepage within lakebeds. J. Res. U.S. Gelogical Surv. 3, p 505.

McCaul, M., Barland, J., Cleary, J., Cahalane, C., McCarthy, T., Diamond, D., 2016. Combining Remote Temperature Sensing with in-Situ Sensing to Track Marine/Freshwater Mixing Dynamics. Sensors 16, 1402.

McCormack, T., Gill, L.W., Naughton, O., Johnston, P.M., 2014. Quantification of

submarine/intertidal groundwater discharge and nutrient loading from a lowland karst catchment. J. Hydrol. 519, 2318–2330.

McCormack, T., Naughton, O., Johnston, P.M., Gill, L.W., 2016. Quantifying the influence of surface water–groundwater interaction on nutrient flux in a lowland karst catchment. Hydrol. Earth Syst. Sci. 20, 2119–2133.

McDonald, M.G., Harbaugh, A.W., 1984. A modular three-dimensional finite-difference groundwater flow model.

Mcmahon, T.G., Patching, J.W., 1984. Fluxes of Organic Carbon in a Fjord on the West Coast of Ireland. -Estuarine, Coast. Shelf Sci. 19, 205–215.

Melia, P., 2014. Toxic gas threat as rotting sea lettuce piles up. Irish Indep.

Mena, C., Reglero, P., Hidalgo, M., Sintes, E., Santiago, R., Martín, M., Moyà, G., Balbín, R., 2019. Phytoplankton Community Structure Is Driven by Stratification in the Oligotrophic Mediterranean Sea. Front. Microbiol. 10.

Menning, D.M., Wynn, J.G., Garey, J.R., 2015. Karst estuaries are governed by interactions between inland hydrological conditions and sea level. J. Hydrol. 527, 718–733.

Met Eireann, 2020. Global radiation, temperature and rainfall dataset, taken from the historical dataset for Athenry (2010-) [WWW Document]. Hist. Data. URL https://www.met.ie/climate/available-data/historical-data

Michael, H.A., Mulligan, A.E., Harvey, C.F., 2005. Seasonal oscillations in water exchange between aquifers and the coastal ocean. Nature 436, 1145–1148.

Monsen, N.E., Cloern, J.E., Lucas, L. V., Monismith, S.G., 2002. A comment on the use of flushing time, residence time, and age as transport time scales. Limnol. Oceanogr. 47, 1545–1553.

Moore, W.S., 2010. The Effect of Submarine Groundwater Discharge on the Ocean. Ann. Rev. Mar. Sci. 2, 59–88.

Moore, W.S., 2008. Fifteen years experience in measuring 224Ra and 223Ra by delayed-coincidence counting. Mar. Chem. 109, 188–197.

Moore, W.S., 2007. Fifteen years experience in measuring 224 Ra and 223 Ra by delayed-coincidence counting.

Moore, W.S., 2000. Ages of continental shelf waters determined from 223Ra and 224Ra. J. Geophys. Res. 105, 117–122.

Moore, W.S., 1999. The subterranean estuary: a reaction zone of ground water and sea water. Mar. Chem. 65, 111–125.

Moore, W.S., 1976. Sampling 228Ra in the deep ocean. Deep. Res. 23, 647–651.

Moore, W.S., Arnold, R., 1996a. Measurement of223Ra and224Ra in coastal waters using a delayed coincidence counter. J. Geophys. Res. 101, 1321–1329.

Moore, W.S., Arnold, R., 1996b. Measurement of 223Ra and 224Ra in coastal waters using a delayed coincidence counter. J. Geophys. Res. 101, 1321–1329.

Moore, W.S., Blanton, J.O., Joye, S.B., 2006. Estimates of flushing times, submarine groundwater discharge, and nutrient fluxes to Okatee Estuary, South Carolina. J.

Geophys. Res. 111, 1–14.

Moore, W.S., Cai, P., 2013. Calibration of RaDeCC systems for 223Ra measurements. Mar. Chem. 156, 130–137.

Moore, W.S., Key, R.M., Sarmiento, J.L., 1985. Techniques for precise mapping of 226Ra and 228Ra in the ocean. J. Geophys. Res.

Moore, W.S., Sarmiento, J.L., Key, R.M., 2008. Submarine groundwater discharge revealed by 228Ra distribution in the upper Atlantic Ocean. Nat. Geosci. 1, 309–311.

Moore, W.S., Shaw, T.J., 2008. Fluxes and behavior of radium isotopes, barium, and uranium in seven Southeastern US rivers and estuaries. Mar. Chem. 108, 236–254.

Morgan, M.G., Henrion, M., 1990. Uncertainty, a guide to dealing with uncertainty in quantitative risk and policy analysis.

Morrison, J.M., Codispoti, L.A., Smith, S.L., Wishner, K., Flagg, C., Gardner, W.D., Gaurin, S., Naqvi, S.W.A., Manghnani, V., Prosperie, L., Gundersen, J.S., 1999. The oxygen minimum zone in the Arabian Sea during 1995. Deep. Res. Part II Top. Stud. Oceanogr. 46, 1903–1931.

Morrissey, P.J., McCormack, T., Naughton, O., Meredith Johnston, P., William Gill, L., 2020. Modelling groundwater flooding in a lowland karst catchment. J. Hydrol. 580, 124361.

Mudarra, M., Andreo, B., Barberá, J.A., Mudry, J., 2014. Hydrochemical dynamics of TOC and NO3− contents as natural tracers of infiltration in karst aquifers. Environ. Earth Sci. 71, 507–523.

Muir, K.S., 1968. Groundwater reconnaissance of the Santa Barbara - Montecito Area, Santa Barbara County, California. U. S. Geol. Surv. Water Supply Pap 1859-A, 28.

Murphy, G.E.P., Romanuk, T.N., Worm, B., 2020. Cascading effects of climate change on plankton community structure. Ecol. Evol. 2170–2181.

Murphy, R.R., Curriero, F.C., Ball, W.P., 2010. Comparison of spatial interpolation methods for water quality evaluation in the chesapeake bay. J. Environ. Eng. 136, 160–171.

Nash, J.E., Sutcliffe, J. V., 1970. River flow forecasting through conceptual models part I - A discussion of principles. J. Hydrol. 10, 282–290.

Nehls, G., Thiel, M., 1993. Large-scale distribution patterns of the mussel Mytilus edulis in the Wadden Sea of Schleswig-Holstein: Do storms structure the ecosystem? Netherlands J. Sea Res. 31, 181–187.

Neilson, B., Costello, M.J., 1999. The relative lengths of seashore substrata around the coastline of Ireland as determined by digital methods in a geographical information system. Estuar. Coast. Shelf Sci. 49, 501–508.

Newell, R.I.E., 2004. Ecosystem influences of natural and cultivated populations of suspension-feeding bivalve molluscs: A review. J. Shellfish Res.

Niemistö, J., Lund-Hansen, L.C., 2019. Instantaneous Effects of Sediment Resuspension on Inorganic and Organic Benthic Nutrient Fluxes at a Shallow Water Coastal Site in the Gulf of Finland, Baltic Sea. Estuaries and Coasts 42, 2054–2071.

Nolan, P., Flanagan, J., 2020. High-resolution Climate Projections for Ireland – A Multi-

model Ensemble Approach.

Nunes, J.P., Ferreira, J.G., Bricker, S.B., O'Loan, B., Dabrowski, T., Dallaghan, B., Hawkins, A.J.S., O'Connor, B., O'Carroll, T., 2011. Towards an ecosystem approach to aquaculture: Assessment of sustainable shellfish cultivation at different scales of space, time and complexity. Aquaculture 315, 369–383.

O'boyle, S., Wilkes, R., Mcdermott, G., Longphuirt, S.N., Murray, C., 2015. Factors affecting the accumulation of phytoplankton biomass in Irish estuaries and nearshore coastal waters: A conceptual model. Estuar. Coast. Shelf Sci. 155, 75–88.

Oberdorfer, J.A., 1996. Numerical modeling of coastal discharge: predicting the effects of climate change, Groundwater discharge in the coastal zone, in: LOICZ IGBP, 69–75, Edited by R.W. Budde- Meier, Pp. 179, LOICZ, Texel, Netherlands, Russian Academy of Science.

Officer C. B., 1976. Physical Oceanography of Estuaries (and Associated Coastal Waters). Bull. Am. Meteorol. Soc. 58.

Officer, C.B., 1980. Box Models Revisited, in: P. Hamilton et Al. (Eds.), Estuarine and Wetland Processes. pp. 65–114.

Officer, C.B., 1979. Discussion of the behaviour of nonconservative dissolved constituents in estuaries. Estuar. Coast. Mar. Sci. 9, 91–94.

Oliveira, A., Baptista, A.M., 1997. Diagnostic modeling of residence times in estuaries. Water Resouces Res. 33, 1935–1946.

Pachepsky, Y., Park, Y., 2015. Saturated Hydraulic Conductivity of US Soils Grouped According to Textural Class and Bulk Density. Soil Sci. Soc. Am. J. 79, 1094–1100.

Paepen, M., Hanssens, D., De Smedt, P., Walraevens, K., Hermans, T., 2020. Combining resistivity and frequency domain electromagnetic methods to investigate submarine groundwater discharge in the littoral zone. Hydrol. Earth Syst. Sci. 24, 3539–3555.

Paerl, H.W., Huisman, J., 2009. Climate change: A catalyst for global expansion of harmful cyanobacterial blooms. Environ. Microbiol. Rep. 1, 27–37.

Palmieri, M.G., Barausse, A., Luisetti, T., Turner, K., 2014. Jellyfish blooms in the Northern Adriatic Sea: Fishermen's perceptions and economic impacts on fisheries. Fish. Res. 155, 51–58.

Parker, M., Dunne, T., Mcardle, J., 1982. Exceptional marine blooms in Irish coastal waters, in: International Council For The Exploration of the Sea.

Paulsen, R.J., Smith, C.F., O'Rourke, D., Wong, T.F., 2001. Development and evaluation of an ultrasonic ground water seepage meter. Ground Water.

Pawlowicz, R., Hannah, C., Rosenberger, A., 2019. Lagrangian observations of estuarine residence times, dispersion, and trapping in the Salish Sea. Estuar. Coast. Shelf Sci. 225, 106246.

Paytan, A., Mclaughlin, K., 2007. The Oceanic Phosphorus Cycle. Chem. Rev. 2007, 563–576.

Peierls, B.L., Hall, N.S., Paerl, H.W., 2012. Non-monotonic responses of phytoplankton biomass accumulation to hydrologic variability: A comparison of two coastal plain

north carolina estuaries. Estuaries and Coasts.

Peltier, W.R., 1994. Ice age paleotopography. Science (80-.).

Petrunic, B., Einsiedl, F., Duffy, G.P., 2012. Major ion chemistry in a coastal karstic groundwater resource located in Western Ireland. Irish J. Earth Sci. 30, 13–30.

Pihl, L., Svenson, A., Moksnes, P.-O., Wennhage, H., 1999. Distribution of green algal mats throughout shallow soft bottoms of the Swedish Skagerrak archipelago in relation to nutrient sources and wave exposure. J. Sea Res. 41, 281–294.

Piló, D., Barbosa, A.B., Teodósio, M.A., Encarnação, J., Leitão, F., Range, P., Krug, L.A., Cruz, J., Chícharo, L., 2018. Are submarine groundwater discharges affecting the structure and physiological status of rocky intertidal communities? Mar. Environ. Res. 136, 158–173.

Platt, T., Gallegos, C.L., Harrison, W.G., 1980. Photoinhibition of Photosynthesis in Natural Assemblages of Marine Phytoplankton. J. Mar. Res.

Platt, T., Jassby, A.D., 1976. The relationship between photosynthesis and light for natural assemblages of coastal marine phytoplankton.

Pluhowski, E., Kantrowitz, I., 1964. Hydrology of the Babylon–Islip Area, Suffolk County, Long Island, New York. US Geol Surv Water Supply Pap 1768, 128.

Plummer, L.N., 1975. Mixing of sea water with calcium carbonate ground water. Mem. Geol. Soc. Am. 142, 219–236.

Pongkijvorasin, S., Roumasset, J., Duarte, T.K., Burnett, K., 2010. Renewable resource management with stock externalities: Coastal aquifers and submarine groundwater discharge. Resour. Energy Econ. 32, 277–291.

Post, V.E.A., Vandenbohede, A., Werner, A.D., Maimun, Teubner, M.D., 2013. Groundwater ages in coastal aquifers. Adv. Water Resour. 57, 1–11.

Pouchar, Y., 2015. Bretagne : pour sa famille, Thierry a été tué par les algues vertes - Le Parisien. Le Paris.

Povinec, P.P., Comanducci, J.F., Levy-Palomo, I., Benjamino Oregioni, 2006. Monitoring of submarine groundwater discharge along the Donnalucata coast in the south-eastern Sicily using underwater gamma-ray spectrometry. Cont. Shelf Res. 26, 874–884.

Price, R.M., Savabi, M.R., Jolicoeur, J.L., Roy, S., 2010. Adsorption and desorption of phosphate on limestone in experiments simulating seawater intrusion. Appl. Geochemistry 25, 1085–1091.

Rabalais, N.N., Turner, R.E., Miseman Jr, W.J., 2002. Gulf of Mexico hypoxia, A.K.A."The dead zone". Ann. Rev. Ecol. Syst. 33, 235–263.

Rabouille, C., Mackenzie, F.T., Ver, L.M., 2001. Influence of the human perturbation on carbon, nitrogen, and oxygen biogeochemical cycles in the global coastal ocean. Geochim. Cosmochim. Acta 65, 3615–3641.

Raine, R., 2014. A review of the biophysical interactions relevant to the promotion of HABs in stratified systems: The case study of Ireland. Deep Sea Res. Part II Top. Stud. Oceanogr. 101, 21–31.

Rama, Moore, W.S., 1996. Using the radium quartet for evaluating groundwater input and

water exchange in salt marshes. Geochim. Cosmochim. Acta 60, 4645–4652.

Rantz, S.E., 1982. Measurement and computation of streamflow: volume 1. Measurement of stage and discharge.

Redfield, A.C., 1958. The biological control of chemical factors in the environment. Am. Sci. 46, 205–221.

Regnier, P., Arndt, S., Goossens, N., Volta, C., Laruelle, G.G., Lauerwald, R., Hartmann, J., 2013. Modelling Estuarine Biogeochemical Dynamics: From the Local to the Global Scale. Aquat. Geochemistry 19, 591–626.

Regnier, P., Steefel, C.I., 1999. A high resolution estimate of the inorganic nitrogen flux from the Scheldt estuary to the coastal North Sea during a nitrogen-limited algal bloom, spring 1995. Geochim. Cosmochim. Acta 63, 1359–1374.

Reid, P.C., 1977. Continuous plankton records: Changes in the composition and abundance of the phytoplankton of the north-eastern Atlantic ocean and North Sea, 1958-1974. Mar. Biol. 40, 337–339.

Reiffenstein, R.J., Hulbert, W.C., Roth, S.H., 1992. Toxicology of hydrogen sulfide. Annu. Rev. Pharmacol. Toxicol. 32, 109–34.

Richards, J.E., Webster, C.P., 1999. Denitrification in the subsoil of the Broadbalk Continuous Wheat Experiment. Soil Biol. Biochem.

Riisgård, H.U., Larsen, P.S., 2014. Physiologically regulated valve-closure makes mussels long-term starvation survivors: Test of hypothesis. J. Molluscan Stud. 81, 303–307.

Riisgård, H.U., Larsen, P.S., Pleissner, D., 2014. Allometric equations for maximum filtration rate in blue mussels Mytilus edulis and importance of condition index. Helgol. Mar. Res. 68, 193–198.

Robertson, W.D., 1995. Development of steady-state phosphate concentrations in septic system plumes. J. Contam. Hydrol. 19, 289–305.

Robinson, Clare, Gibbes, B., Carey, H., Li, L., 2007. Salt-freshwater dynamics in a subterranean estuary over a spring-neap tidal cycle. J. Geophys. Res. Ocean. 112, 1–15.

Robinson, C., Gibbes, B., Li, L., 2006. Driving mechanisms for groundwater flow and salt transport in a subterranean estuary. Geophys. Res. Lett. 33, 3–6.

Robinson, C., Li, L., Barry, D.A., 2007a. Effect of tidal forcing on a subterranean estuary. Adv. Water Resour. 30, 851–865.

Robinson, C., Li, L., Prommer, H., 2007b. Tide-induced recirculation across the aquifer-ocean interface. Water Resour. Res. 43, 1–14.

Robinson, C.E., Xin, P., Santos, I.R., Charette, M.A., Li, L., Barry, D.A., 2017. Groundwater dynamics in subterranean estuaries of coastal unconfined aquifers: Controls on submarine groundwater discharge and chemical inputs to the ocean. Adv. Water Resour. 315–331.

Robinson, M.A., 1998. A finite element model of submarine groundwater discharge to tidal estuarine waters.

Rocha, C., 2008. Sandy sediments as active biogeochemical reactors: Compound cycling

in the fast lane. Aquat. Microb. Ecol. 53, 119–127.

Rocha, C., 2000. Density-driven convection during flooding of warm, permeable intertidal sediments: The ecological importance of the convective turnover pump. J. Sea Res. 43, 1–14.

Rocha, C., 1998. Rhythmic ammonium regeneration and flushing in intertidal sediments of the Sado estuary. Limnol. Oceanogr. 43, 823–831.

Rocha, C., Veiga-Pires, C., Scholten, J., Knoeller, K., Gröcke, D.R., Carvalho, L., Anibal, J., Wilson, J., 2016. Assessing land-ocean connectivity via submarine groundwater discharge (SGD) in the Ria Formosa Lagoon (Portugal): combining radon measurements and stable isotope hydrology. Hydrol. Earth Syst. Sci. 20, 3077–3098.

Rocha, C., Wilson, J., Scholten, J., Schubert, M., 2015. Retention and fate of groundwater-borne nitrogen in a coastal bay (Kinvara Bay, Western Ireland) during summer. Biogeochemistry 125, 275–299.

Rodellas, V., Garcia-Orellana, J., Masqué, P., Feldman, M., Weinstein, Y., 2015a. Submarine groundwater discharge as a major source of nutrients to the Mediterranean Sea. Proc. Natl. Acad. Sci. U. S. A. 112, 3926–3930.

Rodellas, V., Garcia-Orellana, J., Masqué, P., Feldman, M., Weinstein, Y., Boyle, E.A., 2015b. Submarine groundwater discharge as a major source of nutrients to the Mediterranean Sea. Proc. Natl. Acad. Sci. U. S. A. 112, 3926–3930.

Rodellas, V., Garcia-Orellana, J., Trezzi, G., Masqué, P., Stieglitz, T.C., Bokuniewicz, H., Cochran, J.K., Berdalet, E., 2017. Using the radium quartet to quantify submarine groundwater discharge and porewater exchange. Geochim. Cosmochim. Acta 196, 58–73.

Roden, C.M., Rodhouse, P.G., Hensey, M.P., McMahon, T., Ryan, T.H., Mercer, J.P., 1987. Hydrography and the distribution of phytoplankton in Killary Harbour: a fjord in western Ireland. J. Mar. Biol. Assoc. United Kingdom 67, 359.

Rodhouse, P.G., Roden, C.M., Burnell, G.M., Hensey, M.P., McMahon, T., Ottway, B., Ryan, T.H., 1984. Food resource, gametogenesis and growth of Mytilus edulis on the shore and in suspended culture: Killary Harbour, Ireland. J. Mar. Biol. Assoc. United Kingdom 64, 513.

Roxburgh, I.S., 1985. Thermal infrared detection of submarine springs associated with the plymouth limestone. Hydrol. Sci. J. 30, 185.

Rysgaard, S., Thastum, P., Dalsgaard, T., Christensen, P.B., Sloth, N.P., 1999. Effects of Salinitry on NH4+ Adsorption Capacity, Nitrification and Denitrification in Danish Estuarine Sediments. Estuaries 22, 21–30.

Saad, O.A.L.O., Conrad, R., 1993. Temperature dependence of nitrification, denitrification, and turnover of nitric oxide in different soils. Biol. Fertil. Soils 15, 21–27.

Sadat-Noori, M., Santos, I.R., Sanders, C.J., Sanders, L.M., Maher, D.T., 2015. Groundwater discharge into an estuary using spatially distributed radon time series and radium isotopes. J. Hydrol. 528, 703–719.

Sadat-Noori, M., Santos, I.R., Tait, D.R., Maher, D.T., 2016. Fresh meteoric versus recirculated saline groundwater nutrient inputs into a subtropical estuary. Sci. Total

Environ. 566–567, 1440–1453.

Sanford, L.P., Boicourt, W.C., Rives, S.R., 1992. Model for estimating tidal flushing of small embayments. J. Waterw. Port, Coastal, Ocean Eng. 118, 635–654.

Santos, I.R., Bryan, K.R., Pilditch, C.A., Tait, D.R., 2014. Influence of porewater exchange on nutrient dynamics in two New Zealand estuarine intertidal flats. Mar. Chem. 167, 57–70.

Santos, Isaac R, Burnett, W.C., Chanton, J., Dimova, N., Peterson, R.N., 2009. Land or ocean?: Assessing the driving forces of submarine groundwater discharge at a coastal site in the Gulf of Mexico. J. Geophys. Res. 114.

Santos, Isaac R., Burnett, W.C., Dittmar, T., Suryaputra, I.G.N.A., Chanton, J., 2009. Tidal pumping drives nutrient and dissolved organic matter dynamics in a Gulf of Mexico subterranean estuary. Geochim. Cosmochim. Acta 73, 1325–1339.

Santos, I.R., Eyre, B.D., Huettel, M., 2012. The driving forces of porewater and groundwater flow in permeable coastal sediments: A review. Estuar. Coast. Shelf Sci. 98, 1–15.

Savatier, M., Rocha, C., 2021. Rethinking tracer-based (Ra, Rn, salinity) approaches to estimate point-source submarine groundwater discharge (SGD) into coastal systems. J. Hydrol.

Schmidt, A., Schlueter, M., Melles, M., Schubert, M., 2008. Continuous and discrete on-site detection of radon-222 in ground- and surface waters by means of an extraction module. Appl. Radiat. Isot. 66, 1939–1944.

Schneebeli, 1986. Hydraulique souterraine.

Schubert, M., Knoeller, K., Rocha, C., Einsiedl, F., 2015. Evaluation and source attribution of freshwater contributions to Kinvarra Bay, Ireland, using 222Rn, EC and stable isotopes as natural indicators. Environ. Monit. Assess. 187, 1–15.

Schuler, Philip, Duran, L., McCormack, T., Gill, L., 2018. Submarine and intertidal groundwater discharge through a complex multi-level karst conduit aquifer. Hydrogeol. J. 26, 2629–2647.

Schuler, P., Duran, L., McCormack, T., Gill, L.W., 2018. Submarine and intertidal groundwater discharge through a complex multi-level karst conduit aquifer. Hydrogeol. J. 26, 2629–2647.

Schuler, P., Stoeckl, L., Schnegg, P.A., Bunce, C., Gill, L., 2020. A combined-method approach to trace submarine groundwater discharge from a coastal karst aquifer in Ireland. Hydrogeol. J. 28, 561–577.

Schultz, E.A., Simmons, H.B., 1957. Fresh water-salt water density currents, a major cause of siltation in estuaries, Technical bulletin - Committee on Tidal Hydraulics.

Seed, R., 1969. The ecology of Mytilus edulis L. (Lamellibranchiata) on exposed rocky shores - II. Growth and mortality. Oecologia 3, 317–350.

Sekulic, B., Vertacnik, A., 1996. Balance of average annual fresh water inflow into the Adriatic Sea. Water Resour Dev 12, 89–97.

Sharpley, A.N., Curtin, D., Syers, J.K., 1988. Changes in Water-extractability of Soil

Inorganic Phosphate Induced by Sodium Saturation. Soil Sci. Soc. Am. J. 52, 637–640.

Sheldon, J. E. and Alber, M., 2002. A Comparison of Residence Time Calculations Using Simple Compartment Models. Coast. Estuar. Res. Fed. Part B Dedic. Issue Freshw. Inflow Sci. Policy, Manag. Symp. Pap. from 16th Bienn. Estuar. Res. Fed. Conf. (Dec., 2002) 25, 1304–1317.

Shennan, I., Bradley, S.L., Edwards, R., 2018. Relative sea-level changes and crustal movements in Britain and Ireland since the Last Glacial Maximum. Quat. Sci. Rev. 188, 143–159.

Sholkovitz, E., Herbold, C., Charette, M., 2003. An automated dye-dilution based seepage meter for the time-series measurement of submarine groundwater discharge. Limnol. Oceanogr. Methods.

Shuttleworth, E.L., Evans, M.G., Pilkington, M., Spencer, T., Walker, J., Milledge, D., Allott, T.E.H., 2019. Restoration of blanket peat moorland delays stormflow from hillslopes and reduces peak discharge. J. Hydrol. X 2, 100006.

Sierra, C.A., Müller, M., Metzler, H., Manzoni, S., Trumbore, S.E., 2017. The muddle of ages, turnover, transit, and residence times in the carbon cycle. Glob. Chang. Biol. 23, 1763–1773.

Siggins, L., 2016. Ireland's worst storm damage on record was in 2014. Accessed at: https://www.irishtimes.com/news/ireland/irish-news/ireland-s-worst-storm-damage-on-record-was-in-2014-1.2882706. The Irish Times.

Silke, J., O'Beirn, F., Cronin, M., 2005. Karenia mikimotoi : An exceptional dinoflagellate bloom in western Irish waters, summer 2005. Mar. Environ. Heal. Ser. 1–48.

Sin, Y., Wetzel, R.L., Anderson, I.C., 1999. Spatial and temporal characteristics of nutrient and phytoplankton dynamics in the York River Estuary, Virginia: Analyses of long-term data. Estuaries 22, 260–275.

Slomp, C.P., Van Cappellen, P., 2004. Nutrient inputs to the coastal ocean through submarine groundwater discharge: controls and potential impact. J. Hydrol. 295, 64–86.

Smaal, A.C., Vonck, A.P.M.A., 1997. Seasonal variation in C, N and P budgets and tissue composition of the mussel Mytilus edulis. Mar. Ecol. Prog. Ser. 153, 167–179.

Smil, V., 2000. Phosphorus in the environment: Natural Flows and Human Interferences. Annu. Rev. Energy Env. 25, 53–88.

Smith, A.J., 2004. Mixed convection and density-dependent seawater circulation in coastal aquifers. Water Resour. Res. 40.

Smith, A.M., Cave, R.R., 2012. Influence of fresh water, nutrients and DOC in two submarine-groundwater-fed estuaries on the west of Ireland. Sci. Total Environ. 438, 260–270.

Smith, L., Zawadzki, W., 2003. A hydrogeologic model of submarine groundwater discharge: Florida intercomparison experiment. Biogeochemistry 66, 95–110.

Smith, R.L., Böhlke, J.K., Song, B., Tobias, C.R., 2015. Role of Anaerobic Ammonium Oxidation (Anammox) in Nitrogen Removal from a Freshwater Aquifer. Environ. Sci.

Technol. 49, 12169–12177.

Solow, A.R., 2004. Red Tides and Dead Zones. Oceanus 43–45.

Spiteri, C., Slomp, C.P., Tuncay, K., Meile, C., 2008. Modeling biogeochemical processes in subterranean estuaries: Effect of flow dynamics and redox conditions on submarine groundwater discharge of nutrients. Water Resour. Res. 44, 1–18.

Stieglitz, T., Rapaglia, J., Bokuniewicz, H., 2008. Estimation of submarine groundwater discharge from bulk ground electrical conductivity measurements. J. Geophys. Res. Ocean.

Su, N., Burnett, W.C., MacIntyre, H.L., Liefer, J.D., Peterson, R.N., Viso, R., 2014. Natural Radon and Radium Isotopes for Assessing Groundwater Discharge into Little Lagoon, AL: Implications for Harmful Algal Blooms. Estuaries and Coasts 37, 893–910.

Suckow, A., 2014. The age of groundwater - Definitions, models and why we do not need this term. Appl. Geochemistry 50, 222–230.

Sun, Y., Torgersen, T., 1998. The effects of water content and Mn-fiber surface conditions on 224Ra measurement by 220Rn emanation. Mar. Chem. 62, 299–306.

Sverdrup, H.U., 1953. On conditions for the vernal blooming of phytoplankton. ICES J. Mar. Sci. 18, 287–295.

Swarzenski, P.W., Porcelli, D., Andersson, P.S., Smoak, J.M., 2003. The behavior of U- and Th-series nuclides in the estuarine environment. Uranium-series Geochemistry 52, 577–606.

Tamborski, J.J., Cochran, J.K., Bokuniewicz, H.J., 2017. Application of 224Ra and 222Rn for evaluating seawater residence times in a tidal subterranean estuary. Mar. Chem. 189, 32–45.

Tanaka, T., Ono, T., 1998. Contribution of soil water and its flow path to stormflow generation in a forested headwater catchment in central Japan. IAHS-AISH Publ.

Taniguchi, M., 1995. Change in Groundwater Seepage Rate into Lake Biwa, Japan. Japanese J. Limnol. 56, 261–267.

Taniguchi, M., Burnett, W.C., Cable, J.E., Turner, J. V., 2002. Investigation of submarine groundwater discharge. Hydrol. Process. 16, 2115–2129.

Taniguchi, M., Dulai, H., Burnett, K.M., Santos, I.R., Sugimoto, R., Stieglitz, T., Kim, G., Moosdorf, N., 2019. Submarine Groundwater Discharge : Updates on Its Measurement Techniques, Geophysical Drivers, Magnitudes, and Effects. Front. Environ. Sci. 7, 1–26.

Taniguchi, M., Fukuo, Y., 1993. Continuous Measurements of Ground-Water Seepage Using an Automatic Seepage Meter. Groundwater.

Taniguchi, M., Ishitobi, T., Saeki, K.I., 2005. Evaluation of time-space distributions of submarine ground water discharge. Ground Water 43, 336–342.

Tara, B., Sc, K.B., Sciences, N., 2018. An Investigation of the Effects of Submarine Groundwater Discharge on the Coastal Carbon and Nutrient Cycles of a Karstic Aquifer , Kinvara Bay , Co Galway , Ireland.

The Irish Times, 2010. Council says algae are causing brown sludge and foul smells in

Dublin Bay. 22 May.

Thompson, C., Smith, L., Maji, R., 2007. Hydrogeological modeling of submarine groundwater discharge on the continental shelf of Louisiana. J. Geophys. Res. Ocean. 112, 1–13.

Tomasky-Holmes, G., Valiela, I., Charette, M.A., 2013. Determination of water mass ages using radium isotopes as tracers: Implications for phytoplankton dynamics in estuaries. Mar. Chem. 156, 18–26.

Trainer, V.L., Bates, S.S., Lundholm, N., Thessen, A.E., Cochlan, W.P., Adams, N.G., Trick, C.G., 2012. Pseudo-nitzschia physiological ecology, phylogeny, toxicity, monitoring and impacts on ecosystem health. Harmful Algae 14, 271–300.

Tratman, E.K., 1969. The Caves of North-West Clare, Ireland. David and Charles. Newton Abbot. Devon.

Tsabaris, C., Patiris, D.L., Karageorgis, A.P., Eleftheriou, G., Papadopoulos, V.P., Georgopoulos, D., Papathanassiou, E., Povinec, P.P., 2012. In-situ radionuclide characterization of a submarine groundwater discharge site at Kalogria Bay, Stoupa, Greece. J. Environ. Radioact. 108, 50–59.

Tully, O., Clarke, S., 2012. The Status and Management of Oyster (Ostrea edulis) in Ireland. Irish Fish. Investig. 40.

Turner, S.M., Malin, G., Nightingale, P.D., Liss, P.S., 1996. Seasonal variation of dimethyl sulphide in the North Sea and an assessment of fluxes to the atmosphere. Mar. Chem. 54, 245–262.

UISCE, 2010. UISCE report for DAFF on Killary Harbour, August 2010. Prepared by Aquaculture Technical Section, BIM.

UISCE Eirean Irish Water, 2016. Annual Environmental Report 2016 - Kinvara - D0276-01.

Ulman, J.W., Aller, R.C., 1982. Diffusion coefficients in nearshore marine sediments. Limnol. Oceanogr. 27, 552–556.

Valiela, I., Costa, J., Foreman, K., Teal, J.M., Howes, B., Aubrey, D., 1990. Transport of groundwater-borne nutrients from watersheds and their effects on coastal waters. Biogeochemistry 10, 177–197.

Valiela, I., Foreman, K., LaMontagne, M., Hersh, D., Costa, J., Peckol, P., DeMeo-Andreson, B., D'Avanzo, C., Babione, M., Sham, C.H., Brawley, J., Lajtha, K., 1992. Couplings of watersheds and coastal waters: Sources and consequences of nutrient enrichment in Waquoit Bay, Massachusetts. Estuaries 15, 443–457.

Valiela, I., Mcclelland, J., Hauxwell, J., Behr, P.J., Valiela, I., Mcclelland, J., Hauxwell, J., Behr, P.J., Hersh, D., Foreman, K., 1997. Macroalgal Blooms in Shallow Estuaries : Controls and Ecophysiological and Ecosystem Consequences. Oceanogr. Harmful Algal Bloom. 42, 1105–1118.

Van der Molen, D.T., Breeuwsma, A., Boers, P.C.M., 1998. Agricultural Nutrient Losses to Surface Water in the Netherlands: Impact, Strategies, and Perspectives. J. Environ. Qual.

Van Helmond, N.A.G.M., Robertson, E.K., Conley, D.J., Hermans, M., Humborg, C., Joëlle

Kubeneck, L., Lenstra, W.K., Slomp, C.P., 2020. Removal of phosphorus and nitrogen in sediments of the eutrophic Stockholm archipelago, Baltic Sea. Biogeosciences 17, 2745–2766.

Ver, L.M.B., Mackenzie, F.T., Lerman, A., 1999. Carbon cycle in the coastal zone: Effects of global perturbations and change in the past three centuries. Chem. Geol. 159, 283–304.

Visser, A.N., Lehmann, M.F., Rügner, H., D'Affonseca, F.M., Grathwohl, P., Blackwell, N., Kappler, A., Osenbrück, K., 2021. Fate of nitrate during groundwater recharge in a fractured karst aquifer in Southwest Germany. Hydrogeol. J. 1153–1171.

W. Finkl, C., L. Krupa, S., 2003. Environmental Impacts of Coastal-Plain Activities on Sandy Beach Systems: Hazards, Perception and Mitigation. J. Coast. Res. 132–150.

Wai, H.W., Levinton, J.S., 2004. Culture of the blue mussel Mytilus edulis (Linnaeus, 1758) fed both phytoplankton and zooplankton: A microcosm experiment. Aquac. Res. 35, 965–969.

Waite, L., Grant, J., Davidson, J., 2005. Bay-scale spatial growth variation of mussels Mytilus edulis in suspended culture, Prince Edward Island, Canada. Mar. Ecol. Prog. Ser. 297, 157–167.

Walsby, A.E., Hayes, P.K., Boje, R., Stal, L.J., 1997. The selective advantage of buoyancy provided by gas vesicles for planktonic cyanobacteria in the Baltic Sea. New Phytol. 136, 407–417.

Wan, A.H.L., Wilkes, R.J., Heesch, S., Bermejo, R., Johnson, M.P., Morrison, L., 2017. Assessment and characterisation of Ireland's green tides (Ulva species). PLoS One 12.

Wang, X., Du, J., Ji, T., Wen, T., Liu, S., Zhang, J., 2014. An estimation of nutrient fluxes via submarine groundwater discharge into the Sanggou Bay-A typical multi-species culture ecosystem in China. Mar. Chem. 167, 113–122.

Wang, X., Olsen, L.M., Reitan, K.I., Olsen, Y., 2012. Discharge of nutrient wastes from salmon farms: Environmental effects, and potential for integrated multi-trophic aquaculture. Aquac. Environ. Interact. 2, 267–283.

Webb, B.M., Marr, C., 2016. Spatial Variability of Hydrodynamic Timescales in a Broad and Shallow Estuary : Mobile Bay , Alabama. J. Coast. Res. 32, 1374–1389.

Webster, I.T., Hancock, G.J., Murray, A.S., 1995. Modelling the effect of salinity on radium desorption from sediments. Geochim. Cosmochim. Acta 59, 2469–2476.

Welskel, P.K., Howes, B.L., 1992. Differential Transport of Sewage-Derived Nitrogen and Phosphorus through a Coastal Watershed. Environ. Sci. Technol. 26, 352–360.

Werner, A.D., Bakker, M., Post, V.E.A., Vandenbohede, A., Lu, C., Ataie-Ashtiani, B., Simmons, C.T., Barry, D.A., 2013. Seawater intrusion processes, investigation and management: Recent advances and future challenges. Adv. Water Resour. 51, 3–26.

White, W.B., 1988. Geomorphology and hydrology of karst terrains, New York: Oxford University Press.

Wilhelm, S.R., Schiff, S.L., Cherry, J.A., 1994. Biogeochemical Evolution of Domestic Waste Water in Septic Systems: 1. Conceptual Model. Groundwater.

Williams, J., PinderIII, J., 1990. Ground water flow and runoff in a coastal plain stream. Water Resour Bull 26:343–52.

Wilson, A.M., 2005. Fresh and saline groundwater discharge to the ocean: A regional perspective. Water Resour. Res. 41, 1–11.

Wilson, J., Rocha, C., 2014. A remote sensing and geochemical tracing approach for localising groundwater discharge to lakes, in: Neale, C.M.U., Maltese, A. (Eds.), . International Society for Optics and Photonics, p. 92391A.

Wilson, J., Rocha, C., 2012. Regional scale assessment of Submarine Groundwater Discharge in Ireland combining medium resolution satellite imagery and geochemical tracing techniques. Remote Sens. Environ. 119, 21–34.

Winogradow, A., Mackiewicz, A., Pempkowiak, J., 2019. Seasonal changes in particulate organic matter (POM) concentrations and properties measured from deep areas of the Baltic Sea. Oceanologia 61, 505–521.

Wood, C., Harrington, G.A., 2015. Influence of Seasonal Variations in Sea Level on the Salinity Regime of a Coastal Groundwater-Fed Wetland. Groundwater 53, 90–98.

Wood, T., 1979. A modification of existing simple segmented tidal prism models of mixing in estuaries. Estuar. Coast. Mar. Sci. 8, 339–347.

Worthington, S., 1999. A comprehensive strategy for understanding flow in carbonate aquifers. Speleogenes. Evol. Karst Aquifers 1, 1–8.

Worthington, S.R.H., Ford, D.C., Beddows, P.A., 1995. Porosity and permeability enhancement in unconfined carbonate aquifers as a result of solution, in: A.B. Klimchouk, D.C. Ford, A.N. Palmer, and W. Dreybrodt (Eds.), Speleogenesis Evolution of Karst Aquifers: Huntsville, Alabama, National Speleological Society, Inc. pp. 463–472.

Wyatt, T., 2014. Margalef's mandala and phytoplankton bloom strategies. Deep. Res. Part II Top. Stud. Oceanogr. 101, 32–49.

Wyatt, T., Zingone, A., 2014. Population dynamics of red tide dinoflagellates. Deep. Res. II 101, 231–236.

Yakushev, E. V., Neretin, L.N., 1997. One-dimensional modeling of nitrogen and sulfur cycles in the aphotic zones of the Black and Arabian Seas. Global Biogeochem. Cycles 11, 401–414.

Yasumoto, T., Fukui, M., Sasaki, K., Sugiyama, K., 1995. Determinations of marine toxins in foods. J. AOAC Int.

Yasumoto, T., Murata, M., 1993. Marine Toxins. Chem. Rev. 93, 1897–1909.

Yvon-Durocher, G., Jones, J.I., Trimmer, M., Woodward, G., Montoya, J.M., 2010. Warming alters the metabolic balance of ecosystems. Philos. Trans. R. Soc. B Biol. Sci. 365, 2117–2126.

Zanini, L., Robertson, W.D., Ptacek, C.J., Schiff, S.L., Mayer, T., 1998. Phosphorus characterization in sediments impacted by septic effluent at four sites in central Canada. J. Contam. Hydrol. 33, 405–429.

Zektser, I., Dzhamalov, R., 1981. Groundwater discharge to the Pacific Ocean. Hydrol Sci

Bull 26:271–9.

Zektser, I.S., Loaiciga, H.A., 1993. Groundwater fluxes in the global hydrologic cycle: past, present and future. J. Hydrol. 144, 405–427.

Zektzer, I.S., Ivanov, V.A., Meskheteli, A. V., 1973. The problem of direct groundwater discharge to the seas. J. Hydrol. 20, 1–36.

Zhou, Y.Q., Sawyer, A.H., David, C.H., Famiglietti, J.S., 2019. Fresh Submarine Groundwater Discharge to the Near-Global Coast. Geophys. Res. Lett. 46, 5855–5863.

Zimmerman, J.T.F., 1988. Estuarine Residence Times, in: Hydrodynamics of Estuaries. CRC Press, pp. 75–84.

12 General Appendix- Datasets

Note: The standard deviations shown are calculated from triplicate samples taken in separate vials and filtrated independently, so as to account for each sample for the potential bias due to low level contaminations of the sample during filtration. This precaution allowed to build confidence in the values that were the closer from method detection limits.

Appendix 9: Temperature, Salinity, Turbidity, oxidation/reduction potential (ORP), pH, Dissolved oxygen (% saturation) and Electrical conductivity in Kinvarra Bay.

Fieldtrip	Station	Date	Time	X	Y	Distance to spring (km)	Temperature	Salinity	Turbidity	ORP	pH	DO %	EC mS cm^{-1}
Summer 2018 (07)	T1	13/07/2018	07:00	-8.943077	53.166102	-	17.8	27.0	0.0	82.1	8.1	76.5	45.4
Summer 2018 (07)	T2	13/07/2018	09:15	-8.943077	53.166102	-	18.8	32.4	0.0	98.2	8.7	129.3	52.7
Summer 2018 (07)	T3	13/07/2018	11:30	-8.943077	53.166102	-	18.7	27.9	0.0	92.3	8.5	112.2	47.3
Summer 2018 (07)	T4	13/07/2018	13:30	-8.943077	53.166102	-	19.1	23.2	0.0	100.7	9.3	102.3	41.8
Summer 2018 (07)	T5	13/07/2018	15:00	-8.943077	53.166102	-	18.8	37.1	0.0	108.8	8.7	104.6	59.4
Summer 2018 (07)	T6	13/07/2018	16:30	-8.943077	53.166102	-	22.0	35.7	0.0	109.9	8.8	131.6	61.1
Summer 2018 (07)	T7	13/07/2018	19:00	-8.943077	53.166102	-	20.0	37.7	0.0	108.4	8.7	101.7	61.4
Summer 2018 (07)	T8	13/07/2018	21:00	-8.943077	53.166102	-	19.2	38.1	3.6	101.9	8.5	93.6	61.0
Summer 2018 (07)	T9	13/07/2018	23:00	-8.943077	53.166102	-	18.3	31.8	0.0	139.3	7.3	85.3	51.5
Summer 2018 (07)	T10	14/07/2018	01:00	-8.943077	53.166102	-	17.3	20.7	0.0	92.5	7.7	98.0	37.6
Summer 2018 (07)	T11	14/07/2018	03:00	-8.943077	53.166102	-	17.3	21.7	0.0	100.4	7.9	96.1	38.8
Summer 2018 (07)	T12	14/07/2018	05:00	-8.943077	53.166102	-	16.5	26.8	0.0	95.8	8.0	88.7	44.2
Summer 2018 (07)	T13	14/07/2018	07:00	-8.943077	53.166102	-	17.0	30.7	0.0	92.9	8.0	95.9	49.1
Summer 2018 (07)	BH-AM	12/07/2018	10:15	-8.918775	53.126792	-1.7	15.3	7.6	0.0	140.4	7.1	21.8	1.4
Summer 2018 (07)	BH-PM	12/07/2018	17:30	-8.918775	53.126792	-1.7	15.9	1.3	0.0	138.0	7.3	20.8	3.5
Summer 2018 (07)	EM	13/07/2018	17:51	-8.960208	53.176245	4.89	18.3	30.5	0.0	104.5	8.6	102.6	59.8
Summer 2018 (07)	SP	12/07/2018	11:45	-8.92645	53.141673	0	17.9	1.6	0.0	132.5	7.3	57.4	11.1
Summer 2018 (07)	ST1	13/07/2018	17:30	-8.961683	53.162283	3.46	19.9	29.8	0.0	107.3	8.6	104.4	61.4
Summer 2018 (07)	ST2	13/07/2018	18:28	-8.938937	53.145213	1.06	20.2	29.8	0.0	99.9	8.7	64.0	60.9
Summer 2018 (07)	ST3	13/07/2018	18:51	-8.948233	53.155417	2.36	19.1	29.1	0.0	102.0	8.7	104.1	59.9
Summer 2018 (07)	ST4	13/07/2018	17:37	-8.9488	53.164738	3.46	18.8	30.3	0.0	105.7	8.7	103.7	58.8
Summer 2018 (07)	ST5	13/07/2018	17:37	-8.954132	53.166427	3.46	18.8	29.6	0.0	108.8	8.7	104.6	59.4
Autumn 2018 (10)	T1	22/10/2018	10:00	-8.943077	53.166102	-	12.0	30.4	0.0	62.4	7.5	70.5	44.5
Autumn 2018 (10)	T2	22/10/2018	13:00	-8.943077	53.166102	-	12.5	28.4	6.0	79.5	8.0	109.9	42.8
Autumn 2018 (10)	T3	22/10/2018	16:00	-8.943077	53.166102	-	13.2	28.4	0.0	43.5	8.3	104.8	43.4

Autumn 2018 (10)	T4	22/10/2018	19:00	-8.943077	53.166102	-	12.9	29.3	0.0	75.3	8.1	92.2	44.1
Autumn 2018 (10)	T5	22/10/2018	22:00	-8.943077	53.166102	-	13.5	28.1	47.4	68.5	8.1	82.3	43.3
Autumn 2018 (10)	T6	23/10/2018	01:00	-8.943077	53.166102	-	12.5	26.3	10.1	71.5	8.2	83.1	-
Autumn 2018 (10)	T7	23/10/2018	04:00	-8.943077	53.166102	-	12.0	26.9	4.3	81.2	8.4	91.2	40.9
Autumn 2018 (10)	T8	23/10/2018	07:00	-8.943077	53.166102	-	12.2	28.2	4.3	77.5	8.3	89.6	-
Autumn 2018 (10)	T9	23/10/2018	10:00	-8.943077	53.166102	-	12.3	27.9	9.3	75.0	8.4	90.1	42.2
Autumn 2018 (10)	BH	20/10/2018	10:50	-8.918767	53.126792	-1.7	12.1	0.3	0.0	158.5	7.2	42.1	0.5
Autumn 2018 (10)	SP	20/10/2018	08:55	-8.92645	53.141673	0	12.5	0.5	0.0	162.8	6.8	54.2	0.8
Autumn 2018 (10)	ST1	21/10/2018	16:30	-8.942543	53.16705	4	14.3	29.4	0.0	103.0	7.5	98.8	68.8
Autumn 2018 (10)	ST2	21/10/2018	17:00	-8.930507	53.14469	0.5	14.8	10.2	1.0	107.2	7.9	97.4	23.7
Autumn 2018 (10)	ST3	21/10/2018	17:30	-8.952848	53.153857	2	14.0	26.4	0.0	98.5	8.1	102.0	66.8
Autumn 2018 (10)	ST4	21/10/2018	18:30	-8.968368	53.172163	4.6	13.0	30.3	4.2	88.1	8.5	106.4	43.7
Winter 2019 (01)	T1	25/01/2019	17:00	-8.968507	53.171727	-	9.0	28.3	0.0	104.2	8.3	91.4	38.9
Winter 2019 (01)	T2	25/01/2019	20:00	-8.968507	53.171727	-	10.7	29.2	0.0	20.5	8.7	87.9	40.7
Winter 2019 (01)	T3	25/01/2019	23:00	-8.968507	53.171727	-	9.6	29.2	0.0	35.5	8.3	87.7	42.3
Winter 2019 (01)	T4	26/01/2019	02:00	-8.968507	53.171727	-	9.6	28.4	0.0	14.5	8.6	88.9	39.6
Winter 2019 (01)	T5	26/01/2019	05:00	-8.968507	53.171727	-	9.7	26.6	0.0	46.5	8.8	90.2	39.9
Winter 2019 (01)	T6	26/01/2019	08:00	-8.968507	53.171727	-	9.6	29.2	0.0	19.3	8.6	90.5	42.2
Winter 2019 (01)	T7	26/01/2019	11:00	-8.968507	53.171727	-	9.9	27.4	0.0	11.2	8.7	96.2	41.2
Winter 2019 (01)	T8	26/01/2019	14:00	-8.968507	53.171727	-	9.9	27.5	0.0	45.4	8.4	99.0	41.3
Winter 2019 (01)	T9	26/01/2019	17:00	-8.968507	53.171727	-	9.3	28.0	0.0	27.9	8.5	91.0	41.6
Winter 2019 (01)	BH	28/01/2019	16:15	-8.918767	53.126792	-1.7	10.8	0.3	0.0	0.0	0.0	0.0	0.6
Winter 2019 (01)	EM	28/01/2019	12:42	-8.963631	53.180916	5.49	11.1	26.4	0.0	0.0	0.0	0.0	41.3
Winter 2019 (01)	SP	26/01/2019	17:10	-8.92645	53.141673	0	10.2	0.6	0.0	95.4	7.2	67.7	1.3
Winter 2019 (01)	ST1	28/01/2019	11:28	-8.934121	53.143164	0.56	10.6	8.3	0.0	0.0	0.0	0.0	14.2
Winter 2019 (01)	ST2	28/01/2019	11:40	-8.938077	53.14554	0.96	10.7	6.2	0.0	0.0	0.0	0.0	10.9
Winter 2019 (01)	ST3	28/01/2019	11:55	-8.941101	53.151073	1.63	11.0	7.9	0.0	0.0	0.0	0.0	13.5
Winter 2019 (01)	ST4	28/01/2019	12:08	-8.947829	53.158552	2.59	10.6	17.6	0.0	0.0	0.0	0.0	28.6
Winter 2019 (01)	ST5	28/01/2019	12:19	-8.954884	53.165489	3.53	10.8	25.6	0.0	0.0	0.0	0.0	40.2
Winter 2019 (01)	ST6	28/01/2019	12:32	-8.962771	53.171481	4.39	10.6	26.1	0.0	0.0	0.0	0.0	40.9
Spring 2019 (04)	T1	07/04/2019	12:50	-8.968507	53.171727	-	11.5	18.4	14.6	113.0	8.1	120.3	22.6
Spring 2019 (04)	T2	07/04/2019	16:00	-8.968507	53.171727	-	12.6	29.7	6.7	122.9	8.3	121.0	26.3
Spring 2019 (04)	T3	07/04/2019	19:00	-8.968507	53.171727	-	13.0	30.0	16.2	142.8	8.3	107.9	26.4
Spring 2019 (04)	T4	07/04/2019	22:00	-8.968507	53.171727	-	10.7	30.9	39.2	354.5	5.0	100.2	27.4

Spring 2019 (04)	T5	08/04/2019	01:00	-8.968507	53.171727	-	10.9	28.6	0.0	383.0	7.7	94.7	35.4
Spring 2019 (04)	T6	08/04/2019	04:00	-8.968507	53.171727	-	9.3	28.5	62.7	149.0	7.9	101.4	35.9
Spring 2019 (04)	T7	08/04/2019	07:00	-8.968507	53.171727	-	9.1	29.7	4.3	162.0	7.6	86.0	35.7
Spring 2019 (04)	T8	08/04/2019	10:00	-8.968507	53.171727	-	10.3	29.0	1.3	164.4	8.1	122.3	35.3
Spring 2019 (04)	T9	08/04/2019	13:00	-8.968507	53.171727	-	11.8	27.1	4.6	116.9	8.3	134.0	34.5
Spring 2019 (04)	BH	08/04/2019	15:00	-8.918767	53.126792	-1.7	11.1	0.2	0.0	259.7	5.6	52.5	0.6
Spring 2019 (04)	EM	06/04/2019	16:58	-8.962164	53.181533	5.72	11.5	31.9	0.0	161.2	8.5	183.3	29.5
Spring 2019 (04)	SP	07/04/2019	14:00	-8.92645	53.141673	0	11.9	0.4	0.2	130.7	7.5	72.5	0.8
Spring 2019 (04)	SPUP	08/04/2019	13:30	-8.92645	53.141673	0	11.7	0.0	0.0	111.1	7.6	77.0	1.2
Spring 2019 (04)	ST1	06/04/2019	15:10	-8.935724	53.142924	0.64	11.8	12.8	1.5	130.4	7.7	173.8	21.5
Spring 2019 (04)	ST2	06/04/2019	15:32	-8.938942	53.146	1.14	11.6	14.3	0.0	155.0	8.0	174.8	21.2
Spring 2019 (04)	ST3	06/04/2019	15:45	-8.941683	53.151315	1.79	11.3	23.2	0.0	151.0	8.3	186.6	25.2
Spring 2019 (04)	ST4	06/04/2019	16:02	-8.949191	53.159132	2.81	11.3	30.9	0.0	153.1	8.5	189.4	28.3
Spring 2019 (04)	ST5	06/04/2019	16:25	-8.957427	53.165856	3.67	10.8	32.4	0.0	176.6	8.5	188.4	29.5
Spring 2019 (04)	ST6	06/04/2019	16:43	-8.963944	53.17228	4.63	11.6	33.5	0.0	216.9	8.5	182.6	29.5

Appendix 10: Water temperature, Salinity, Turbidity, oxidation/reduction potential (ORP), pH, Dissolved oxygen and Electronic conductivity in Killary Harbour and in River Bunowen (R1), River Erriff (R2), River Bundoragha (R3)

Fieldtrip	Station	Date	Time	X	Y	Distance to Erriff river	Temperature	Salinity	Turbidity	ORP	pH	DO %	EC mS cm^{-1}
Summer 2017 (08)	1D	24/08/2017	09:50	-9.856568	53.622383	14.83	15.6	39.1	0.0	98.3	8.5	98.3	69.1
Summer 2017 (08)	1S	24/08/2017	09:35	-9.856568	53.622383	14.83	15.9	25.0	0.0	87.9	8.5	98.6	53.7
Summer 2017 (08)	2D	24/08/2017	10:20	-9.820283	53.613233	13.69	16.5	32.1	0.0	93.6	8.6	98.8	72.4
Summer 2017 (08)	2S	24/08/2017	10:12	-9.820283	53.613233	13.69	16.1	28.9	0.0	80.0	8.6	95.1	58.4
Summer 2017 (08)	3D	24/08/2017	11:05	-9.794417	53.604533	12.5	15.9	32.6	0.0	99.9	8.6	97.7	72.4
Summer 2017 (08)	3S	24/08/2017	10:42	-9.794417	53.604533	12.5	16.2	23.8	0.0	86.0	8.6	98.0	52.5
Summer 2017 (08)	4D	24/08/2017	11:50	-9.782892	53.5997	9.9	15.8	30.1	0.0	106.4	8.5	95.8	69.5
Summer 2017 (08)	4S	24/08/2017	11:39	-9.782892	53.5997	9.9	16.0	20.5	0.0	102.6	8.7	97.2	48.6
Summer 2017 (08)	5D	24/08/2017	12:40	-9.757333	53.600783	6.53	15.0	31.1	0.0	99.4	8.9	97.3	37.9

Summer 2017 (08)	5S	24/08/2017	12:30	-9.757333	53.600783	6.53	15.8	21.3	0.0	92.5	8.5	87.8	67.6
Summer 2017 (08)	6S	24/08/2017	13:12	-9.72395	53.601033	3.66	15.6	11.0	0.0	99.9	8.8	99.6	14.9
Summer 2017 (08)	EM	24/08/2017	09:02	-9.721692	53.600626	15.89	15.9	32.5	0.0	88.8	8.3	98.3	62.3
Summer 2017 (08)	R1	26/08/2017	00:00	-9.778207	53.583583	8.58	16.1	0.3	0.0	118.0	7.7	99.2	0.5
Summer 2017 (08)	R2	26/08/2017	00:00	-9.670602	53.615819	0	17.4	0.2	0.0	119.7	8.0	103.4	0.3
Summer 2017 (08)	R3	26/08/2017	00:00	-9.753155	53.606967	6.38	17.4	0.0	0.0	104.0	6.7	104.0	0.1
Winter 2018 (02)	T1	18/02/2018	13:00	-9.730128	53.6002	-	9.1	26.2	13.1	115.0	0.0	99.1	28.1
Winter 2018 (02)	T2	18/02/2018	16:00	-9.730128	53.6002	-	8.8	26.6	2.6	146.5	7.4	99.0	28.3
Winter 2018 (02)	T3	18/02/2018	19:00	-9.730128	53.6002	-	9.1	26.0	1.4	107.2	7.4	96.9	27.9
Winter 2018 (02)	T4	18/02/2018	22:00	-9.730128	53.6002	-	9.0	23.7	3.6	174.0	7.6	95.0	25.6
Winter 2018 (02)	T5	19/02/2018	01:00	-9.730128	53.6002	-	9.1	14.5	3.1	98.6	7.8	97.9	16.4
Winter 2018 (02)	T6	19/02/2018	04:00	-9.730128	53.6002	-	9.1	15.2	2.5	101.2	7.9	98.7	17.1
Winter 2018 (02)	T7	19/02/2018	07:00	-9.730128	53.6002	-	10.9	16.8	3.2	109.5	7.9	100.0	19.6
Winter 2018 (02)	T8	19/02/2018	10:00	-9.730128	53.6002	-	9.6	17.8	2.5	111.5	7.9	97.1	20.0
Winter 2018 (02)	T9	19/02/2018	13:00	-9.730128	53.6002	-	9.9	14.7	0.2	105.6	7.8	103.1	16.9
Winter 2018 (02)	5D	17/02/2018	09:30	-9.721692	53.600626	3.93	-	-	-	-	-	-	-
Winter 2018 (02)	K16-1D	16/02/2018	12:20	-9.877823	53.630149	15.01	7.8	32.1	5.4	111.3	7.9	102.0	32.6
Winter 2018 (02)	K16-1S	16/02/2018	12:14	-9.877823	53.630149	15.01	6.5	31.5	2.5	133.2	8.2	98.0	31.0
Winter 2018 (02)	K16-2D	16/02/2018	13:35	-9.857046	53.620501	13.14	7.9	32.9	7.7	112.2	7.8	100.1	33.4
Winter 2018 (02)	K16-2S	16/02/2018	13:27	-9.857046	53.620501	13.14	6.1	30.0	2.5	103.1	8.3	98.1	29.3
Winter 2018 (02)	K16-3D	16/02/2018	13:35	-9.812439	53.610216	10.26	7.5	33.2	8.8	108.7	7.9	100.1	33.4
Winter 2018 (02)	K16-3S	16/02/2018	14:30	-9.812439	53.610216	10.26	5.9	21.9	3.2	113.1	8.2	98.2	22.0
Winter 2018 (02)	K16-4D-5S	16/02/2018	15:40	-9.758291	53.60135	6.16	5.6	33.5	1.0	108.4	8.3	99.0	14.4

Winter 2018 (02)	K16-4S	16/02/2018	15:32	-9.758291	53.60135	6.16	6.8	14.0	0.5	119.0	8.4	97.1	31.4
Winter 2018 (02)	K16EM	16/02/2018	11:32	-9.721692	53.600626	16.49	7.1	31.7	2.7	114.8	8.1	98.8	33.2
Winter 2018 (02)	K17-1D	17/02/2018	07:30	-9.877823	53.630149	13.14	8.2	31.5	10.1	86.4	7.2	100.7	32.4
Winter 2018 (02)	K17-1S	17/02/2018	07:30	-9.877823	53.630149	13.14	6.2	28.5	3.8	95.7	8.0	97.0	28.1
Winter 2018 (02)	K17-2D	17/02/2018	07:45	-9.857046	53.620501	11.25	7.3	31.6	9.3	101.0	8.1	100.3	31.7
Winter 2018 (02)	K17-2S	17/02/2018	07:45	-9.857046	53.620501	11.25	6.4	27.8	3.8	109.4	8.1	96.5	27.6
Winter 2018 (02)	K17-3D	17/02/2018	08:00	-9.812439	53.610216	8.22	7.4	31.8	8.0	102.5	8.0	100.1	32.0
Winter 2018 (02)	K17-3S	17/02/2018	08:00	-9.812439	53.610216	8.22	5.5	17.2	4.1	102.3	8.1	98.3	17.3
Winter 2018 (02)	K17-4D	17/02/2018	08:45	-9.758291	53.60135	6.16	7.5	31.9	5.7	97.6	8.0	96.6	32.2
Winter 2018 (02)	K17-4S	17/02/2018	08:45	-9.758291	53.60135	6.16	5.4	18.4	4.3	97.7	8.0	98.9	18.4
Winter 2018 (02)	K17-5S	17/02/2018	09:30	-9.721692	53.600626	3.93	5.6	10.4	4.8	91.1	8.2	99.7	10.9
Winter 2018 (02)	R1	18/02/2018	00:00	-9.778207	53.583583	8.58	9.2	0.2	6.7	73.4	8.4	100.7	0.3
Winter 2018 (02)	R2	18/02/2018	00:00	-9.670602	53.615819	0	8.2	0.1	4.2	79.9	8.0	100.1	0.1
Winter 2018 (02)	R3	18/02/2018	00:00	-9.753155	53.606967	6.38	8.6	0.0	1.3	97.8	7.9	99.8	0.1
Summer 2018 (07)	T1	16/07/2018	13:00	-9.85983	53.620311	-	17.2	39.3	0.0	66.0	8.6	131.8	49.0
Summer 2018 (07)	T2	16/07/2018	15:00	-9.85983	53.620311	-	13.4	40.2	2.6	22.8	8.8	144.0	50.0
Summer 2018 (07)	T3	16/07/2018	17:00	-9.85983	53.620311	-	15.8	30.6	24.9	85.2	8.2	109.8	38.3
Summer 2018 (07)	T4	16/07/2018	19:00	-9.85983	53.620311	-	15.7	34.7	0.0	74.0	8.2	104.4	42.4
Summer 2018 (07)	T5	16/07/2018	21:00	-9.85983	53.620311	-	15.5	34.3	0.0	70.8	8.1	101.4	41.8
Summer 2018 (07)	T6	16/07/2018	23:00	-9.85983	53.620311	-	15.4	31.9	0.0	59.1	8.2	101.9	39.1
Summer 2018 (07)	T7	17/07/2018	01:00	-9.85983	53.620311	-	15.4	35.0	0.0	45.9	8.1	87.4	42.4
Summer 2018 (07)	T8	17/07/2018	03:00	-9.85983	53.620311	-	15.4	31.4	26.2	58.5	7.7	78.5	38.6
Summer 2018 (07)	T9	17/07/2018	05:00	-9.85983	53.620311	-	15.1	31.8	0.0	49.4	8.1	99.0	38.7

Summer 2018 (07)	1D	16/07/2018	08:23	-9.856568	53.622383	13.82	13.8	32.1	3.6	1029.0	8.1	93.9	37.9
Summer 2018 (07)	1S	16/07/2018	08:37	-9.856568	53.622383	13.82	15.1	31.1	0.0	106.9	8.0	102.0	38.0
Summer 2018 (07)	2D	16/07/2018	08:57	-9.820283	53.613233	11.14	14.8	34.5	0.0	110.0	8.1	94.7	41.4
Summer 2018 (07)	2S	16/07/2018	09:18	-9.820283	53.613233	11.14	16.2	36.7	0.0	110.9	8.3	101.4	45.2
Summer 2018 (07)	3D	16/07/2018	09:39	-9.794417	53.604533	9.26	15.0	36.1	0.0	87.0	8.2	94.4	43.3
Summer 2018 (07)	3S	16/07/2018	10:00	-9.794417	53.604533	9.26	15.2	33.1	0.0	97.7	8.3	102.1	40.3
Summer 2018 (07)	4D	16/07/2018	10:16	-9.782892	53.5997	8.13	14.8	30.9	0.0	108.7	8.2	95.8	37.5
Summer 2018 (07)	4S	16/07/2018	10:32	-9.782892	53.5997	8.13	15.1	30.2	0.0	110.7	8.1	100.4	36.9
Summer 2018 (07)	5D	16/07/2018	10:58	-9.757333	53.600783	6.36	15.0	33.1	0.0	113.6	8.2	96.8	40.1
Summer 2018 (07)	5S	16/07/2018	11:25	-9.757333	53.600783	6.36	15.6	29.1	0.0	117.2	8.1	99.7	36.1
Summer 2018 (07)	6S	16/07/2018	11:52	-9.72395	53.601033	4.15	16.4	32.7	0.0	119.4	8.2	98.7	40.9
Summer 2018 (07)	EM	16/07/2018	08:10	-9.721692	53.600626	15.36	14.9	32.6	0.0	90.2	8.3	104.0	39.5
Summer 2018 (07)	R1	16/07/2018	15:45	-9.778207	53.583583	8.58	16.9	0.3	0.0	73.3	8.9	100.5	0.5
Summer 2018 (07)	R2	15/07/2018	15:45	-9.670602	53.615819	0	19.9	0.4	0.0	130.9	7.4	99.6	0.7
Summer 2018 (07)	R3	15/07/2018	14:30	-9.753155	53.606967	6.38	19.1	0.2	0.0	112.4	7.6	100.5	0.3
Autumn 2018 (10)	1D	25/10/2018	08:30	-9.825283	53.614507	11.2	12.9	33.6	0.0	17.7	8.5	91.1	38.5
Autumn 2018 (10)	1S	25/10/2018	08:15	-9.825283	53.614507	11.2	12.6	30.7	0.0	38.7	8.1	91.7	35.3
Autumn 2018 (10)	2D	25/10/2018	09:30	-9.789332	53.601092	7.87	12.9	32.2	0.0	16.4	8.4	86.3	37.2
Autumn 2018 (10)	2S	25/10/2018	09:15	-9.789332	53.601092	7.87	12.0	28.6	0.0	49.2	8.2	92.3	32.6
Autumn 2018 (10)	3D	25/10/2018	10:00	-9.759552	53.600582	5.89	12.9	31.7	0.0	25.7	8.4	83.8	36.6
Autumn 2018 (10)	3S	25/10/2018	09:45	-9.759552	53.600582	5.89	12.1	25.4	0.0	39.0	8.5	91.7	29.4
Autumn 2018 (10)	4S	25/10/2018	10:20	-9.722391	53.600944	3.61	12.0	26.2	0.0	38.2	8.2	92.2	30.2
Autumn 2018 (10)	EM	25/10/2018	08:00	-9.881891	53.63162	15.24	13.4	30.1	0.0	72.5	7.7	91.9	

Autumn 2018 (10)	R1 - Bunowen	24/10/2018	00:00	-9.778207	53.583583	8.58	12.8	0.3	0.0	83.1	7.9	95.5	0.5
Autumn 2018 (10)	R2 - Erriff	24/10/2018	14:45	-9.670602	53.615819	0	12.1	0.1	0.0	91.8	7.7	96.3	0.2
Autumn 2018 (10)	R3 - Bundoragha	24/10/2018	13:30	-9.753155	53.606967	6.38	12.3	0.1	0.0	67.7	8.0	95.5	0.2
Winter 2019 (01)	T1	24/01/2019	05:00	-9.73165	53.598464	-	12.5	15.3	0.0	107.8	6.9	95.0	33.8
Winter 2019 (01)	T2	24/01/2019	08:00	-9.73165	53.598464	-	9.0	16.6	0.0	57.3	7.6	71.4	38.1
Winter 2019 (01)	T3	24/01/2019	11:00	-9.73165	53.598464	-	9.5	16.0	0.0	48.8	7.8	92.4	36.9
Winter 2019 (01)	T4	24/01/2019	14:00	-9.73165	53.598464	-	9.4	11.3	19.6	43.6	7.6	93.4	27.6
Winter 2019 (01)	T5	24/01/2019	17:00	-9.73165	53.598464	-	9.1	13.9	0.0	27.5	7.5	90.6	34.2
Winter 2019 (01)	T6	24/01/2019	20:00	-9.73165	53.598464	-	10.0	14.3	0.0	45.3	7.6	87.7	33.0
Winter 2019 (01)	T7	24/01/2019	23:00	-9.73165	53.598464	-	9.7	15.3	1.9	43.1	7.6	87.9	34.4
Winter 2019 (01)	T8	25/01/2019	02:00	-9.73165	53.598464	-	9.6	10.0	1.7	33.8	8.5	88.2	24.3
Winter 2019 (01)	T9	25/01/2019	05:00	-9.73165	53.598464	-	9.5	15.3	0.0	83.5	8.0	88.6	33.6
Winter 2019 (01)	1D	23/01/2019	08:55	-9.817082	53.612233	10.62	8.2	34.7	0.0	137.2	8.3	90.6	58.2
Winter 2019 (01)	1S	23/01/2019	08:25	-9.817082	53.612233	10.62	7.8	26.6	0.0	0.0	8.3	90.5	52.4
Winter 2019 (01)	2D	23/01/2019	09:25	-9.778845	53.599833	7.7	8.9	33.8	0.0	91.9	7.9	91.5	56.7
Winter 2019 (01)	2S	23/01/2019	09:15	-9.778845	53.599833	7.7	7.0	17.1	0.0	86.2	8.0	90.5	46.6
Winter 2019 (01)	3D	23/01/2019	09:55	-9.758313	53.600483	6.28	9.0	34.0	0.0	99.0	8.3	86.8	53.2
Winter 2019 (01)	3S	23/01/2019	09:45	-9.758313	53.600483	6.28	6.9	12.1	0.0	96.6	8.5	91.5	36.9
Winter 2019 (01)	4D	23/01/2019	10:37	-9.742187	53.600933	5.41	9.1	33.8	0.0	76.1	8.2	89.7	58.0
Winter 2019 (01)	4S	23/01/2019	10:27	-9.742187	53.600933	5.41	6.9	10.8	0.0	59.2	8.7	91.4	33.5
Winter 2019 (01)	5S	23/01/2019	10:55	-9.73033	53.60095	4.37	6.9	9.4	0.0	59.5	8.8	90.5	29.2
Winter 2019 (01)	6S	23/01/2019	11:30	-9.715354	53.601058	3.49	6.4	9.8	0.0	74.9	8.4	91.7	30.5
Winter 2019 (01)	EM	23/01/2019	07:46	-9.881891	53.63162	15.34	9.0	28.7	0.0	61.7	7.7	90.7	57.2

Winter 2019 (01)	R1	24/01/2019	15:30	-9.778207	53.583583	8.58	10.0	0.2	0.0	83.1	7.6	92.7	0.3
Winter 2019 (01)	R2	24/01/2019	14:30	-9.670602	53.615819	0	9.1	0.1	0.0	76.2	8.1	96.1	0.4
Winter 2019 (01)	R3	23/01/2019	15:00	-9.753155	53.606967	6.38	7.9	0.1	0.0	109.9	8.6	94.5	0.5
Spring 2019 (04)	T1	02/04/2019	21:00	-9.73165	53.598464	-	9.5	33.3	0.0	65.4	7.6	97.7	35.3
Spring 2019 (04)	T2	02/04/2019	00:00	-9.73165	53.598464	-	8.0	29.1	0.0	70.2	7.8	98.3	33.2
Spring 2019 (04)	T3	03/04/2019	03:00	-9.73165	53.598464	-	7.0	20.7	0.0	119.4	8.1	99.5	30.6
Spring 2019 (04)	T4	03/04/2019	06:00	-9.73165	53.598464	-	8.0	30.7	0.0	91.1	7.9	98.9	33.8
Spring 2019 (04)	T5	03/04/2019	09:00	-9.73165	53.598464	-	8.2	30.5	0.0	106.0	8.1	100.5	33.7
Spring 2019 (04)	T6	03/04/2019	12:00	-9.73165	53.598464	-	8.3	25.2	0.0	107.1	7.8	100.9	31.8
Spring 2019 (04)	T7	03/04/2019	15:00	-9.73165	53.598464	-	9.0	26.7	0.0	137.6	7.2	105.2	31.7
Spring 2019 (04)	T8	03/04/2019	18:00	-9.73165	53.598464	-	9.5	28.0	0.0	153.2	7.7	105.1	33.0
Spring 2019 (04)	T9	03/04/2019	21:00	-9.73165	53.598464	-	8.1	30.1	0.0	148.9	7.6	101.1	33.5
Spring 2019 (04)	1D	04/04/2019	07:47	-9.817082	53.612233	11.34	8.3	34.9	0.0	162.0	8.3	101.6	29.6
Spring 2019 (04)	1S	04/04/2019	07:46	-9.817082	53.612233	11.34	7.2	31.7	0.0	142.9	8.1	101.9	28.4
Spring 2019 (04)	2D	04/04/2019	08:45	-9.778845	53.599833	9.38	8.3	35.0	0.0	160.0	8.3	101.9	29.5
Spring 2019 (04)	2S	04/04/2019	08:40	-9.778845	53.599833	9.38	8.0	31.3	0.0	217.0	8.3	102.0	27.0
Spring 2019 (04)	3D	04/04/2019	09:20	-9.758313	53.600483	7.08	8.7	33.9	0.0	171.0	8.5	102.0	29.4
Spring 2019 (04)	3S	04/04/2019	09:15	-9.758313	53.600483	7.08	8.5	27.6	0.0	208.0	8.5	101.6	27.2
Spring 2019 (04)	4D	04/04/2019	10:05	-9.742187	53.600933	5.58	12.9	34.0	0.0	165.7	8.3	100.0	29.3
Spring 2019 (04)	4S	04/04/2019	10:00	-9.742187	53.600933	5.58	7.9	26.4	0.0	170.0	8.1	102.0	26.8
Spring 2019 (04)	5S	04/04/2019	10:15	-9.73033	53.60095	4.34	8.2	26.8	0.0	151.2	8.4	102.0	26.7
Spring 2019 (04)	6S	04/04/2019	10:28	-9.715354	53.601058	3.58	8.2	23.3	0.0	154.4	8.5	101.0	25.1
Spring 2019 (04)	7S	03/04/2019	14:45	-9.681944	53.609871	1.2	0.0	0.0	0.0	0.0	0.0	0.0	0.0

Spring 2019 (04)	EM	04/04/2019	06:58	-9.881891	53.63162	16.02	7.4	34.9	0.0	142.6	7.5	103.3	29.8
Spring 2019 (04)	R1	03/04/2019	10:00	-9.778207	53.583583	8.58	6.0	0.1	0.0	93.0	8.2	100.0	0.4
Spring 2019 (04)	R2	03/04/2019	12:00	-9.670602	53.615819	0	7.8	0.1	0.0	77.0	8.5	99.9	0.5
Spring 2019 (04)	R3	04/04/2019	13:30	-9.753155	53.606967	6.38	8.1	0.1	0.0	150.6	7.0	101.7	0.3

Appendix 11: Nutrient data for Kinvarra Bay

Fieldtrip	Station	Date	Time	X	Y	km from river	Salinity (kg m^{-3})	TOxN (µmol L^{-1})	Stdev TOXN	NH_3 (µmol L^{-1})	Stdev NH3	NO_2 (µmol L^{-1})	Stdev NO_2	SRP (µmol L^{-1})	Stdev SRP
Summer 2018 (07)	T1	13/07/2018	07:00	-8.943077	53.166102	-	27.0	0.3	0.0	2.1	0.77	0.3	-	0.5	0.11
Summer 2018 (07)	T2	13/07/2018	09:15	-8.943077	53.166102	-	32.4	1.5	0.2	1.0	0.27	0.3	0.07	0.1	0.01
Summer 2018 (07)	T3	13/07/2018	11:30	-8.943077	53.166102	-	27.9	0.7	1.0	0.7	0.06	0.5	0.04	0.5	0.04
Summer 2018 (07)	T4	13/07/2018	13:30	-8.943077	53.166102	-	23.2	8.5	0.9	0.6	0.08	0.4	0.13	0.3	0.08
Summer 2018 (07)	T5	13/07/2018	15:00	-8.943077	53.166102	-	37.1	0.2	0.0	0.7	0.23	0.2	0.02	0.2	0.07
Summer 2018 (07)	T6	13/07/2018	16:30	-8.943077	53.166102	-	35.7	0.2	0.1	0.7	0.19	0.2	0.03	0.2	0.04
Summer 2018 (07)	T7	13/07/2018	19:00	-8.943077	53.166102	-	37.7	0.3	0.6	2.8	2.20	0.2	0.05	0.4	0.24
Summer 2018 (07)	T8	13/07/2018	21:00	-8.943077	53.166102	-	38.1	0.2	0.2	0.9	0.29	0.3	0.29	0.2	0.03
Summer 2018 (07)	T9	13/07/2018	23:00	-8.943077	53.166102	-	31.8	0.3	0.0	1.3	0.66	0.2	0.04	0.1	0.03
Summer 2018 (07)	T10	14/07/2018	01:00	-8.943077	53.166102	-	20.7	13.6	0.5	0.6	0.15	0.3	0.23	0.3	0.02
Summer 2018 (07)	T11	14/07/2018	03:00	-8.943077	53.166102	-	21.7	3.7	0.4	0.8	0.56	0.3	0.10	0.1	0.10
Summer 2018 (07)	T12	14/07/2018	05:00	-8.943077	53.166102	-	26.8	0.2	0.1	0.5	0.04	0.1	0.02	0.1	0.04
Summer 2018 (07)	T13	14/07/2018	07:00	-8.943077	53.166102	-	30.7	0.2	0.1	0.6	0.12	0.1	0.03	0.1	0.06
Summer 2018 (07)	BH-AM	12/07/2018	10:15	-8.918775	53.126792	-1.7	7.6	63.6	1.2	<0.1	0.14	2.2	0.21	0.2	0.08
Summer 2018 (07)	BH-PM	12/07/2018	17:30	-8.918775	53.126792	-1.7	1.3	63.0	4.3	<0.1	0.19	0.2	0.20	0.2	0.09
Summer 2018 (07)	EM	13/07/2018	17:51	-8.960208	53.176245	4.89	30.5	0.2	0.1	0.8	0.06	0.2	0.03	0.1	-
Summer 2018 (07)	SP	12/07/2018	11:45	-8.92645	53.141673	0	1.6	87.6	4.0	0.4	0.60	0.3	0.11	0.4	0.05
Summer 2018 (07)	ST1	13/07/2018	17:30	-8.961683	53.162283	3.46	29.8	0.2	0.0	0.6	0.09	0.2	0.02	0.2	0.01
Summer 2018 (07)	ST2	13/07/2018	18:28	-8.938937	53.145213	1.06	29.8	0.2	0.2	0.5	0.10	0.2	0.06	0.2	0.04
Summer 2018 (07)	ST3	13/07/2018	18:51	-8.948233	53.155417	2.36	29.1	0.3	0.1	0.6	0.23	0.2	0.14	0.2	0.04
Summer 2018 (07)	ST4	13/07/2018	17:37	-8.9488	53.164738	3.46	30.3	0.2	0.1	0.5	0.08	0.1	<0.02	0.1	0.02
Summer 2018 (07)	ST5	13/07/2018	17:37	-8.954132	53.166427	3.46	29.6	0.2	0.1	0.5	0.05	0.2	<0.02	0.2	0.01
Autumn 2018 (10)	T1	22/10/2018	10:00	-8.943077	53.166102	-	30.4	7.5	0.3	1.1	0.11	0.8	<0.02	0.6	0.03
Autumn 2018 (10)	T2	22/10/2018	13:00	-8.943077	53.166102	-	28.4	15.4	0.5	0.7	0.02	0.8	0.04	0.4	0.04

Autumn 2018 (10)	T3	22/10/2018	16:00	-8.943077	53.166102	-	28.4	9.0	1.3	1.1	0.25	1.4	0.61	0.4	0.02
Autumn 2018 (10)	T4	22/10/2018	19:00	-8.943077	53.166102	-	29.3	7.1	0.8	0.8	0.04	0.7	0.06	0.4	0.07
Autumn 2018 (10)	T5	22/10/2018	22:00	-8.943077	53.166102	-	28.1	8.1	0.4	0.7	0.12	0.6	0.08	1.0	0.02
Autumn 2018 (10)	T6	23/10/2018	01:00	-8.943077	53.166102	-	26.3	26.5	1.0	3.6	5.02	0.7	0.05	0.3	0.05
Autumn 2018 (10)	T7	23/10/2018	04:00	-8.943077	53.166102	-	26.9	17.2	0.8	0.7	0.09	0.7	0.00	0.4	0.12
Autumn 2018 (10)	T8	23/10/2018	07:00	-8.943077	53.166102	-	28.2	10.4	2.3	7.6	6.06	0.6	0.04	0.3	0.04
Autumn 2018 (10)	T9	23/10/2018	10:00	-8.943077	53.166102	-	27.9	11.9	2.2	0.8	0.09	0.7	0.15	0.6	0.08
Autumn 2018 (10)	BH	20/10/2018	10:50	-8.918767	53.126792	-1.7	0.3	70.9	6.0	2.3	2.40	1.2	0.58	0.4	0.02
Autumn 2018 (10)	SP	20/10/2018	08:55	-8.92645	53.141673	0	0.5	134.9	6.8	2.1	1.57	0.8	0.37	0.5	0.05
Autumn 2018 (10)	SPmidhightide	20/10/2018	-	-8.92645	53.141673	0	0.0	-	-	-	-	-	-	-	-
Autumn 2018 (10)	ST1	21/10/2018	16:30	-8.942543	53.16705	4	29.4	7.1	0.4	1.1	0.50	0.8	0.17	0.4	0.04
Autumn 2018 (10)	ST2	21/10/2018	17:00	-8.930507	53.14469	0.5	10.2	69.0	1.2	2.1	2.30	0.4	0.13	0.3	0.01
Autumn 2018 (10)	ST3	21/10/2018	17:30	-8.952848	53.153857	2	26.4	3.8	0.5	1.0	0.23	0.7	0.17	0.3	0.03
Autumn 2018 (10)	ST4	21/10/2018	18:30	-8.968368	53.172163	4.6	30.3	1.6	1.8	1.2	0.03	0.6	<0.02	0.2	0.05
Winter 2019 (01)	T1	25/01/2019	17:00	-8.968507	53.171727	-	28.3	32.4	2.1	3.9	5.43	0.8	0.31	0.4	0.11
Winter 2019 (01)	T2	25/01/2019	20:00	-8.968507	53.171727	-	29.2	15.9	10.0	0.4	0.35	0.6	0.16	0.4	0.05
Winter 2019 (01)	T3	25/01/2019	23:00	-8.968507	53.171727	-	29.2	14.4	0.5	0.7	0.05	0.4	0.20	0.2	0.09
Winter 2019 (01)	T4	26/01/2019	02:00	-8.968507	53.171727	-	28.4	33.6	18.2	0.4	0.30	0.4	0.16	0.2	0.07
Winter 2019 (01)	T5	26/01/2019	05:00	-8.968507	53.171727	-	26.6	20.3	3.0	0.7	0.17	0.9	0.12	0.3	0.06
Winter 2019 (01)	T6	26/01/2019	08:00	-8.968507	53.171727	-	29.2	18.6	0.3	0.7	0.03	0.8	0.17	0.4	0.06
Winter 2019 (01)	T7	26/01/2019	11:00	-8.968507	53.171727	-	27.4	16.1	2.0	0.6	0.03	0.7	0.28	0.3	0.02
Winter 2019 (01)	T8	26/01/2019	14:00	-8.968507	53.171727	-	27.5	21.2	0.9	0.6	0.05	0.7	0.19	0.4	0.05
Winter 2019 (01)	T9	26/01/2019	17:00	-8.968507	53.171727	-	28.0	21.8	1.0	0.7	0.01	0.9	0.46	0.3	0.04
Winter 2019 (01)	BH	28/01/2019	16:15	-8.918767	53.126792	-1.7	0.3	101.4	5.5	0.6	0.47	0.3	0.08	0.1	0.04
Winter 2019 (01)	EM	28/01/2019	12:42	-8.963631	53.180916	5.49	26.4	28.4	1.1	0.7	0.06	0.5	0.13	0.4	0.04
Winter 2019 (01)	SP	26/01/2019	17:10	-8.92645	53.141673	0	0.6	252.0	133.4	24.1	0.29	0.3	<0.02	0.2	0.17
Winter 2019 (01)	ST1	28/01/2019	11:28	-8.934121	53.143164	0.56	8.3	85.0	2.6	0.3	0.06	0.7	0.12	0.1	0.08
Winter 2019 (01)	ST2	28/01/2019	11:40	-8.938077	53.14554	0.96	6.2	97.1	3.8	0.2	0.03	0.7	0.16	0.2	0.10
Winter 2019 (01)	ST3	28/01/2019	11:55	-8.941101	53.151073	1.63	7.9	87.1	3.4	0.3	0.05	0.7	0.32	0.1	0.02
Winter 2019 (01)	ST4	28/01/2019	12:08	-8.947829	53.158552	0	17.6	53.4	3.3	0.5	0.06	0.4	0.39	0.3	0.08
Winter 2019 (01)	ST5	28/01/2019	12:19	-8.954884	53.165489	3.53	25.6	31.3	1.5	0.7	0.10	0.4	0.15	0.3	0.07
Winter 2019 (01)	ST6	28/01/2019	12:32	-8.962771	53.171481	4.39	26.1	28.1	0.5	0.6	0.03	0.4	<0.02	0.2	0.07
Spring 2019 (04)	T1	07/04/2019	12:50	-8.968507	53.171727	-	18.4	28.8	13.7	1.9	2.17	0.3	0.09	0.2	0.04
Spring 2019 (04)	T2	07/04/2019	16:00	-8.968507	53.171727	-	29.7	33.3	6.0	0.6	0.52	0.6	0.04	0.5	0.02

Spring 2019 (04)	T3	07/04/2019	19:00	-8.968507	53.171727	-	30.0	8.8	0.7	0.8	0.69	0.5	0.05	0.3	0.03
Spring 2019 (04)	T4	07/04/2019	22:00	-8.968507	53.171727	-	30.9	2.4	0.3	0.9	0.14	0.4	<0.02	0.6	0.05
Spring 2019 (04)	T5	08/04/2019	01:00	-8.968507	53.171727	-	28.6	15.6	0.5	0.8	0.01	0.4	0.07	0.3	0.03
Spring 2019 (04)	T6	08/04/2019	04:00	-8.968507	53.171727	-	28.5	19.3	1.3	0.9	0.02	0.4	<0.02	0.5	0.20
Spring 2019 (04)	T7	08/04/2019	07:00	-8.968507	53.171727	-	29.7	5.4	0.3	0.9	0.09	0.5	0.11	0.2	0.04
Spring 2019 (04)	T8	08/04/2019	10:00	-8.968507	53.171727	-	29.0	5.2	0.5	0.8	0.32	0.4	0.06	0.2	0.06
Spring 2019 (04)	T9	08/04/2019	13:00	-8.968507	53.171727	-	27.1	20.0	0.5	0.8	0.07	0.4	0.05	0.2	0.03
Spring 2019 (04)	BH	08/04/2019	15:00	-8.918767	53.126792	-1.7	0.2	80.7	22.0	0.2	0.15	0.4	0.19	0.1	0.08
Spring 2019 (04)	EM	06/04/2019	16:58	-8.962164	53.181533	5.72	31.9	9.7	0.7	1.4	0.41	0.5	0.09	0.2	0.01
Spring 2019 (04)	SEDSP	06/04/2019	14:00	-8.92645	53.141673	0	14.3	42.1	15.3	12.2	1.82	1.4	0.65	-	-
Spring 2019 (04)	SP	07/04/2019	14:00	-8.92645	53.141673	0	0.4	109.9	18.5	<0.1	0.12	0.6	0.66	0.2	0.06
Spring 2019 (04)	SPDown	08/04/2019	13:30	-8.92645	53.141673	0	0.0	-	-	-	-	-	-	-	-
Spring 2019 (04)	SPUP	08/04/2019	13:30	-8.92645	53.141673	0	0.0	-	-	-	-	-	-	-	-
Spring 2019 (04)	ST1	06/04/2019	15:10	-8.935724	53.142924	0.64	12.8	45.6	1.8	0.4	0.34	0.5	0.11	0.3	0.13
Spring 2019 (04)	ST2	06/04/2019	15:32	-8.938942	53.146	1.14	14.3	43.2	0.9	0.4	0.33	0.3	<0.02	0.2	0.08
Spring 2019 (04)	ST3	06/04/2019	15:45	-8.941683	53.151315	1.79	23.2	19.1	10.2	0.9	0.06	0.6	0.23	0.1	0.03
Spring 2019 (04)	ST4	06/04/2019	16:02	-8.949191	53.159132	2.81	30.9	7.8	0.2	0.7	0.61	0.8	0.08	0.2	0.03

Appendix 12: TDN, SI and DON data for Kinvarra Bay

Fieldtrip	Station	Date	Time	X	Y	km from river	Salinity (kg m-3)	TDN (µmol L^{-1})	Si (µmol L^{-1})	Stdev Si	DON (µmol L^{-1})
Winter 2019 (01)	BH	28/01/2019	16:15	-8.918767	53.126792	-1.7	0.34816	167.8	-	-	65.8
Winter 2019 (01)	EM	28/01/2019	12:42	-8.963631	53.180916	5.49	26.4192	46.0	-	-	16.8
Winter 2019 (01)	SP	26/01/2019	17:10	-8.92645	53.141673	0	0.5632	352.7	-	-	70.5
Winter 2019 (01)	ST6	28/01/2019	12:32	-8.962771	53.171481	4.39	26.112	48.1	-	-	19.4
Spring 2019 (04)	BH	08/04/2019	15:00	-8.918767	53.126792	-1.7	0.24576	114.2	45.1	1.3	33.4
Spring 2019 (04)	EM	06/04/2019	16:58	-8.962164	53.181533	5.72	31.9488	1.4	3.9	0.1	<0.3
Spring 2019 (04)	SP	07/04/2019	14:00	-8.92645	53.141673	0	0.3584	158.5	49.3	0.6	48.5
Spring 2019 (04)	ST1	06/04/2019	15:10	-8.935724	53.142924	0.64	12.8	70.3	24.2	2.7	24.2
Spring 2019 (04)	ST2	06/04/2019	15:32	-8.938942	53.146	1.14	14.336	64.3	22.1	1.2	20.6
Spring 2019 (04)	ST3	06/04/2019	15:45	-8.941683	53.151315	1.79	23.2448	24.3	10.6	0.5	2.8
Spring 2019 (04)	ST4	06/04/2019	16:02	-8.949191	53.159132	2.81	30.9248	5.1	4.7	0.7	<0.3
Spring 2019 (04)	ST5	06/04/2019	16:25	-8.957427	53.165856	3.67	32.3584	11.6	4.6	0.7	3.0
Spring 2019 (04)	ST6	06/04/2019	16:43	-8.963944	53.17228	4.63	33.4848	10.6	4.3	0.3	2.9

Appendix 13: Nutrient data for Killary Harbour

Fieldtrip	Station	Date	Time	X	Y	km from river	Salinity (kg m^{-3})	TOxN (µmol L^{-1})	Stdev TOXN	NH_3 (µmol L^{-1})	Stdev NH_3	NO_2 (µmol L^{-1})	Stdev NO_2	SRP (µmol L^{-1})	Stdev SRP
Summer 2017 (08)	1D	24/08/2017	09:50	-9.856568	53.622383	14.83	39.1	1.0	0.06	2.4	0.10	0.8	0.01	0.1	0.01
Summer 2017 (08)	1D-0824	24/08/2017	13:30	-9.87475	53.629917	-	0.0	0.9	0.16	0.9	0.10	0.7	0.07	-	-
Summer 2017 (08)	1S	24/08/2017	09:35	-9.856568	53.622383	14.83	25.0	1.5	0.06	0.9	0.06	0.8	0.01	0.1	0.08
Summer 2017 (08)	1S-0824	24/08/2017	13:20	-9.87475	53.629917	-	0.0	0.3	0.01	1.0	0.20	0.8	0.09	-	-
Summer 2017 (08)	2D	24/08/2017	10:20	-9.820283	53.613233	13.69	32.1	0.9	0.01	1.8	0.26	0.8	0.03	0.1	0.03
Summer 2017 (08)	2S	24/08/2017	10:12	-9.820283	53.613233	13.69	28.9	1.6	0.10	0.9	0.05	0.8	0.05	0.1	0.02
Summer 2017 (08)	3D	24/08/2017	11:05	-9.794417	53.604533	12.5	32.6	1.1	0.04	3.0	0.06	0.8	0.05	0.4	0.24
Summer 2017 (08)	3S	24/08/2017	10:42	-9.794417	53.604533	12.5	23.8	1.5	0.02	2.5	0.08	0.7	0.01	0.1	0.03
Summer 2017 (08)	4D	24/08/2017	11:50	-9.782892	53.5997	9.9	30.1	1.4	0.01	3.8	0.33	0.9	0.07	0.3	0.01
Summer 2017 (08)	4S	24/08/2017	11:39	-9.782892	53.5997	9.9	20.5	1.6	0.16	1.1	0.74	0.6	0.01	0.1	0.01
Summer 2017 (08)	5D	24/08/2017	12:40	-9.757333	53.600783	6.53	31.1	1.9	0.06	1.0	0.03	0.9	0.01	0.5	0.01
Summer 2017 (08)	5S	24/08/2017	12:30	-9.757333	53.600783	6.53	21.3	1.0	0.04	0.5	0.01	0.6	0.04	0.1	0.01
Summer 2017 (08)	6S	24/08/2017	13:12	-9.72395	53.601033	3.66	11.0	1.1	0.70	0.9	0.70	0.4	0.09	0.1	0.02
Summer 2017 (08)	EM	24/08/2017	09:02	-9.721692	53.600626	15.89	32.5	1.0	0.09	1.7	0.05	0.8	0.04	0.1	0.08
Summer 2017 (08)	R1 - Bunowen	26/08/2017	00:00	-9.778207	53.583583	8.58	0.3	0.1	0.20	0.4	0.04	0.2	0.02	-	-
Summer 2017 (08)	R2 - Erriff	26/08/2017	00:00	-9.670602	53.615819	0	0.2	2.4	0.03	0.6	0.12	0.3	0.01	0.2	0.06
Summer 2017 (08)	R3 - Bundoragha	26/08/2017	00:00	-9.753155	53.606967	6.38	0.0	4.2	0.20	0.4	0.13	0.2	0.04	<0.1	-
Winter 2018 (02)	T1	18/02/2018	13:00	-9.730128	53.6002	-	26.2	6.0	0.34	0.7	0.12	0.6	0.20	0.2	0.10
Winter 2018 (02)	T2	18/02/2018	16:00	-9.730128	53.6002	-	26.6	6.1	1.38	0.8	0.17	0.7	0.15	0.3	0.05
Winter 2018 (02)	T3	18/02/2018	19:00	-9.730128	53.6002	-	26.0	7.0	0.48	0.9	0.14	0.5	0.12	0.2	0.10
Winter 2018 (02)	T4	18/02/2018	22:00	-9.730128	53.6002	-	23.7	5.1	0.46	0.8	0.07	0.3	0.10	0.2	0.09
Winter 2018 (02)	T5	19/02/2018	01:00	-9.730128	53.6002	-	14.5	6.6	0.12	0.6	0.03	0.5	0.12	0.1	0.10
Winter 2018 (02)	T6	19/02/2018	04:00	-9.730128	53.6002	-	15.2	6.3	0.19	0.5	0.14	0.4	0.21	0.1	0.05
Winter 2018 (02)	T7	19/02/2018	07:00	-9.730128	53.6002	-	16.8	5.9	0.45	0.6	0.03	0.3	0.03	0.2	0.11
Winter 2018 (02)	T8	19/02/2018	10:00	-9.730128	53.6002	-	17.8	5.8	0.50	0.7	0.12	0.4	0.12	0.2	0.07
Winter 2018 (02)	T9	19/02/2018	13:00	-9.730128	53.6002	-	14.7	5.8	0.07	0.7	0.22	0.6	0.19	0.1	0.06
Winter 2018 (02)	5D	17/02/2018	09:30	-9.721692	53.600626	3.93	0.0	1.2	0.24	0.4	0.04	0.5	0.32	<0.1	-
Winter 2018 (02)	K16-1D	16/02/2018	12:20	-9.877823	53.630149	15.01	32.1	5.3	0.19	0.9	0.08	0.6	0.07	0.4	0.02
Winter 2018 (02)	K16-1S	16/02/2018	12:14	-9.877823	53.630149	15.01	31.5	8.1	0.15	0.7	0.00	0.6	0.38	0.3	0.05
Winter 2018 (02)	K16-2D	16/02/2018	13:35	-9.857046	53.620501	13.14	32.9	6.4	2.06	0.9	0.19	0.5	0.23	0.5	0.02

Winter 2018 (02)	K16-2S	16/02/2018	13:27	-9.857046	53.620501	13.14	30.0	3.4	0.21	<0.1	1.20	0.5	0.06	0.2	0.01
Winter 2018 (02)	K16-3D	16/02/2018	13:35	-9.812439	53.610216	10.26	33.2	3.6	0.79	0.9	0.16	0.5	0.18	0.4	0.01
Winter 2018 (02)	K16-3S	16/02/2018	14:30	-9.812439	53.610216	10.26	21.9	3.2	0.95	0.6	0.04	0.4	0.05	0.1	0.01
Winter 2018 (02)	K16-4D-5S	16/02/2018	15:40	-9.758291	53.60135	6.16	33.5	6.0	1.26	0.7	0.07	0.5	0.10	0.2	0.06
Winter 2018 (02)	K16-4S	16/02/2018	15:32	-9.758291	53.60135	6.16	14.0	3.8	1.95	0.7	0.04	0.4	0.11	0.2	0.03
Winter 2018 (02)	K16EM	16/02/2018	11:32	-9.721692	53.600626	16.49	31.7	7.1	1.64	0.7	0.21	2.4	0.49	0.3	0.06
Winter 2018 (02)	K17-1D	17/02/2018	07:30	-9.877823	53.630149	13.14	31.5	8.1	1.41	0.8	0.03	0.7	0.16	0.4	0.02
Winter 2018 (02)	K17-1S	17/02/2018	07:30	-9.877823	53.630149	13.14	28.5	6.5	1.50	0.6	0.03	0.4	0.09	0.1	0.01
Winter 2018 (02)	K17-2D	17/02/2018	07:45	-9.857046	53.620501	11.25	31.6	4.0	0.57	0.9	0.07	0.8	0.17	0.6	0.08
Winter 2018 (02)	K17-2S	17/02/2018	07:45	-9.857046	53.620501	11.25	27.8	5.5	0.88	0.7	0.02	0.7	0.23	0.1	0.01
Winter 2018 (02)	K17-3D	17/02/2018	08:00	-9.812439	53.610216	8.22	31.8	10.0	0.19	0.8	0.09	0.7	0.02	0.4	0.02
Winter 2018 (02)	K17-3S	17/02/2018	08:00	-9.812439	53.610216	8.22	17.2	3.3	1.75	0.3	0.81	0.4	0.06	0.2	0.07
Winter 2018 (02)	K17-4D	17/02/2018	08:45	-9.758291	53.60135	6.16	31.9	9.0	0.87	0.1	1.35	0.5	0.11	0.4	0.02
Winter 2018 (02)	K17-4S	17/02/2018	08:45	-9.758291	53.60135	6.16	18.4	6.5	1.99	0.7	0.30	0.4	0.20	0.1	0.04
Winter 2018 (02)	K17-5S	17/02/2018	09:30	-9.721692	53.600626	3.93	10.4	5.0	0.20	0.6	0.15	0.4	0.14	0.2	0.10
Winter 2018 (02)	R1 - Bunowen	18/02/2018	00:00	-9.778207	53.583583	8.58	0.2	1.2	0.24	0.4	0.04	0.5	0.23	<0.1	-
Winter 2018 (02)	R2 - Erriff	18/02/2018	00:00	-9.670602	53.615819	0	0.1	6.1	0.69	0.6	0.25	0.3	0.04	<0.1	-
Winter 2018 (02)	R3 - Bundoragha	18/02/2018	00:00	-9.753155	53.606967	6.38	0.0	4.1	0.32	0.6	0.29	1.2	0.37	<0.1	-
Summer 2018 (07)	T1	16/07/2018	13:00	-9.85983	53.620311	-	39.3	0.3	0.06	0.6	0.01	0.5	0.03	0.3	0.08
Summer 2018 (07)	T2	16/07/2018	15:00	-9.85983	53.620311	-	40.2	0.6	0.49	0.7	0.27	0.5	0.06	0.3	0.06
Summer 2018 (07)	T3	16/07/2018	17:00	-9.85983	53.620311	-	30.6	0.3	0.07	0.5	0.14	0.5	0.29	0.3	0.07
Summer 2018 (07)	T4	16/07/2018	19:00	-9.85983	53.620311	-	34.7	0.4	0.06	0.6	0.09	0.3	0.37	0.2	0.09
Summer 2018 (07)	T5	16/07/2018	21:00	-9.85983	53.620311	-	34.3	0.3	0.06	0.4	0.36	0.4	0.26	0.2	0.05
Summer 2018 (07)	T6	16/07/2018	23:00	-9.85983	53.620311	-	31.9	0.3	0.06	0.6	0.05	0.5	0.03	0.1	0.09
Summer 2018 (07)	T7	17/07/2018	01:00	-9.85983	53.620311	-	35.0	6.4	0.34	0.6	0.04	0.6	0.02	0.4	0.08
Summer 2018 (07)	T8	17/07/2018	03:00	-9.85983	53.620311	-	31.4	0.6	0.14	0.5	0.03	0.6	0.34	0.4	0.06
Summer 2018 (07)	T9	17/07/2018	05:00	-9.85983	53.620311	-	31.8	0.3	0.08	0.5	0.13	0.3	0.21	0.3	0.08
Summer 2018 (07)	1D	16/07/2018	08:23	-9.856568	53.622383	13.82	32.1	0.4	0.03	0.5	0.18	0.4	0.03	0.3	0.06
Summer 2018 (07)	1S	16/07/2018	08:37	-9.856568	53.622383	13.82	31.1	0.3	0.05	0.6	0.03	0.4	0.24	0.1	0.04
Summer 2018 (07)	2D	16/07/2018	08:57	-9.820283	53.613233	11.14	34.5	0.3	0.06	0.6	0.08	0.4	0.26	0.2	0.06
Summer 2018 (07)	2S	16/07/2018	09:18	-9.820283	53.613233	11.14	36.7	0.3	0.09	0.5	0.10	0.4	0.00	0.1	0.03
Summer 2018 (07)	3D	16/07/2018	09:39	-9.794417	53.604533	9.26	36.1	0.2	0.01	0.3	0.31	0.4	0.24	0.3	0.06
Summer 2018 (07)	3S	16/07/2018	10:00	-9.794417	53.604533	9.26	33.1	0.3	0.01	0.3	0.29	0.4	0.08	0.1	0.06

Summer 2018 (07)	4D	16/07/2018	10:16	-9.782892	53.5997	8.13	30.9	0.3	0.07	0.6	0.05	0.4	0.24	0.2	0.05
Summer 2018 (07)	4S	16/07/2018	10:32	-9.782892	53.5997	8.13	30.2	0.3	0.03	0.6	0.03	0.4	0.01	0.2	0.04
Summer 2018 (07)	5D	16/07/2018	10:58	-9.757333	53.600783	6.36	33.1	0.3	0.10	0.5	0.11	0.4	0.26	0.2	0.07
Summer 2018 (07)	5S	16/07/2018	11:25	-9.757333	53.600783	6.36	29.1	0.3	0.01	0.6	0.11	0.4	0.02	0.2	0.03
Summer 2018 (07)	6S	16/07/2018	11:52	-9.72395	53.601033	4.15	32.7	0.3	0.05	0.5	0.11	0.4	0.01	0.2	0.07
Summer 2018 (07)	EM	16/07/2018	08:10	-9.721692	53.600626	15.36	32.6	0.3	0.01	0.4	0.11	0.4	0.24	0.1	0.05
Summer 2018 (07)	R1 - Bunowen	16/07/2018	15:45	-9.778207	53.583583	8.58	0.3	5.8	0.48	0.2	0.07	0.5	0.37	0.1	0.03
Summer 2018 (07)	R2 - Erriff	15/07/2018	15:45	-9.670602	53.615819	0	0.4	3.9	0.09	0.5	0.18	0.4	0.22	<0.1	-
Summer 2018 (07)	R3 - Bundoragha	15/07/2018	14:30	-9.753155	53.606967	6.38	0.2	6.9	0.77	0.4	0.52	0.4	0.03	<0.1	-
Autumn 2018 (10)	1D	25/10/2018	08:30	-9.825283	53.614507	11.2	33.6	0.8	1.32	0.9	0.07	0.6	0.10	0.3	0.07
Autumn 2018 (10)	1S	25/10/2018	08:15	-9.825283	53.614507	11.2	30.7	0.8	0.33	0.9	0.04	0.6	0.18	0.3	0.02
Autumn 2018 (10)	2D	25/10/2018	09:30	-9.789332	53.601092	7.87	32.2	3.0	0.28	1.0	0.14	0.9	0.11	0.3	0.04
Autumn 2018 (10)	2S	25/10/2018	09:15	-9.789332	53.601092	7.87	28.6	1.1	1.18	0.8	0.04	0.7	0.19	0.2	0.01
Autumn 2018 (10)	3D	25/10/2018	10:00	-9.759552	53.600582	5.89	31.7	3.5	0.18	0.9	0.08	1.0	0.02	0.4	0.04
Autumn 2018 (10)	3S	25/10/2018	09:45	-9.759552	53.600582	5.89	25.4	2.2	0.98	0.6	0.03	0.6	0.04	0.2	0.02
Autumn 2018 (10)	4S	25/10/2018	10:20	-9.722391	53.600944	3.61	26.2	1.2	0.26	0.7	0.07	0.7	0.03	0.2	0.01
Autumn 2018 (10)	EM	25/10/2018	08:00	-9.881891	53.63162	15.24	30.1	3.2	1.39	29.7	25.08	0.9	0.24	0.4	0.02
Autumn 2018 (10)	R1 - Bunowen	24/10/2018	00:00	-9.778207	53.583583	8.58	0.3	2.3	0.17	0.3	0.02	1.3	0.58	0.2	0.03
Autumn 2018 (10)	R2 - Erriff	24/10/2018	14:45	-9.670602	53.615819	0	0.1	4.6	0.36	0.3	0.04	0.5	1.10	0.1	0.04
Autumn 2018 (10)	R3 - Bundoragha	24/10/2018	13:30	-9.753155	53.606967	6.38	0.1	5.2	0.33	0.2	0.06	0.3	0.03	0.1	0.03
Winter 2019 (01)	T1	24/01/2019	05:00	-9.73165	53.598464	-	15.3	8.3	0.56	10.5	4.15	0.6	0.03	0.3	0.03
Winter 2019 (01)	T2	24/01/2019	08:00	-9.73165	53.598464	-	16.6	7.0	1.52	0.8	0.33	0.5	0.17	0.2	0.02
Winter 2019 (01)	T3	24/01/2019	11:00	-9.73165	53.598464	-	16.0	7.4	0.49	0.9	0.39	0.5	0.13	5.6	0.13
Winter 2019 (01)	T4	24/01/2019	14:00	-9.73165	53.598464	-	11.3	12.4	1.10	7.9	8.53	0.5	0.04	0.2	0.02
Winter 2019 (01)	T5	24/01/2019	17:00	-9.73165	53.598464	-	13.9	7.6	1.15	0.6	0.33	0.5	0.23	0.2	0.01
Winter 2019 (01)	T6	24/01/2019	20:00	-9.73165	53.598464	-	14.3	8.1	0.26	3.5	3.08	0.5	0.12	0.1	0.01
Winter 2019 (01)	T7	24/01/2019	23:00	-9.73165	53.598464	-	15.3	7.1	0.52	0.4	0.06	0.5	0.82	0.2	0.03
Winter 2019 (01)	T8	25/01/2019	02:00	-9.73165	53.598464	-	10.0	6.9	1.51	0.5	0.04	0.5	0.12	0.2	0.02
Winter 2019 (01)	T9	25/01/2019	05:00	-9.73165	53.598464	-	15.3	6.5	0.19	0.5	0.05	0.7	0.21	0.5	0.07
Winter 2019 (01)	1D	23/01/2019	08:55	-9.817082	53.612233	10.62	34.7	10.5	2.51	1.8	0.82	0.6	0.07	0.4	0.01
Winter 2019 (01)	1S	23/01/2019	08:25	-9.817082	53.612233	10.62	26.6	8.1	0.21	1.5	0.19	0.6	0.03	0.3	0.02
Winter 2019 (01)	2D	23/01/2019	09:25	-9.778845	53.599833	7.7	33.8	8.1	0.21	1.8	0.11	0.7	0.04	0.5	0.07

Winter 2019 (01)	2S	23/01/2019	09:15	-9.778845	53.599833	7.7	17.1	5.9	0.47	0.6	0.17	0.3	0.03	0.2	0.02
Winter 2019 (01)	3D	23/01/2019	09:55	-9.758313	53.600483	6.28	34.0	8.1	0.76	1.6	0.62	0.4	0.20	0.5	0.02
Winter 2019 (01)	3S	23/01/2019	09:45	-9.758313	53.600483	6.28	12.1	7.2	1.27	0.6	0.39	0.4	0.01	0.2	0.06
Winter 2019 (01)	4D	23/01/2019	10:37	-9.742187	53.600933	5.41	33.8	8.4	0.76	9.2	14.40	0.4	0.09	0.5	0.01
Winter 2019 (01)	4S	23/01/2019	10:27	-9.742187	53.600933	5.41	10.8	8.5	1.23	1.3	0.74	0.7	0.20	0.2	0.01
Winter 2019 (01)	5S	23/01/2019	10:55	-9.73033	53.60095	4.37	9.4	8.1	0.92	1.0	0.42	0.4	0.04	0.3	0.02
Winter 2019 (01)	6S	23/01/2019	11:30	-9.715354	53.601058	3.49	9.8	8.7	1.03	2.5	1.93	0.4	0.06	0.2	0.05
Winter 2019 (01)	EM	23/01/2019	07:46	-9.881891	53.63162	15.34	28.7	8.2	1.54	6.1	7.12	0.7	0.03	0.3	0.04
Winter 2019 (01)	R1 - Bunowen	24/01/2019	15:30	-9.778207	53.583583	8.58	0.2	5.7	0.31	0.4	0.20	0.3	0.26	0.1	-
Winter 2019 (01)	R2 - Erriff	24/01/2019	14:30	-9.670602	53.615819	0	0.1	11.3	2.30	1.4	1.14	0.4	0.04	0.1	0.01
Winter 2019 (01)	R3 - Bundoragha	23/01/2019	15:00	-9.753155	53.606967	6.38	0.1	6.3	0.19	0.4	0.19	0.4	0.14	0.1	0.01
Spring 2019 (04)	T1	02/04/2019	21:00	-9.73165	53.598464	-	33.3	7.4	1.46	1.6	0.74	0.2	0.44	0.3	0.03
Spring 2019 (04)	T2	02/04/2019	00:00	-9.73165	53.598464	-	29.1	4.4	1.03	0.8	0.09	0.2	0.17	0.2	0.01
Spring 2019 (04)	T3	03/04/2019	03:00	-9.73165	53.598464	-	20.7	3.4	0.63	0.8	0.09	0.2	0.14	0.3	0.06
Spring 2019 (04)	T4	03/04/2019	06:00	-9.73165	53.598464	-	30.7	4.8	0.51	0.9	0.05	0.3	0.19	0.2	0.08
Spring 2019 (04)	T5	03/04/2019	09:00	-9.73165	53.598464	-	30.5	4.3	0.38	1.1	0.20	0.2	0.22	0.3	0.01
Spring 2019 (04)	T6	03/04/2019	12:00	-9.73165	53.598464	-	25.2	4.0	0.82	0.5	0.46	0.1	0.09	0.1	0.01
Spring 2019 (04)	T7	03/04/2019	15:00	-9.73165	53.598464	-	26.7	4.2	0.36	0.9	0.08	0.2	0.16	0.2	0.01
Spring 2019 (04)	T8	03/04/2019	18:00	-9.73165	53.598464	-	28.0	2.4	0.39	0.8	0.07	0.2	0.11	0.2	0.02
Spring 2019 (04)	T9	03/04/2019	21:00	-9.73165	53.598464	-	30.1	2.3	0.74	0.8	0.05	0.2	0.17	0.2	0.02
Spring 2019 (04)	1D	04/04/2019	07:47	-9.817082	53.612233	11.34	34.9	6.2	0.04	3.2	1.32	0.3	0.29	0.4	0.04
Spring 2019 (04)	1S	04/04/2019	07:46	-9.817082	53.612233	11.34	31.7	5.8	1.50	1.3	0.11	0.4	0.37	0.2	0.04
Spring 2019 (04)	2D	04/04/2019	08:45	-9.778845	53.599833	9.38	35.0	6.1	0.19	2.5	0.11	0.5	0.31	0.3	0.02
Spring 2019 (04)	2S	04/04/2019	08:40	-9.778845	53.599833	9.38	31.3	3.6	0.75	1.0	0.12	0.3	0.22	0.2	0.03
Spring 2019 (04)	3D	04/04/2019	09:20	-9.758313	53.600483	7.08	33.9	5.3	0.45	2.1	0.17	0.5	0.29	0.1	0.05
Spring 2019 (04)	3S	04/04/2019	09:15	-9.758313	53.600483	7.08	27.6	3.0	0.78	0.5	0.45	-	0.22	0.1	0.05
Spring 2019 (04)	4D	04/04/2019	10:05	-9.742187	53.600933	5.58	34.0	5.6	0.37	1.8	0.12	0.5	0.28	0.4	0.02
Spring 2019 (04)	4S	04/04/2019	10:00	-9.742187	53.600933	5.58	26.4	3.8	0.56	0.9	0.09	0.3	0.23	0.1	0.01
Spring 2019 (04)	5S	04/04/2019	10:15	-9.73033	53.60095	4.34	26.8	3.2	0.20	0.8	0.02	0.4	0.24	0.1	0.01
Spring 2019 (04)	6S	04/04/2019	10:28	-9.715354	53.601058	3.58	23.3	3.7	0.34	0.8	0.07	0.2	0.18	0.2	0.03
Spring 2019 (04)	7S	03/04/2019	14:45	-9.681944	53.609871	1.2	0.0	-	-	-	-	-	-	-	-
Spring 2019 (04)	EM	04/04/2019	06:58	-9.881891	53.63162	16.02	34.9	2.0	0.47	2.0	0.39	0.2	0.09	0.4	0.03

Spring 2019 (04)	R1 - Bunowen	03/04/2019	10:00	-9.778207	53.583583	8.58	0.1	3.3	0.31	0.3	0.06	0.4	0.37	0.1	0.03
Spring 2019 (04)	R2 - Erriff	03/04/2019	12:00	-9.670602	53.615819	0	0.1	7.6	0.35	0.1	0.13	-	0.73	0.1	0.02
Spring 2019 (04)	R3 - Bundoragha	04/04/2019	13:30	-9.753155	53.606967	6.38	0.1	5.7	0.11	0.3	0.07	0.3	0.35	0.2	0.06

Appendix 14: TDN, Si, DON values for Killary Harbour.

Fieldtrip	Station	Date	Time	X	Y	km from river	Salinity (kg m-3)	TDN (µmol N L^{-1})	Si (µmol L^{-1})	Stdev Si	DON (µmol N L^{-1})
Spring 2019 (04)	1D	04/04/2019	07:47	-9.817082	53.612233	11.34	34.9184	9.7	7.6	3.9	0.4
Spring 2019 (04)	1S	04/04/2019	07:46	-9.817082	53.612233	11.34	31.744	3.3	6.7	0.8	<0.3
Spring 2019 (04)	2D	04/04/2019	08:45	-9.778845	53.599833	9.38	35.0208	13.9	4.6	0.1	5.3
Spring 2019 (04)	2S	04/04/2019	08:40	-9.778845	53.599833	9.38	31.3344	1.1	7.0	0.8	<0.3
Spring 2019 (04)	3D	04/04/2019	09:20	-9.758313	53.600483	7.08	33.8944	4.1	6.5	2.1	<0.3
Spring 2019 (04)	3S	04/04/2019	09:15	-9.758313	53.600483	7.08	27.648	17.9	8.6	0.4	14.3
Spring 2019 (04)	4D	04/04/2019	10:05	-9.742187	53.600933	5.58	33.9968	5.7	7.8	0.4	<0.3
Spring 2019 (04)	4S	04/04/2019	10:00	-9.742187	53.600933	5.58	26.4192	13.4	9.3	1.0	8.7
Spring 2019 (04)	5S	04/04/2019	10:15	-9.73033	53.60095	4.34	26.8288	<0.3	9.1	1.1	<0.3
Spring 2019 (04)	6S	04/04/2019	10:28	-9.715354	53.601058	3.58	23.3472	5.0	10.9	0.3	0.5
Spring 2019 (04)	EM	04/04/2019	06:58	-9.881891	53.63162	16.02	34.9184	-	-	-	-
Spring 2019 (04)	R1 - Bunowen	03/04/2019	10:00	-9.778207	53.583583	8.58	0.12288	<0.3	3.4	1.2	<0.3
Spring 2019 (04)	R2 - Erriff	03/04/2019	12:00	-9.670602	53.615819	0	0.14336	13.6	23.8	0.4	9.9
Spring 2019 (04)	R3 - Bundoragha	04/04/2019	13:30	-9.753155	53.606967	6.38	0.09216	<0.3	29.9	0.9	<0.3

Appendix 15: ^{223}Ra and ^{224}Ra data for Kinvarra Bay

Station	Date	Time	X	Y	Distance from spring	Salinity	^{224}Ra (dpm 100L^{-1})	^{223}Ra (dpm 100L^{-1})	^{224}Ra/ ^{223}Ra
BH-AM	12/07/2018	10:15	-8.918775	53.126792	-1.7	7.6	7.4	0.7	10.0
BH-PM	12/07/2018	17:30	-8.918775	53.126792	-1.7	1.3	8.2	0.6	13.6
EM	13/07/2018	17:51	-8.960208	53.176245	4.89	30.5	7.2	1.2	6.1
SP	12/07/2018	11:45	-8.92645	53.141673	0	1.6	5.8	0.6	9.8
ST1	13/07/2018	17:30	-8.961683	53.162283	3.46	29.8	8.0	1.5	5.4
ST2	13/07/2018	18:28	-8.938937	53.145213	1.06	29.8	11.3	1.7	6.7
ST3	13/07/2018	18:51	-8.948233	53.155417	2.36	29.1	8.7	1.3	6.7
BH	20/10/2018	10:50	-8.918767	53.126792	-1.7	0.3	5.9	0.7	8.7
SP	20/10/2018	08:55	-8.92645	53.141673	0	0.5	2.8	0.2	11.9
ST1	21/10/2018	16:30	-8.942543	53.16705	4	29.4	6.6	0.9	7.5
ST2	21/10/2018	17:00	-8.930507	53.14469	0.5	10.2	7.9	1.3	6.0
ST3	21/10/2018	17:30	-8.952848	53.153857	2	26.4	9.7	1.3	7.5
ST4	21/10/2018	18:30	-8.968368	53.172163	4.6	30.3	13.0	1.6	8.2
BH	28/01/2019	16:15	-8.918767	53.126792	-1.7	0.3	4.3	0.3	15.2
EM	28/01/2019	12:42	-8.963631	53.180916	5.49	26.4	5.7	1.1	5.4
SP	26/01/2019	17:10	-8.92645	53.141673	0	0.6	2.6	0.3	9.5
ST1	28/01/2019	11:28	-8.934121	53.143164	0.56	8.3	3.7	0.4	8.9
ST2	28/01/2019	11:40	-8.938077	53.14554	0.96	6.2	2.3	0.3	8.0
ST3	28/01/2019	11:55	-8.941101	53.151073	1.63	7.9	4.2	0.5	8.7
ST6	28/01/2019	12:32	-8.962771	53.171481	4.39	26.1	5.0	0.9	5.8
BH	08/04/2019	15:00	-8.918767	53.126792	-1.7	0.2	8.7	0.7	12.8
EM	06/04/2019	16:58	-8.962164	53.181533	5.72	31.9	3.8	0.8	5.0
SP	07/04/2019	14:00	-8.92645	53.141673	0	0.4	2.9	0.2	12.6
ST1	06/04/2019	15:10	-8.935724	53.142924	0.64	12.8	4.7	0.6	8.4
ST2	06/04/2019	15:32	-8.938942	53.146	1.14	14.3	5.6	0.7	7.6
ST3	06/04/2019	15:45	-8.941683	53.151315	1.79	23.2	6.4	0.8	8.5
ST4	06/04/2019	16:02	-8.949191	53.159132	2.81	30.9	4.3	0.6	7.1
ST5	06/04/2019	16:25	-8.957427	53.165856	3.67	32.4	3.9	0.6	6.2
ST6	06/04/2019	16:43	-8.963944	53.17228	4.63	33.5	3.6	0.4	9.3

Appendix 16: ^{223}Ra and ^{224}Ra data for Killary Harbour. R1 = Bunowen, R2= Erriff, R3 = Bundoragha

Station	Date	Time	X	Y	Distance from river Erriff	Salinity	^{224}Ra (dpm 100L^{-1})	^{223}Ra (dpm 100L^{-1})	^{224}Ra/ ^{223}Ra
1D	24/08/2017	09:50	-9.856568	53.622383	14.83	39.1	3.0	0.4	7.7
1S	24/08/2017	09:35	-9.856568	53.622383	14.83	25.0	10.3	1.1	9.2
3S	24/08/2017	10:42	-9.794417	53.604533	12.5	23.8	10.3	0.6	17.1
4D	24/08/2017	11:50	-9.782892	53.5997	9.9	30.1	10.8	1.2	8.7
4S	24/08/2017	11:39	-9.782892	53.5997	9.9	20.5	17.8	1.8	9.7
6S	24/08/2017	13:12	-9.72395	53.601033	3.66	11.0	8.2	0.6	13.4
EM	24/08/2017	09:02	-9.721692	53.600626	15.89	32.5	4.5	0.5	9.0
5D	17/02/2018	09:30	-9.721692	53.600626	3.93	0.0	4.5	0.4	10.2
K16-1D	16/02/2018	12:20	-9.877823	53.630149	15.01	32.1	10.8	1.0	10.5
K16-1S	16/02/2018	12:14	-9.877823	53.630149	15.01	31.5	30.9	3.3	9.4
K16-2D	16/02/2018	13:35	-9.857046	53.620501	13.14	32.9	7.5	0.7	10.8
K16-2S	16/02/2018	13:27	-9.857046	53.620501	13.14	30.0	4.9	0.7	6.8
K16-3D	16/02/2018	13:35	-9.812439	53.610216	10.26	33.2	17.1	1.2	14.2
K16-3S	16/02/2018	14:30	-9.812439	53.610216	10.26	21.9	4.5	0.5	10.0
K17-3D	17/02/2018	08:00	-9.812439	53.610216	8.22	31.8	5.1	0.5	10.2
K17-3S	17/02/2018	08:00	-9.812439	53.610216	8.22	17.2	16.8	1.5	11.3
K17-5S	17/02/2018	09:30	-9.721692	53.600626	3.93	10.4	10.5	0.7	14.6
1S	16/07/2018	08:37	-9.856568	53.622383	13.82	31.1	3.4	0.4	7.7
2S	16/07/2018	09:18	-9.820283	53.613233	11.14	36.7	4.1	0.7	5.9
3S	16/07/2018	10:00	-9.794417	53.604533	9.26	33.1	4.4	0.5	8.5
4S	16/07/2018	10:32	-9.782892	53.5997	8.13	30.2	5.8	0.8	7.5
5S	16/07/2018	11:25	-9.757333	53.600783	6.36	29.1	9.4	0.9	9.9
6S	16/07/2018	11:52	-9.72395	53.601033	4.15	32.7	12.4	0.9	14.2
EM	16/07/2018	08:10	-9.721692	53.600626	15.36	32.6	5.6	0.5	11.4
R1 - Bunowen	16/07/2018	15:45	-9.778207	53.583583	8.58	0.3	3.1	0.1	26.2
R2 - Erriff	15/07/2018	15:45	-9.670602	53.615819	0	0.4	3.4	0.1	45.6
R3 - Bundoragha	15/07/2018	14:30	-9.753155	53.606967	6.38	0.2	2.7	0.1	18.6
2D	25/10/2018	09:30	-9.789332	53.601092	7.87	32.2	8.9	0.6	14.3
2S	25/10/2018	09:15	-9.789332	53.601092	7.87	28.6	5.2	0.6	8.5
3S	25/10/2018	09:45	-9.759552	53.600582	5.89	25.4	8.2	1.1	7.5
4S	25/10/2018	10:20	-9.722391	53.600944	3.61	26.2	17.2	0.9	18.8
EM	25/10/2018	08:00	-9.881891	53.63162	15.24	30.1	6.7	0.7	9.9
R1 - Bunowen	24/10/2018	00:00	-9.778207	53.583583	8.58	0.3	4.0	0.1	29.6
R2 - Erriff	24/10/2018	14:45	-9.670602	53.615819	0	0.1	9.9	0.2	51.3
R3 - Bundoragha	24/10/2018	13:30	-9.753155	53.606967	6.38	0.1	8.2	0.1	56.6
1D	23/01/2019	08:55	-9.817082	53.612233	10.62	34.7	5.2	0.5	9.5
1S	23/01/2019	08:25	-9.817082	53.612233	10.62	26.6	3.5	0.3	11.4
2S	23/01/2019	09:15	-9.778845	53.599833	7.7	17.1	7.1	0.4	16.1
3S	23/01/2019	09:45	-9.758313	53.600483	6.28	12.1	8.2	0.4	20.6
4S	23/01/2019	10:27	-9.742187	53.600933	5.41	10.8	7.3	0.4	18.5
6S	23/01/2019	11:30	-9.715354	53.601058	3.49	9.8	10.3	0.4	26.1

R2 - Erriff	24/01/2019	14:30	-9.670602	53.615819	0	0.1	3.3	0.2	17.3
1D	04/04/2019	07:47	-9.817082	53.612233	11.34	34.9	3.1	0.4	8.5
1S	04/04/2019	07:46	-9.817082	53.612233	11.34	31.7	5.3	0.6	9.0
2S	04/04/2019	08:40	-9.778845	53.599833	9.38	31.3	7.5	0.4	16.9
3D	04/04/2019	09:20	-9.758313	53.600483	7.08	33.9	5.9	0.5	12.1
3S	04/04/2019	09:15	-9.758313	53.600483	7.08	27.6	9.2	0.6	14.3
4S	04/04/2019	10:00	-9.742187	53.600933	5.58	26.4	13.2	0.6	21.6
5S	04/04/2019	10:15	-9.73033	53.60095	4.34	26.8	11.8	0.7	17.1
6S	04/04/2019	10:28	-9.715354	53.601058	3.58	23.3	18.2	0.7	25.7
7S	03/04/2019	14:45	-9.681944	53.609871	1.2	0.0	32.9	1.1	28.6
EM	04/04/2019	06:58	-9.881891	53.63162	16.02	34.9	5.4	0.4	14.9
R1 - Bunowen	03/04/2019	10:00	-9.778207	53.583583	8.58	0.1	3.0	0.1	39.4
R2 - Erriff	03/04/2019	12:00	-9.670602	53.615819	0	0.1	4.2	0.1	33.7
R3 - Bundoragha	04/04/2019	13:30	-9.753155	53.606967	6.38	0.1	3.1	0.1	28.4

Appendix 17: Radon samples in Killary Harbour

Fieldtrip	Station	Date	Time	X	Y	km from river Erriff	Salinity (kg m^{-3})	^{222}Rn (Bq m^{-3})	Stdev ^{222}Rn (Bq m^{-3})
Summer 2018 (07)	T1	16/07/2018	13:00	-9.85983	53.620311	-	39.3	635	370
Summer 2018 (07)	T2	16/07/2018	15:00	-9.85983	53.620311	-	40.2	37	81
Summer 2018 (07)	T3	16/07/2018	17:00	-9.85983	53.620311	-	30.6	72	83
Summer 2018 (07)	T4	16/07/2018	19:00	-9.85983	53.620311	-	34.7	156	176
Summer 2018 (07)	T5	16/07/2018	21:00	-9.85983	53.620311	-	34.3	86	130
Summer 2018 (07)	T6	16/07/2018	23:00	-9.85983	53.620311	-	31.9	152	196
Summer 2018 (07)	T7	17/07/2018	01:00	-9.85983	53.620311	-	35.0	23	64
Summer 2018 (07)	T8	17/07/2018	03:00	-9.85983	53.620311	-	31.4	231	203
Summer 2018 (07)	T9	17/07/2018	05:00	-9.85983	53.620311	-	31.8	67	133
Summer 2018 (07)	1D	16/07/2018	08:23	-9.856568	53.622383	13.82	32.1	87	93
Summer 2018 (07)	1S	16/07/2018	08:37	-9.856568	53.622383	13.82	31.1	294	84
Summer 2018 (07)	2D	16/07/2018	08:57	-9.820283	53.613233	11.14	34.5	385	184
Summer 2018 (07)	2S	16/07/2018	09:18	-9.820283	53.613233	11.14	36.7	77	89
Summer 2018 (07)	3S	16/07/2018	10:00	-9.794417	53.604533	9.26	33.1	214	163
Summer 2018 (07)	4D	16/07/2018	10:16	-9.782892	53.5997	8.13	30.9	23	64
Summer 2018 (07)	5D	16/07/2018	10:58	-9.757333	53.600783	6.36	33.1	163	120
Summer 2018 (07)	5S	16/07/2018	11:25	-9.757333	53.600783	6.36	29.1	421	93
Summer 2018 (07)	EM	16/07/2018	08:10	-9.721692	53.600626	15.36	32.6	142	182
Summer 2018 (07)	R2 - Erriff	15/07/2018	15:45	-9.670602	53.615819	0	0.4	400	397
Autumn 2018 (10)	1D	25/10/2018	08:30	-9.825283	53.614507	11.2	33.6	25	70
Autumn 2018 (10)	1S	25/10/2018	08:15	-9.825283	53.614507	11.2	30.7	143	169
Autumn 2018 (10)	2D	25/10/2018	09:30	-9.789332	53.601092	7.87	32.2	374	261
Autumn 2018 (10)	2S	25/10/2018	09:15	-9.789332	53.601092	7.87	28.6	95	144
Autumn 2018 (10)	4S	25/10/2018	10:20	-9.722391	53.600944	3.61	26.2	23	64
Autumn 2018 (10)	EM	25/10/2018	08:00	-9.881891	53.63162	15.24	30.1	345	205

Appendix 18: Radon samples in Kinvarra Bay. Values are averages of triplicate samples.

Fieldtrip	Station	Date	Time	X	Y	km from river	Salinity (kg m^{-3})	^{222}Rn (Bq m^{-3})	Stdev ^{222}Rn (Bq m^{-3})
Summer 2018 (07)	T10	14/07/2018	01:00	-8.943077	53.166102	-	20.7	1879	392
Summer 2018 (07)	T11	14/07/2018	03:00	-8.943077	53.166102	-	21.7	3306	667
Summer 2018 (07)	T12	14/07/2018	05:00	-8.943077	53.166102	-	26.8	3765	1132
Summer 2018 (07)	T1	13/07/2018	07:00	-8.943077	53.166102	-	27.0	857	281
Summer 2018 (07)	T2	13/07/2018	09:15	-8.943077	53.166102	-	32.4	849	297
Summer 2018 (07)	T3	13/07/2018	11:30	-8.943077	53.166102	-	27.9	394	222
Summer 2018 (07)	T4	13/07/2018	13:30	-8.943077	53.166102	-	23.2	2073	491
Summer 2018 (07)	T5	13/07/2018	15:00	-8.943077	53.166102	-	37.1	631	353
Summer 2018 (07)	T9	13/07/2018	23:00	-8.943077	53.166102	-	31.8	264	307
Summer 2018 (07)	BH-AM	12/07/2018	10:15	-8.918775	53.126792	-1.7	7.6	11105	1355
Summer 2018 (07)	BH-PM	12/07/2018	17:30	-8.918775	53.126792	-1.7	1.3	11049	1728
Summer 2018 (07)	EM	12/07/2018	17:51	-8.960208	53.176245	4.89	30.5	1361	193
Summer 2018 (07)	SP	12/07/2018	11:45	-8.92645	53.141673	0	1.6	8177	1743
Summer 2018 (07)	ST1	13/07/2018	17:30	-8.961683	53.162283	3.46	29.8	2091	215
Summer 2018 (07)	ST2	13/07/2018	18:28	-8.938937	53.145213	1.06	29.8	480	193
Summer 2018 (07)	ST3	13/07/2018	18:51	-8.948233	53.155417	2.36	29.1	1776	661
Summer 2018 (07)	ST5	13/07/2018	17:37	-8.954132	53.166427	3.46	29.6	4727	546
Autumn 2018 (10)	T1	22/10/2018	10:00	-8.943077	53.166102	-	30.4	1391	653
Autumn 2018 (10)	T2	22/10/2018	13:00	-8.943077	53.166102	-	28.4	1490	423
Autumn 2018 (10)	T3	22/10/2018	16:00	-8.943077	53.166102	-	28.4	788	270
Autumn 2018 (10)	T4	22/10/2018	19:00	-8.943077	53.166102	-	29.3	3027	575
Autumn 2018 (10)	T5	22/10/2018	22:00	-8.943077	53.166102	-	28.1	1349	374
Autumn 2018 (10)	T6	23/10/2018	01:00	-8.943077	53.166102	-	26.3	3509	479
Autumn 2018 (10)	T7	23/10/2018	04:00	-8.943077	53.166102	-	26.9	1542	533
Autumn 2018 (10)	T8	23/10/2018	07:00	-8.943077	53.166102	-	28.2	1865	753
Autumn 2018 (10)	T9	23/10/2018	10:00	-8.943077	53.166102	-	27.9	2056	844
Autumn 2018 (10)	BH-AM	20/10/2018	10:50	-8.918767	53.126792	-1.7	0.3	3602	1406
Autumn 2018 (10)	BHBlack	20/10/2018	16:45	-	-	-	0.5	5711	2931
Autumn 2018 (10)	SP	20/10/2018	08:55	-8.92645	53.141673	0	0.5	11747	6883
Autumn 2018 (10)	SPmidhightide	20/10/2018	-	-8.92645	53.141673	0	0.0	7851	4316
Autumn 2018 (10)	ST1	21/10/2018	16:30	-8.942543	53.16705	4	29.4	810	345
Autumn 2018 (10)	ST2	21/10/2018	17:00	-8.930507	53.14469	0.5	10.2	2414	874
Autumn 2018 (10)	ST3	21/10/2018	17:30	-8.952848	53.153857	2	26.4	1055	195
Autumn 2018 (10)	ST4	21/10/2018	18:30	-8.968368	53.172163	4.6	30.3	1070	246
Winter 2019 (01)	T1	25/01/2019	17:00	-8.968507	53.171727	-	28.3	546	280
Winter 2019 (01)	T2	25/01/2019	20:00	-8.968507	53.171727	-	29.2	143	135
Winter 2019 (01)	T3	25/01/2019	23:00	-8.968507	53.171727	-	29.2	40	75
Winter 2019 (01)	T4	26/01/2019	02:00	-8.968507	53.171727	-	28.4	291	234
Winter 2019 (01)	T5	26/01/2019	05:00	-8.968507	53.171727	-	26.6	144	160
Winter 2019 (01)	T6	26/01/2019	08:00	-8.968507	53.171727	-	29.2	21	38

Winter 2019 (01)	T7	26/01/2019	11:00	-8.968507	53.171727	-	27.4	85	111
Winter 2019 (01)	T8	26/01/2019	14:00	-8.968507	53.171727	-	27.5	295	194
Winter 2019 (01)	T9	26/01/2019	17:00	-8.968507	53.171727	-	28.0	67	83
Winter 2019 (01)	BH	28/01/2019	16:15	-8.918767	53.126792	-1.7	0.3	3238	656
Winter 2019 (01)	EM	28/01/2019	12:42	-8.963631	53.180916	5.49	26.4	240	157
Winter 2019 (01)	SedimentSpring	26/01/2019	17:10	-8.92645	53.141673	0	0.0	5120	732
Winter 2019 (01)	SP	26/01/2019	17:10	-8.92645	53.141673	0	0.6	7997	490
Winter 2019 (01)	ST1	28/01/2019	11:28	-8.934121	53.143164	0.56	8.3	5120	732
Winter 2019 (01)	ST2	28/01/2019	11:40	-8.938077	53.14554	0.96	6.2	784	284
Winter 2019 (01)	ST3	28/01/2019	11:55	-8.941101	53.151073	1.63	7.9	3366	1012
Winter 2019 (01)	ST4	28/01/2019	12:08	-8.947829	53.158552	2.59	17.6	1001	510
Winter 2019 (01)	ST5	28/01/2019	12:19	-8.954884	53.165489	3.53	25.6	116	161
Winter 2019 (01)	ST6	28/01/2019	12:32	-8.962771	53.171481	4.39	26.1	327	365
Spring 2019 (04)	T1	07/04/2019	12:50	-8.968507	53.171727	-	18.4	1039	262
Spring 2019 (04)	T2	07/04/2019	16:00	-8.968507	53.171727	-	29.7	675	334
Spring 2019 (04)	T3	07/04/2019	19:00	-8.968507	53.171727	-	30.0	152	207
Spring 2019 (04)	T4	07/04/2019	22:00	-8.968507	53.171727	-	30.9	157	146
Spring 2019 (04)	T5	08/04/2019	01:00	-8.968507	53.171727	-	28.6	591	310
Spring 2019 (04)	T6	08/04/2019	04:00	-8.968507	53.171727	-	28.5	566	298
Spring 2019 (04)	T7	08/04/2019	07:00	-8.968507	53.171727	-	29.7	229	195
Spring 2019 (04)	T8	08/04/2019	10:00	-8.968507	53.171727	-	29.0	250	98
Spring 2019 (04)	T9	08/04/2019	13:00	-8.968507	53.171727	-	27.1	296	163
Spring 2019 (04)	BH	08/04/2019	15:00	-8.918767	53.126792	-1.7	0.2	11926	649
Spring 2019 (04)	EM	06/04/2019	16:58	-8.962164	53.181533	5.72	31.9	342	208
Spring 2019 (04)	SP	07/04/2019	14:00	-8.92645	53.141673	0	0.4	7496	2012
Spring 2019 (04)	SPDown	08/04/2019	13:30	-8.92645	53.141673	0	0.0	8203	1103
Spring 2019 (04)	SPUP	08/04/2019	13:30	-8.92645	53.141673	0	0.0	5554	1525
Spring 2019 (04)	ST1	06/04/2019	15:10	-8.935724	53.142924	0.64	12.8	1828	488
Spring 2019 (04)	ST2	06/04/2019	15:32	-8.938942	53.146	1.14	14.3	1483	525
Spring 2019 (04)	ST3	06/04/2019	15:45	-8.941683	53.151315	1.79	23.2	1010	475
Spring 2019 (04)	ST4	06/04/2019	16:02	-8.949191	53.159132	2.81	30.9	186	124
Spring 2019 (04)	ST5	06/04/2019	16:25	-8.957427	53.165856	3.67	32.4	117	117
Spring 2019 (04)	ST6	06/04/2019	16:43	-8.963944	53.17228	4.63	33.5	615	235